Pulverised Biomass Flame Propagation

Muhammad Azam Saeed

Submitted in accordance with the requirements for the degree of
Doctor of Philosophy

The University of Leeds

School of Chemical and Process Engineering

June, 2016

The candidate confirms that the work submitted is his own, except where work which has formed part of jointly-authored publications has been included. The contribution of the candidate and the other authors to this work has been explicitly indicated below. The candidate confirms that appropriate credit has been given within the thesis where reference has been made to the work of others.

List of publications

A list of publications are listed below that are part of this present study. The contribution from each individual for each joint publication is explicitly explained.

- **Muhammad Azam Saeed**, Clara Huéscar Medina, Gordon E. Andrews, Herodotos N. Phylaktou, David Slatter and Bernard M. Gibbs, Agricultural waste pulverised biomass: MEC and flame speeds. Journal of Loss Prevention in the Process Industries, 2015. 36(0): p. 308-317.

The candidate as primary author for this publication led the experimental procedure and writing up of the publication. Clara Huescar Medina and David Slatter as co-authors participated in carrying out the experiments. Prof. Gordon, Dr. Phylaktou and Prof. Bernard were co supervisors of the research work, participated in the analysis of results and proof-read the publication.

- **Muhammad Azam Saeed**, Clara Huéscar Medina, Gordon E. Andrews, Herodotos N. Phylaktou, David Slatter & Bernard M. Gibbs. Agricultural waste pulverised biomass: Lean flammability and flame speeds in Tenth International Symposium on Hazards, Prevention, and Mitigation of Industrial Explosions. 2014. Bergen, Norway.

The candidate as primary author for this publication led the experimental procedure and writing up of the publication. Clara Huescar Medina and David Slatter as co-authors participated in carrying out the experiments. Prof. Gordon, Dr. Phylaktou and Prof. Bernard were co supervisors of the research work, participated in the analysis of results and proof-read the publication. Prof. Gordon presented this paper in the conference as an oral presentation.

- **Muhammad Azam Saeed**, Gordon E. Andrews, Herodotos N. Phylaktou & Bernard M. Gibbs. Global kinetics of the rate of volatile release from biomasses in comparison to coal, in 1st Chemistry in Energy Conference (1st CEC), Royal Conference of Chemistry Conference, 2015: Edinburgh, UK. *(Published in 'Fuel Journal')*

The candidate as primary author for this publication led the experimental procedure and writing up of the publication. Prof. Gordon, Dr. Phylaktou and Prof. Bernard were co supervisors of the research work, participated in the analysis of results and proof-read the publication. Prof. Gordon presented this

paper in the conference as an oral presentation. This paper is now published in the Fuel Journal.

- **Muhammad Azam Saeed**, Gordon E. Andrews, Herodotos N. Phylaktou, David Slatter, Clara Huéscar Medina & Bernard Gibbs. Flame propagation of pulverised biomass crop residues and their explosion characteristics. 25th International Colloquium on the Dynamics of Explosions and Reactive Systems (ICDERS). 2015. Leeds, UK.

The candidate as primary author for this publication led the experimental procedure and writing up of the publication. Also the candidate presented this paper as an oral presentation in the conference. David Slatter as co-author participated in carrying out the experiments. Clara Huescar Medina guiding in learning software for extracting explosibility results. Prof. Gordon, Dr. Phylaktou and Prof. Bernard were co supervisors of the research work, participated in the analysis of results and proof-read the publication. This paper is accepted for Journal of Combustion, Science and Technology and in the publishing phase.

- **Muhammad Azam Saeed**, Gordon E. Andrews, Herodotos N. Phylaktou & Bernard M. Gibbs. Effect of steam exploded treatment on the reactivity of wood sample. Proceedings of the 8th Int. Conference on Sustainable Energy and Environmental Protection (SEEP2015). 2015. Paisley, Scotland, UK.

The candidate as primary author for this publication led the experimental procedure and writing up of the publication. Prof. Gordon, Dr. Phylaktou and Prof. Bernard were co supervisors of the research work, participated in the analysis of results and proof-read the publication. Prof. Gordon presented this paper in the conference as an oral presentation. This paper is now published in the International Journal of Hydrogen Energy.

- **Muhammad Azam Saeed**, Herodotos N. Phylaktou, Gordon E. Andrews & Bernard M. Gibbs. Reactivity of biomass crop residues based on MEC and flame speed. Proceedings of the 14th International Symposium on Handling and Hazards of Materials in Industry, ANQUE+ICCE+BIOTEC+14th HANHAZ. Madrid, Spain. ISBN: 978-84-697-0726-5

The candidate as primary author for this publication led the experimental procedure and writing up of the publication. Prof. Gordon, Dr. Phylaktou and Prof. Bernard were co supervisors of the research work, participated in the analysis of results and proof-read the publication.

- **Muhammad Azam Saeed**, Gordon E. Andrews, Herodotos N. Phylaktou, Hamed Sattar, Clara Huescar-Medina, David Slatter, Herath, P. & Bernard M. Gibbs. Improvements to the Hartmann dust explosion equipment for MEC measurements that are compatible with gas lean limit measurements. 10th Asia-Oceania Symposium on Fire Science and Technology (10th AOSFST). 2015. Tsukuba, Japan.

The candidate as primary author for this publication led the experimental procedure and writing up of the publication. Also the candidate presented this paper as an oral presentation in the conference. This paper was written based on the current along with the previous experimental results of Hamed Sattar, David Slatter, P Herath and Huescar Clara Media as co-authors for this publication. Prof. Gordon, Dr. Phylaktou and Prof. Bernard were co supervisors of the research work, participated in the analysis of results and proof-read the publication. This paper is in the publishing phase for the *journal of Procedia Engineering on the Elsevier Science Direct system*.

- **Muhammad Azam Saeed**, Aysha Irshad, Gordon E. Andrews, Herodotos N. Phylaktou & Bernard M. Gibbs. Agricultural waste biomass energy potential in Pakistan. Proceedings of the International Bioenergy (Shanghai) Exhibition and Asian Bioenergy Conference, European Biomass and Energy Conference (EUBCE), 2015. Shanghai, China, DOI: http://dx.doi.org/10.5071/IBSCE2015-1CO.1.2

The candidate as primary author for this publication reviewed the literature and performed some calculations for the biomass waste based on statistics. Aysha Irshad as co-author performed the energy calculation for wood, seed oils and banana trees. Both the candidate and Aysha were involved in writing up of the publication. Prof. Gordon, Dr. Phylaktou and Prof. Bernard were co supervisors of the research work, participated in the analysis of results and proof-read the publication. Prof. Gordon presented this paper as oral presentation in the conference.

- Nieves Fernandez-Anez, David J. F. Slatter, **Muhammad Azam Saeed**, Herodotos N. Phylaktou, Gordon E. Andrews, Javier Garcia-Torrent (20150. Ignition sensitivity of coal / waste / biomass mixtures. Proceedings of the 8th Int. Conference on Sustainable Energy and Environmental Protection (SEEP2015), 2015, Paisley, Scotland.

The candidate participated in training the primary author (Nieves Fernandez-Anez) on the experimental unit and use of software for extracting results. David was involved in supervising during the experimental phase. Nieves followed the writing up of the publication. Dr. Phylaktou, Prof. Andrews and Dr. Javier were co-supervisors of the research work, participated in the analysis of results and proof-read the publication.

- **Muhammad Azam Saeed**, Gordon E. Andrews, Herodotos N. Phylaktou, Bernard M. Gibbs, Richard Walton & Lukasz Niedzweicki. (2016). Flame propagation of coarse wood mixture: raw and torrefied. Proc. 8th International Seminar on Fire and Explosion Hazards (ISFEH8), Heifei, China. USTC Press.

The candidate as primary author for this publication led the experimental procedure and writing up of the publication. Also the candidate presented this paper as an oral presentation in the conference. Prof. Gordon, Dr. Phylaktou and Prof. Bernard were co supervisors of the research work, participated in the analysis of results and proof-read the publication. Ricard Walton and Lukasz Niedzweicki provided the raw and torrefied materials for this work. They also assisted in writing the torrefaction process adopted for the studied torrefied sample.

- **Muhammad Azam Saeed**, David Slatter, Gordon E. Andrews, Herodotos N. Phylaktou & Bernard M. Gibbs. Flame speed and Kst reactivity data for pulverised corn cobs and peanut shells. 11th International Symposium on Hazards, Prevention, and Mitigation of Industrial Explosions. 2016. Dalian, China.

The candidate as primary author for this publication led the experimental procedure and writing up of the publication. David Slatter helped in the carrying out the experimental work. Prof. Gordon, Dr. Phylaktou and Prof. Bernard were co supervisors of the research work, participated in the analysis of results and proof-read the publication.

- **Muhammad Azam Saeed**, David Slatter, Gordon E. Andrews, Herodotos N. Phylaktou & Bernard M. Gibbs. The burning velocity of pulverised biomass: The influence of particle size. 7th International Conference on Safety and Environment in the Process & Power Industry. 2016. Ischia, Italy. (Accepted for oral presentation)

The candidate as primary author for this publication led the experimental procedure, compiled data and writing up of the publication. David Slatter helped in the carrying out the experimental work. Prof. Gordon, Dr. Phylaktou and Prof. Bernard were co supervisors of the research work, participated in the analysis of results and proof-read the publication. This paper will be included in the Chemical Engineering Transaction Journal.

Conference posters

- **Muhammad Azam Saeed**, Gordon E. Andrews, Herodotos N. Phylaktou & Bernard M. Gibbs. Influence of biomass pellet composition on the pulverised pellet flame propagation and minimum explosible concentration. 25th International Colloquium on the Dynamics of Explosions and Reactive Systems (ICDERS). 2015. Leeds, UK.

The candidate led the experimental work and presented them in the form of poster in the conference. Prof. Gordon, Dr. Phylaktou and Prof. Bernard participated in the analysis of results and proof-read the publication.

- **Muhammad Azam Saeed**, Aysha Irshad, Gordon E. Andrews, Herodotos N. Phylaktou & Bernard M. Gibbs. Biomass energy potential in Pakistan. 1st Biomass Emission Conference. 2015. Leeds, UK.

The candidate and Aysha performed the calculations and presented in the form of poster in the conference. Prof. Gordon, Dr. Phylaktou and Prof. Bernard participated in the analysis of results and proof-read the publication.

Acknowledgements

I am extremely grateful to my supervisors, Prof. Gordon Andrews, Dr. Herodotos Phylaktou and Prof. Bernard Gibbs for their guidance during the course of the past years, for many hours of discussions and for trusting me and giving me confidence to undertake this research.

I am grateful to the University of Engineering and Technology, Lahore, Pakistan for awarding me Faculty Development Program Scholarship to pursue my PhD study. I am also grateful to Energy Program (EPSRC, ESCR, NERC, BBSRC and STFC, Grant EP/H048839/1) for financial support for part of this project, and to all sample suppliers: Sea2Sky Energy UK Ltd and Zilkha Biomass Energy.

I would also like to thank all of my colleagues: Hamed Sattar, Clara Huescar Medina, Dave Slatter, Aziz Alarifi and Aysha Irshad. I wish them all the best for the future.

I am also most grateful to Bob Boreham, Adrian Cunliffe, Sara Dona, Ed Woodhouse and Susanne Patel for their patience, help and advice with all technical issues, which were numerous.

Very special thanks to my parents who have given me every opportunity in life and who, together with my brothers and sisters, have been an endless source of encouragement. I am also grateful to the rest of my family and friends both in Pakistan and the UK. The best reward is to spend time with all of them.

Abstract

A resource analysis for Pakistan has demonstrated that abundant **crop residues** offer a viable, and environmental-friendly alternative to currently inadequate, oil-based power generation. Similarly, in many countries there is legislative pressure and incentives to replace coal with biomass, in electricity production. Efficient and safe exploitation of such biofuels requires data on flame propagation rates and explosibility characteristics.

Crop residues (bagasse, rice husk, wheat-straw, corn-cob and peanut-shell) and different raw and thermally treated woods were tested using the modified Hartmann tube and the modified 1 m^3 explosion vessel. The modified Hartmann tube was operated for varying ignition delays using a digital timer. A hemispherical disperser with drilled pipe was calibrated for the testing of fibrous and coarse size biomass mixtures.

Thermogravimetric analysis data from these materials enabled the application of two different models for the determination of volatile release kinetics. Biomass samples were found to have lower activation energies with higher volatile release rates at low temperatures, compared to coals.

Despite their higher ash content, pulverised crop-residues showed leaner minimum explosible concentrations (0.2-0.5 equivalence-ratio) than woods (0.3-0.7) - depending on particle size. Biomass samples were more sensitive to explosion than coal, resulting in flame propagation in coarse-size-range fractions (300-500-µm) that was not experienced with coals. Maximum explosion pressures of near 9 barg were measured for the fine size fraction (less than 63-µm) samples, with no less than 7 barg for coarse size fraction (less than 1 mm).

Milling of thermally treated biomass samples resulted in higher fines fraction than untreated biomass, for the same sieve size and this was considered as one of the reasons of the higher reactivity (higher flame speed and higher deflagration index of these samples).

The detailed data from this work are usable in the design of safe and efficient combustion systems for power generation from crop residues and other biomass fuels.

Table of Contents

List of Tables

List of Figures

Nomenclature

Abbreviations

A/F	Air to fuel ratio
daf	Dry ash free basis
dP/dt	Rate of pressure rise (bar/s)
E	Activation energy (KJ/mol)
FC	Fixed carbon (%)
GCV	Gross calorific value (MJ/Kg)
GHG	Greenhouse gases
GHRR	Global heat release rate (MW/m^2)
k	Rate constant
K_G	Cubic law gas constant (bar m/s)
K_{st}	Cubic law dust constant/ Deflagration index (bar m/s)
LFL	Lean flammability limit
LOC	Limiting Oxygen Concentration
MEC	Minimum Explosible Concentration
MIE	Minimum Ignition Energy
Pm/Pi	Normalised maximum explosion pressure (bar)
P_{red}	Reduce Pressure (bar)
s_f	Turbulent flame speed (m/s)
s_L	Laminar flame speed (m/s)
SEM	Scanning Electron Microscopy
SMD/$d_{3,2}$	Surface Mean Diameter (µm)
U_L	Laminar burning velocity (m/s)
VM	Volatile matter (%)
VMD/$d_{4,3}$	Volume Mean Diameter

Greek/Latin symbols

Ø	Equivalence ratio
β	Turbulent factor
λ	layer thickness
ρ	density

Subscripts

b	burnt
c	corrected
i	initial
L	laminar
m	maximum
T	turbulent
u	unburnt

Chapter 1 INTRODUCTION

In this chapter, the historical dominancy of different energy sources is explained. The feasibility of biofuels for extraction of energy with their pros and cons and the techniques to avoid biomass related problems are discussed. Energy conversion routes of biomass and their applications are presented. The risks of fire and explosion associated with these biofuels are briefly discussed. In the end, the project background with the lists of UK's Biomass Power-Plants (current and planned) is presented. Finally the objectives of the work are presented briefly.

1.1 Background of energy sources in practice

For thousands of years, biomass was the important energy source known to mankind. The fossil fuels had taken over that role during the last centuries. At the end of the 19th century, the use of coal started to increase. After World War II, inexpensive gasoline became available leading to an increasing oil usage. Fossil fuel reserves cannot last longer due to the increasing energy requirement. Also the combustion of fossil fuels have proven to be harmful for the environment due to hazardous emissions. Concentration of carbon dioxide (CO_2), causing global warming, increased in the atmosphere due to the large-scale utilization of fossil fuels. The energy community started to look for the substitutes of fossil fuels as all the estimated fossil fuels energy sources in the world last for 70-80 years on average and the energy sources have to be shifted to the others. This transition towards a low carbon energy demands the detailed assessment of new source before its application. Careful considerations and efforts are needed to modify/change the existing technology suitable for the new fuel [1].

1.2 Greenhouse gas emissions

Fossil fuels are the main source of hazardous GHG's emissions causing serious threats to the environment. The Kyoto Protocol is an international binding agreement under the United Nations to commit its parties for reducing overall emission of CO_2 [2]. During its first period, it was committed by 37 industrialized countries and European Community to reduce the GHG's emission to an average of 5% against 1990 level. In the second agreement, it is committed reducing the GHG's emission up to 18% against 1990 in the period of eight years from 2013 to 2020.

Table 1.1: Four Carbon budgets to meet the target for GHG's reduction [3]

Budget		Carbon budget level	% reduction below base year
1st carbon budget	2008-2012	3018MtCO_2e	23%
2nd carbon budget	2013-2017	2782MtCO_2e	29%
3rd carbon budget	2018-2022	2544MtCO_2e	35% by 2020
4th carbon budget	2023-2027	1950MtCO_2e	50% by 2025

The 'Climate Change Act' established a target for the UK in 2008 that aims to reduce UK's GHG's up to 80% by 2050 from the baseline year of 1990 [3]. To monitor and regulate the progress in the reduction of carbon credits, four carbon budgets consisting of five years each were established that are presented in table 1.1 [3];

1.3 Role of renewable energy sources

In the current era, the scope for renewable energy has emerged to have significant potential as it is environment friendly and economically desirable especially for agricultural countries. There are different renewable energy options e.g. solar, hydro, wind, biomass, geothermal etc. [4]. Adoption of local available renewable sources for energy generation is therefore increasing.

In the US, about a 13% share of electricity was generated from renewable sources in 2014 as shown in Figure 1.1 [5]. In the UK, provisional calculations, using a methodology set by the EU renewable directive, showed that a 7% share of energy consumed in 2014 was from renewable sources compared to 5.6% in 2013 (About a 25% increase) [6].

The UK has already initiated shift away from coal power plants to renewable biofuels. According to DUKES, the percentage of electricity from renewable fuel was 10.7% in 2012 which increased to 13.8% in 2013 (About 29% increase based on 2012) [6]. The electricity generation using different shares of renewable energy is shown in fig 1.2.

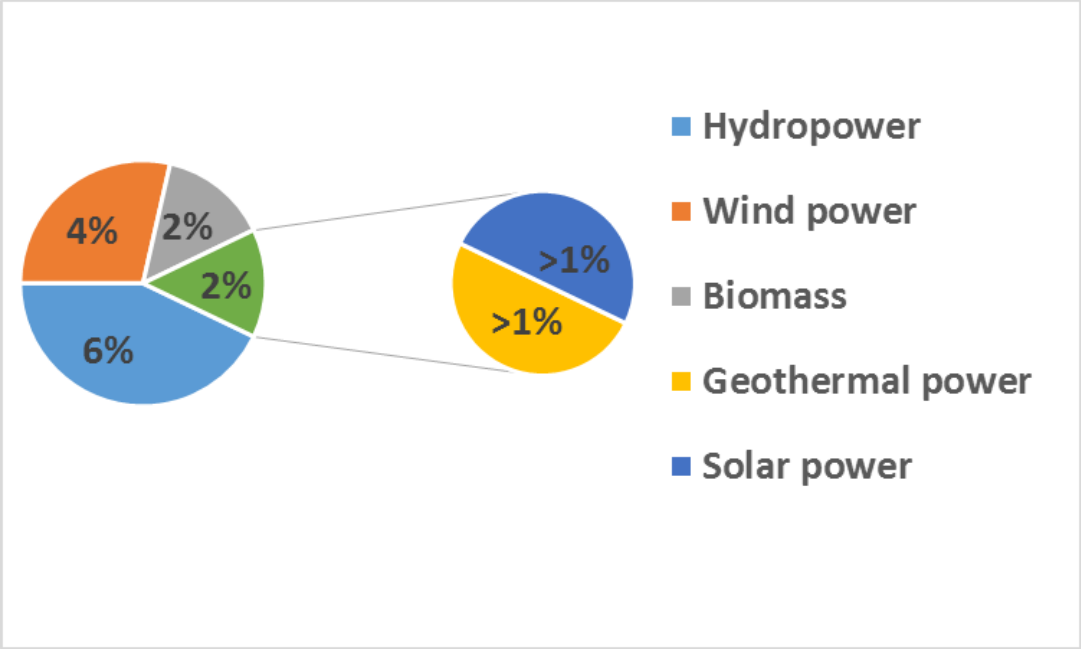

Figure 1.1: US Shares of renewable sources for electricity generation in 2014 [5]

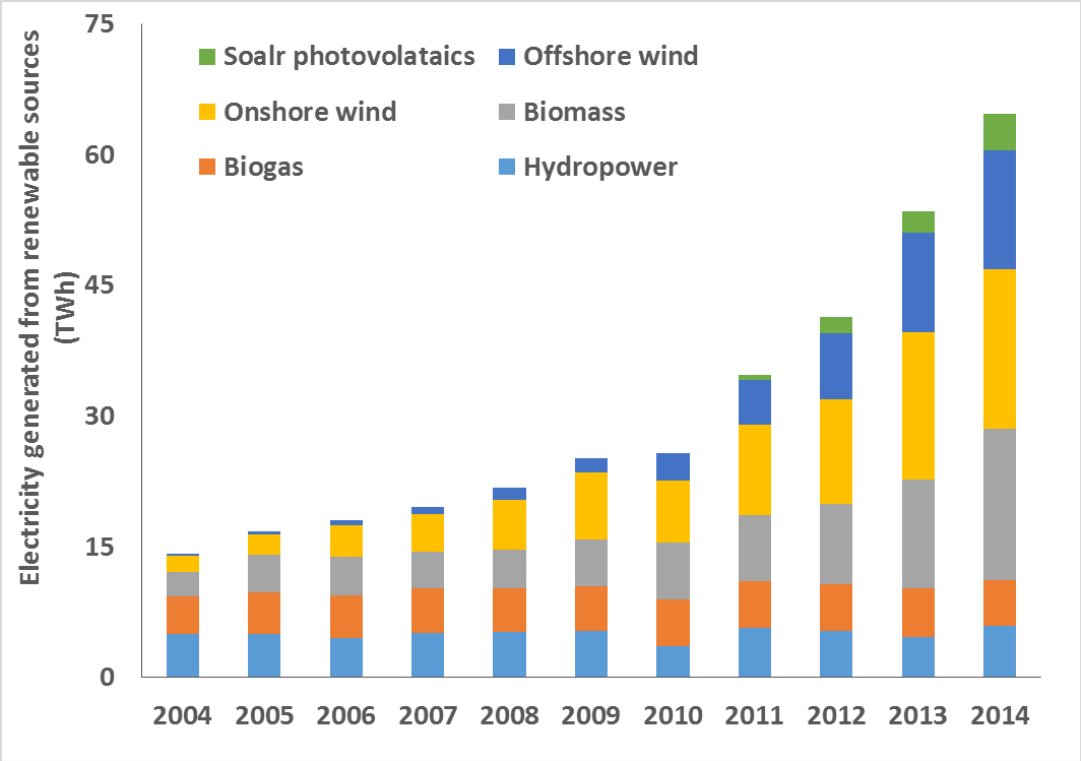

Figure 1.2: UK's electricity generation from different renewable sources [6]

1.4 Role of bioenergy for sustainable conversion

Renewable energy in 2014 was utilised for various applications as shown in Figure 1.3 [6]. Biomass conversion to energy is an appropriate and reliable source of energy after balancing their consistent growth with consumption. Biomass samples do not require much time for their growth as used for fossil fuels and follow the cyclic process. Due to the short time period of their 'carbon-cycle', they are CO_2 neutral fuels [1]. Utilization of the renewable biofuels has a vital contribution for achieving these targets. According to the EU Commission's recent report, the conclusion was drawn that the use of different types of biomass reduce GHG's emissions by 55 to 98% even when transported internationally [7].

In fact, in May 2007, the UK's government published its biomass strategy coupled with the Energy White Paper for the intention of government to expand the utilization and application of the biomass as the renewable source of energy that includes

- A EU target of 20% renewable energy by 2020
- From April 2008 to 2010, the transport fuel obligation program of 5% of UK forecourt fuel to make up from renewable source.

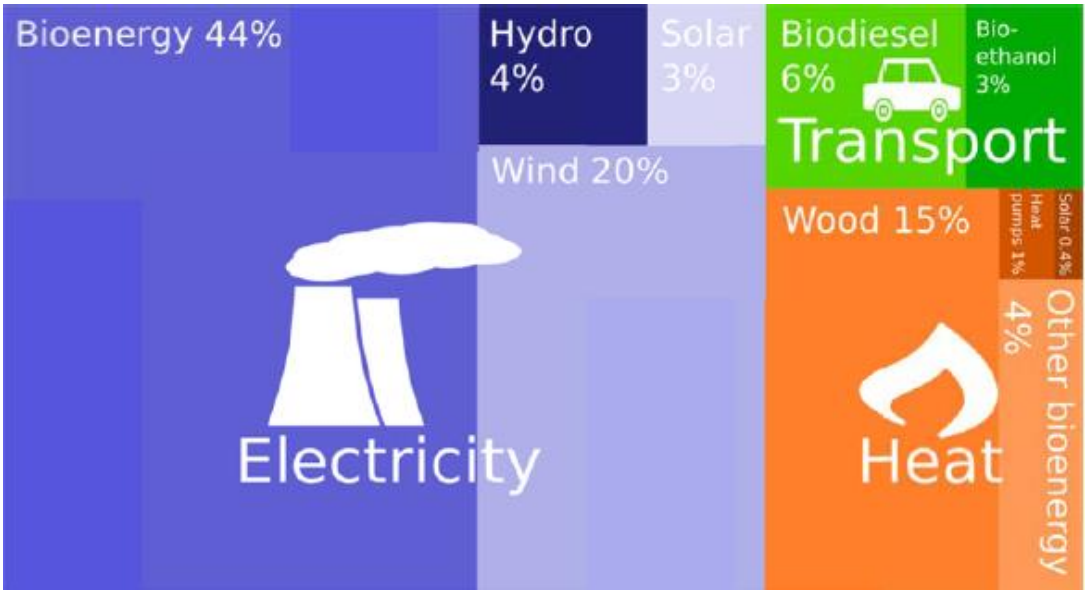

Figure 1.3: UK's share of renewable sources for electricity generation in 2014 [6]

Digest of the United Kingdom's Energy Statistics estimated 30% share of Coal in national grid electricity in 2014 [6]. Burning of this coal in the power generation plants is the biggest source of carbon emissions. These coal power plants are scheduled to either close or switch to other renewable fuel, to meet the environmental regulations. Biofuels are the most appropriate substitute of coal for the existing coal power generation plants.

Biomass is recognized as 'material originates from living and recently dead biological materials e.g. wood, agricultural residues and animal remainder'. A major share of this biomass is used as cattle's feed-stocks. Some of the woody biomass is used in the wood industries for construction. There are still thousands of tonnes of this biomass mainly agricultural waste without any use and incinerated or dumped for disposal whereas some is left on land to replenish soil fertility.

According to UK Department of Business, Enterprise and Regulatory Reforms (BERR), the UK's energy crops include short rotation coppice, Miscanthus (Elephant Grass), willow and poplar, Reed Canary Grass and Oil Seed Rape. The largest and most effective Brigg renewable straw fired power station is in Cambridgeshire, UK [8]. This 36MW plant has the generation capacity of over 270GWh/y that facilitates to approximately 80,000 homes for heating and lighting. The total yearly straw consumption of this Power station is 200,000 tonnes collected from the farms located in the radii of 50mile [8].

Agricultural countries like Pakistan have enormous amounts of crop residues. Some of this biomass are needed for soil fertility but a large amount has no end use. These waste residues after some pre-treatments can be a viable option as fuels for the electric power generation. There is a detailed Pakistan statistics and calculations of these crop residues in the second chapter.

In practice energy is used by farmers in planting and harvesting crops. So the process is not strictly carbon neutral and auditing this upstream CO_2 leads to figure on the sustainability of biomass or the efficiency of the CO_2 reduction. The EU and USA have drawn up sustainability criteria for biomass and any biomass used for power generation has to meet the approved sustainability criteria considering emission for upstream activities. Similar procedures would have to be adopted in Pakistan to ensure that the production of biomass was sustainable.

1.4.1 Compositional analysis of biomass

The main components of biomass include cellulose, hemicellulose, lignin, proteins, lipids, simple sugars, starches, water, HC, ash and other compounds. The main elemental components of the biomass include carbon, hydrogen, oxygen, nitrogen, sulphur and some of the alkali metals. Generally all the dry (moisture free) biomass materials contain the carbon, as the principal component, in between 30-60%. Oxygen the 2nd largest component and hydrogen, the third largest component in between 4-6% with remaining nitrogen and sulphur usually below 1% [9].

Biomass materials contain high amount of oxygen and hydrogen compared to coal as shown in Van Krevelen plot in Figure 1.4. The chemical characterization of a number of biomasses was compiled and listed by Vassilev et al. (2012) in the review paper [10]. Also biomass materials contain higher volatiles than coals. There are discrepancies in the biomasses depending on their type and origin. These oxygenated biofuels with higher volatiles make them very reactive [11].

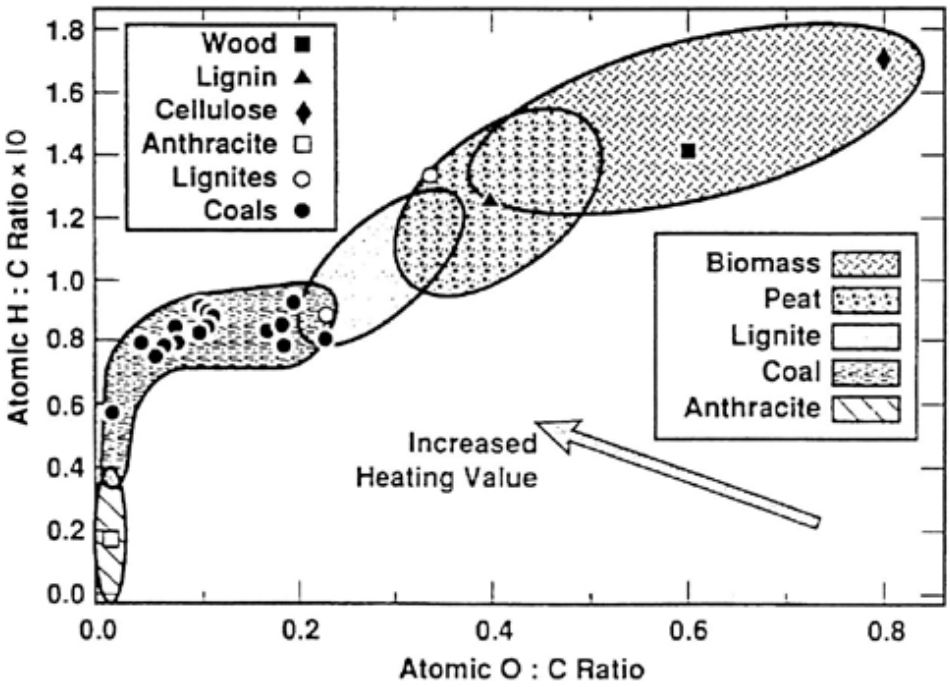

Figure 1.4: H/C v. O/C molar plots for biomass in comparison to different types of coal samples

1.4.2 Challenges and techniques to improve biofuels for its exploitation

Biofuels can be employed for various application after refining its properties using different pre-treatments as shown in Figure 1.5. There are some issues related to handling of these biomass due to low bulk density and high moisture content [12]. Transporting raw biomass with relatively high water content, high ash content (for agricultural biomass) and low bulk density would be prohibitively expensive. To overcome this problem biomass is washed to reduce ash, dried using external heat and densified by being formed into pellets [13]. Some thermal treatments are also applied for more refinement depending on their use.

The compact shape of pellet or briquetted biomass enables more biomass to be stored in a fixed volume and hence increase the energy density of the transport costs. As pellets are pre-pulverised at source and only need to be broken up in the coal mills, they are the preference for large scale use in pulverized coal power stations. However, for smaller power generation steam cycles using briquettes of dried compressed biomass is more practical. There are two types of densification available: simple compression of dried biomass into briquettes, as available in China, and pulverisation of the biomass into a powder which is dried and then compressed into pellets [14, 15].

Biomass based on wood is generally low in ash, but biomass based on agricultural wastes, as advocated in this work have variable ash content. Ash is a problem as it reduces the CV per kg of biomass. However, its main problem is the ash consists of various metals such as potassium, iron, magnesium, manganese, sodium etc. and this creates boiler fouling and corrosion problems.

Some typical biomass ash and water contents from the work of the author are shown in table 1.2. Some of the agricultural waste are very high in ash and this would have to be refined by applying some pretreatments. Also a special feature of biomass ash that was not well known and this is that milling of the biomass into a finer powder <63 µm, concentrates the ash in the finer fraction.

The alkaline earth metals are released from the soil into the biomass in the growing process and potassium is one of the key ingredients in agricultural waste ash. For the utilization of agricultural waste biomass for power generation, washing is applied to reduce these alkali metals.

Table 1.2: Water and Ash Content of a Range of Biomass [17-19]

Biomass	H_2O (% mass)	Ash (% mass)	CV (MJ/kg)
Rice Husk	7.7	17.9	15.2
Rice Husk <63µm	6.56	31.2	14
Bagasse	7.2	20.1	15.6
Bagasse (<63µm)	6.85	23.4	15.05
Wheat Straw	6.8	22.8	14.5
Wheat Straw <63µm	3.98	49.2	13.93
Lycopodium	1.6	4.1	29.6
Corn flour	11.6	3.8	16.4
Walnut Shells	4.95	6.3	18.75
Pistachio nut shells	2.7	8.3	17.8
Pine wood	4.27	4.4	19.2

Simply washing by water or acid leaching techniques are the effective in controlling the alkali metals release from biomass [16]. Simple water leaching can reduce alkali metals of up to 70-80% [16].

Thermal treatments like 'Torrefaction' can be carried out by heating the biomasses in the absence of air or in an inert environment at a temperature in the range of 200-300^{0}C for small time duration (20 minutes). The resultant process gives a very dry biomass and drives off some volatiles [20], that may be used for the heating requirements of the process. The main effect is to destroy the fibrous nature of woody biomass and makes the fibers brittle. The material is more easily pulverized in coal mills at power plants. A further benefit of torrefaction is to enhance the calorific value and to reduce the moisture contents. However there is small enhancement of ash that has to be controlled by performing it in combination with washing. This extensive pretreatment of biomass can lead to better boiler performance and hence to a higher thermal efficiency of the power generation plant.

The consistency in the supply of biomass to the power generation plants is another challenge. Utilization of some crop residues as power plants feedstock is also dependent on their seasonal harvesting that also depends on the environmental conditions. After their harvesting, their collection and safe

storage for a period of utilization requires short and long term planning. This includes the incentives to the local farmers and rural developments to encourage them for the targeted collection and transportation using local transports to a common storage point in the power generation plant. There should be strategies to keep the fertility of the soil for continuous utilization of land for harvesting. Biomass materials with small compositional variations can be consumed as mixture as also demonstrated in this research work. All of these planning and strategies should also have backing and support by the Government to ensure the process streamlined.

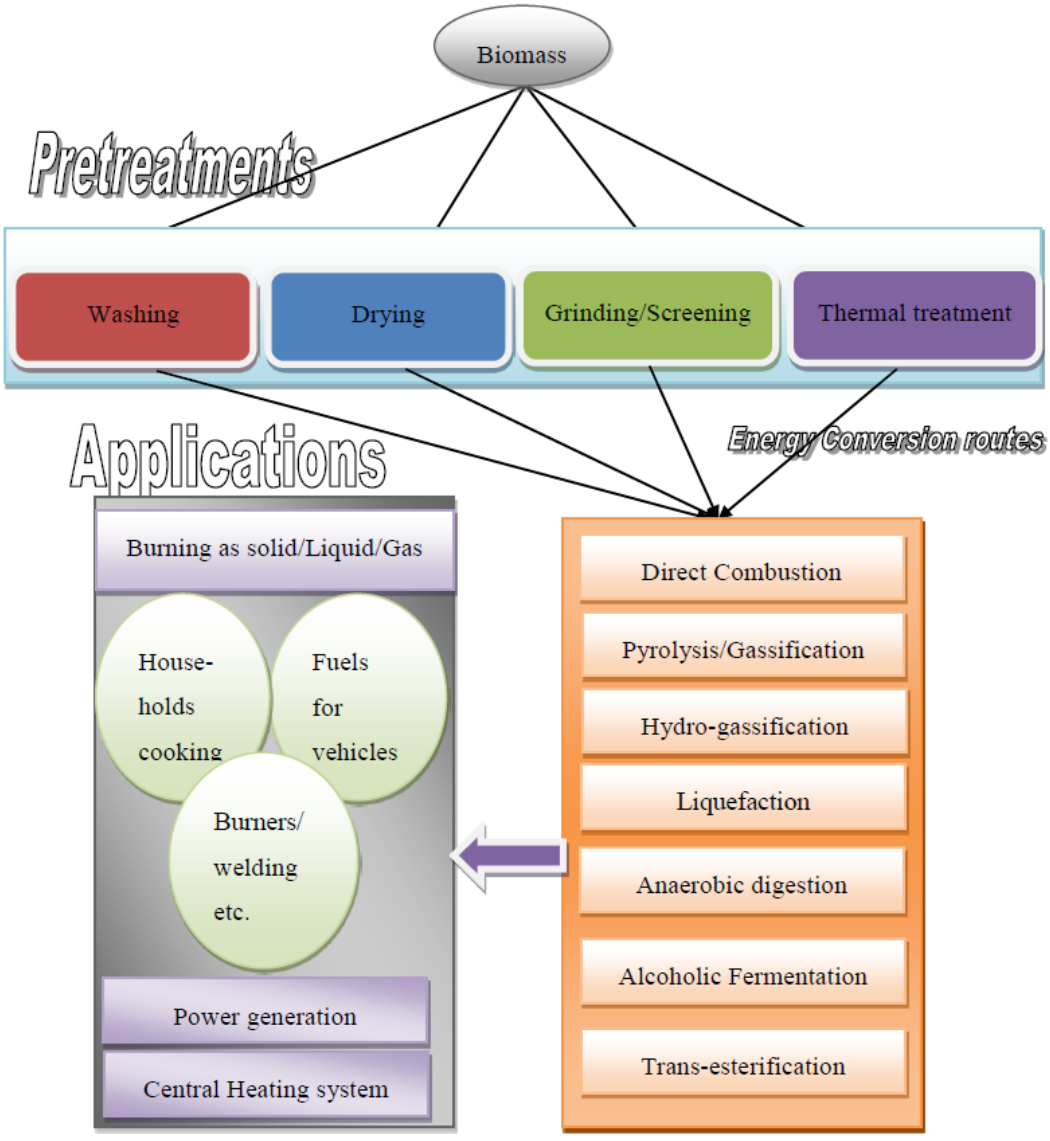

Figure 1.5: Biomass energy conversion routes using different technologies

Also the biomass materials are very reactive and need careful attention in handling, storing, conveying, milling and combustion. Lots of fire/explosion incidents involving pulverised biomass dust have been reported in the literature as detailed in Chapter 03. This is because of the scarce established data of its explosibility characteristics [17, 18, 21-24].

1.4.3 Fire/ Explosibility hazards of biomass

Biofuels are very reactive and carry fire and explosion hazards in pulverized form. Different explosibility parameters need to be evaluated for these solid dusts for safe working environment and for the design of the emergency systems that activate to overcome/suppressing the hazards for post explosion events. Also the existing methodologies have some flaws in accurately determining the explosiblity hazards or are incapable for fibrous biomass. These existing techniques needs to be modified and refined to acquire the reliable explosibility measurements.

The use of biomass in pulverized form gives the efficient combustion with the least excess air. However, the use of pulverised biomass as a fuel in power generation is relatively new and started as co-firing with coal. However, there are now large scale 100% pulverized biomass combustion steam generation plant as shown in table 1.3. There is a dearth of data on the fundamental combustion properties of pulverised biomass, in terms of data on flame propagation rates that are necessary for burner design. Also there are fundamental safety problems for which there is a lack of data. Flash back of biomass in the supply tubes is a problem due to its enhanced reactivity relative to coal, which this work will demonstrate. Also biomass dust explosions can occur in biomass storage silos, in transfer lines from pulverisers to the burners and in the pulveriser system.

1.5 Project background

There is a great concern in the energy security and the environmental threats for air pollution. In the Britain, major share of electricity comes from the burning of coal. All the electricity generated from power stations utilizing coal are scheduled to close or switch to other renewable fuels, to meet the environmental regulations. As biomass energy application reduces carbon dioxide emissions 55 to 98% even when transported to long distances compared to fossil fuels. Utilization of biomass (crop residues, woody and thermally treated) reserves

without any end-use can play a vital role in keeping the coal power generation plants in operation.

As shown in table 1.3, the current, planned and proposed power plants in the UK utilizing biomass are listed with the generation output. Many of the plants have adopted retrofit systems without considering the fire/explosibility hazards associated with the pulverized biomass fuel. This improper retrofitting is very dangerous and has serious risks involved. The massive use of the renewable biomass have to be favoured only in the safe working boundaries. The accurate knowledge of the explosibility data and the flame propagation mechanism needs to be explored as this is also required for the design of the protecting systems. The existing methodologies needs to be refined and modified for the accurate measurements of explosibility hazards of fibrous biomass. Also effect of different parameters, acting actively or passively, on the pulverised biomass flame propagation needs to be established. Especially the effect of particle size that has major influence on the explosibility hazards. Laboratory based methodologies are only suitable for fine sized dust particles that cannot be applied for commercial power generation plants. Besides raw biomass testing, thermally treated biomass samples gaining attention need to be assessed and compared with raw biomass samples.

The release of the volatiles in the propagation of flame plays a vital role for the burning of the dust particles. The kinetics for the release of volatiles needs to be investigated for agricultural waste and woody biomass samples. Also the role of fine sized particles along-with coarse particles needs to be studied. Fire and explosibility data of new biomass fuels needs to be established for their safe application in the power generation with minimum risk of danger. Also the existing methodologies for dust explosibility measurements have flaws giving inaccurate results that needs to be refined for reliable measurements of explosibility characteristics.

Table 1.3: UK's Biomass power stations (Current & Planned) [25]

		Current		
Project	**Location**	**Company**	**Fuel**	**Output**
Balcas Timber	Enniskillen, NI	Balcas	Wood	2.5 MW_e
Balcas Timber	Invergordon	Balcas	Wood	8 MW_e
Eccleshall Biomass	Eccleshall, Staffs		Miscanthus	2.6 MW_e
Ely	Ely, Cambridgeshire	EPRL	Straw	38 MW_e
Eye	Eye, Suffolk	EPRL	Poultry litter	12.7 MW_e
Glanford	Scunthorpe, N Lines	EPRL	MBM, Poultry litter	13.5 MW_e
Goosey Lodge	Northants		Biomass	16 MW_e
Grainger Sawmill	Enniskeane, Ireland		Wood	2 MW_e
Newry Biomass	Newry, NI	Kedco	Wood	2 MW_e(+2 MW_e) CHP
PDM Group	Widnes, Cheshire	PDM Group	Food residues	9.5 MW_e
Slough Heat and Power	Slough, Berks	SSE	Wood+Fibre	35 MW_e+12 MW_e
Stevens Croft	Lockerbie, Scotland	E.ON	Wood	44 MW_e
Thetford	Thetford, Norfolk	EPRL	Chicken litter	38.5 MW_e
Tilbury B	Tilbury, Essex	RWE	Wood pellets	750 MW_e
Tyrone	Strabane, NI	Tyrone Energy	Recycled wood	2.1 MW_e
UPM Caledonian	Irvine, Scotland	UPM	Papermill residues	26 MW_e
UPM Shotton	Shotton, Wales	UPM	Papermill sludge	20 MW_e
West Field	Fife, Scotland	EPRL	Chicken litter	9.8 MW_e
Western Wood Energy	Port Talbot, Wales	Eco2	Wood	14 MW_e
Wilton 10	Middlesborough	Sembcorp	Wood	30 MW_e
Total				**1090.2 MW_e**
		In Planning		
Project	**Location**	**Company**	**Fuel**	**Output**
Avonmouth	Avonmouth	Helius	Pellets	100 MW_e
Billingham	Teesside	Gaia Power	Recycled wood	45 MW_e
Blackburn Meadows	Sheffield	E.ON	Wood	25 MW_e
Brigg	North Lincolnshire	Eco2	Straw	40 MW_e
Castle Cary	Castle Cary	Bronzeoak	Wood	12.7 MW_e
Drax	Yorkshire	Drax	Pellets	2000 MW_e
Dundee	Dundee	Forth Energy	Wood	100 MW_e
Enfield Biomass	London	Kedco	Wood	12 MW_e CHP
Ferrybridge	Nr. Castleford	SSE	Multifuel, RDF	68 MW_e
Grangemouth	Grangemouth	Forth Energy	Wood	100 MW_e
Hollyhead	Hollyhead	Anglesey Aluminium	Wood	300 MW_e
Ironbridge	Ironbridge	E.ON	Pellets	1000 MW_e
Rosyth	Rosyth	Forth Energy	Wood	100 MW_e
Mendlesham	Mendlesham, Suffolk	Eco2	Straw	40 MW_e
Nevis Power	Newport	Welsh Power	Biomass	50 MW_e
Pollington	Pollington	Dalkin Bioenergy		52 MW_e
Portbury Docks	Bristol	E.ON	Wood	150 MW_e
Rosyth	Rosyth	Forth Energy	Wood	120 MW_e
Rothes Distiller CoRD	Rothes Moray	Helius	DDG	7.2 MW_e CHP
Sleaford	Lincolnshire	Eco2	Straw	40 MW_e
Stallingborough	Stallingborough Lines	Helius/RWE npower	Wood	65 MW_e
Tansterne	Hull	GB Bio	Straw	12.5 MW_e
Tees Rep Tesco	Middlesborough	MGT Power	Wood	300 MW_e
Tibury Biomass	Tilbury	RWE npower	Pellets	870 MW_e
Tilbury Green Power	Tilbury	Express Energy	Biomass & SRF	60 MW_e
Markinch CHP	Fife	RWE npower	Wood residues	49.9 MW_e CHP
Tyne REP	Tyneside	MGT Power	Imported wood	295 MW_e
Wetwang	Yorkshire	E yortks Power	Wood & Straw	15 MW_e
Total				**5319.3 MW_e**
		Proposed		
Project	**Location**	**Company**	**Fuel**	**Output**
Blyth	Blyth	RE Systems	Wood	100 MW_e
Claycross	Derbyshire	Kedco	Wood	12 MW_e CHP
Drakelow	Drakelow	E.ON	Wood	
Greenpower 54	Wolverhampton	Express Energy	Biomass & SRF	30 MW_e
Hull	Hull	Dong		300 MW_e

Peterborough	Peterborough	Peterborough RE	Agricultural waste	66 MW_e
Southampton	Southampton	Helius	Pellets	100 MW_e
Thetford Wood	Thetford	EPRL	Wood	40 MW_e
Total				**648 MW_e**

1.6 Objectives of the present study

The objective of the present study includes

- Feasibility and statistical analysis of Pakistani crop residues as a source of energy for the rural development and the challenges for their effective utilization.
- Study of kinetic models for the volatiles release rate at low heating Thermogravimetric analysis.
- Determination of the minimum explosible concentration (MEC) of the agricultural waste residues and other biomass dusts as a function of particle size distribution using the modified Hartmann tube.
- Calibration of the modified Hartmann tube for the optimum ignition delay for explosibility measurements representative to fully dispersed concentration.
- Determination of the explosibility parameters like MEC, maximum explosion pressure, flame speed, burning velocity and K_{st} for different Pakistani and other biomass dusts using the modified ISO $1m^3$ vessel.
- Testing and comparison of explosiblity hazards of fine and coarse particle sized mixture
- For all selected powders, comprehensive analysis of raw and post explosion residues including proximate and ultimate analyses, particle size distribution, calorific value measurement, Scanning Electron Microscope for surface morphology. true density, porosity and surface area analysis to understand the flame propagation mechanism.
- Model for the propagation of flame in fine and coarse sized range fractions

1.7 Thesis structure

This research work focussed on the use of biomass specially the crop residues with no significant use with their flame and explosibility characteristics for their safe exploitations.

In the first chapter, the adverse environmental impacts of the fossil fuels and the role of renewable energy particularly the biofuels for the generation of clean

energy is explained. The possible challenges for the effective utilization of biomass mixtures are also mentioned.

Second chapter is particularly related to Pakistan, for the feasibility and statistical analysis of the crop residue waste as feedstock, in the power generation.

Third chapter is related to the hazards involved in the handling, processing and flame propagation of pulverised biomass mixture (dust). Different parameters, affecting the flame propagation rate and explosibility characteristics, are listed and explained based on the findings in the literature.

The fourth chapter includes the description of the analytical techniques and experimental method for the testing of pulverised biomass flame propagation. It incorporates the modifications to the existing methods for their refinement and testing of fibrous and coarse biomass mixtures.

Fifth chapter is related to the kinetic study of the volatile release rate of biomass in comparison to the coals. It also includes the chemical characterisation of the selected biomass samples for this research work.

Chapters 6 and 7 include the experimental results from the modified Hartmann tube and modified $1m^3$ vessel for selected biomass samples (crop residues, woods and thermally treated woods) for different size fractions. Different explosibility characteristics results are listed and compared with coal in combination with the effect of particle size.

Chapter 8 is the conclusions based on this research work and the future plan is listed to expand it further.

Chapter 2 ENERGY REPORT ON PAKISTAN

Pakistan has a major electricity supply problem with urban areas having a very intermittent supply of electricity. The supply gap at periods of high demand is 6 GW. Pakistan has a large agricultural economic sector and produces a substantial amount of waste material that has little current economic use. This work shows that these agricultural wastes are a significant energy resource that could be used to generate electricity using relatively small biomass generator sets that could take all the waste biomass from the surrounding agricultural area. Pakistan currently imports most of the oil used for electricity generation. The costs of this result in high cost electricity and bio-electricity could be generated competitively in Pakistan. It was estimated, based on a 30% thermal efficiency of electric power generation, that the annual production of crop residues have the potential to generate 76% of the annual electricity requirements of Pakistan. For this to come from agricultural wastes in farmland, transport costs would have to be minimised. It is proposed that a series of about 10MWe plants should be established (which are commercially available) with all farms in about a 10km radius delivering their agricultural solid waste to the plant at the farmers cost with direct payment by the power generator.

2.1 Introduction

The current total population of Pakistan is about 190 million, with an annual growth of 1.9%. It is much larger than any individual European country. Pakistan currently faces a crisis of electrical energy supply with demand outstripping supply and frequent power cuts. Pakistan has over 30% of its 55 million population with no access to electricity [26]. The summer monsoon season has a peak electricity demand [27], due to the extensive use of air conditioning.

People in urban areas are facing 6-12 hours load-shedding whereas in the rural areas, it is worse. According to official statistics there is no electricity shortage, as the total production potential of energy in Pakistan was 94.65 billion KWh in 2014 utilizing all the available sources, whereas the energy consumption was 70.1 billion KWh [28]. However, this electricity consumption is the amount paid for and is not the real amount of electricity used. In reality at times of peak demand there is insufficient supply of electricity.

The trend in supply and demand for electricity in Pakistan is shown in Figure

2.1 for 2008 – 2015 [29]. Every year in there was an electricity delivery shortfall and this has got worse in recent years. The production of electricity has increased each year since 2008 but the demand is increasing faster [29]. The shortfall of electricity was 6 GW in 2012 and ranged from 4 to 6 GW between 2008 and 2015. The main reason for this shortfall in electricity is the line losses and electricity theft. Also 45% of the total electricity generated is wasted as revealed by the water and power ministry [29]. Figure 2.2 is an example of the electricity theft in Pakistan, where there is no control of connections to the grid distribution. The new Government of Pakistan has taken actions against this and a task force is dealing to tackle this.

Pakistan has reduced its demand for imported oil for transportation by utilizing compressed natural gas as fuel for road transport vehicles [30]. Pakistan generation of electricity is currently dominated by hydro, oil and natural gas [31]. The electricity supply shortfall is worst in winter when hydro plants start losing capacity due to the freezing temperature of hydro reservoirs. This leads to a demand for more electricity from gas plants to balance the gap between supply and demand. In summer, the high consumption of electricity due to the use of air conditioners in the hot humid climate, compels the government to import large amounts of furnace oil for the diesel electric power generation. This cost is not affordable for the Government and the import cost of the furnace oil destabilizes the economy. Industrial investors are not willing to invest in factories in Pakistan as the electric power supply cannot be guaranteed. About 60 to 70% of the local textile industry has shifted to China, Bangladesh and India [32].

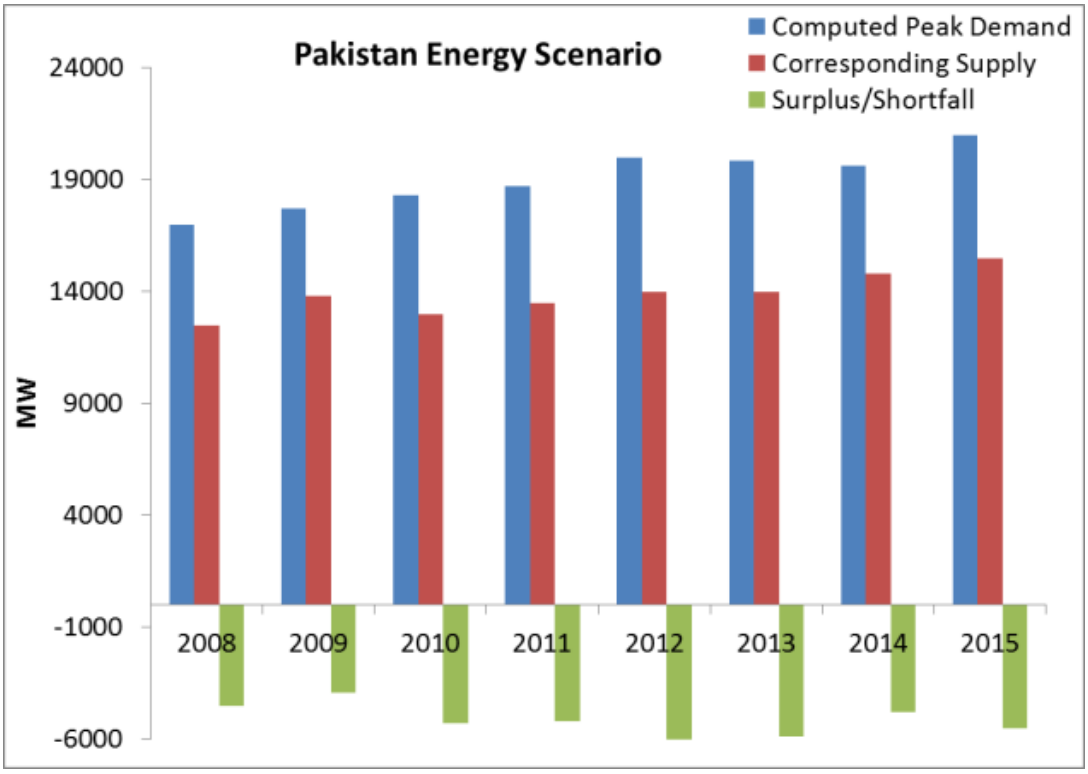

Figure 2.1: Pakistan yearly energy scenario [29, 33]

Figure 2.2: An example of distribution losses due to electricity theft in Pakistan

2.2 GHG emissions from electricity generation

2.2.1 Fossil fuels

The major source of greenhouse gases in Pakistan is from the combustion of fossil fuels in electricity generation power plants and road vehicles, 151.6 MMT in 2010 [34]. The major component of GHG's was carbon dioxide [35]. Figure 2.3 shows the fuel sources of electric power in Pakistan in 2011. Expensive fuel oil accounts for 35% of electricity generation [33]. The other major fuels are gas, hydro and nuclear. There is currently no use of biomass to generate electricity and negligible use of coal. During 2011-2012, 19.2 million metric tons of petroleum products of worth US $15.2 billion were imported, 40 % of which was used for the generation of electricity [36]. Little attention has been given to the renewable electricity options, including the use of biomass. As the limited fossil fuels reserves start to be depleted [37] and no new reserves of fossil fuels have been discovered, the Government of Pakistan is now showing an interest in the renewable energy options and especially bio based energy options.

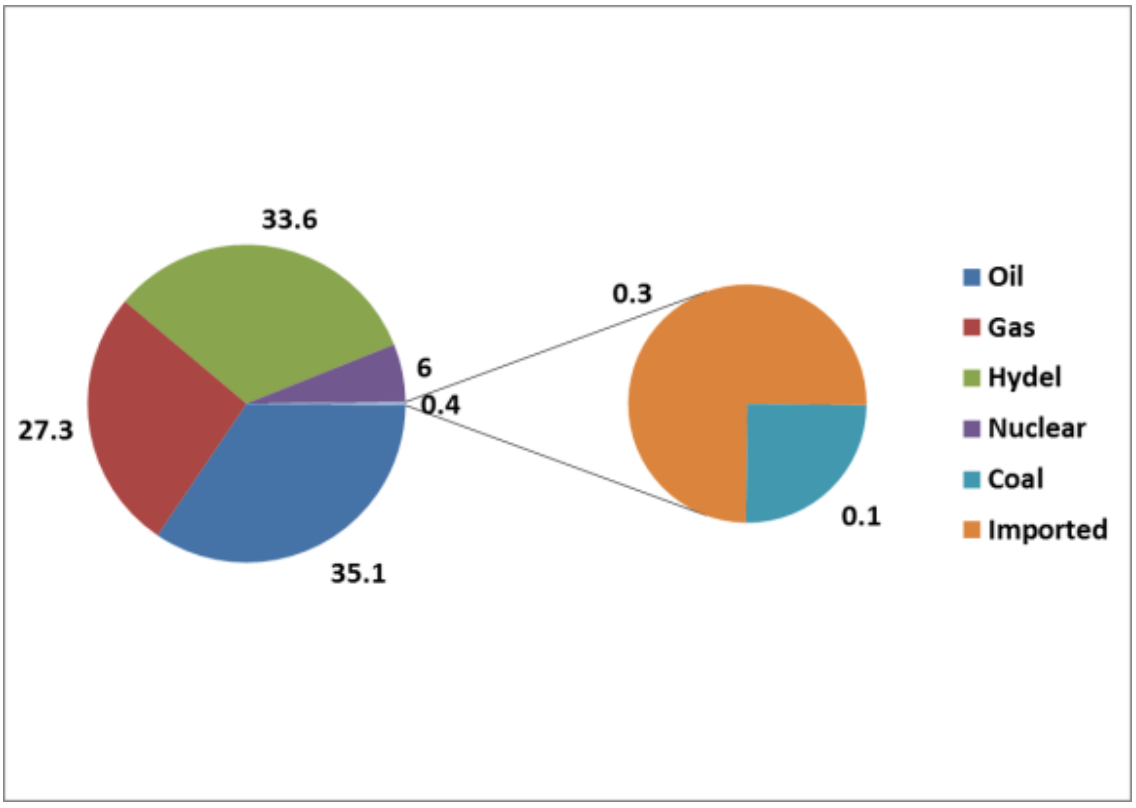

Figure 2.3: Fuel sources of electricity generation in Pakistan in 2011 [31]

2.2.2 Renewable energy in Pakistan

The current status of fossil fuel in Pakistan is shown in Table 2.I. More than half of the proven reserves have been consumed. The limited reserves of oil and natural gas force Pakistan to seriously consider renewable sources of energy. Farooq and Kumar [38] assessed the potential of renewable source of energy for Pakistan. They studied the current and the future potential of solar, wind, small hydro and biomass. The statistics of each renewable source was estimated and calculations for generation of electricity generation potential were carried out. The total technical potential of solar based electricity was estimated to be 358 TWh in 2010 with a projected potential of 708 TWh for 2050. Clearly Solar is a renewable energy source that should be developed in Pakistan, but there is currently no infrastructure to install solar panels and no government subsidy to do so. Wind energy potential is mainly in the southern coastal areas of Pakistan and Farooq and Kumar [38] estimated the potential wind electrical power generation to be 34 TWh per year. The total potential of small hydroelectricity was identified to be 3 GW.

Table 2.1: Fossil fuels reserves statistics in Pakistan

	Oil	**Natural Gas**	**Coal**
	Million Tonnes of Oil Equivalent 'MTOE'		
Resource potential	3622	6849	78450
Proven recoverable reserves	130	1067	845
Cumulative production so far	88	568	89
Remaining recoverable reserves	41	499	797
Annual Production	3.3	29.3	1.6
Reserve to Production ratio (# of years)	12	17	528

Farooq and Kumar [38] estimated the total potential of bio based electricity generation to be 20.3 TWh for 2010 and the projected potential for 2050 was 55.6 TWh. They used an assumed thermal efficiency of the biomass electricity plants to be 30%, which is conservative but realistic for small scale plant. A 30% thermal efficiency of small scale biomass steam generation electricity generating plant has also been assumed in the present work. However, it is shown in the present work that Farooq and Kumar [38] underestimated the current potential of biomass electricity in Pakistan. Biomass energy was rated by Farooq and Kumar [38] at the top of the list of the various renewable energy technologies for the generation of electricity.

If all of these renewable fuels were utilized then the current reliance on fossil fuels could be minimized [38]. The Government of Pakistan has taken steps towards liquid biofuel utilization in transport fuels by approved a policy to have the minimum 5% by volume of biodiesel in diesel and targeted this to increase to 10% in 2025 [39]. This is essentially the European policy with the implementation date for 10% biofuels five years later than Europe. However, there is currently no policy on the encouragement of biomass for electric power generation.

Among the various renewable energy sources, bio based energy is attractive for Pakistan, as substantial agricultural biomass residues are generated each year and their disposal is already a problem [40, 41]. The size of these residues is estimated in the present work based on the published yields of food crops. Renewable biomass is a very important alternative source of energy contributing 10-14 % of the energy needs of world today [42]. Pakistan is a major agricultural country with multiple crops produced every year as a result of its favorable climate. More than 70% of the population of Pakistan live in rural areas and are farmers [43]. Urban areas of Pakistan generate ~20 MT/yr of solid wastes, ~82.12 MT/yr of crop residue and over 365 MT/yr of animal manure [44].

Agriculture is the mainstay of Pakistan’s economy. It accounts for 24% of the GDP and employs 48.4% of the total labour force. Agriculture contributes to growth as a supplier of raw materials to industry as well as a market for industrial products and also contributes 60% to Pakistan’s export earnings [45].

Pakistan is in a geographic location that has all the climates. The cool dry winter season is from December to February and from March to May, there is a warm spring, then from mid-May to November is summer and the monsoon season [27]. There are two principal crop seasons in Pakistan namely “Kharif”, with sowing beginning in April and harvest between October and December and “Rabi” beginning in October-December and ending in April-May. Rice, sugar cane, cotton, maize and millet are Kharif crops, while wheat, gram, tobacco, rapeseed, barley and mustard are Rabi crops.

2.3 Previous estimates of biomass energy potential in Pakistan

Amur and Bhattacharya [46] estimated biomass and their residues for various applications in Pakistan. The major application of biomass is in the household sector which is 86% of total biomass energy. The traditional cooking stoves employed in rural areas of Pakistan are currently the major end users of biomass energy and utilizes 80% of current bioenergy. About 64% of the population in Pakistan is utilizing biomass for cooking [26]. In proposing an increased use of agricultural waste biomass for electric power generation in this work, we are referring to agricultural wastes that are not currently used for domestic cooking.

Mirza et al. [47] surveyed the potential of biomass to contribute to Pakistan’s energy needs and concluded that biomass was a potential source of significant energy in Pakistan. They advocated that biomass based energy could be made more efficient using advanced co-generation (power and heat) technology. However, as Pakistan has a negligible building heating requirement and a significant building cooling requirement, the advocacy of CHP is inappropriate as it needs a heating load greater than the electric power demand in order to achieve the best overall thermal efficiencies of around 80%.

Mirza et al. [47] advocated that municipal solid waste and nutrients could be utilized in electric power generation. The use of municipal waste for power generation is established technology, but needs capital investment to build the plants and reduce waste going to landfill. However, animal dung is a dispersed source of fuel and needs collecting by farmers. The transport cost to distance large power generation plants is not realistic and hence it has the same issues as the utilization of agricultural wastes that are discussed in this work. Plants that can burn agricultural waste biomass can also burn dried animal dung. It will

be shown in this work that agricultural waste biomass and waste wood biomass in Pakistan are a much greater resource than those discussed by Mirza et al. [47].

Bhutto et al. [48] demonstrated biomass as a major renewable source of energy, with some issues in implementing, as it has a lower calorific value with slow burning compared to coal or hydrocarbon fuels. They presented biomass statistics and the scope of contribution to energy output. The possible transportation means for the biomass were elaborated. The potential energy conversion of these biomasses was estimated using assumed electric power conversion efficiencies, depending on the type of biomass and the route/technology used.

The existing and future projects of the generation of biogas from the animal dung were discussed by Bhutto et al. [48]. Although biogas can be generated by anaerobic digestion from animal waste, it is a very high capital cost intensive solution to the energy crisis. Current costs are approximately £5B per GW of generating capacity, roughly the same as offshore wind generation costs. Also the process costs more for small scale of the plant and for a 100 cow farm is about £100K for 10 kW electric, which is roughly 10 times the current cost of solar electric energy. Advocating expensive solutions to the Pakistan energy problem is not helpful. The direct burning of biomass to generate steam and then electricity in small scale power plants, which is advocated in the present work is considered to be a lower cost option, that would nevertheless require Government funding to make the local generation of electricity strategy, that is advocated, work in a large number of areas.

Currently there is little industrial application of biomass. The purpose of this work is to demonstrate that the potential for biomass electricity in Pakistan is greater than has been estimated in previous publications. It is advocated that biomass generation of electricity should be adopted as a major part of the Government of Pakistan’s renewable energy policy.

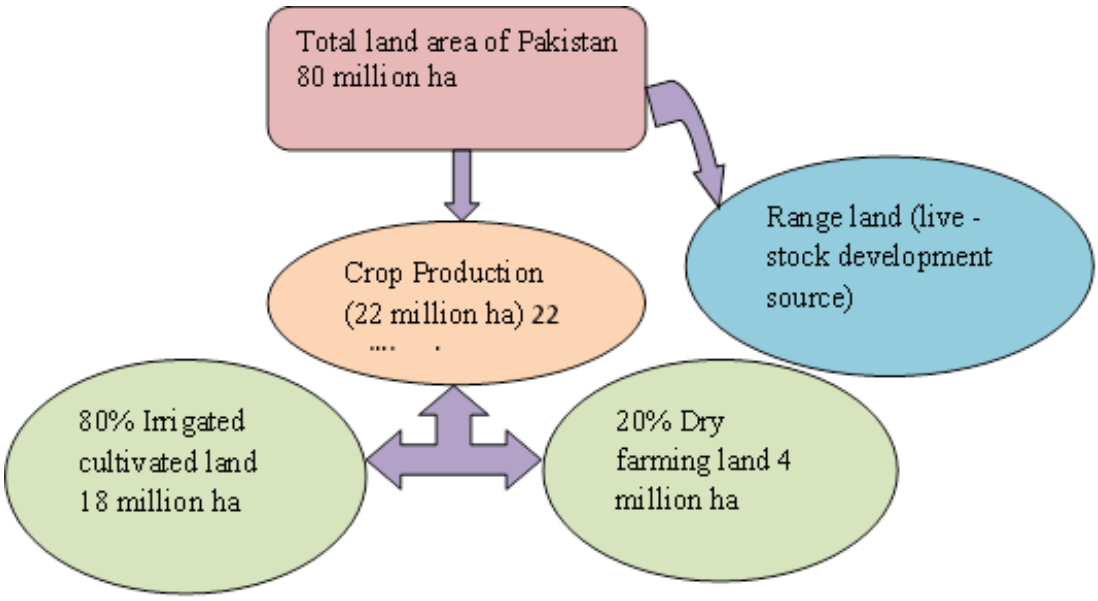

Figure 2.4: Pakistan land distribution [49]

2.4 Biomass energy resources in Pakistan

2.4.1 Distribution and share of biomass materials

Figure 2.4 shows the major uses of the 80M ha of land in Pakistan [49]. 44M ha is identified agricultural land, but there is a large proportion (>40%) of range land, which has potential for an expansion of this sector, particularly as grazing land.

Figure 2.5 classifies the proportion of different crops in Pakistan [50]. Five major crops: wheat, cotton, sugar cane, rice and maize account for about 87% of fertilizer consumption [49]. Wheat accounts for about 45% of fertilizer use followed by cotton with a share of 23%. Sugar cane is the third crop; nutrient use per ha is highest for this crop.

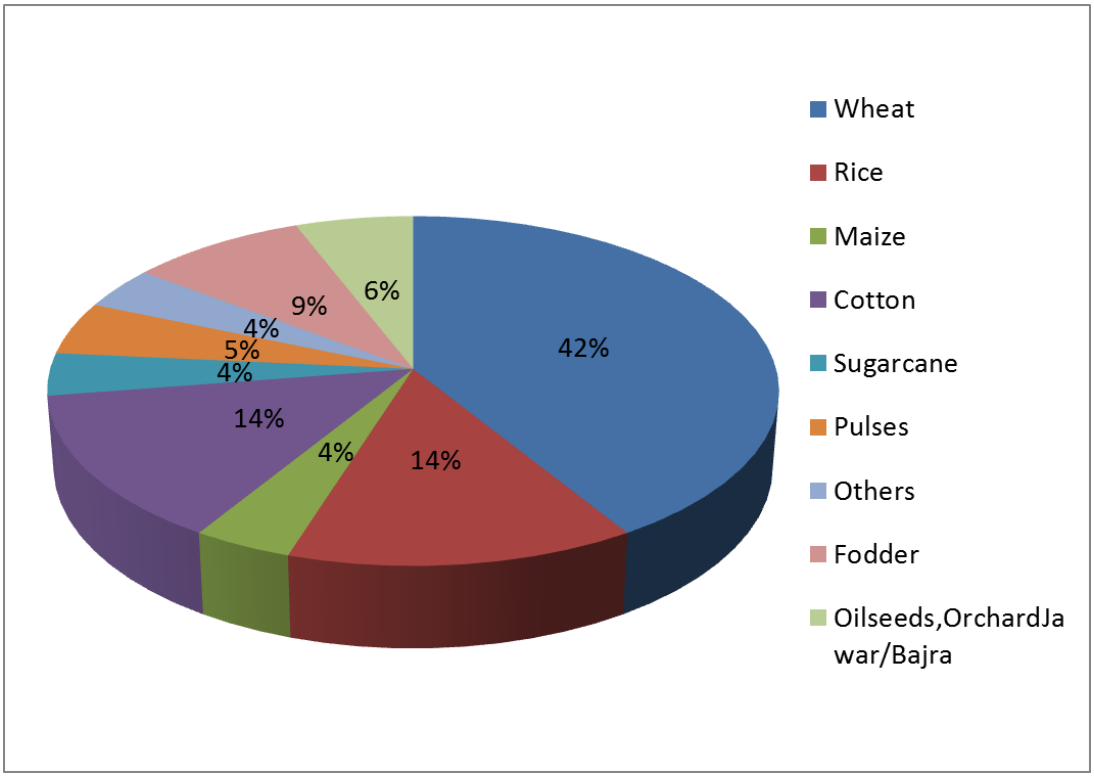

Figure 2.5: Percentage of crop area under various crops [50]

Table 2.2: Summary of Agricultural Waste Resources in Pakistan (Updated from [48, 51])

Name of the crop	Annual production 1000 MT*	Type of residue	Crop to residue ratio residue/kg crop	Total residue 1000 MT	Energy Potential MTOE**
Rice	6160[1]	Husks	0.2[(3)]	1232	0.529
		Stalks	1.5[(3)]	9241	3.973
		Straw	1.5[(3)]	9241	3.973
Cotton lint and cotton seed	6605[1]	Boll shell	1.1[(3)]	7266	3.124
		Husk	1.1[(3)]	7266	3.124
		Stalks	3.8[(3)]	25100	10.791
Wheat	25,214[1]	Pod	0.3[(3)]	7564	3.252
		Stalks	1.5[(3)]	37820	16.260
Sugar cane	55,309[1]	Bagasse	0.33[(3)]	18252	7.847
		Top and leaves	0.05[(3)]	2766	1.189
Maize/Corn	4270.9[1]	Cobs	0.3[(3)]	1281	0.551
		Stalks	2[(3)]	8542	3.672
Millet	304[1]	Cobs	0.33[(3)]	100	0.043
		Husks	0.3[(3)]	91	0.039
		Stalks	2[(3)]	607	0.261
Barley	71.2[1]	Stalks	1.3[(3)]	93	0.040
Dry chilly	203[1]	Stalks	1.5[(3)]	304	0.131
Walnuts	10.4[1]	Shells	0.5[(E)]	5.2	0.002
Pistachio nuts	0.7[1]	Shells	0.5[(E)]	0.4	0.0002
Pine nuts	21[2]	Cone	50[(4)]	1050	0.451
		Shells	0.3[(E)]	6.3	0.003
Peanuts	87.9[1]	Shells	0.3[(E)]	26.4	0.011
Coconut	10.1[1]	Shells	0.5[(E)]	5.1	0.002
Castor oil seed	4[1]	Residue after oil extraction	0.55[(E)]	2.2	0.001
Peaches and nectarines	54.4[1]	Pit	0.5[(E)]	27.2	0.012
Papayas	7.8[1]	Seeds	0.2[(E)]	1.6	0.001
Plums and sloes	54.5[1]	Pit	0.3[(E)]	16.4	0.007
Rape seed	195[1]	Residue after oil extraction	0.5[(E)]	97.4	0.042
Sun flower seed	404[1]	Residue after oil extraction	0.5[(E)]	202.2	0.087
Total					59.42
Biomass energy conversion efficiencies[(5)]					20%
Transmission and distribution losses[(6)]					20%
Total energy available					9.51
Energy consumption per year [(6)]					6.37
Total energy available from a year collection of residues = 1.5 years					

(1) [52], (2) [53], (3)[51], (4)[54], (5)[12]
(6) [28], (E) Estimated this work
* Annual production data for the year 2012- except for pine nut shells where 1994 data is used
** 1 MTOE = 11.6 TWh [55]

2.5 Yearly growth of crops and the electricity generation potential

2.5.1 Agricultural waste crop residues potential for electricity generation

The statistics for growth of biomass can be explained on the basis of three main terms: the area available, the production and the crop yield [56]. Crop area is the surface of land on which a crop is grown. In general, the area measured for cadastral purposes includes, in addition to the area cultivated, headlands, ditches and other non-cultivated areas may give additional crop growing areas. Crop production is obtained by multiplying the average yield per unit of area by the corresponding crop area harvested.

Crop yield is the measurement of the amount of a crop that was harvested per unit of land area. This measurement is often used for a cereal, grain or legume and is normally measured in metric tons per hectare (or kilograms per hectare). Crop yield can also refer to the actual seed generation from the plant. For example, a grain of wheat yielding three new grains of wheat would have a crop yield of 1:3. It is also referred to as "agricultural output".

The production of most of the crops in Pakistan with their respective residues and their energy potential is summarised in Table 2.2, which is based on the present work and previous estimates [24, 38]. Energy potential is calculated assuming heat capacity of 18MJ/kg for all the biomass and assuming a very poor thermal efficiency of the power generation plant of 20%. It can be seen in Table 2.2 that if Pakistan collects all the residues for a year, these are alone sufficient to fulfil the requirements for energy production for up to 1.5 years (this calculation assumes 100% collection efficiency).

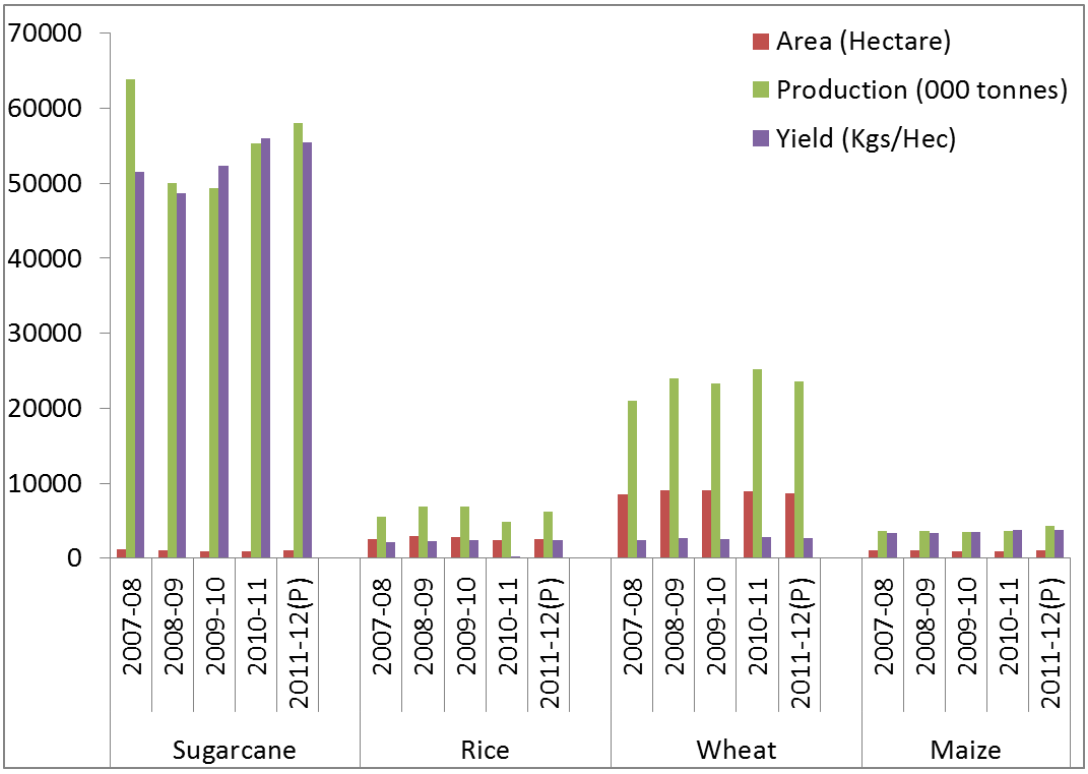

Figure 2.6: Production trends of major crops in Pakistan [57]

Table 2.2 shows that the most import agricultural waste crops in Pakistan for power generation are rice, cotton, wheat, sugar cane and maize. However, the other smaller amounts such as nut shells are significant as the process of collection of this biomass is already organised for the production of nuts. Thus the nut shells are all in one place and could be used for power generation there. Nut shells pulverise in a sumilar way to coal as they are brittle and Sattar et al. [18] has shown that they are quite reactive and will propagate flames.

Tables 2.3 shows that four of the main crops which are abundantly grown in Pakistan are sugarcane, wheat, rice and maize [28, 57]. Figure 2.6 shows the trends in production of these four main crops in Pakistan from 2007 to 2012. The residues obtained from these major crops are enormous, as shown in Tables 2.2 and 2.3, but are currently wasted. Utilization of these residues for biomass energy is a valuable potential source of renewable electricity.

Figure 2.6 shows that sugarcane is a major crop in Pakistan and has the greatest yield per hectare. During 2010-11, the area under sugarcane cultivation was 1,029,000 hectares which is 4% of the total cropped area. Sugar cane waste, which constitutes 10% of the sugarcane, is currently burnt in the fields.

During 2010-11, around 64 MMT of sugarcane was grown in Pakistan, which resulted in biomass waste generation of around 6 MMT. The bioenergy potential of cane waste is around 9.5 TWh per year [58].

For each 10 tonnes of sugarcane crushed, a sugar factory produces nearly 3 tonnes of wet bagasse [20]. Since bagasse is a by-product of the cane sugar industry, the quantity of production in each country is in line with the quantity of sugarcane produced [59]. There are more than 70 sugar producing factories in Pakistan that are generating million of tonnes of bagasse and should be the basis of electric power generation from this waste [60]. Utilization of bagasse in cogeneration could enable sugar mills to provide 700 MW surplus power to the national grid [61]. The potential annual electricity production from bagasse has been estimated to be 5700 GWh [62].

Table 2.3 shows different biomass crop residues production for Pakistan in the year 2010-2011 that were calculated from the production mass of the food part of the crops [57] and using crop to residue ratios [48]. The residues of biomass were conservatively assumed to be collected with a 35% collection efficiency [38]. Table 2.3 shows that the total energy that could be produced from these four biomass samples in Pakistan with 30% electrical generator efficiency was 40 TWh/y and this is 56% of the demand for electricity in Pakistan.

Similarly calculations performed by my research fellow ‘Aysha’ showed that unused woody biomass, oilseed crop residue and banana tree wastes have the potential to generate 9.5%, 2.4% and 8.2% respectively of the annual electricity demand in Pakistan.

Table 2.3 : Yearly Energy yield from four major crop residues

Major Crops	Crops Production ($x10^3$) 'tonnes'	Crop wastes	Residue to Crop ratio	Residue Production ($x10^3$) 'tonnes'	Collection ($x10^3$) 'tonnes'	Calorific Value 'MJ/Kg'	Heat Contents ($x10^6$) 'GJ'
Rice	4823.3	Husks	0.2	964.7	337.63	15.16	5.12
		Stalks	1.5	7234.95	2532.23	10.05	25.4
		Straw	1.5	7234.95	2532.23	10.05	25.4
Wheat	25213.8	Pod	0.3	7564.14	2647.45	14.49	38.4
		Stalks	1.5	37820.7	13237.2	16.5	218.4
Sugar-cane	55308.5	Bagasse	0.33	18251.8	6388.13	15.63	99.8
		Top and Leaves	0.05	2765.4	967.9	18.4	17.8
Maize/Corn	3706.9	Cobs	0.3	1112.0	389.22	16.12	6.3
		Stalks	2	7413.8	2594.83	14.65	38
Total heat contents of the four major biomass residues 'GJ/y'							$4.7x10^8$
Total energy obtained TWh/y							1300
With 30% Efficiency TWh/y							40
Total average requirement in Pakistan in 2014 TWh/y [28]							70
Almost 56% of the annual demand for electricity can be met by the utilisation of agricultural waste in Pakistan for an electrical generator steam turbine thermal efficiency of 30%.							

2.6 Comparison of energy estimates of bioenergy electricity potential in Pakistan

A comparison of the energy estimates for different renewable feedstocks were presented in table 2.4. It was observed that solar renewable sources have the greater potential for the generation of electricity. Different biomass resources also have the potential to contribute a major share for electricity

requirement in Pakistan. Farooq and Kumar (2013) estimated a low electricity potential from biofuel resources for 2010 and therefore projected inappropriate for 2050. However the actual potential of these biofuels for electricity generation was much greater as in this work, only four major crops were considered for the utilization of their unused residues with electricity potential of 40 TW h. After including with the wood, oilseed and banana waste, then the total electricity potential was estimated to be around 54.2 TWh which has a share of 76% of annual Pakistan electricity requirement for 2014.

2.7 Cost comparison

Among the different renewable energy technologies, biomass conversion to energy is one of the most economical and simple technology. The size of the plant for the biomass conversion to energy can be built in the 1-20 MW capacity range or higher [44]. The use of smaller plant sizes is advocated so that they can be located where the waste biomass resources are. This enables the transport costs to be minimized.

Figure 2.7 shows the comparison of the cost of renewable energy options for various regional areas in the world [63]. The large colored bars represent the typical LCOE (Levelized Cost of Energy) range by technology and the colored horizontal lines the weighted average. Biomass renewable energy is lower capital cost than wind energy and considerably lower than diesel electric power generation. Biomass energy thus has significant potential in Pakistan.

Table 2.4: Previous estimates in comparison to current calculations for bioenergy

Authors	Year Published	Feedstock	Electric TWh Estimated	Projected Electric TWh	Electrical efficiency
Farooq and Kumar [38]	2013	Solar (PV+ thermal)	358 (2010)	708 (2050)	
		Wind energy	34 (2010)	-	
		Field crop residues	9.93 (2010)	21 (2050)	30%
		Animal waste	9.2 (2010)	23.57 (2050)	30%
		MSW	1.13 (2010)	11 (2050)	
Memon [64]	2006	Crop residues	35.5 (2005)	51.5 (2030)	30%
Amur & Bhattacharya [46]	1999	Major crop residues	88 (293.5 thermal) (1994)	142.1 (473.7 thermal) (2010)	30%
		Woody fuels	27.8 (92.56 thermal) (1994)	26 electric (86.82 thermal) (2010)	
Awam & Rashid [62]	2012	Biogas from livestock residues	55 – 106 Biogas		
		Biogas from fibrous residues	5.7		
This work	**2014 data**	**Residues of four major crops**	**40 (54.2 considering residues+wood+oilseed+ banana waste)**		**30%**

2.8 Local electric power generation in small units

Figure 2.8 shows the overview of the envisaged small scale biomass power generation based in the locality in which the agricultural waste materials are generated so that the transportation costs are minimised. A radius of 10 km around a small power plant would have sufficient waste biomass material to operate a 10 MW power plant.

The summation of the above four main agricultural waste materials in combination with woody biomass could generate a total of 76 % of Pakistan's electricity supply. The peak electricity demand is 20 GW and about 15GW could be generated from biomass. If 10 MW small scale biomass electric power plants are installed then to meet the 15GW peak demand 1500 units would be required. The total farmed land area in Pakistan is 240,000 km^2 and all the waste biomass is assumed to come from this area. This would give a farmed area of 160 km^2 to supply the biomass for each 10 MW power plant. This is a square around the power plant of 13 km and would give a journey length of almost 7km for the most distant farmer. This is a practical distance for animal driven carts to transport the biomass to the plant and hence is feasible from a low cost transport viewpoint.

Pakistan has already made a start on a biomass electric generation strategy and Tables 2.5 and 2.6 list the biomass power plants which are being built (Table 2.5) and co-firing (Table 2.6) for the generation of the electricity [65]. Most of these power plants are establishing by the private investors or the industrial stakeholders. Three of the biomass plants are of the above size of about 10 MW for the biomass feedstock to come from farm agricultural waste in easy animal powered transport distance of the plant. Other power plants are larger and being built to supply power to the industry that has generated the biomass waste.

As Pakistan has substantial coal reserves, and if these are exploited and coal fired power-plants built then these can be used for co-firing with waste biomass. Some of the cogeneration projects using biomass under considerations in Pakistan generating heat and power simultaneously are presented in Table 2.6 [66].

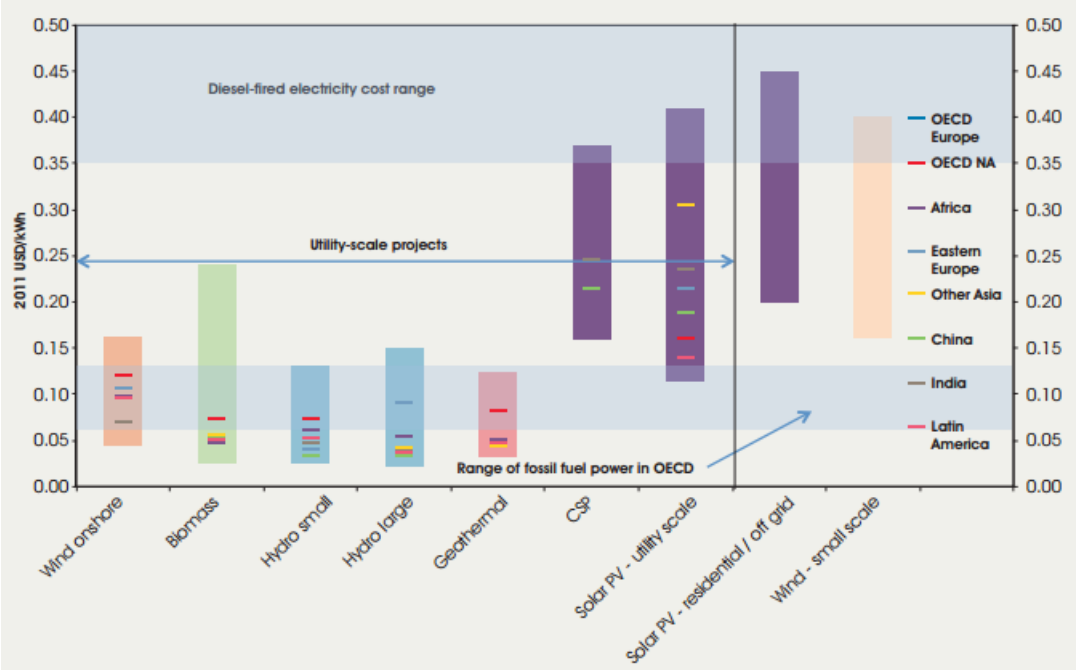

Figure 2.7: Cost comparisons of different energy options [63]

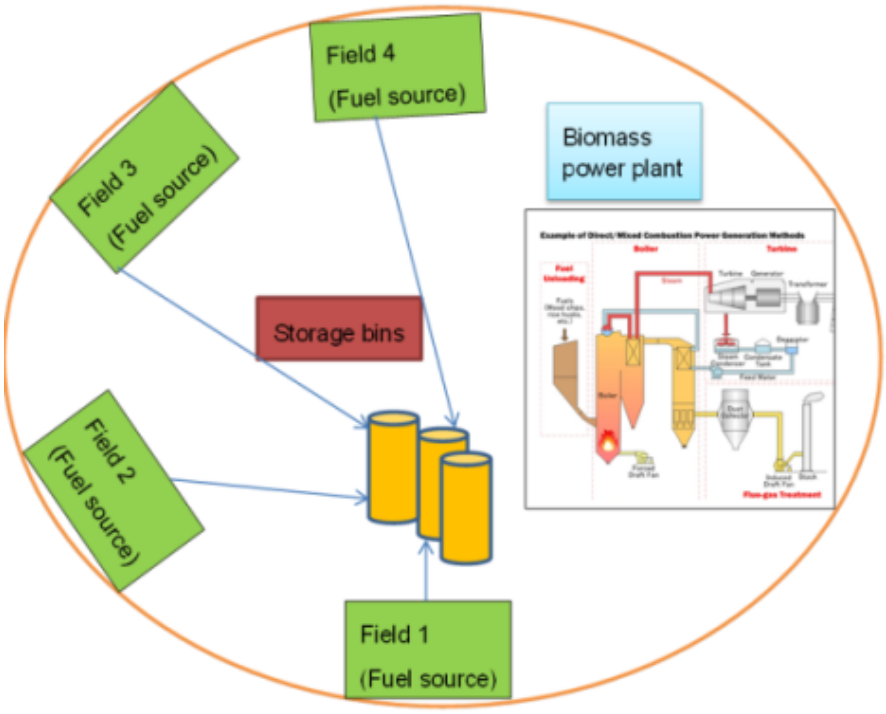

Figure 2.8: Imaginary layout of small plant in the vicinity of agricultural land

Table 2.5: Biomass Poer plants in Pakistan in progress [65]

Location of Plant	**Power generation**	**Size of Plant (fuels utilization) 'tonnes' (x10^3)**	**Agricultural crops**	**Sponsorship & Cost in $**	**Biomass supply source**
Jhang, Punjab	12 MW (Steam turbine)	90-110 at 70-80% plant capacity factor in a year	Cotton stalk, rice husk, sugarcane trash, bagasse, wheat chaff and other crops as multi-fuel sources	Lumen Energia Pvt Ltd U.S $ 14.38 Million on debt / equity ratio of 80:20	Rice & Sugar factories in the vicinity
Mirwah Gorchani Town, Mirpurkhas, Sindh.	12 MW (Steam turbine)	**Open yard storage**:24.5 (equivalent to 45days full load operation), **Covered storage**: 2.2(Equivalent to 4 days full load operation)	Primary fuels: Bagasse, Rice husk Secondary fuels: Cotton Stalks, Wood Chips	Investors from US and local entrepreneurs the SSJD Bioenergy Generation	Al-Abbass sugar Mills Ltd, Tharparkar Sugar Mills Ltd,Digri Sugar Mills Ltd, Najma (Thar) Sugar Mills Ltd,Mirpurkhas Sugar Mills Ltd
Faisalabad, Punjab	12 MW	-------	rice husk, corn cob, cotton sticks, agricultural by-products	M/s Masood Textile Mills	-------
Mardan, Khyber Pakhtunkhwa	200 MW	-------	-------	M/s Greensure Environmental Solutions (Pvt) Ltd	TMA, Mardan
Matli, Sindh	9 MW	-------	Biogas (Based on sugar molasses)	Pak Ethanol (Pvt) Ltd	-------

National Electric Power Regulatory Authority 'NEPRA' has taken a landmark decision of supporting bagasse based co-generation projects. In order to attract the sugar mills to generate 3GW of potential biomass electricity through the use of waste bagasse. An IRR (Internal rate of return) of 18% will be given as an incentive which is 3% higher than the IRR allowed to thermal projects on RFO (Residual Fuel Oil)/Gas [33].

Table 2.6: Biomass Co-generation Power plants in Pakistan in progress [66]

Sr. No.	*Project*	*Sponsor/Company Name*	Feedstock	*Location*	*Net Capacity (MW)*
1	JDW Cogeneration Project	JDWP/JSML	Bagasse/Coal	Near Rahim Yar Khan, Punjab	80
2	Ramzan Cogeneration Project	Ramazan Energy/Sharif Group, Ramaz Sugar Mills	Bagasse/Coal	Bhawana, Jhang Road Chiniot, Punjab	100
3	Janpur Cogeneration Project	Janpur Energy/RYK Mills	Bagasse/Coal	Janpur, District Rahim Yar Khan, Punjab	60
4	Fatima Cogeneration Project	Fatima Energy/Fatima Sugar Mills	Bagasse/Coal	Sanawan, Kot Addu, Muzaffargarh, Punjab	100
5	Chishtia Cogeneration Project	CPL/CSML	Bagasse/Coal	Sillanwali - Sahiwal road District Sargodha, Punjab	65
6	Dewan Cogeneration Project	Dewan Energy Ltd	Bagasse/Coal	Dewan City 20 Km from Sujawal on Sujwal-Badin Road, Sindh	120
7	Etihad Cogeneration Project	Etihad Power Generation Ltd	Bagasse/Coal	Karamabad District Rahim Yar Khan Punjab	60

2.9 Conclusions

Pakistan is one of the developing countries which are struggling hard to meet the demand for electric power generation. Pakistan currently relies on fossil fuel sources of energy that are expensive and bad for climate change. Renewable and sustainable biomass was shown to have the potential to generate 76% of the peak demand for electricity in Pakistan. Sugarcane, wheat straw, rice husk and maize are the main agricultural waste materials that could generate 56% of Pakistan's electricity. It was concluded that utilization of these local resources for power generation are the feasible option for agricultural countries like Pakistan as they are cheap and available in enormous amount without any end use.

Chapter 3 REVIEW OF DUST EXPLOSION LITERATURE

This chapter focuses on the description of different explosibility hazards associated with dust particles. The dust explosion and its mechanism are explained in comparison to gas explosion. The fire and explosion hazards associated with dust and a database of dust incidents are listed. Different parameters used to characterize the dust are mentioned and standard equipment adopted to measure the explosibility parameters are explained. The theory of dust flame propagation and different factors affecting its mechanisms are summarized. The discrepancies in the physical properties of biomass are the key reasons to define a unique criterion for biomass. The low bulk density of biomass require higher cost for its transportation. The pelletizing and torrefaction are the pre-treatments applied for the easy handling and storage of biomass for various applications as discussed previously. Findings of the works led by various researchers in the areas of dust explosion are summarized. Different parameters affecting the dust explosion are discussed one by one at the end of the Chapter.

Dust is considered as tiny particles which may settle due to their own weights but remain airborne. According to previous National Fire Protection Association, 2007 (NFPA) statement [67], 'Any finely divided particle of size 420 μm or capable of passing through the U.S. No. 40 Standard sieve is considered to be a dust'. According to NFPA-13 [68], combustible dust is defined as 'A finely divided combustible particulate solid that presents a flash fire hazard or explosion hazard when suspended in air or the process-specific oxidizing medium over a range of concentrations'.

These finely divided particles pose less hazards in settled condition but present a greater explosion hazards when suspended in the form of a cloud accompanied with some oxidizing medium (Figure 3.1). Settled particles undergo slow burning with slow generation of heat whereas there is instantaneous burning of dust cloud called dust explosion with high bulid up of pressure if contained in some confined space.

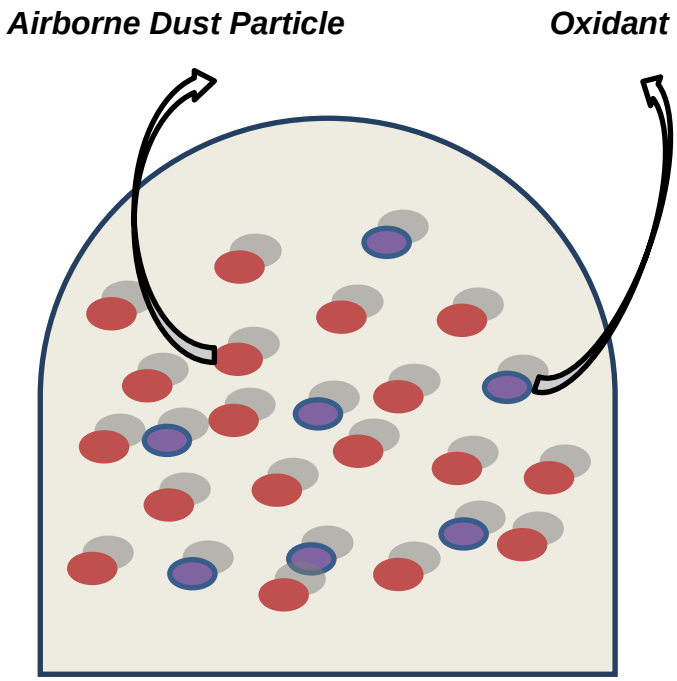

Figure 3.1: Dust air suspension

3.1 Combustion & Explosion

Combustion is the oxidation of the substance releasing heat and combustion products. Explosion is defined as the sudden release of heat with the generation of pressure waves in the confined volume. Explosion is the uncontrolled combustion with the release of destructive pressure waves depending on the combustible fuel and confinement. All the explosible materials must be combustible but all the combustible materials might not necessarily be explosible.

Fire is the visible phenomenon of combustion that follows the principle of the fire triangle comprising of fuel, oxidizing agent (air/oxygen) and ignition source (electrical/chemical) (Figure 3.2(a). The combustion proceeds with the oxidation of fuel releasing heat of combustion and the combustion products. Explosion follows the explosion pentagon (Figure 3.2(b) comprising of;

- fuel (combustible dust)
- oxidizing medium (Air/ Oxygen)
- Ignition source (Electrical/ Chemical)
- dispersion of fuel in oxidizing medium
- confinement to some degree

(a)

- Slow burning
- Slow release of energy
- No/less sound

(b)

- Fast/Flash burning
- Rapid release of energy
- Less/Medium/Loud sound
- Pressure waves in confined space resulting destruction

Figure 3. 2: a) Fire triangle b) Explosion pentagon

3.2 Dust explosion

A dust explosion is defined as the sudden flare up due to the release of pressure waves as a result of chemical reaction of the explosible solid dust particles.

The dispersion of the dust as a cloud or suspension results in the effective interaction of the dust particles with the oxidizing agent that favours the rapid burning of the dust. As shown in Figure 3.3, a 1mm layer of settled dust of concentration 500 kg/m^3 when dispersed forms a cloud of 100 kg/m^3 in a 5 m^3 confined volume. The burning of the particles causes the rapid build-up of pressure in confined space. The expansion of the pressure waves, if restricted with weak confinement results in the destruction. This expansion effect is due to the propagation of the flame with heat release. The explosion strength in the laboratory scale equipments is determined in adiabatic conditions with no heat loss to the surrounding. The flame speed range in the small enclosure varies in order from one metre per second to hundreds of metre per second [69].

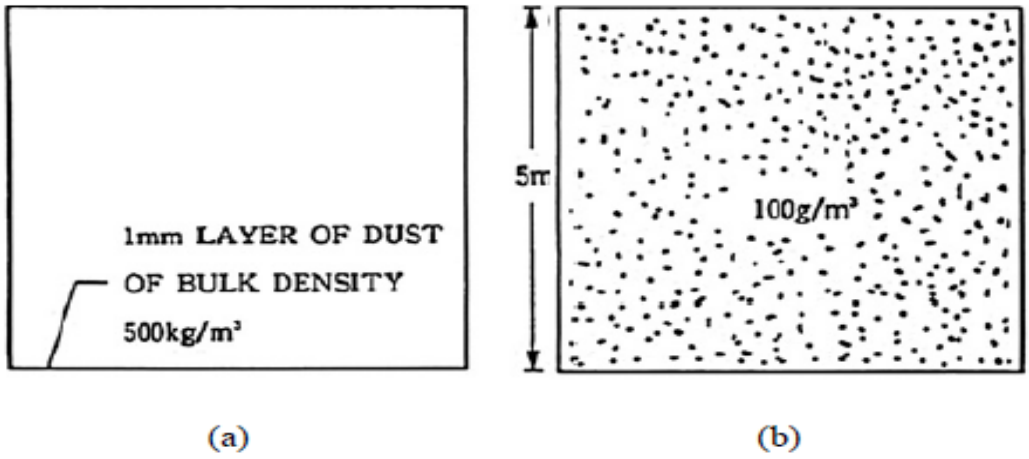

Figure 3.3: (a) 1mm settled dust layer of bulk density 500kg/m³ (b) Formation of cloud of concentration 100g/m³ in a 5m³ room from the settled dust [70]

3.3 Comparison of gas and dust explosions

There are a number of differences between the gas and dust explosions on the basis of explosion characteristics [71, 72]. The dust explosion differs from the gas explosion in the following ways;

- Gas explosion is a homogeneous reaction whereas the dust explosion follows the homogeneous reaction with the release of volatiles and heterogeneous reaction with the solid char.
- The reaction zone in the dust cloud is relatively thicker than the gas cloud due to heterogeneous reaction.
- Dusts have variable particle size and shape whereas the gas have uniform molecules.
- Analogies exist between different gas combustion reactions whereas there is a significant discrepancy among different dusts due to wide variations in their properties.
- Difficulties in proper mixing with the oxidant and the degree of uniformity of the dust with the oxidizing agent have strong dependence on the explosion whereas for gases, this is not a big problem.
- There are some phenomena that happen with dust, such as agglomeration and generation of electrostatic charges that affect the explosion.

- Turbulence in the dust explosion has a significant role in ensuring the particles to remain suspended unlike gas explosion.

Two main differences were highlighted as [73, 74]

- Explosive gases have specified combustible concentration ranges whereas flame propagation in the dust cloud is not bound to the flammable dust concentration range. A stationary layer of dust may also exhibit a role in the sustained flame propagation due to presence of trapped oxygen in the pores.
- The basic physics in the cloud generation and sustainment for the dust and gas is very different.

With respect to dust explosion, the main property of the dust explosion is the size of the particles which influences the surface area available for the reaction. The decrease in the size of the particles results in the increase in the surface area and the ease in the release of the volatiles. The higher the release of volatiles, the faster the reaction. This work has shown that the speed of flame propagation is a strong function of the particles size. Larger size particles of biofuels can be exploded as dust cloud in contrast to coals that don't support the flame propagation for coarse particle sizes.

3.4 Flame propagation of dust cloud

The generation and spreading of the flame through the dust cloud is dependent on the uniformity of the dust cloud. The non-uniform propagation of flame was experienced due to the irregularities of the dust cloud. The flame propagation depends on a number of factors such as composition of the dust, fuel to oxidant ratio, size of the particles, turbulence and uniformity of the suspension, temperature and pressure conditions and quenching distance. The results revealed that the peak flame speeds for solid dusts were measured at excess of the stoichiometric fuel concentration (concentration of the fuel higher than the stoichiometric concentration). This behaviour of solid dust is in contrast with gases that have their maximum flame speed at near stoichiometric concentration. Another point of contrast is observed that the weighed concentration of the dust does not fully participate in the dust explosion and a substantial amount remains unburnt after the explosion. Following this work, flame propagation in the confined vessel revealed the presence of a proportion of unburnt mass as indicated by post explosion residue analysis. Explosion wind

drives some of the particle towards the vessel wall resulting in an unburnt layer sticking to the wall or dropping off some of the particles after hitting the wall as explained later in this work. This unburnt mass was accounted to determine the actual representative burnt concentration in this work.

On the basis of the severity of the explosion, the dust explosions are categorized as;

3.4.1 Deflagration

According to NFPA (2013), propagation of a combustion zone at a velocity that is less than the speed of sound in the unreacted medium ahead of flame front is recognized as Deflagration.

3.4.2 Detonation

If the speed of the flame as a result of explosion is higher than the speed of sound (supersonic), it is known as detonation. Pressure waves generated in the detonation are known as shock waves.

3.5 Primary and secondary explosions

In the primary explosion, the explosion pentagon results the generation of pressure waves due to burning of the dust particles. The dust explosion transmits the pressure waves through the atmosphere causes disturbance of the settled/deposited dust and blows this dust to form a secondary suspension as shown in Figure 3.4. The ignition of these secondary suspensions of dust by the propagating flame is the secondary explosion. The secondary explosion is a more devastating and a bigger hazard than the primary explosion. The basic principle of the protection of dust explosion is the avoidance of this secondary explosion with good housekeeping.

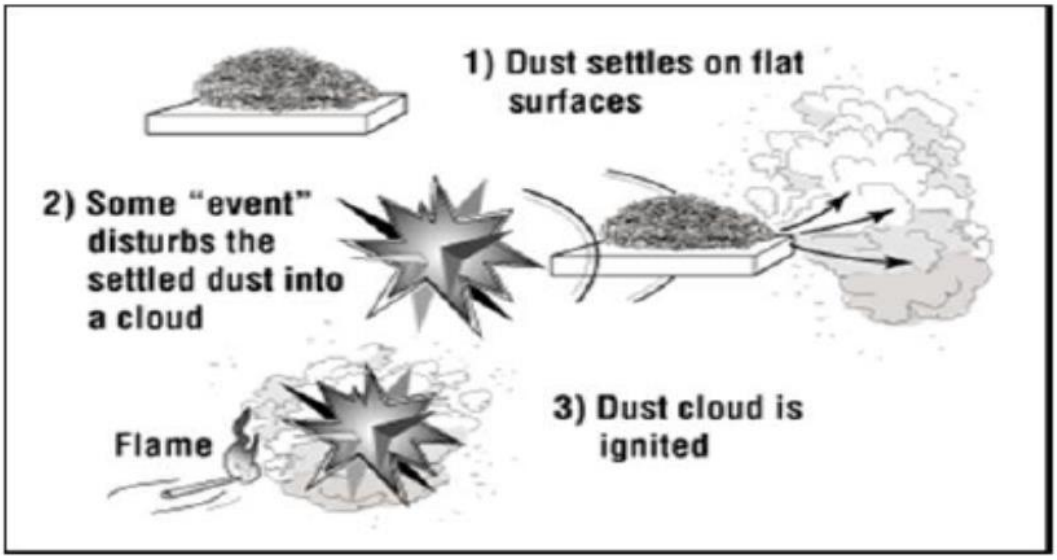

Figure 3.4: Dust explosion from settled dust layer [75]

The initiation of the dust explosion is achieved by the ignition source or achieving the auto-ignition temperature. The minimum ignition temperature is not a fundamental property of the dust and depends on the size and shape of the instrument used. It also depends on the moisture contents and size of the particles. Auto ignition temperature is achieved by minimum ignition energy that initiates the dust explosion. The existing experimental methods included the introduction of a spark of known ignition energy in the dust cloud to observe whether ignition occurs or not. Some methods have used a low energy (as low as 0.1mJ) synchronized capacitive spark for the determination of minimum ignition energy however later it was realized to have some hidden error in it [76].

The minimum ignition temperature is measured in a modified Godbert-Greenwald Furnace apparatus as shown in Figure 3.5 [77]. It consists of a silica furnace tube mounted vertically in a thermally insulated metal case. The temperature of the silica furnace tube is varied by an externally heated electric winding. The top of this tube after a 90^{o} bend is linked with the dust holder, mounted horizontally. The dust holder is connected with the dispersion air reservoir. The bottom of the silica tube is open to the atmosphere. The furnace temperature is maintained to approximately $1000^{o}C$ thermostatically and the dust is dispersed by the dispersing air through the furnace. The ignition is detected by the observation of the flame at the bottom of the tube. The ignition is detected by the lowering of the furnace temperature until the difference is less

than 10ºC are obtained for the dust cloud to be ignited. This temperature is called the minimum ignition temperature.

There are lots of hazards associated with the handling of the dust. A number of dust fires and explosion incidents have happened in the past and on average, one dust incident happens each day [78]. The summaries of some of the recent incidents related to dust fire and explosion are listed in Table 3.1 below (also in Appendix A).

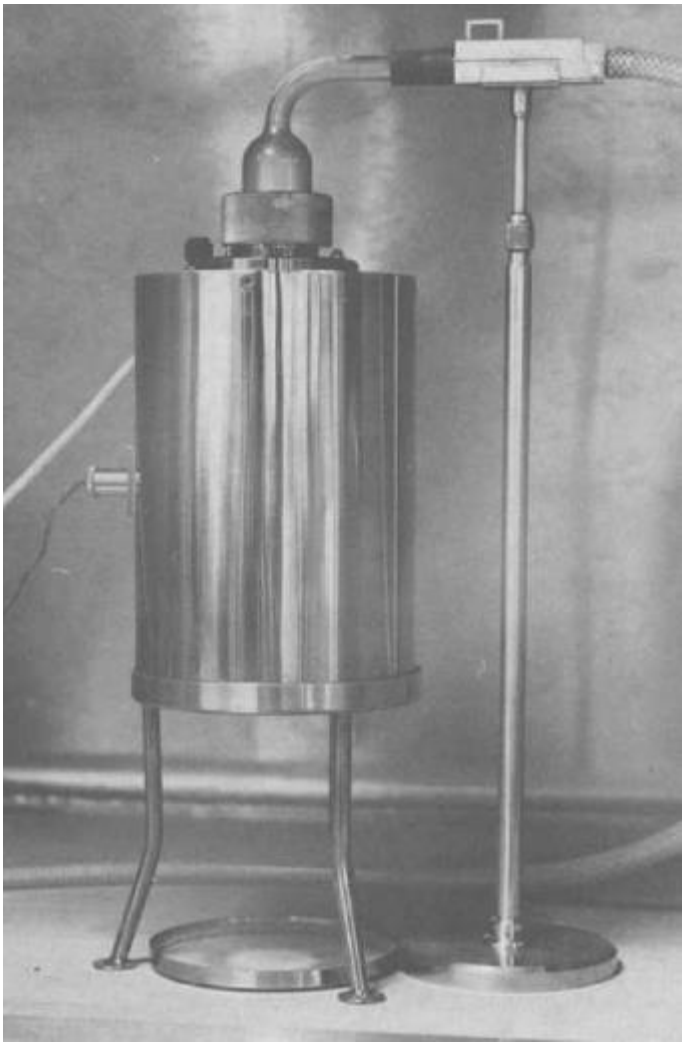

Figure 3.5: Godbert Greenwald Furnace Apparatus

Table 3.1: Summaries of recent dust fire/explosion incidents

Date	Type	Plant	Summary
July 17, 2015	Fire + explosion	Bosley wood flour mill, Macclesfield	➢ Fire and explosion in wood flour mill resulted four causalities. ➢ Cause of the incident is still under investigation.
February 05, 2015	Fire	Boyne City wood pellet factory	➢ Fire broke out in a dust collector. ➢ Suppression activated but failed to put out all the fire. ➢ No injuries were reported.
April 28, 2014	Fire + explosion	German Pellets plant in Woodville	➢ Dust caught fire inside silo and resulted explosion affecting another silo next to it. ➢ No injuries were reported.
March 29, 2014	Fire	Energex American plant	➢ An office and sawdust storage warehouse damaged. ➢ One firefighter was injured only.
September 03, 2013	Fire + explosion	Rotokawa wood pellet plant,	➢ Fire and explosion originated inside the silo and duct system. ➢ No injuries were reported.
April 09, 2013	Fire	Charleston Pellet plant	➢ Fire caught by the pellets started in the pellet plant ➢ No injuries were reported.
April 05, 2013	Fire	Dewys Manufacturing in MARNE, Mich.(WOOD)	➢ Five fire departments were called to Dewys Manufacturing in Marne after a fire sparked Friday morning. ➢ The fire started just in a dust collecting unit in the building. No one was hurt and the fire did not spread to any other part of the structure.
April 01,2013	Explosion	Glendale Heights sheet metal plant	➢ Two people were hurt in an apparent explosion at a Glendale Heights sheet metal plant. ➢ It happened around noon at the Northstar Metal Products facility in the 500-block of Mitchell. ➢ Smoke was seen coming from inside the building, but no exterior damage was immediately apparent. ➢ An employee said, it appeared aluminium dust in the company's grinding room might have ignited to trigger the explosion, but the exact cause is still under investigation.
March 18,2013	Fire	Rochester industrial plant	➢ Dust inside the ductworks caused a fire at Spaulding Composites Inc. ➢ There were smoldering fires throughout the ducts ➢ None of the workers or firefighters sustained injuries from the fire
March 14,2013	Fire	Barefoot Pellet, Troy, PA	➢ Fire broke out shortly in a dry storage shed at Barefoot Pellet Company in Troy Township. ➢ One worker suffered smoke inhalation ➢ It was believed that a malfunction occurred in a front end loader, catching sawdust in the storage shed on fire.
March 04,2013	Fire	Point Wakefield, Australia	➢ The Country Fire Service (CFS) says the fire was reported at a hay processing plant at Bowmans ➢ At the height of the fire, 18 fire fighters and five fire trucks attended the blaze, which is burning about 100 metres from the nearest building. ➢ Spontaneous combustion has been identified as the cause of the blaze.
February 11,2013	Fire	Oakley Paper Plant Kreamer, PA	➢ District Fire Chief Gregory A. Potter said the fire started in the ventilation system of the one-story paper plant. ➢ No one was hurt. ➢ The cause of the fire was determined to be debris in the vents above the roller drying system.
February 05,2013	Fire	DALTON, Ga. Chemical Plant (AP)	➢ Fire broke out in the sawdust collection system at a woodworking plant ➢ No injuries have been reported. ➢ Fire-fighters dealt with the blaze about a mile away.
February 01,2013	Fire	Redmond wood pellet plant	➢ An extensive fire in exterior ductwork caused damage to a Redmond wood pellet plant ➢ No injuries were reported
January 28,2013	Explosion	Tandil Argentina grain silo agricultural plant	➢ An explosion in a grain silo at an agricultural plant killed 1 and injured another
January 04,2013	Fire	Huntingdonshire straw factory	➢ Three tonnes of straw caught fire in a tub grinder. ➢ The straw was removed from the machine and separated to put out the fire, which was accidental and believed to be caused by metal in the grinder. ➢ This is the fifth time a fire has broken out at the straw processing factory in 18 months

3.6 Operations involving dust

The operations, in which dust are generated or handled are comprised of [73];

1. Size reduction (e.g. Crushing, Grinding, Cutting)
2. Conveying—manual or mechanical (e.g. Belt conveyer, Rotary conveyer, Pneumatic conveyer etc.)
3. Pneumatic separation
4. Settling chambers (e.g. Sedimentation, Clarifying vessel)
5. Cyclones (Dry or Wet cyclone)
6. Filters (e.g. filter through septum, rotary filter, Plate filter)
7. Scrubbers
8. Electrostatic precipitator
9. Driers (e.g. Tray driers, Rotary driers, Fluidized bed driers, Pneumatic driers, Spray driers)
10. Screening and classifying operations
11. Mixing and blending operations
12. Storage
13. Packing
14. Dust fired heaters.

Dust is generated in the handling means as shown in Figure 3.6. It was observed that approximately 14.8% of dust was generated during grinding [54]. There should be a proper term for specifying the level of dust particles in a volume of air. Dustiness is defined as ‘number of particles per litre of air’.

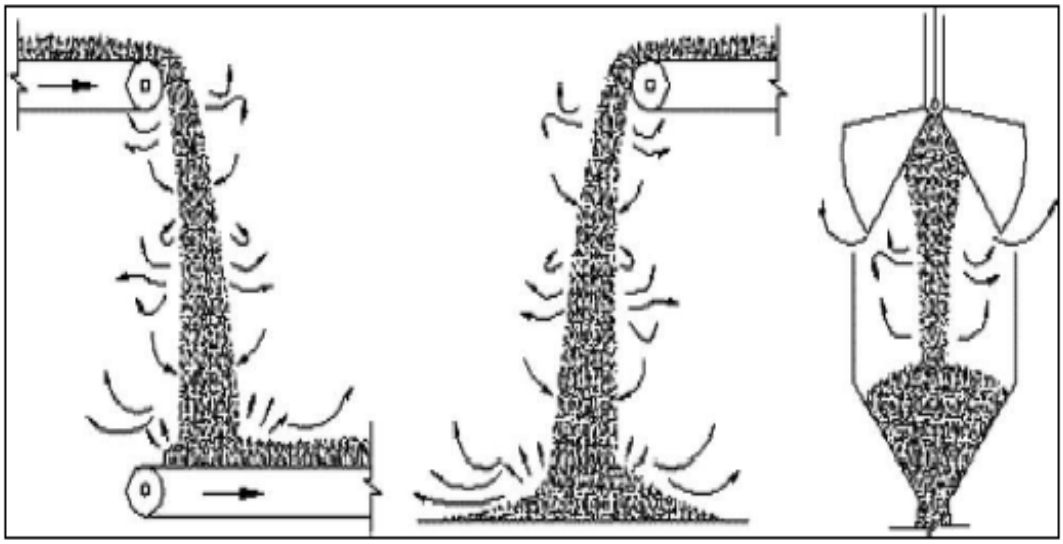

Figure 3.6: Generation of dust in handling of biomass [79]

The industries involved in the handling of the dust are as follows;

- Woodworking
- Plastics
- Agricultural
- Coal mining
- Chemical, including dyestuffs
- Foodstuff, human and animal
- Metals
- Pharmaceuticals

etc.

For the safe operation of handling dusts in many industries, it is necessary to characterize the dust for their explosibility characteristics using the standard reliable techniques.

3.7 Dust explosion testing equipment

The first equipment adopted for measuring the burning properties of dust was the Explosion tube. According to US Bureau of Mines classification of the test apparatus, three test apparatuses were recognized for the dust explosion tests.

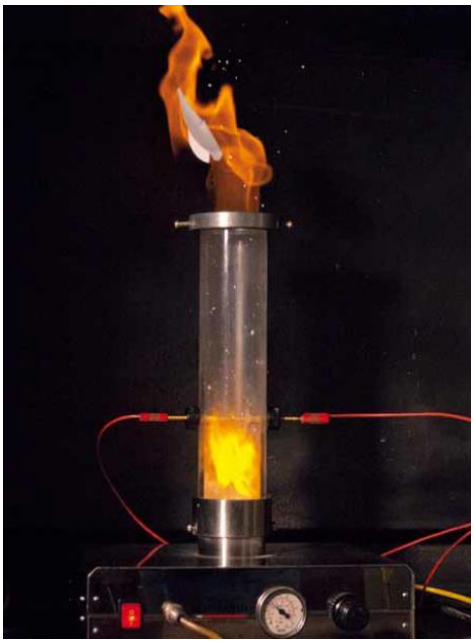

Figure 3.7: Hartmann tube

- Vertical tube (Dispersion of dust vertically upward)
- Horizontal tube (Dispersion of dust in the horizontal direction)
- Inflammator (Dispersion of dust vertically downward)

The closed tube is known as a 'Bomb' and the open tube from the top covered with some venting material known as a 'Hartmann tube', were employed by the US Bureau of Mines for determining different explosible parameters. The most experimental works has been performed on a 20L and 1 m^3 vessels. The universally adopted standard ISO 1 m^3 vessel was recognized as the approved testing equipment for the determinations of the explosibility measurements [73].

The Hartmann tube apparatus, as shown in Figure 3.7, was primarily employed for 'go' or 'no go' screening tests to determine whether the dust can ignite or not. For some weak explosive dusts, spark ignition is possible to fail due to the small ignition energy. Later it was modified to measure the minimum ignition energy by varying spark energy. Huescar et al., (2013) further modified the Hartmann tube to measure the minimum explosible concentration (MEC) using some suitable ignition criteria [19]. The Hartmann tube due to its small size, requires only small amounts of materials to be tested. It is more time efficient and portable. There are still many influencing factors depending on the accurate determination of the explosion characteristics. The presence of a pre-existing

spark under or over-estimates the combustion characteristics due to stratified concentration at the time of ignition. Due to its small diameter, the wall effects are more severe in it which acts as quenching in the propagation of flame. However there were no dispersion problems associated with the fibrous dust and was found to be the only unit suitable for testing of fibrous dust.

20 L sphere as shown in Figure 3.8 is called the small version of big ISO 1 m^3 vessel that has chemical igniters having higher ignition energy. The spark is activated in the centre of the vessel. The wall effect on the propagation of the flame is associated with the strong chemical igniter [80]. Dahoe et al. (1996) found that it was only suitable for the chemical igniter of 2.5 kJ energy or smaller than this due to the interaction of flame with the wall. Different dispersion devices like moving hose and rebound nozzle are used on the side or bottom of the vessel to increase dispersion.

The most accepted standard ISO 1 m^3 vessel is known as the universal vessel for the dust explosion tests and is shown in Figure 3.9. The results obtained for the explosibility data using this device are more reliable. According to dust standards, any test failing on the Hartmann tube or 20L sphere must be validated on the ISO 1m^3 vessel. The chemical igniter of strong ignition energy (10Kj) is used to ignite the dusts. This result in the generation of spherical flame with no wall effects. However due to its large size, a huge amount of dust is required to undertake tests. It is also more time consuming than the others dust explosion methods. There is a provision of different designed dispersers that can be used. However these dispersers after designing need proper calibration compared with the standard C ring disperser and no major work has been done for the calibration of these dispersers.

The summary of some of the units that have been adopted for the determination of the explosibility parameters are mentioned below in table 3.2.

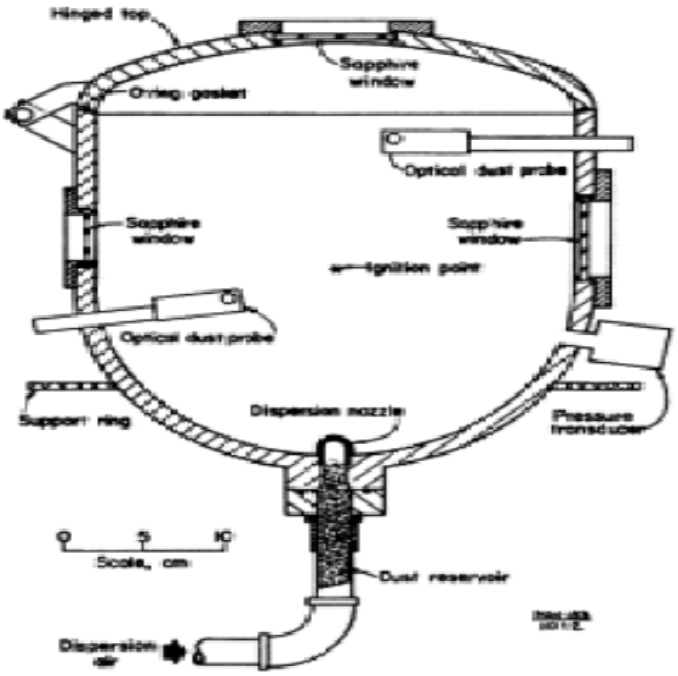

Figure 3.8: Pittsburg laboratory 20L chamber [81]

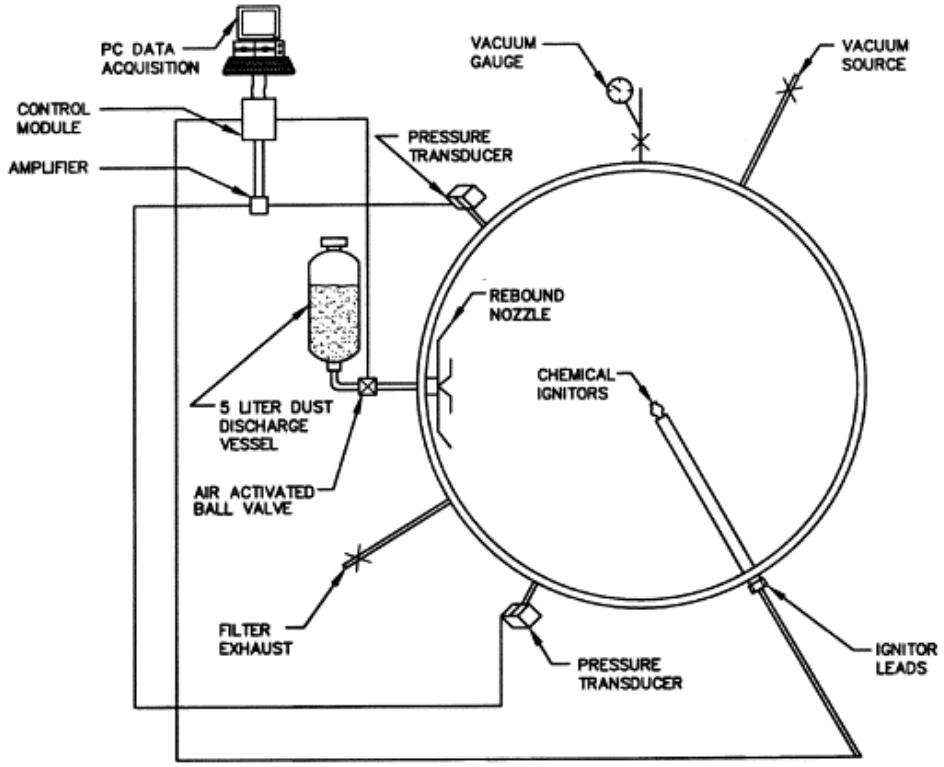

Figure 3.9: Vertical cross section of Fike 1m^3 vessel [81]

Table 3.2: Summary of some equipment's used for dust explosibility testings [73]

Author	Year	Equipment	Description
Holtzwart and von Meyer	1891	50 cm^3 capacity glass tube	Pair of Platinum electrode for spark, Short compressed air blast generated dust cloud in the area of spark
Engler	1907	250-500 cm^3 capacity Glass flask	---------
Trostel and Frevert	1924	1.4 L capacity explosion bomb	Small cup for dust at the bottom and air was injected from the bottom via tube to blast the dust heap with 180 degree rotation facing downward.
Hartmann et al.	1943	1.2 L vertical cylinder	Air was introduced axially from the bottom and deflected into dust by a small conical hat, Explosibility measurements published by US Bureau of Mines based on this unit
Meek and Dallavalle	1954	60 L chamber	Dust was introduced through funnel shaped cup, tailored with special dispersion cone.
Carpenter and Davies	1958	275 cm^3 combustion vessel	Detached dust dispersion cup of 2cm diameter at the bottom
Helwig	1965	43 L closed bomb	Air was blasted through 100cm^3 whirling cylinder in the fluidization chamber
Nagy et al.	1971	1 L to 14 m^3	Used different air blast methods
Moore	1979	1 to 43 L three different vessels	---------
Enright	1984	1 to 20 L three different vessels	---------
Bartknecht	1971	1 m^3	Dust was dispersed through U or C ring disperser.
Siwek	1977	20 L	Starting with 5L, 10L and then finishing to 20L to have comparative results as 1 m^3 vessel.
Cashdollar and Hertzberg	1985	20 L	Included interchangeability dust dispersion system

Table 3.3: Explosibility characterisation of dust and influencing factors

Explosibility of dust
Explosibility characteristics
➢ Minimum explosible concentration ➢ Maximum explosive pressure ➢ Maximum rate of pressure rise ➢ Flame speed and burning velocity ➢ Minimum ignition energy ➢ Minimum ignition temperature ➢ Limiting oxygen concentration
Physical properties of fuel
➢ Shape/surface area ➢ Particle size distribution ➢ Inert (Moisture+Ash contents) ➢ Volatile matter ➢ Porosity of the sample ➢ Fluidity of fuel/Inter particle forces ➢ Some alkaline metals as catalyst
Process conditions
➢ Oxidizing medium ➢ Temperature and Pressure ➢ Turbulence level ➢ Uniformity and dispersion ➢ Humidity level ➢ Ignition energy ➢ Congestion level

Different explosible dusts are characterised by their explosibility characteristics. Determination of the explosibility characteristics is a function of physical properties of the fuel, methodology adopted and the process conditions as listed in table 3.3. Physical parameters favouring the effective propagation of a flame

include higher surface area with a larger proportions of fine particles, minimum inerts, higher volatile yield with porous structure for its fast release, ease of fuel dispersibility and the presence of some alkaline metals which catalysing the rate of flame propagation, however it is still not well established. Similarly, the process conditions affect the measurements of explosibility characteristics. Comparison of these properties for different fuels should be based on the same process conditions for distinguishing the fuels. Measurement of these explosibility properties for varying oxygen concentration (oxygen limited or oxygen rich environment) yield different results. Similarly, initial temperature, pressure, humidity, ignition energy, turbulence level and congestion will directly or indirectly affect the measurements results. The influence of these parameters on the explosibility characteristics will be explained in detail later in this chapter.

Also the improper experimental methodology may under or overestimate the burning properties of dust. The existing design and their experimental methodologies still have some limitations. Most of these methods are applicable for uniform shaped symmetrical particles without any dispersion problems. However for biomass materials, the fibrous nature and high voluminous dust makes it difficult for their testings. Improvements were made in the modified Hartmann tube and 1 m^3 vessel in this area as part of this work.

Old version of the Hartmann tube were refined for reliable measurements of explosibility characteristics especially minimum explosible concentration. The poor ignition criteria and visual observation of flame propagation was refined based on physical measurements. It was further refined as will be discussed in detail in the corresponding chapter.

The standard 1 m^3 vessel with a 5L dust pot was not suitable to test the wide range of concentration and for low bulk density fibrous biomass dust, it was more limited for testing of concentration. This 5L pot was extended to a 10L volume by placing another 5L pot in series to accommodate high voluminous biomass dusts. This 10L volume was calibrated by varying dispersion pressure to result in the same turbulence level as that with standard settings [82]. The optimum dispersion pressure was measured to be 10 bar for the 10L pot instead of 20bar (for 5L pot) for producing same turbulence giving comparable results of explosibility characteristics [82]. Also testing of irregular shaped coarse/fibrous dust resulted in choking/Plugging in the standard C-ring disperser and small spherical dispersers, they were only suitable for uniform

fine dust with d90<100µm based on laser diffraction technique. Standard procedure defined in the EN 14034-2:2006 (E) states that 'the starting concentration for explosibility testing should be 500 g/m^3. After this, the successive concentrations should be with an increment of 250 g/m^3 above and 50% below this 500 g/m^3 in a sequence as shown below';

…..,1000, 750, 500, 250, 125, 60, 30, 15……. g/m^3

Based on this, if a concentration of 125 g/m^3 ignites and the next 60 g/m^3 fails to ignite, then the safe side of minimum explosible concentration is 60 g/m^3. But with this, there is a significant error in these measurements. As if the actual lean limit is 90 g/m^3 then there is an error of almost 33% in the measurements. Similarly after 60 g/m^3, the next successive concentration is 30 g/m^3 however if the actual lean limit is say 40 g/m^3, then there is still an error of 25%. This may be one of the reason for very lean limits of HCO dust in comparison to HC fuels. As the gaseous explosion measurements have percentage error of less than 1% for tube methods. In this work, the successive concentrations tested near the lean side were narrow for more accurate determination of MEC and ignored the statement of 50% or 250 g/m^3 successive concentration. However, some of the dusts, because of their limited amount were tested based on this standard procedure as mentioned in the EN 14034-2:2006.

The concentration of the dust usually represented as g/m^3 is classified as.

- Minimum explosible concentration

The minimum concentration of dust, in the presence of excess oxidizing agent, that can sustain the explosion in accordance with the standard. According to NFPA 68-13, 'The minimum concentration of a combustible dust cloud that is capable of propagating a deflagration through a uniform mixture of the dust and air under the specified conditions of test'.

- Stoichiometric concentration

The concentration of dust that is sufficient to consume the entire oxidizing agent under the specified condition of test.

- Worst case concentration

The concentration of dust, that gives the maximum explosion rate under the specified condition of test. It may be also called the most reactive concentration.

- Maximum explosible concentration

The maximum concentration of dust in the presence of limiting oxidizing agent that can sustain the explosion as specified by Standard under the specified condition of test. It is similar to upper flammability limit as used for gaseous mixtures.

3.8 Hazard Index

The extent of the explosive nature of the dust is specified by the Hazard index which was established by the US Bureau of Mines. This hazard index is used to compare the sensitivity and severity of explosibility hazard of different dusts. Different ratios are used to measure the Hazard index. The hazard index or index of explosibility of the dust can be obtained by multiplying the ratios as shown in eq. 3.1.

$$Index\ of\ explosibility = Ignition\ sensitivity \times Explosion\ severity \quad [3.1]$$

Ignition sensitivity and explosion severity are the empirical dimensionless ratios for classifying the dust hazards by comparing with the explosibility characteristics of standard reference Pittsburgh coal sample. Minimum ignition temperature, minimum ignition energy and minimum explosible concentration are used to measure the ignition sensitivity whereas maximum explosion pressure and maximum rate of pressure rise are used to measure the explosion severity of the selected dust in comparison to Pittsburgh coal sample (Table 3.4).

$$Ignition\ sensitivity = \frac{(Min.ign.temp. \times Min.ign.energy \times Min.ign.conc.)_{reference\ dust}}{(Min.ign.temp. \times Min.ign.energy \times Min.ign.conc.)_{sample\ dust}} \quad [3.2]$$

$$Explosion\ severity = \frac{(Max.explosion\ press. \times Max.rate\ of\ pressure\ rise)_{sample\ dust}}{(Max.explosion\ press. \times Max.rate\ of\ pressure\ rise)_{reference\ dust}} \quad [3.3]$$

Based on the ignition sensitivity and explosion severity, different dusts were classified for their degree of hazard severity as weak, moderate, strong and severe by Jacobson et al. (1961) [83] as shown in Figure 3.10.

Table 3.4: Explosibility data of standard pittsburgh coal

Minimum explosible concentration	55 g/m^3
Minimum ignition energy	0.06 J
Minimum ignition temperature	610^{o}C
Maximum explosion pressure	5.7 barg
Maximum rate of pressure rise	158.6 bar/s

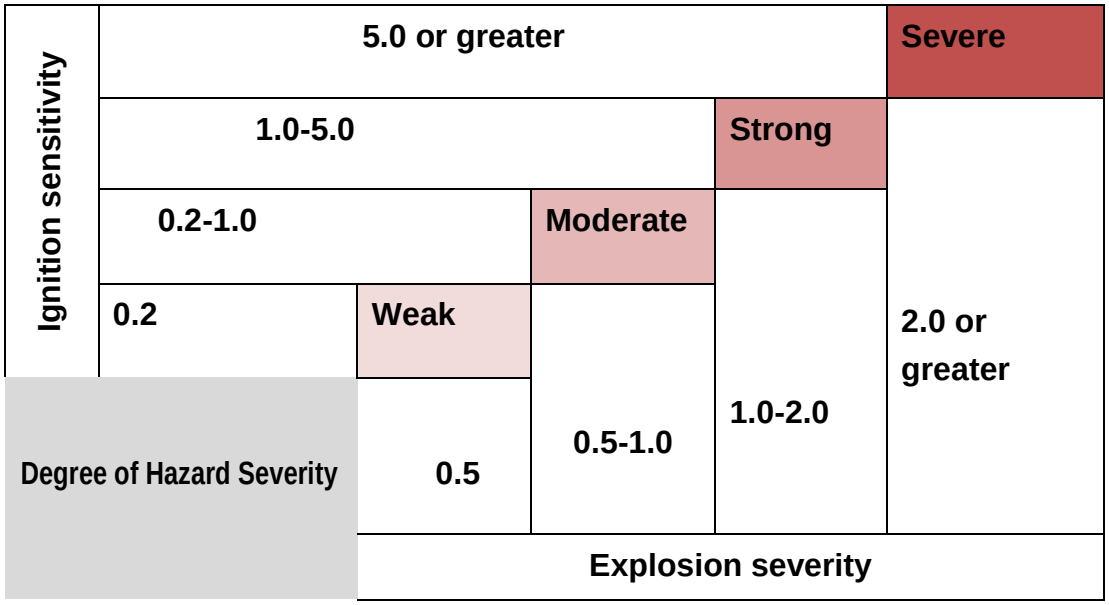

Figure 3.10: Degree of hazard severity based on explosion severity and ignition sensitivity

Most of these explosibility properties were determined using the Hartmann dust explosion equipment except the minimum ignition temperature that was measured using Godbert Greenwalt furnace [77].

Further classification based on the explosion severity of the explosible dusts was done using dust constant K_{st} measurements as explained below.

3.9 Cube root law

Idealized isothermal treatment predicts that the maximum rate of pressure rise is inversely proportional to the radius of the confined vessel that is the cube root of the confined vessel volume. The cube root law is also known as the volume normalized method, used as a scaling method for the dust explosions [73]. Mathematically it is expressed as,

$$Deflagration\ index\ or\ dust\ constant, k_{st} = \frac{dP}{dt} V^{1/3} \quad [3.4]$$

It is strictly valid as a scaling relationship under the following hypothetical circumstances;

1) Both the test vessels should have the same mass burning rate when rate of pressure rise reaches its peak value. (i.e. Same products of the burning velocity, same flame area, same density of the unburnt mixture)

Necessary things for the validity of this assumption are;

- Geometrically similar vessels
- Central point ignition with negligible energy input by the igniter
- Identical flow properties (Same turbulence level)
- Changes in the unburnt mixture (Pressure, Temperature and turbulence) caused by the expansion of the flame front towards unburnt mixture are similar in both the vessels
- No significant net flow in the vessel at the time of ignition (it disturbs the growing spherical flame)

2) Thickness of the flame should be negligible as compared to the radius of the explosion vessel.(Non spherical flame results uneven propagation of the flame front that reaches the inflexion point and quenching results due to the effect of walls)

In Figure 3.11, the Pressure time plot in the dust explosion is shown. First, injection of dust in the evacuated vessel raises the pressure to ambient atmospheric pressure and then explosion of the dispersed dust cloud results in the build-up of pressure in the confined vessel that quenches after reaching the wall as shown.

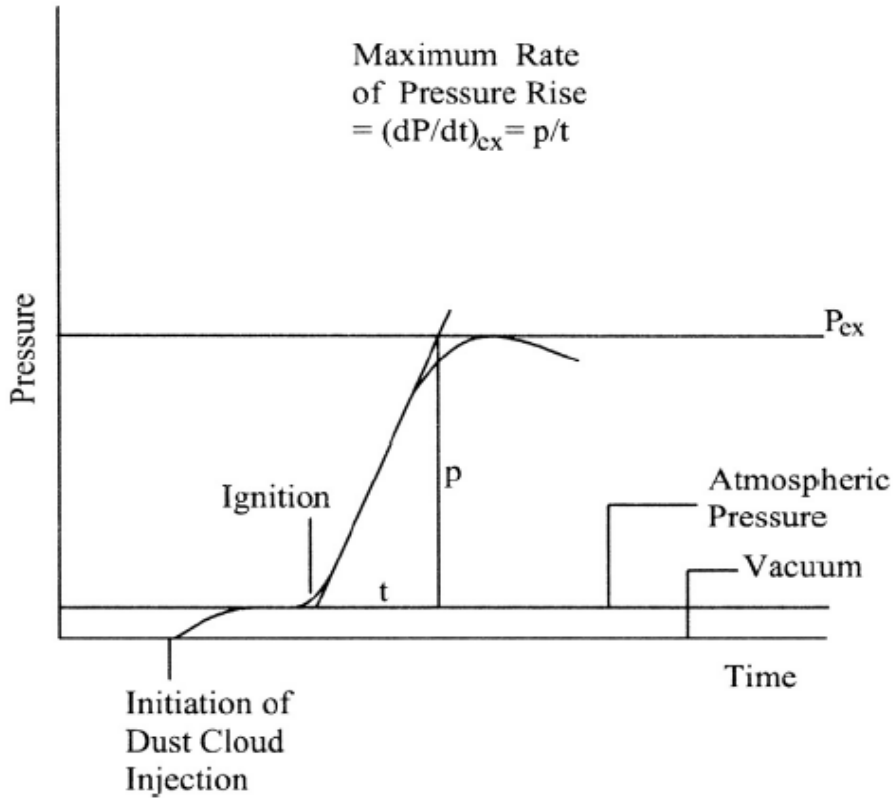

Figure 3.11: Pressure-time record of a dust explosion test [84]

Maximum rate of pressure rise is measured using the slope for the steep rise of explosion pressure. Later this peak rate of pressure rise is volume normalised by multiplying it with the cube root of the vessel volume. These values are the quantitative determination of the explosion severity (Table 3.5) and are used in the protection design.

Table 3.5: Explosion severity classification based on Pressure rise (P_{max}) and deflagration index (K_{st})

Hazard Class	Kst (bar m/s)	Pmax (bar)	Explosion severity
St.1	≤200	10	Moderate
St.2	201-300	10	Strong
St.3	≥300	12	Very strong

Dusts with higher values of the deflagration index and higher explosion pressure are extremely hazardous and require accurate and reliable protection design for safe working environment [68].

Hertzberg and Cashdollar (1987) gave the relationship for the propagation of the fireball generated spherically due to central point ignition using the spherical constant volume vessel e.g. 20L sphere related as [85];

$$\frac{P_{(t)} - P_o}{P_{max} - P_o} = k \frac{V_{(t)}}{V_o} \qquad [3.5]$$

Here the proportionality constant 'k' is a correction factor accounting the compressibility difference between burnt and unburnt mixture.

$P_{(t)}$= Pressure development of the fire ball at any time 't'

P_o=Initial pressure in the constant volume vessel

P_{max}=Maximum explosion pressure

$V_{(t)}$= Volume of the expanding fire ball in constant volume vessel at any time 't'

V_o= Constant volume of the vessel

For spherical propagation of the fireball,

$$\frac{V_t}{V_0} = [\frac{r_{(t)}}{r_0}]^3 \qquad [3.6]$$

Where

$r_{(t)}$= Variation in the radius of fireball during its propagation at time 't'

r_0= Radius of the fixed constant volume vessel

Flame speed can be estimated by placing 'S_b t' in place of '$r_{(t)}$' where S_b is known as the flame speed of the fireball.

Flame speed can be related with the turbulent burning velocity using the following relation as;

$$S_b = \frac{\rho_u}{\rho_b} S_u \qquad [3.7]$$

Here ρ_u= Density of unburnt gas and ρ_b is the density of the burnt gas at constant pressure.

3.10 Types of flames

There are two types of flame [86]

3.10.1 Nusselt flames

Pure heterogeneous combustion occurring at the surface of individual particles and is sustained by diffusion of oxygen towards the particle surface.

3.10.2 Volatile flames

Local homogeneous combustion of the released volatiles mixed with the oxidant. It is the homogeneous flame of a single phase.

Using pulverized biomass for wide applications require its explosibility characteristics to be accessed as these are very reactive and carry fire and explosion hazards. Biomass are so diverse in their chemical characterisation depending on their type and local conditions of their origin. Vessilev et al. (2012) compiled the chemical characterisation of a number of biomass of different types from various studies as shown in Figure 3.12. It can be seen in Figure 3.12 that the range of O/C molar ratio is 0.1-0.9 whereas for H/C molar ratio is 0.7-2.4. These biomass after some suitable pre-treatments can be refined for their consistent properties as discussed before. These biomass as a continuous feedstock for renewable generation of energy can be used as a substitute of coal in the existing coal power generation plants. The objective of this research work is to focus on various types of biomass for measuring the explosion characteristics for their safe exploitation.

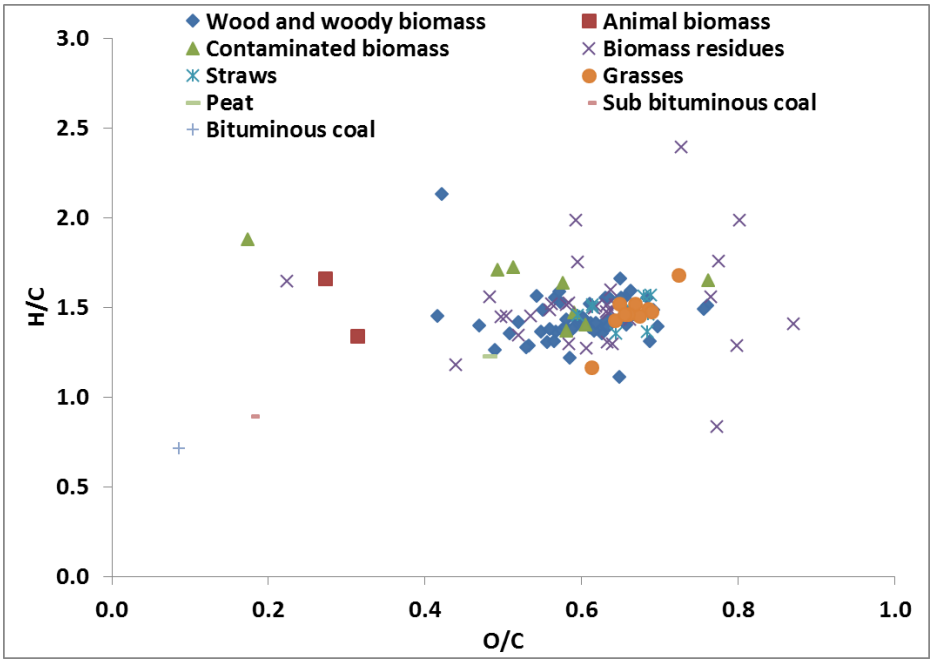

Figure 3.12: Elemental molar ratios of different types of biomass in comparison to different classes of coal

It was showed that the maximum flame speed occurred at equivalence ratio 'Ø' of ~ 2 compared with Ø ~1.05 for hydrocarbon gas/air mixtures [18, 22]. It occurs for all HCO type dusts due to possible gasification for rich concentration mixtures [73]. This was not realized in the dust explosion literature, as the dust concentrations had not been expressed in terms of Ø, but only as g/m^3 [24]. To determine Ø, the elemental analysis of the fuel is required so that the stoichiometric Ø as g/m^3 can be calculated, as will be described later in this work for stoichiometric calculations.

Similarly the reactivity of biomass was measured to be greater than coal samples. Two thermally treated biomass and their raw samples were tested on the modified Hartmann tube and the results were compared with the coal samples. Lean flammability results in terms of equivalence ratio showed that biomass materials (treated and untreated) were more reactive than the kellingley coal [19]. The reactivity of the torrefied biomass is affected by the torrefaction condition. The severe the torrefaction condition, the less would be the volatiles but there would be enhancement in the brittleness that on crushing gives more fine particles (and ash in the finer size fraction). So, the torrefaction severity results the loss of volatiles of the biomass but the explosibility is

counterbalance due to the augmentation in the number of fine particles due to more brittleness [87].

3.11 Effect of size and shape of the particles

Effect of particle size is an additional parameter for the degree of freedom to specify the dust explosion. Changing the particle size affects the lean flammable limits of the fuel. There is some characteristic diameter (minimum diameter) of the dust below which the lean limit of that dust become independent on the size of the particle. Similarly there is also an upper limit of the diameter at which the flame propagation ceases due to absorption of heat by the excess surface [85].

The shape of the particles also has a strong impact on the severity of the dust explosion. The regular shaped particles have low explosbility index than the irregular shaped particles due to low surface area of the regular shaped particles [88].

Nifuku & Katoh (2001) studied the particle size's effect on the minimum ignition energy for the ignition of dust. They observed that the reduction in the size of the particle facilitates the burning of the particles due to high exposed surface area. They also observed that the average particle concentration in the dust-air suspension is also strongly dependent on the minimum ignition energy and the ignition sensitivity of the particles [89]. Burning rate of dust particles is directly proportional to its surface area. Compression of a spherical particle of diameter 5 microns into a 0.2 micron thickness of flake with a length of 20 microns results in the augmentation of the surface area by 8 times [73].

Gao et al. (2013) studied the effect of particle size distribution on the propagation of the flame using Octadecanol dust. The flame was visualized by high speed camera combined with band width filter. It was concluded that the flame developed by fines was regular shape and continuous due to high release of the volatiles whereas the flame developed by coarse particles was discrete and discontinuous due to less release of volatile and burning of the solid particles. Flame imaging revealed that the flame colour changed to blue as the particle size varied from fine to coarse [90].

The particle size distribution and the volatiles have a significant influence on the reactivity of the biomass. It has been determined that the biomass comprising of coarse particles greater than 150 microns sustain the flame propagation. The reactivity of the biomass increases as the size of the particles is reduced that

increase the expose surface area of the particles. The coarse particles burn in the presence of fines as the fines have more surface to volume ratio. It was noted that the biomass particles are not spherical but elongated cylinder like shape that have higher surface to volume ratio. The higher reactivity of the biomass dust reflect the release of volatile might include some reactive gases like Hydrogen or Carbon Monoxide having equivalence ratio smaller than the hydrocarbon gases. It is assumed that the variation of the characteristics of the biomass particles like size, shape, density with the process conditions like temperature influence the reactivity of the biomass particles in terms of release of volatile quantity and reactive species [91].

Eckhoff (2013) explained the effect of nm sized particles along with agglomeration phenomenon on the explosion severity. Decrease in size of the particles intensifies the explosion severity however most of the nm size particles have the tendency to agglomerate due to strong inter-particles forces that results in the formation of bigger particles counter-balancing the increased reactivity. So, the existing preventive design of explosion for micron sized particles should be suitable with nm sized particles [92].

3.12 Flammable limits of the dust

Coal and biomass fuels have specified lower limit of flammability but no upper flammability limit. As the concentration of the fuel is increased, it acts as an inert in suppressing the dust explosion with only 50% of the nominal dusts take part in the explosion whereas the other 50% remains unburnt. So it is agreed that some amount of the biomass may be burnt in the higher concentration leaving the remaining amount unburnt. However some attempts have been done to predict the upper flammability limit.

The concentration of the dust also plays a vital role in the propagation of the flame. The flame thickness increases as the concentration of the dust starting from the lean limit increases and starts to decrease again as the concentration is much higher than the stoichiometric concentration. The concentration of the dust near the minimum explosible concentration develops the thinner flame having a thickness of approximately 10cm whereas at higher concentration, the thickness of the flame is about 50-100cm [69].

Deguingand & Galant (1981) employed a weak spark ignition for the determination of the upper flammable limit and found apparent upper flammable

limit of coal dust to be ~4kg/m^3 which was in fact more an ignitability limit rather than flammable limit because of weak ignition source [93].

Eckhoff, Fuhre & Pedersen (1987) used the Hartmann bomb (closed tube) for the measurements of the flammability limits of low moisture maize dust. The minimum explosible concentration was measured to be 70g/m^3 at the ambient temperature and pressure whereas the maximum explosible concentration was estimated to be probably somewhere in the concentration range of 1500-2500g/m^3. In a specially constructed top vented steel silo of volume 236m^3, the most/worst explosive concentration for maize starch was found to be 600-700g/m^3 whereas the minimum explosible concentration was estimated to be of the order of 100g/m^3 [94]. Wolanski (1992) found that increasing the concentration reduced the flame temperature below its limit value and postulated that the dusts do not have an upper flammability limit [95]. Mintz (1993) used the technique of reducing oxygen content and enhancing the particle size to calculate the upper flammability limit of some of the dusts [96].

Cashdollar & Chathrathi (1993) used 20 L chamber and 1 m^3 vessel for determining the minimum explosible concentration of gilsonite, bituminous coal and anthracite coal using different igniters. They observed that the 20L chamber with 2500 J igniter and 1 m^3 vessel with10 kJ igniter gave the comparable results for the minimum explosible concentration. High ignition energy greater than 2500J in 20L chamber resulted in the overdriven of the measurements.

The lean limit of the Pittsburgh seam bituminous coal was determined to be 90g/m^3 with an error of ±0.01 kg/m^3 and rich flammability limit could not be judged even at concentration up to 4kg/m^3 using 20L vessel [97]. The lean limit of Pittsburgh coal was higher than the previous measured results (55g/m^3) using the Hartmann tube showing the discrepancies in the experimental result. Cashdollar (2000) used a 20 L chamber with 2500J igniter and found that for high volatile coal dust and polyethylene showed an explosion even at concentration beyond 4kg/m^3 [98].

Yuan et al. (2012) proposed a new method to calculate the minimum explosible concentration based on the combustion duration time rather than the maximum pressure. The maximum pressure for different concentration of coal in Siwek 20L sphere was found to depend on the ignition time delay. Measurement of MEC were not reliable without having the optimized ignition time delay. On the

other hand, the combustion time instead of maximum explosion pressure was not much dependent on the ignition delay time. Concentration-combustion time graph having a peak value for a given sized dust, resulted the more reliable MEC [99].

3.13 Effect of turbulence & the burning velocity on explosion

3.13.1 Burning velocity

It is defined as 'the velocity of the burning zone relative to the unburnt zone that causes compression of the unburnt zone and enhance the turbulence'.

Burning velocity is classified as laminar burning velocity and turbulent burning velocity. These are very important parameters in the design of a burner. Lots of work has done in estimating the burning velocity of the dusts. There are some peculiar features in the dust burning velocities which were identified by many researchers. It is difficult to stabilize the laminar dust flame without significant cooling due to emission of radiations as explained by Lee (1987& 1988). Cooling reduces the actual temperature of the flame less than the adiabatic temperature and the system approaches towards non-adiabatic condition. The average burning velocity is lower for this non-adiabatic flame. It was showed experimentally that the burning velocity for Aluminium air cloud increased with the decreasing particle diameter [86].

Nagy, Conn and Verakis. (1969) derived an expression of temperature and pressure dependence for the adiabatic flame propagation in a spherical vessel related as [100]

$$T_u = T_o \left(\frac{P}{P_o}\right)^{\frac{(\gamma_u - 1)}{\gamma_u}} \qquad [3.8]$$

$$T_b = T_m \left(\frac{P}{P_m}\right)^{\frac{(\gamma_b - 1)}{\gamma_b}} \qquad [3.9]$$

Here T_u the mixture burning temperature

T_o the initial temperature

T_b the temperature of the combustion product

T_m the overall temperature when flame reaches the vessel wall

P/P_o the pressure ratio relative to initial pressure

P/P_m the pressure ratio relative to maximum explosion pressure

γ_b and γ_u are the specific heat ratios of burnt and unburnt mixtures respectively.

Laminar burning velocity of the coal air dust flame at atmospheric pressure showed the following results [101];

- Peak burning velocity was measured at rich dust concentration higher than the stoichiometric concentration.
- Peak burning velocity was proportional to the specific surface area.
- Decreasing the particles diameter moved the peak burning velocity towards the lean side concentration instead of rich side with the peak increased towards the lean side concentration.
- Higher the volatiles (smaller diameter particles), higher the peak burning velocity towards the lean side.
- Oxygen enhancement or the formation of hybrid mixture increased the burning velocity.
- Steady, laminar Flame thickness of the coal dust particles was directly proportional to the size of the dust particles.
- Measured peak flame temperature was measured in the range from 1000 to 1500K that was smaller than the real flame temperature.
- The extent of the release of volatiles from the coal was proportional to the coal dust concentration.

Model for the coal dust combustion in air was proposed including the following three stages [85].

1. Heating and release of the volatiles.
2. Mixing of the volatile with the air to form the gaseous mixture
3. Gas phase burning of this mixture.

For small particles and low dust concentration, the stage 3 would be the rate limiting step whereas for larger diameter particles and higher dust concentration, heating to release sufficient volatile (stage 1) would be the rate limiting step.

Table 3.6: Works done for burning velocity measurements [73]

Author	Year	Material	Parameter	Findings
Kaesche-Krischer and Zehr	1958, 1959	Lycopodium -air and Polyvinyl alcohol-air	Burning velocity	• Stable Lycopodium/air flame for concentration range 200 to 500g/m^3 • Flame was blue similar to the rich HC mixtures. • High burning velocity for high volatiles and enhanced oxygen ignition.
Mason and Wilson	1967	Lycopodium -air	Burning velocity	• Similar results as that of Kaesche-krischer, • Temperature was measured at 140g/m^3 dust and found that at 2mm below the flame front, the temperature was 300-350K whereas at 1.5mm above the flame front, the temperature was 1800K which is also in complete agreement with Kaescher,1958
Ballal	1983	Coal-air	Burning velocity	• Free fall explosion tube with Zero gravity condition. • Laminar burning velocity were measured to be 0.11-0.25m/s depending on the volatile proportion. • Universally accepted relation is proposed which is the total quenching time for the laminar dust flame is equal to the sum of the time of devolatalization and the time for the gas phase chemical reaction. • Burning velocity was found to be strongly dependent on the particle size, concentration, volatiles, heat losses and a mass transfer number of the particle
Bradley et al.	1986	graphite with methane-air and coal air	Burning velocity	• Theoretical calculation of the laminar burning velocity.
Proust and Veyssiere	1988	Maize starch	Burning velocity	• A laser tomography system was used to control the homogeneity of the dust cloud. • The quenching distance was determined to be 7 mm which was the minimum at about stoichiometric conc. of 235 g/m^3. • Laminar burning velocity was determined as 0.27m/s.

Different researchers measured the burning velocity using various techniques are listed in table 3.6.

Modelling of gas and dust explosions requires knowledge of the laminar burning velocity, U_L, which is a major area of research for gas flames. For dust flames there is no agreed methodology for its measurement and hence no agreed values that can be used in explosion protection design or in pulverised biomass burner design. Andrews and Bradley (1972) [102] showed that there were systematic errors in most methods of determining the laminar burning velocity of gases and these were related to the finite thickness of the flame and the assumption of an infinitely thin flame in many of the measurement methods. As the flame thickness of dust flames is greater than gas flames, the measurement problems for S_L for dusts are likely to be greater than for gas flames. Some recommended values of burning velocity for gases using measurement methods with low errors were recommended by Andrews and Bradley [102] and adopted by the NFPA-68 (2013) in their gas explosion protection standard [68]. For dusts no data base exists for laminar burning velocities, as few measurement methods exist, due to the need for turbulence to keep the dusts in suspension. The lack of a reference standard for the measurement of S_L contrasts with the area of gas flammability limits, where standards do exist [97].

In gas or dust explosion protection using venting or suppression there has always been a legal requirement to take into account, in the vent design process, the reactivity of the most reactive mixture that the vent is a protection against. In the absence of agreed methods to determine S_L an alternative and less fundamental parameter has been used for many years known as deflagration parameter, K. For gases this is usually referred to as K_G and for dusts K_{st}. It should be noted that if the pressure rise is expressed relative to the initial pressure, P_i, then

$$\frac{K}{P_i} = \frac{(\frac{dP}{dt})_{max}}{P_i} V^{\frac{1}{3}} \qquad 'm/s'$$

How dP/dt_{max} is measured is detailed in a European Standards for gas [103] and dust [104] explosions. Also required to be measured is the peak explosion pressure and there are standards on how to do this [105]. These reactivity parameters are embedded in the European standards for gas [106] and dust venting [107], but are not used in the wider area of combustion modelling. The

measurement procedures for the dust reactivity, K_{st}, require the ISO standard [108] 1m^3 spherical explosion vessel to be used to determine P_{msx} and dp/dt_{max} and this is one of the experimental equipment used in the present work.

The standard dust explosion techniques are based on a turbulent injection process as turbulence is required to keep the dust dispersed. The average turbulence can be calibrated by undertaking laminar gas explosions and then operating the air injection system into a premixed gas air mixture to generate the same turbulence as occurs in the dust explosion [109, 110] and this method was used in the present work to calibrate the turbulence in the new injection systems for coarse fibrous biomass.

For gases K_G is measured in a laminar explosion in a 5L spherical vessel and Bartknecht [111] has published K_G for a wide range of gases in a 5L sphere and these values are quoted in the design standards [106]. Till 2012 the K_G reactivity parameter for gases and Bartknecht's list of values of K_G was part of the gas venting design standards in the USA [112] but have been replaced by a more fundamental gas venting design procedure based on S_L as the reactivity parameter [68]. However, they have not chosen to regulate how S_L is measured but have specified a reference value for propane, 0.46 m/s that the measurement method must be corrected to. Dust standards also continue to use K_{st} as the reactivity parameter for dust, due to the lack of reliable data for dust S_L. The problem with the K_G approach to gas reactivity is that it is dependent on the vessel volume [24, 112, 113], which is a reflection of the dependence of laminar flame propagation on the distance from the spark [114], due to self-acceleration of the flame caused by the formation of cellular flames. The procedures of Chippett [114] are used to increase S_L due to this effect in the USA gas venting standards [68], but there is no procedure to take this into account in the European gas venting standards [106].

Andrews and Phylaktou [24] showed that for gases the K_G/P_i and S_L gas reactivity parameters are linearly related by eq. 3.10. They also showed that for reasonable values of S_L and adiabatic P_m/P_i the predicted values of K_G were in reasonable agreement with experimental K_G measurements.

$$\frac{K_G}{P_i} = 3.16 \left(\frac{P_{max}}{P_i} - 1\right) S_L E_P \qquad [3.10]$$

Where E_p is the constant pressure expansion ratio which is the unburnt gas to burnt gas density ratio. For dusts, E_p could be determined as the ratio of peak pressure to initial pressure in a closed vessel dust explosion [110, 112]. It is quite difficult to calculate expansion factor for dust as it is influenced by the water and ash content as well as the elemental composition of the dust. This approach was used in the present work. The key assumption in the derivation of eq. 3.10 is that the explosion flame speed is constant across the vessel diameter with no account taken of the rise in pressure, P, and temperature, T, in the later stages of the explosion. The change in S_L with T and P was computed by Bradley and Mitcheson [115] and the results show that the final value of S_L would only be 20% higher than the initial value which is a relatively small error. Kumar [116] has derived an equation similar to eq. 3.10 that includes the P and T dependence of S_L but give similar values to those from eq. 3.10. Sattar et al. [110] showed for the first time experimentally that K_G and S_L were linearly related as eq. 3.10 predicted, but only if both reactivity parameters were measured in the same explosion vessel. They showed that the ISO 1 m^3 vessel was the ideal vessel size to measure S_L and was the minimum size that made the common assumption of an infinitely thin flame to be valid for the closed vessel explosion technique. Sattar et al. also showed that the ISO 1 m^3 explosion vessel could be used for gas explosions to measure the constant pressure explosion laminar flame speed using arrays of exposed junction thermocouple to determine the flame arrival time. The infinitely thin flame front assumption then enables the laminar burning velocity U_L to be determined by eq. 3.11.

$$U_L = \frac{S_L}{E_P} \qquad [3.11]$$

Sattar et al. [110] used this approach to determine the maximum burning velocity of methane-air to be 0.42 m/s which they showed to be in good agreement with a wide range of other measurements using reliable techniques [102]. This approach was adapted for determining the laminar burning velocity of dust air mixture and is applied to a range of pulverised biomass in the present work, using the measured P_m/P_i in the ISO 1 m^3 vessel for E_p [98].

3.13.2 Laminar burning velocity of dusts

The most common method of burning velocity measurements is to use the vertical tube method with dust falling from the top and ignition at the bottom.

Proust and Veyssiere [117] showed that laminar flames could be achieved, but Andrews and Bradley [102] showed that this method did not give reliable values of laminar burning velocity for gas/air mixtures and the same is likely for dusts/air explosions. Improvements to the method were made by using the dust particle motion ahead of the flame to determine the gas velocity ahead of the flame, so that the burning velocity was the difference between the flame speed up the tube and the gas velocity ahead of the flame [118], a technique that Andrews and Bradley first used for gas flames in closed vessel explosions using a hot wire anemometer to measure the gas velocity ahead of the flame [102]. The dust burning results of Proust and Veyssiere [117] from this method showed considerable data scatter of the order of +/-100% and hence did not demonstrate a methodology that could be relied on for dust explosion reactivity characterisation. Their maximum laminar burning velocity results for maize starch was 0.3 m/s, but Wolanski [119] reported a value of 0.55 m/s for maize starch using a similar technique, but using a larger diameter tube. Proust and Veyssiere [117] also showed a very poor correlation between the K_{st} measured in the ISO 1 m^3 equipment and laminar burning velocity using the tube method.

Mazarkiewicz and Jorisade measured the maximum laminar burning velocity of cornstarch at 0.14 m/s. Nagy and Veritas [120] developed a method to use the Hartmann vertical tube dust explosion equipment to measure the maximum laminar burning velocity for a wide range of materials with maximum burning velocities in the range 0.02 – 0.1 m/s, which are very low values. Dahoe et al. [121] reported the maximum laminar burning velocity of cornflour as 0.63 m/s and Smoot et al. [122] determined the maximum laminar burning velocity of lignite as 0.31 m/s for 10 µm particles and 0.21 m/s for 33 µm particles.

Dahoe et al. (2002) established the efficient and reliable method for the determination of the laminar burning velocity. The laminar burning velocity was measured by ‘Laser Doppler Anemometry’ [121]. In this method, the burner was used to produce a stable flame of the cornstarch and utilizing a suitable parameter as ‘Markstein length’ that accounted the variation due to the stretch in the propagation of the flame. The Markstein length is the dust property and is fixed for a given dust flame. Due to insufficient knowledge of its dependence on the physical and chemical properties of dust, the theoretical and experimental determination of this Markstein length was not specific and need more work in accurately determining the laminar burning velocity [121].

Phylaktou et al. [123] measured the laminar burning velocity of several dusts, for the maximum reactivity mixtures, using the ISO 1 m^3 spherical vessel. They increased the ignition delay between the start of dust injection and the firing of the ignitor. The reference time delay is 0.6s after the start of air flowing into the vessel [111]. The ignition delay was increased in stages up to 4s delay, by which time the injection turbulence had decayed to laminar conditions. Unfortunately in most cases, before laminar conditions had been achieved the peak overpressure started to fall, indicating that significant proportions of the dust injected had fallen out under gravity. This then resulted in the concentration of the mixture that the flame propagated through varying with time. However, this method indicated that the laminar burning velocity for maize starch was 0.25 m/s, derived from their value for the laminar flame speed and their measured peak pressure and using Eq. 2. For biscuit flour the laminar burning velocity was 0.20 m/s, for a coal it was 0.17 m/s, for milk powder it was 0.14 m/s and for resin powder, which is mainly a hydrocarbon dust, it was 0.48 m/s which is typical of high MW hydrocarbon gas burning velocities. However, this method had the weakness of the result being an extrapolation of the curve fit of the laminar flame speed as a function of the ignition delay to infinite delay and although the above laminar burning velocity data are reasonable it is difficult to make a case for the absolute accuracy of this method of measurement.

Sattar et al. [110] developed an alternative method for using the ISO 1 m^3 dust explosion equipment for laminar burning velocity measurements, which has been used in the present work for pulverised biomass. This method determined the mean turbulence levels in the ISO 1m^3 dust explosions, for the standard ignition delay, using laminar and turbulent methane/air explosions to determine the turbulence enhancement factor and then applied this to the measured turbulent dust/air flame speeds to determine the laminar flame speed and then the laminar burning velocity was calculated with the expansion ratio determined from the measured peak to initial pressure ratio [98]. This work measured the maximum laminar burning velocity of cornflour as 0.55 m/s, walnut shell dust (an agricultural waste biomass) as 0.55 m/s and Kellingley coal as 0.17 m/s. Sattar et al. [110] also showed that measurements of K_{st} and U_L on the same ISO 1 m^3 equipment gave a good linear correlation between the measured K_{st} and U_L.

3.14 Role of turbulence

There are two types of turbulence in the explosion which are;

- Turbulence before combustion

Turbulence generated by the dispersion of the dust by some flowing medium (small effect on the dynamics of explosion)

- Turbulence after combustion

Turbulence generated in the unburnt mixture by the expansion of flame front due to the combustion (More strong effect on the dynamics of explosion)

The turbulence generated by the expanding flame in the unburnt zone has major influence on the dynamics of explosion and a little work is done to drive the expression for this type of turbulence. Alternatively, Instead of observing the change due to the turbulence generated after combustion, the burning velocity was examined.

The effect of the induced turbulence for dispersing the dust in the closed vessels was investigated on the basis of the turbulent to laminar burning velocity and the maximum rate of pressure rise. It was revealed from the experiments that the increase in the ignition delay results in the decay of pre-explosion turbulence and the severity of the explosion was reduced. The mixture of corn-starch-air and Methane air were tested in the 6, 26 and 950 litres closed vessel with the varying ignition delay [124]. It was determined that the combustion of corn-starch have the maximum explosion pressure rise close to the corresponding lean methane-air mixture (5-5.5%) at the low turbulence intensities (u'<1m/s) and to the corresponding rich methane-air mixture (>7.5%) at the high turbulence intensities. It was also observed that the effect of turbulence is significant in the corn-starch air mixture as compared to Methane air mixture [124].

Stoichiometric and thermodynamic considerations like adiabatic flame temperature are of limited use for combustible dust-air suspension as reactions are incomplete with some portion of the dust not participating in the flame propagation. Turbulence has a dominant effect in experimentally determining the burning rates of the dust explosion. The geometry and flame structure for laminar dust flames are not stable and poorly defined for burners as explained by Lee (1988). For cornstarch-air mixture, lowering the turbulence intensity in

the constant volume vessel reduced the explosion pressure indicating the less burnt mass [125] & [126].

Amyotte & Pegg (1989) observed higher burning velocity at higher turbulence levels lead to increased rates of combustion and reduce heat loss to the walls [127]. They demonstrated the quantitative effect of turbulence on the explosibility parameters of the dust explosion. The effect of ignition delay on the maximum rate of pressure rise for lycopodium dust of size approximately 30µm was presented for a series of ignition delays from 40ms to 900ms using dust concentrations of 0.1-1kg/m^3. It was observed that the

- Maximum rate of pressure rise decreases with increasing ignition delay for fixed dispersion pressure
- Higher air pressure from reservoir for the dispersion of dust results in the higher maximum rate of pressure rise for short ignition delay (40-180ms), approximately constant maximum rate of pressure rise at moderate ignition delay (180-200ms) and at further higher ignition delay (>200ms), it starts decreasing.
- The root mean square velocity which is a measure of turbulence decreases with the increase in the ignition delay.

For this work, a systematic approach was developed to see the effect of turbulence on the ignition properties in the Hartmann bomb. A parameter $K_{st}/K_{st,max}$ was also established to measure the turbulence decay parameter.

The trend of the particle falling freely based on the semi-analytical mathematical modelling in the dust propagating flame under the influence of various forces. The thermophoretic force has the key and dominating role as the particle approaches to flame leading to a stagnant zone where the particle velocity is zero and due to the strong thrust force, the particle velocity trend is reversed [128].

Serafin et al. (2013) used the modified Spherical apparatus 0.25m^3 to study the effect of turbulence on the explosion severity of the dust explosion. In this work, five dusts (Wheat flour, Brown flour, powdered sugar, Meant bone powder and Torula yeast) were utilized to see the effect of the turbulence on the explosibility parameters such as maximum pressure and the rate of pressure rise. It was experienced from the experimental results that the enhancing of the turbulence by increasing the speed of the stirrer placed in the Explosion vessel results in

the augmentation of the explosibility parameters. The effect of turbulence on maximum pressure is more pronounced for powdered sugar and the wheat flour and on maximum rate of pressure rise for all the dusts except meat bone powder. It was concluded that enhancing the turbulence for some dusts can double the explosion outcomes than that at the static condition. So, the design of the vent for the safe operation of the explosion tests in the laboratory and commercial scale should include the effect of the turbulence [129].

There are number of methods available for the investigation of the turbulence in the gas and solid dispersed cloud such as [73] (Among all these, the most versatile method is ‘Laser Doppler Anemometer’);

- Hot wire or hot film anemometer
- Laser Doppler anemometry
- Flow visualization by means of small particles (<1micron) as ‘markers’
- Flow visualization by thermal markers (Successive heating of gas volume by hot wires , Poor spatial resolution)
- Acoustic anemometer
- Electric discharge anemometer
- Cold wire anemometer

In the presence of turbulence, the uniformity of the dust concentration is affected due to the local variation and particle size distribution due to vortices [130]. As shown in Figure 3.13, the burning of solid particles in the vertical duct is accompanied under different phenomena. Suitable level of turbulence with good uniformity results in good combustion with less unburnt particles. The uniformity of the dust air dispersion has a significant influence on the combustion properties of the dusts as the ignition in the vertical tube without proper ignition delay may result in the discrepancy in the local variation of the uniformity which may results the under or overestimation of the ignition properties. This area is part of this research work and will be discussed later under the Hartmann results.

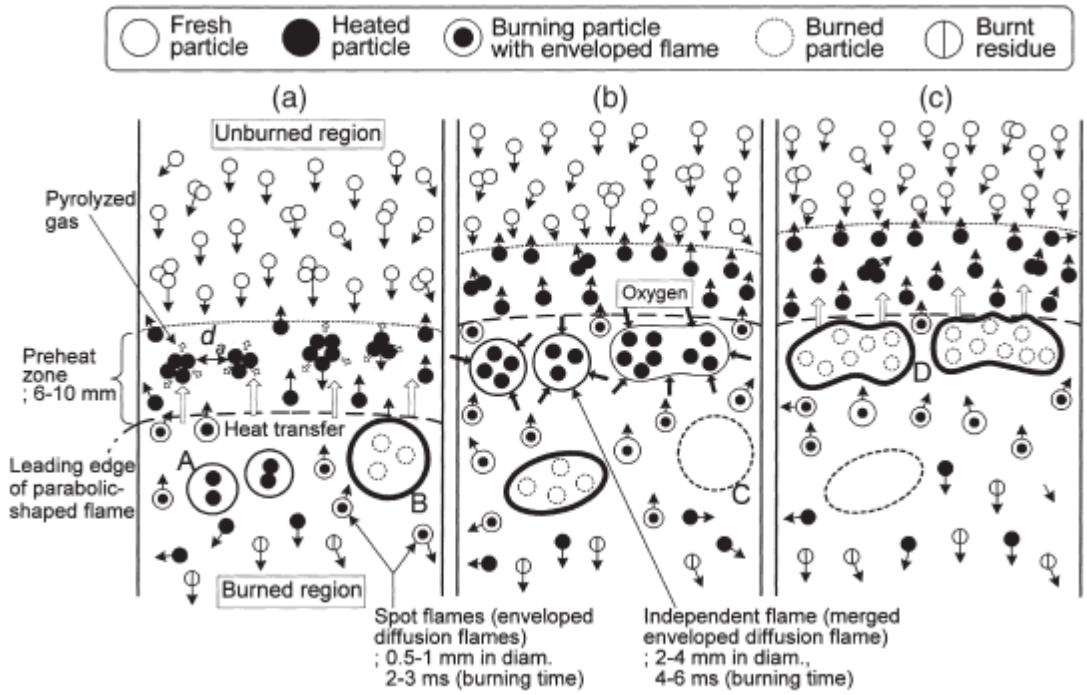

Figure 3.13: Flame propagation of lycopodium air mixture in vertical duct [131]

3.15 Effect of Oxygen concentration

Higher concentration of oxygen gives the higher maximum explosion pressure and maximum rate of pressure rise. As quoted by Eckhoff (2003), 'reduction in maximum explosion pressure is proportional to the reduction in the oxygen content, as would be expected from thermodynamic considerations'.

Pakistani biomass and coal were studied by TGA in the low (1%) and high oxygen concentration (3%) environment. It was found that the conversion of the biomass char and coal in the high oxygen concentration environment was higher [132]. The maximum explosion pressure was observed to fall much sharply at lower oxygen concentration than at higher oxygen concentration [70].

Similarly the oxygen enriched environment boosts up the explosion severity as demonstrated by the combustion of coal in the oxygen enhanced environment. The higher concentration of oxygen in the dust cloud lowers the minimum explosible concentration of the dust, the minimum ignition temperature, minimum ignition energy and enhances the peak explosion pressure, peak rate of pressure rise, speed of the combustion and the temperature of the propagating flame [133].

Mittal (2013) determined the limiting oxygen concentration of the coal dust using the 20 L explosion vessel. Different tests were performed by varying the concentration of the oxygen by the partial pressure method. The oxygen analyser was also used to verify the oxygen concentration. It was determined that the limiting oxygen concentration has a direct influence on the explosibility of the dust and the explosion severity can be suppressed by reducing the amount of oxygen with the enhancement of inert gas [84].

3.16 Effect of initial pressure

Cashdollar and Hertzberg (1985) used 20L explosion vessel to study the effect of initial pressure on the flame propagation of Polyethylene dust [134]. Initial pressure was tested from 0.5 to 2.5 bar and a linear dependence of initial pressure on the lean flammability limit similar to gaseous mixtures was observed.as shown in the Figure 3.14.

Garcia & Torrent (1998) studied the effect of initial pressure and the turbulence on the severity of the biomass dust explosion. It was inferred that the turbulence (higher injection impulse 2-3.5MPa depending on the concentration) has more vibrant role in enhancing the maximum rate of pressure rise in 1 m^3 vessel than the higher initial pressure (1-1.5MPa) [135]. Increasing the initial pressure with higher amount of dispersing air consumes more mass of dust.

Two dust deposits pot in series were introduced in this work to increase the air density for increasing initial dispersing pressure. For irregular shape and low density of biomass, the irregularities affected the flame front propagation due to inhomogeneous dust cloud formation.

It was also observed that at very high initial pressure, the rate of pressure was levelled off. This was due to increasing particles to particle closeness and high bulk density. High turbulence accelerates the movement of the particles resulting more interaction with the oxygen leading to fast propagation of flame even at high initial pressure. So a strong safety measures is needed to be established. The limestones and oxygen are the most influential parameters to impede and accelerate respectively the dust explosion [136].

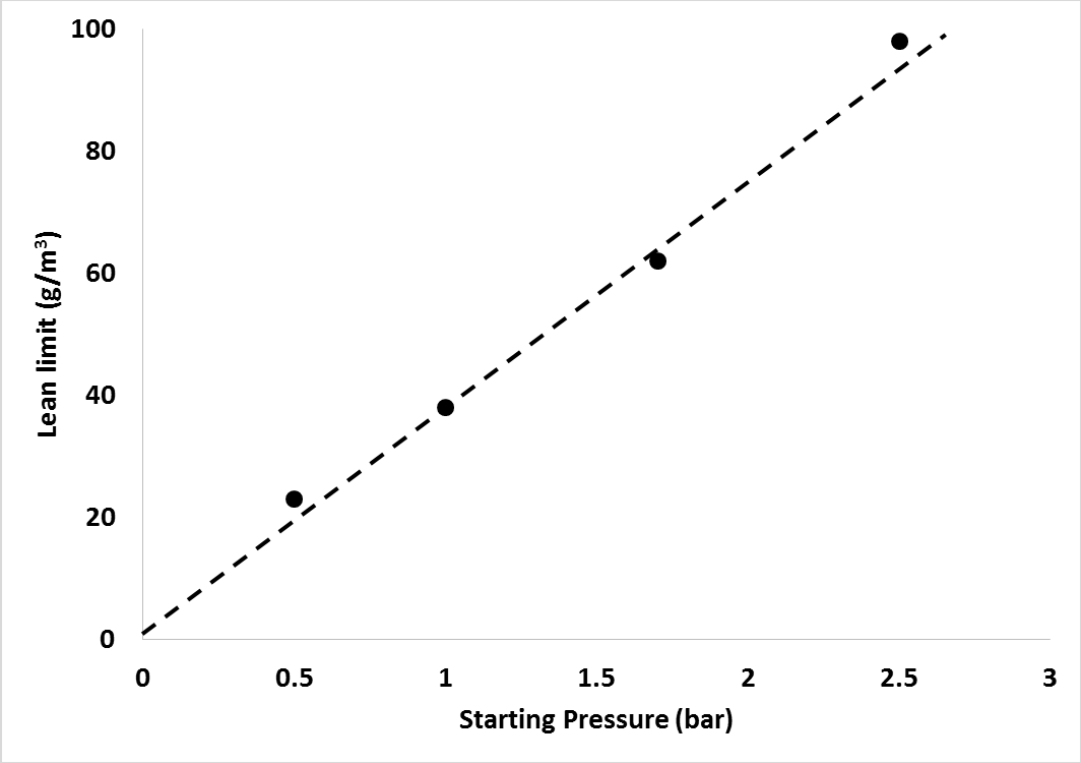

Figure 3.14: Linear dependence of MEC of Polyethylene dust with initial pressure [134]

3.17 Effect of moisture contents

The Hartmann bomb was used to investigate the effect of the moisture contents on the rate of pressure rise. It was observed that higher mass after certain concentration and the moisture contents, lower the rate of pressure rise with the same injection pressure. This was due to the poor dispersibility of the higher mass of dust with higher concentration and the agglomeration phenomenon due to the high moisture contents. It was concluded as the generalized statement that the correlation to study the effect of moisture contents on the rate of pressure rise does not reflect the genuine effect. It was because of the high influence of the turbulence with the variation of the ignition delay that affect the quality of the dust dispersion [137].

Yuan et al. (2014) studied the effect of moisture content on the explosion parameters [138]. Three coal samples of micron sized were tested on 20L Siwek vessel with 5Kj igniter as shown in Figure 3.15. It was found that increase in the moisture content directly influence in reducing the explosion parameters P_{max}, $dP/dt_{,max}$ and increasing the MEC. Coal samples with fine particle size distribution after moisture content of approximately 12.5% showed sharp

decrease in explosion sensitivity and severity whereas for coarse particle size distribution, there was a linear relationship of moisture content and explosion parameters. This was due to strong inter-particle forces among fine particles with increase in moisture resulting formation of agglomerate of large size demonstrated by SEM images [138]. Experimental findings are summarized in table 3.7 as shown below.

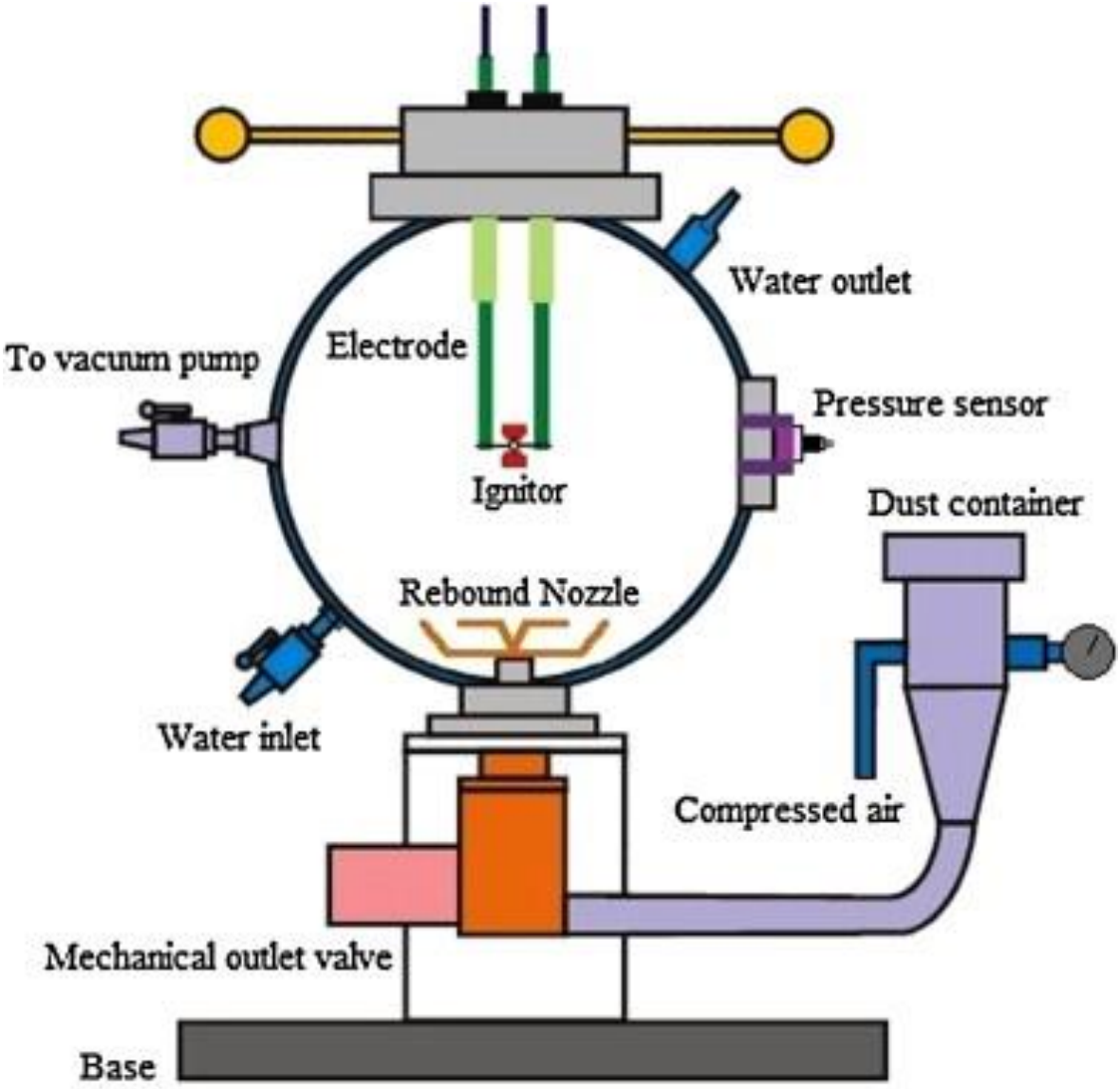

Figure 3.15: 20L Siwek explosion vessel [138]

Table 3.7: Effect of moisture content on explosion parameters for different sized coal samples for range of most reactive concentrations (500-700g/m^3) [138]

		500 g/m^3		600g/m^3		700g/m^3		
Coal dust	**Moisture content (wt%)**	**Pex (bar)**	**(dp/dt)ex (bar/s)**	**Pex (bar)**	**(dp/dt)ex (bar/s)**	**Pex (bar)**	**(dp/dt)ex (bar/s)**	**MEC (g/m^3)**
No. 1 43–75 µm	2.4	5	239	4.8	256	4.6	271	43
	5	4.9	211	4.7	241	4.5	248	51
	10	4.3	124	4.1	135	4	148	66
	12	3.5	84	3.3	93	3	102	–
	13	3	68	2.7	75	2	83	103
No. 2 75–125 µm	2.4	4.8	180	4.6	188	4.5	195	45
	5	4.6	168	4.4	174	4.3	180	55
	10	3.7	113	3.7	120	3.5	132	74
	12	3.6	92	3.4	96	3.1	105	–
	13	3.4	79	3	83	2.3	90	90
No. 3 125–550 µm	2.4	3.6	94	3.5	101	3.5	111	57
	4	2.9	68	3	75	3	87	75
	5	2.3	60	2.6	64	2.5	75	86

3.18 Effect of igniter and ignition energy

Cashdollar and Chatrathi (1993) measured the apparent lean flammability limits of gillsonite and bituminous coal using different ignition energies on 20 L and 1 m^3 vessels. The results as shown in Figure 3.16 were restricted to three data points for 1 m^3 vessel whereas there were six data points plotted using 20 L sphere. Minimum explosible concentration of the selected dust samples were measured to decrease with increase in ignition energies until a critical value is achieved after that ignition energy becomes irrelevant for MEC measurements. It was also noted that MEC were leaner using 20 L vessel compared to 1 m^3 vessel for the same ignition energy that was due to overdriven effect in the small 20L vessel later explained by Dahoe et al. (1996).

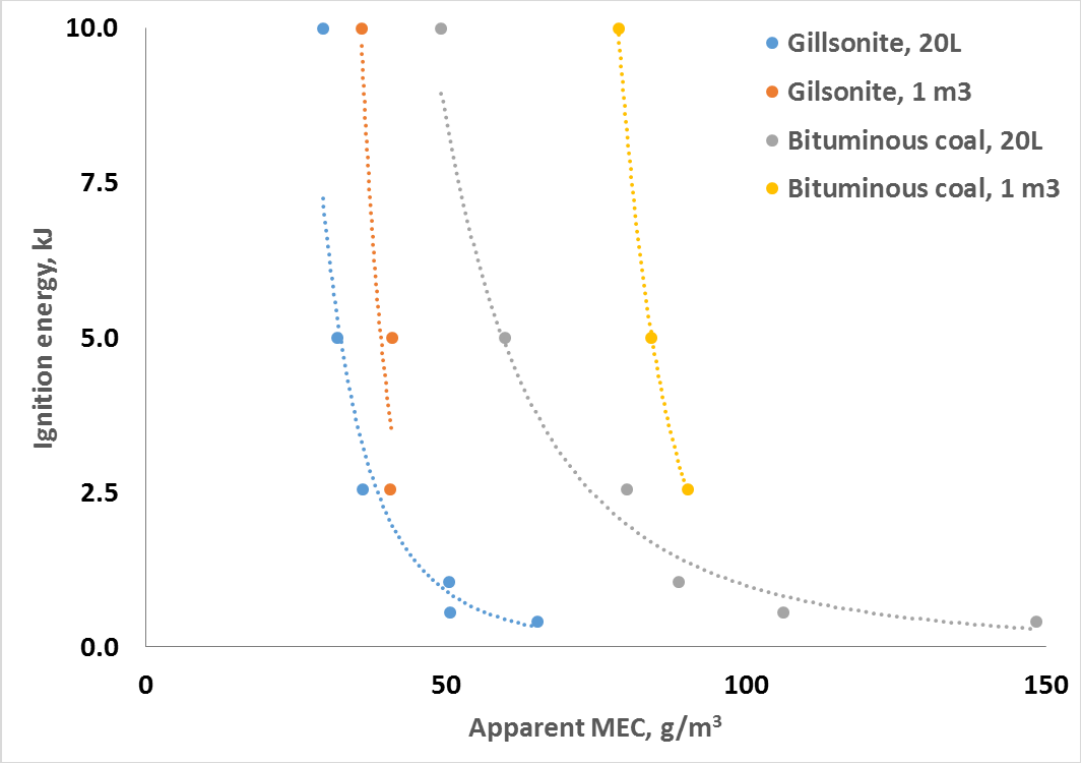

Figure 3.16: Effect of ignition energy on the measurement of MEC for gillsonite and bituminous coal using 20L and 1m³ vessels [139]

The accurate determination of the MIE has strong dependence on lower limit of ignition energy of the apparatus. Randeberg et al. (2005) established the most advance method for the determination of MIE using synchronized spark down to the order of 0.03 mJ [76].

Janes et al. (2008) studied the comparison of the measured minimum ignition energy obtained from MIKE 3 and Hartmann apparatus. The main factors affecting the minimum ignition energy are the delay between the dispersion of the dust and the spark over, dispersion method, spark characteristics (type, its duration and energy) and the nominal amount of dust/particles placed on the disperser. They concluded on the basis of experiments performed with a number of dusts (Polymer, biomass, coal, metals) using these two units that the minimum ignition energies obtained from MIKE 3 unit was equal or smaller than the Hartmann unit in the range of energies 1-10 mJ and above 100 mJ. So, it was concluded that the MIKE 3 unit was more effective and efficient in the discrimination of the dust on the basis of their ignition sensitivity. However, other parameters like particle size distribution, the method of dispersion, concentration in the region of ignition due to the varying turbulence by varying

the ignition delay are also the influential parameters for the determination of the minimum ignition energy [140].

The effect of the type of igniters and the ignition energy on the explosibility parameters were investigated by Gao et al. (2013) [141]. It was observed that the chemical igniters with different ignition energies overdrive the results whereas the electrostatic igniters of different ignition energies underdrive the results. Chemical igniters in comparison to electrostatic igniters act as booster in achieving the maximum overpressure quickly and have higher deflagration index. Ignition energies have direct effect on the measurements of the explosibliity parameters.

Kuai et al. (2013) pointed out the flaw in the European Standard to accommodate the effect of ignition energy in the explosion severity. A variation of the ignition energy offsets the accurate prediction of the explosion parameters results. The authors proposed that the explosion parameters should be evaluated at the critical ignition energy and for this, two methods were proposed; one was ‘flame thickness method’ and the second was ‘induction time method’ instead of relying on pressure-time graph. The estimation of the explosion parameters at this value of critical ignition energy gave the more reliable results. Inappropriate ignition energy have more pronounced effect on carbonaceous materials where the combustion takes place after the release of volatiles and ignition energy has strong dependence on the kinetics of release of volatiles [142].

3.19 Heat transfer mechanism in dust explosion

A radiative ignition model was developed theoretically for the solid fuel by Kashiwagi (1974). The effect of the in-depth absorption of the radiation and exposure time on the solid fuel was investigated. It was found that the role of gases have major influence in the ignition of the solid fuels. These pyrolysis gases have some activation energy related to the lower limit and the upper limit for ignition and beyond this domain, no ignition was predicted [143].

A thermal radiation theory for plane flame on a burner based on coal dust flame had been used. Some assumption were used that are;

- Unidirectional flow
- No mixing of the burnt particles with the unburnt mixture.

Heat liberated ahead of the flame by the heat transfer mode ‘radiation’ that is first absorbed by the dust particles then heat is lost from the dust particles to the ambient air through heat transfer mode conduction. The absorbed and loss heat results the ignition temperature of the dust to be achieved. The volatiles and non-volatiles contents of the dust were included for the stoichiometric calculations means the complete involvement of all the coal dust particles [69].

Proust (2006) explored some fundamental aspects related to ignition and flame propagation of dust clouds. In his work, it was revealed that the radiation energy has insignificant role in the propagation of the flame rather than this energy is lost in the combustion process. The propagation of flame by the heterogeneous burning (particles burning leading to pyrolysis) due to conduction phenomenon was suggested with a constraint of particle size less than 100 microns. This argument was verified by employing ‘Tomographic techniques’ as explained on the basis of characteristics time scale [117]. It was concluded that radiative heat transfer in the metallic dust flame propagation is a vital driving force due to extremely high flame temperature [144].

3.20 Explosion behaviour of the hybrid mixtures

The propagation of flame in the nicotinic acid-gas air hybrid mixture was studied in the open tube [145]. Stages of flame propagation was classified in four different phases. Initial phase 1 was spherical with the development of flame. Phase 2 was the propagating flame reaching the wall, phase 3 was the steady state flat propagating flame and the phase 4 was the oscillating flame at the end. It was concluded that development of flame in phase 1 without any significant effect of the turbulence depicted the laminar burning velocity and the phase 3 depicted the higher burning velocity with the significant influence of the turbulence. The phases 2 and 4 were ignored due to the wall effect and the venting effects. It was also concluded that the effect of turbulence needed to be accounted for the accurate determination of the stretched flame [145].

The sensitivity of the hybrid mixture on the explosion severity was investigated using modified 20L and Hartmann tube. It was observed that the hybrid mixture containing as low as 1% vol. explosive vapours were more sensitive than the pure dust cloud. It was found that introduction of the explosive vapour in the dust-air mixture results in the drastic change in shifting the rate limiting step from boundary diffusion to homogeneous gas phase reaction. However different

models (Bartknecht and Le Chatelier) proposed for interpreting the results due to these changes are not always conservative due to influential parameters [146].

The explosion behaviour of the hybrid mixture of nanometre sized carbon black particles and the propane gas was investigated using 20L explosion vessel [147]. Due to very fine particles, SEM reflected some agglomeration of the carbon black particles. This hybrid mixture was different than other hybrid mixtures as it was not ignited for the concentration of solid and liquid fuel lower than their flammability limits contrast to other hybrid mixtures. Incremental addition of the propane gas higher than the LEL to the carbon black particles resulted in the enhance explosion with less ignition delay time [147].

Khalil (2013) work rejected the null hypothesis that the severity of the Hydrogen-air mixture is always greater than the heterogeneous mixture of activated carbon-hydrogen and air having the same amount of hydrogen as in the binary mixture. He concluded that the hybrid mixture of Activated carbon-Hydrogen-air mixture have higher deflagration index than the respective binary mixture of Hydrogen and air having the same concentration of the Hydrogen. Therefore a more safety measure was needed to be applied for the hybrid mixtures [148].

3.21 Role of pyrolysis in dust explosion

The propagation of the dust flame is strongly dependent on the composition of the dust. It was experienced that the coal dusts containing volatiles less than 12.5% are non-explosive dusts. The biomass contains higher volatiles contents than coals and flame propagation initially supported by these volatiles, may build up sufficient heat to compel the char particles to be burnt in the explosion. The rate of volatile release of the dust vary with the particle size of the dust. Fine particles of dust contribute efficiently with fast release of volatiles due to high exposed surface area [69].

For actual modelling of flame propagation, the composition of the burning mixture and its variation with flame progression needs to be accounted. Release of volatile with the exposure of spark also alter the composition of the remaining dust. Dahoe (2000) and Dahoe et al. (2001) first demonstrated the variation of composition in the pre-heating zone due to liberation of volatile components just before the ignition [126, 149].

To express the burning rate of the dust, the key parameters are turbulent burning velocity and volumetric heat release rate. There are lots of difficulties in accurately defining and measuring the burning velocity, even for gases [150]. This is because of the difficulty in sharply identifying the area of the burning zone due to strain propagation of flame causing compression in the unburnt zone.

The rapid pyrolysis of the agricultural residues was performed at 800 and 1000^0C using free fall reactor [151]. It was concluded that reduction in the size of the crop dusts favour the higher heating rate with high yield of Hydrogen whereas low yield of solid char. Also cracking of the biomass residue, at higher temperature resulted higher volatiles and low char yield.

The surface morphological study of the explosion residues spotted the blowing holes confirming the release of volatile in the combustion of coal and Cork dust [152]. It was assumed that these volatiles were responsible for the propagation of the flame.

By proposing one dimensional single particle pyrolysis model, role of pyrolysis gases in the organic dust explosion was studied. Rate limiting steps for the combustion of the organic dust was strongly dependent on the particle size distribution and the combustion conditions as also validated by experimental approach using modified Godbert-Greenwald furnace for pyrolysis under argon atmosphere with gas chromatography as the gas analysing instrument. It was assumed that the generation of volatiles from pulverized combustion of biomass have major role in enhancing the reactivity of the biomass [153].

Flame propagation behaviour of Octadecanol dust was studied for different particle size distribution. The flame was visualized by high speed camera combined with band width filter. Photographic results showed that the flame developed by fines is regular shape and continuous due to high release of volatiles whereas the flame developed by coarse particles was discrete and discontinuous due to less release of volatile and burning of the solid particles. The colour of the flame also changed to blue with the burning of coarse particles showing the incomplete combustion of coarse size particles [90].

Burhene, Damiani & Aicher (2013) studied the influence of the biomass feedstock moisture contents and the pyrolysis temperature on the Pyrolysis gases and the yield of the char produced. The Norway spruce wood chips were

employed with an initial moisture content of 2.4%, 16.4% and 55.4% and pyrolysed at temperature of 500 and 800^{o}C in the tubular batch reactor. It was observed that the increase in the moisture content result in the higher yield of the condensable gases and low yield of char at both lower and higher pyrolysis temperature, However the gaseous products at the low pyrolysis temperature decreased with the moisture contents because of the loss of the CO_2 with the higher moisture contents going into the condensable gases whereas at the higher pyrolysis temperature, the non-condensable gaseous products increased with the feedstock moisture contents due to the higher generation of the CO. The surface features of the produced char were also analysed in terms of pore (meso and macro sizes) and BET surface area. It was observed that initial moisture contents have a little effect on the produced char reactivity. However, at the low pyrolysis temperature, the char showed higher reactivity but at higher temperature, the char reactivity decreased. This was assumed as might be due to the thermal annealing effect [154].

3.22 Protection techniques for the dust explosion

There are number of safety measure that can be taken to ensure the protection from the dust explosions such as;

- Discourage the formation of the dust cloud

This can be done by two ways;

  i. Depleting the amount of fuel in comparison to the oxidant to such an extent that it cannot support explosion

  ii. Depleting the amount of oxidant in comparison to the fuel to such an extent that it cannot support explosion

- Elimination of any ignition source in the area of dust cloud that is capable of igniting the dust cloud
- Apply some explosion protection measures to mitigate the ignition

  i. Explosion suppression (Inerting techniques)

  ii. Explosion containment (Explosion resistant construction)

  iii. Explosion relief venting (By means of rupture disc/pressure relief flaps etc.)

  iv. Explosion isolation measure

The most attractive and adopted protection method is to prevent the ignition of the dust cloud [69]. Other methods include the elimination of the ignition source and the reduction of the oxidizing agent to fuel ratio. The lowering of the oxidant to fuel ratio is achieved by introducing the inert material that dilutes the dust cloud so that, the level of oxygen does not support the flame propagation. The amount of inert use for the suppression of the dust explosion depends on the nature and composition of dust and the selection of the inerting material.

Two inerting gases such as nitrogen and carbon dioxide are the most likely to be available. These gases have little different inerting effect due to difference in density and the specific heats. The carbon dioxide is more effective as inert than nitrogen however; the difference in inerting capabilities is very small.

Beside the inert gas, there are number of diluents used to prevent dust explosion such as carbonates, bicarbonates, sulphates, halides, oxides and dioxides. The term diluent is referred to the inert dust. The diluent added to the combustible dust acts as heat sink and retards the build-up of heat necessary to sustain the dust explosion. It was observed that for the pure coal dust, the addition of 5% diluents can reduce the flame speed of up to 20 to 50% whereas the addition of 40% diluents can reduce the flame speed of up to 50 to 90% [69].

Kletz outlined some of the inherent safe process design techniques [155]. He is known as the father of the inherent safe process design concept. Example of the inherent safe operation is the flow of mass through silos and hopper instead of funnel flow (first central column flow then redial flow start to the centre) that is inherently safe operation.

Different parameters studied by various researchers and their findings were summarised in table 3.8.

Table 3.8: Different parameters Studied by Various Researchers

Scientist	Year	Equipment	Material	Effect of	Effect on	Results
Dyduch et al.	2016	20L, 1 m^3		Transient flow velocity	Explosibility characteristics	Large discrepancy in explosibliity characteristics from different experimental methods was due to difference in transient flow velocity as measured using Bi-directional velocity probe (BDVP).
Li et al.	2016	20L	Coal samples	Particle size and dispersibility	Explosibility characteristics	Small particle size and small dispersibility yielded more volatiles, that affect the flame propagation with higher P_{max} and $dP/dt_{,max}$.
Soundarara-jan et al.	1996	20L	Iron sulphide	Particle size	P_m and dP/dt	Higher the particle size, lower the explosibility characteristics and vice versa
Sweiss and Sinclair	1985	-	Natural and synthetic organic dust	Particle size	LOC	Limiting oxygen conc. decreased with decreasing particle size down to 100 microns and below 100microns, it became independent on d_p.
Wiemann	1984	-	Brown coal	Particle size	LOC	Small influence of dust particles size on LOC.
Addai et al.	2016	Modified Goldbert Greenwald furnace and	Combustible solids (Toner, Lycopodium, Starch, Niacin, brown coal) and	Inert concentration	Ignition sensitivity (MIT and MIE)	

		Hartmann tube	inert (Magnesium oxide, Sand and Ammonium sulphate			
Walther and Schacke	1986	20L ISO vessel	Polymer material	Oxygen content	Maximum explosion pressure	Max. permissible conc. for inserting cloud of polymer was independent on initial pressure over the range 1-4bara. Trend over this was represented by $P_{max}=0.35*P_0$ * (vol% of O_2)
Hartmann	1948	Godbert-Greenwald furnace	Pittsburg coal dust<74micron	Oxygen content	Minimum ignition temperature	Increase in MIT with the reduction in the vol % of oxygen.
Ballal	1980		Various materials(Ti, C, Al, Mg) of mean particle diameter of 45µm	Oxygen content	Minimum electric spark ignition energy	Increase in the oxygen content resulted the smooth decrease in the minimum ignition energy
Glarner	1948		Melamine, Pea Flour, Lycopodium	Oxygen content	minimum ignition energy	As the reduction in oxygen content approached the limit for flame propagation, a much steeper rise in MIE was observed.
Zabetakis	1965		Gaseous HC in air	Initial temperature	MEC	Linear relationship between ignition temperature and minimum explosible concentration was proposed.
Wiemann	1987	$1m^3$ closed vessel with 10 kJ chemical igniter	Peat, Beech, Coals, Methyl Cellulose	Initial temperature	MEC	Reduction of ignition temperature resulted in the increase in the MEC

Glarner	1983	20 L vessel with 10 kJ igniter.	Coals, Lycopodium, Melamine polymer	Initial temperature	MEC	Reduction of ignition temperature resulted in the increase in the MEC
Glarner	1984		Lycopodium, Maize, Starch,Mud,Pea flour, Melamine polymer, Cellulose Herbicide.Oye C	Initial temperature	Minimum electric spark ignition energy	Decrease in initial temperature of dust cloud resulted in the increase in MIE (A common convergence point was at 100^{o}C and 0.088mJ is indicated for organic materials.)
Wiemann	1987	1m^3 closed vessel	Bituminous coal	Dust concentration ,Initial temperature, Initial pressure	P_{max} and dP/dt	**1)** Low temperature resulted reduction in P_{max} due to the reduction of O_2 conc. per unit volume of dust cloud at given P_i. **2)** The trend for dP/dt showed the involvement of complex kinetics. **3)** Peak P_{max} & Dust conc. giving peak pressure was proportional to the initial pressure
Walther and Schacke	1986	20L	Polymer material	Initial pressure	P_{max}	Increase in the initial pressure approximately resulted in the linear increase in the peak pressure.
Bartknecht	1978	Const. volume vessel	Starch	Initial pressure	P_{max}	Increase in the initial pressure approximately resulted in the linear increase in the peak pressure.

Pedersen and Wilkins	1988	15 L closed bomb	Sub-bituminous coal	Initial pressure	P_{max} and dP/dt	Approximately linear relationship (linear increase) was predicted.
Hertzberg and Cashdollar	1988		Coal,Polyethylene and Methane	Initial pressure	MEC	MEC increased with increasing the initial pressure. (More increase with coal, Almost similar change of Polyethylene and Methane)
Engler	1885	0.25 m^2 Wooden explosion box	**Hybrid mixture,** Charcoal, Methane	vol % of gas	ignition sensitivity	Addition of 2.5 vol % of methane in charcoal dust that is lower than the lean limit; resulted explosion.
Reeh	1979		**Hybrid mixture,** Coal dust, Methane	vol % of gas	volatiles of coal for flame propagation	Critical minimum content of volatiles requirements was decreased with the addition of Methane. Flame propagation needs 14% volatile with no methane, 13% volatile with 1% methane, 12% volatiles with 2% methane and only 9% volatile for 3% methane.)
Cardillo and Anthony	1978		**Hybrid mixture,** Propane, Polypropylene, Polyethylene and Iron	vol % of gas	MEC of dust	An empirical correlation was developed relating MEC of dust and propane. It was observed that addition of 1%propane resulted in the reduction in iron conc. from 200 to 100g/m^3.
Franke	1978		**Hybrid mixture,** Methane, coal and air	vol % of gas	MIE	Appreciable reduction in MIE of the order of 100 was

						observed with the addition of methane from 0% to 3%.
Pellmont	1979		Hybrid mixture, Propane, PVC, Polyethylene, Cellulose and Hansa Yellow.	vol % of gas	MIE	Linear decrease in MIE with increase in vol % of propane.
Foniok	1985		Hybrid mixture, Methane, Coal	vol % of gas	MIE	Reduction in MIE with the addition of gas. (A reduction of the most sensitive concentration of coal (volatiles=31%) from 750 to 200g/m^3 was observed with the addition of methane from 0 to 3.5 %.)
Nagy and Portman	1961	28 L closed vessel	Hybrid mixture, Coal, Methane	2vol% of methane	P_{max} and dP/dt	Hybrid mixture resulted the high P_{max} and dP/dt
Ryzhik and Makhin	1978		Hybrid mixture, Coal, Methane	vol % of gas	Ignition behaviour	A reduction of the induction time was observed for the ignition of the hybrid mixture.
Reeh	1978		Hybrid mixture, Coal, Methane	vol % of gas	Explosion violence	Influence of methane addition on the explosion severity was significant at the initial phase of explosion.
Bartknecht	1978		**Hybrid mixture,** PVC dust, Methane	vol % of gas	Explosion violence	High violence as the vol % of methane was increased.
Dahn	1986	20 L closed bomb vessel	**Hybrid mixture,**Xylene, Toluene, Hexane and Waste dust	vol % of gas	Explosion violence	High vol % of gas resulted high violence of the explosion

Chapter 4 EXPERIMENTAL METHODOLOGY

This chapter focuses on the techniques employed for the chemical characterization of the samples. Different analyzers techniques are described in detail with the methodology adopted. Different analyses are performed include Ultimate analysis, TGA proximate analysis, Bomb calorimetry, Bulk and true density, Particle size distribution, BET surface area, Ash characterization and Scanning electron microscopy (SEM). Some unit operations like sieving and milling were also performed and explained briefly.

Testing of the biomass crop residues was performed on the modified Hartmann dust explosion tube and modified ISO 1m^3 vessel. The modified Hartmann tube was used for the measurements of the minimum explosible concentration, rate of pressure rise and flame speed. The distribution and development of the flame was also monitored, frame by frame, using a high speed camera. The modified Hartmann tube was also operated for different ignition delays in combination with photographic imaging. Detailed experimental methodology of the modified Hartmann tube is presented to measure the reactivity of the solid dusts.

ISO 1 m^3 vessel was used for the measurements of explosibility indices such as maximum explosion pressure relative to ambient atmospheric, deflagration index 'K_{st}', turbulent, laminar flame speed and burning velocity. Complete analysis of the post explosion residue was also performed and the results were compared with the raw samples to study the flame propagation mechanism. This ISO 1m^3 vessel was used with different calibrated dispersers due to the inability of the standard C ring disperser to effectively disperse the fibrous biomass dusts. A calibrated hemispherical disperser was also utilized to study the effect of particle size on the reactivity of dusts as it has the same method as Hartmann for dispersing the dust from the open hemispherical cup placed inside the vessel at the bottom of the vessel. Experimental methodology for the modified ISO 1m^3 vessel along-with the calibration procedure of hemispherical disperser was explained in detail.

Finally the significance of the modified Hartmann tube for minimum explosible concentration measurement was explained in comparison to other experimental methodologies. It was concluded that the modified Hartmann tube gives good resolution as that of gas flammability testing for the measurement of minimum explosible concentration than the modified ISO 1m^3 vessel. However, the

ignition delay affects the measurement of reactivity and an optimum ignition delay for the fine fraction of biomass was found to be in the range 50-120ms.

4.1 Raw and treated samples tested

Biomass crop waste were used primarily for this research work. However some woody and treated biomass samples were also tested and compared with the raw samples. Most of the agricultural waste samples including sugarcane bagasse, wheat straw, rice husk, corn cob and peanut shell were sourced from Pakistan based on the higher production of their respective crops. Some portion of these agricultural wastes are used as food for cattle however a big residual portion is left on land as waste and disposed without making use of it. Some wood pellets that are the feedstock of boilers were also tested using modified Hartmann tube. A 20kg sample of steam exploded pine wood pellets was provided by Zilkha biomass energy along-with a small portion of its raw pine wood (10g) for Hartmann testing. Also a 15kg sample of mixed woods containing spruce, fir and pine with its torrified sample were provided by Renewable fuel technologies for testing on modified ISO $1m^3$ vessel. All these samples were milled and sieved to specific sizes (Listed later in table 4.2) before testing for explosibility characteristics. A detailed list of biomass and its treated samples with their origin/suppliers is shown in table 4.1.

4.2 Chemical characterization

Selected solid samples were characterised for elemental, TGA proximate, Particle size distribution using Laser diffraction technique, Calorific value using bomb calorimetry, bulk and true density. Some crop residues were also analysed for the ash characterisation using X-ray flouresence technique. Scanning electron microscopy was also performed of the raw and post explosion residue samples. Stoichiometric concentration were also calculated based on elemental and TGA analysis in terms of Air to fuel ratio by mass.

Table 4.1: Biomass and treated samples for reactivity measurements

Sample	Origin/Supplier	Specifications (As received)
Bagasse	Pakistan (Local plant)	<1 mm
Wheat straw	〃	<1 mm
Rice husk	〃	<1 mm
Corn cob	〃	<0.5mm
Peanut shell	〃	<0.5mm
Pine wood pellets	Blazer wood, Clifford Jones Timber, UK	4-20 mm
HW Sawdust wood pellet	Duffield wood pellet, Yorkshire, UK	4-20 mm
Construction wood waste	Dalkia wood pellet	4-20 mm
Raw pine wood chips	Zilkha biomass energy	
steam exploded pine wood	〃	4-20 mm
Raw SPF wood mixture	Renewable fuel technologies	<3 mm
Torrefied SPF wood mixture	〃	<3 mm (302.9^{o}C, 7min)

4.2.1 Ultimate analysis

The elemental analysis of biomass crop residues was carried out using a Flash 2000 Thermo Scientific Analyser. It consisted of a reactor in which the small amount of sample (< 4 mg) was burnt at 1800°C and converted to the respective combustion gases like CO_2, H_2O, NO_2 and SO_2. These combustion gases were then passed through the chromatographic column using carrier gas (nitrogen) where they are separated before passing through a thermal conductivity detector (TCD) and a flame photometric detector. Different elements were quantified with the output signal proportional to the concentration of the elemental oxides present in the mixture. The results were obtained as a percentage of individual elements with oxygen found by subtraction method using the following eq;

$$\%O = 100 - (\%C + \%H + \%N + \%S + \%Moisture + \%Ash)$$

Each sample was tested in duplicate provided the percentage deviation <5% and the average of the two readings was taken. Calibration of this Thermo Scientific flash 2000 was routinely done using standard samples of known elemental analysis.

4.2.2 Proximate analysis

Proximate analysis was carried out using a Shimadzu TGA-50 thermo gravimetric analyser. It consisted of a mass balance attached to a ceramic sample pan in a furnace. It recorded the weight loss with time and temperature that helped in quantitative determination of the moisture content, volatiles, fixed carbon and ash contents. The release pattern of a material within three stages mentioned in Figure 4.1;

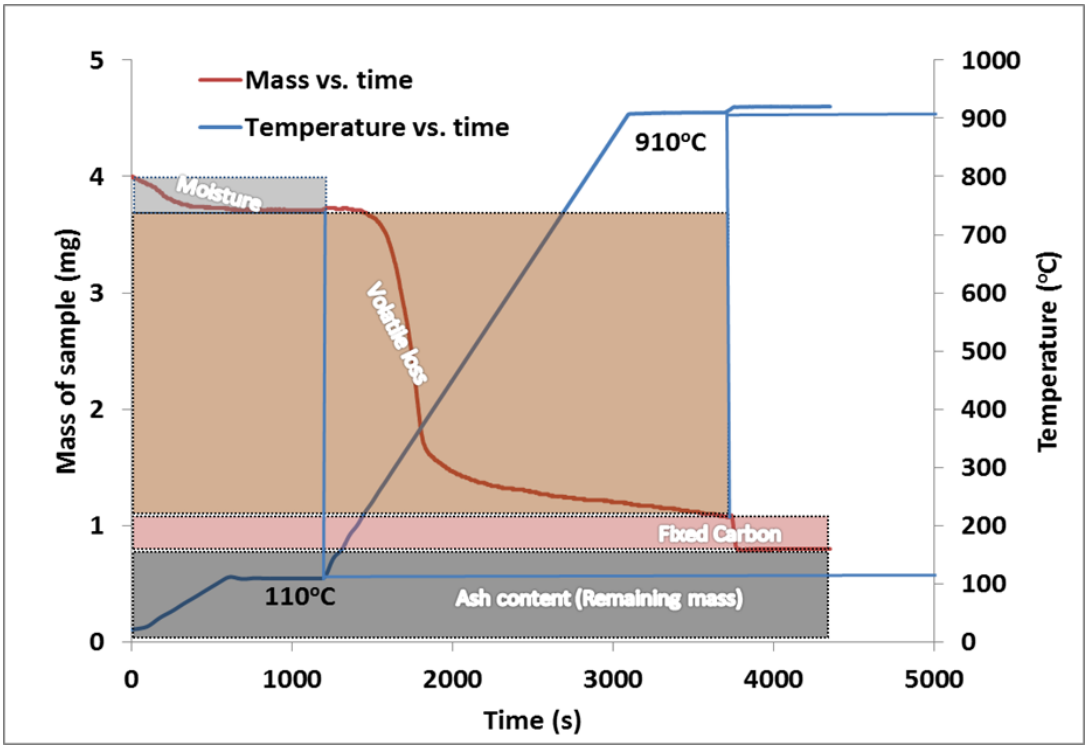

Figure 4.1: % Weight loss and temperature vs. time: TGA plot

A temperature program was set for the TGA analysis as;

- The sample was heated up under a nitrogen environment from ambient temperature to 110^{o}C at the rate of 10^{o}C/min and maintaining it at 110^{o}C for 10 minutes. This results in driving off the moisture content from the sample, giving the mass of moisture content in the sample.

- The temperature was then heated further at a rate of 25^{o}C/min up to 910^{o}C with a hold time of 10 min to release the volatile loss.

- After this, air was introduced, to completely burn out the remaining sample. This mass loss here was known as the fixed carbon content of the material.

- The remaining inert material left after this was the ash content (Calculated by difference method).

This TGA equipment was operated with a relatively slow heating rate and this might give a slower volatile release than that of actual flame heating. The sample to be tested was also small, in a crucible and packed together, producing more of a layer than particles, all of which may underestimate (reduce) volatile release. However, existing methods for determining the volatile content of coal or biomass also involve slow heating rates and so the results are comparable with other measurements.

4.2.3 Calorific value by Bomb Calorimeter

A Parr 6200 Oxygen Bomb Calorimeter was used for the determination of gross calorific value. Calorific value was measured by comparing the heat released from the sample with that of standard material. A representative sample of nearly 1g was first pelletised using Specac Hydraulic Manual press. This pellet was then placed in the small crucible that was held in the bomb head. A loop of fused wire placed above the sample without touching the sample and crucible. The bomb head was secured with the bomb cylinder and screwed tightly with no air leakage. Bomb was then filled with oxygen to a pressure of 25 bar and placed in the chamber in the calorimeter containing 2kg water with a thermistor and stirrer in the water. The lid of the bomb calorimeter was then closed and ignition activated through the fused wire. Sample was burnt in a high-pressure oxygen atmosphere in a metal pressure vessel or bomb.

The energy released by the combustion is absorbed within the calorimeter and the resulting temperature change was recorded and used to measure the

heating value of sample. The bomb calorimeter was routinely calibrated using ten measurements of standard benzoic acid pellets of known calorific values.

Calorific values were also calculated for biomass samples based on elemental analysis using OLS correlation with percentage errors less than 5%;

$$CV\ (kJ/kg) = 1.87\%C^2 - 144\%C - 2802\%H + 63.8\%C\%H + 129\%N + 20147$$

Where %C, H and N were on as received basis.

4.2.4 Particle size distribution

The particle size distribution was performed on a Malvern Mastersizer 2000, using the laser diffraction technique. The range of particle size distribution was from 0.1-1000 µm. Small amount of sample was first well mixed in a suitable medium (normally deionised water) with few drops of reagent 'IGEPAL' if necessary to avoid the formation of large clumps. This well mixed mixture of sample was added in the dispersion unit which is fitted with a stirrer and an optical lens. The particles in the cell were passed through a focused laser beam which scatters the light at an angle that is inversely proportional to the size of a particle. This angular intensity of the scattered light is measured by a series of photosensitive detectors. The stirrer was set to a rotating speed of 2000 rpm for better dispersion. The laser beam was passed through the dispersion and the map of scattering intensity versus angle was used to calculate the particle size. Measurements of particle size distribution were taken for 10 runs with three repeats giving a total of 30 measurements. Particle size distributions were measured in terms of d_{10}, d_{50}, d_{90}, $d_{3,2}$ and $d_{4,3}$ as the average of these 30 runs. Here d_{10}, d_{50} and d_{90} show the average particle sizes of the 10%, 50% and 90% of the cumulative volume respectively whereas $d_{3,2}$ and $d_{4,3}$ show the surface mean and volume mean diameters respectively.

4.2.5 Bulk and true density

Bulk and true densities of solid fuels are important properties to consider for their transportation. For the measurement of bulk density, a measuring cylinder of around 25 ml was used. The empty cylinder was first weighed after cleaning thoroughly. Solid fuel in powder form for less than 63µm fraction was added in this cylinder gradually with gentle tapping of the cylinder until it was filled to 25 ml. After filling the cylinder to 25 ml, the mass of the cylinder with solid powder

was measured again and the net mass of solid powder was calculated after subtracting the empty cylinder mass. This tapped mass of solid powder when divided with 25 ml volume gave the value of bulk density. Each sample was repeated ten times and the average value was considered as bulk density with a percentage error less than 10%.

True or particle density is known as the actual particle density excluding spaces. A micromeritics AccuPyc 1330 gas displacement pycnometer was used for the true density measurement for less than 63µm fraction. The unit contains a calibrated cell that was filled with powdered. This cell was then pressurised causing the compression and then the pressure was released. This process was repeated couple of times and the average value of actual true density was displayed using the actual particle volume excluding the void spaces of the measured mass.

4.2.6 BET surface area

Surface areas of the solid fuel plays an important role in their reactivity. Higher surface area results in more interaction of the oxidizing agent with particles facilitating the oxidation reaction. A Micromeritics Tristar 3000 surface area and porosity analyser was used. Sample of around 0.3g was first filled in a clear sample tube using a flexible tube to avoid particle deposition on the wall of the sample tube. The nitrogen flow needle was placed in the sample tube after pre-set degassing temperature of 120^{o}C in the degassing Flow Prep 060. After 4 hours, the sample tubes were weighed again to measure the net degassed mass of the respective sample. These sample tubes were then attached using fittings with the main Tristar unit after filling the 4 L Dewar with liquid nitrogen. Sample name and net mass of the degassed sample were entered for the corresponding sample tube pot. The unit was then started to measure the BET surface area, pore volume and pore diameter. This unit cools the sample using liquid nitrogen and allows inert gas to adsorb on the particle surface. Number of gas molecules adsorbed were then plotted against actual to saturation pressure of the adsorbed gas. BJH adsorption and desorption isotherms were plotted and based on BET calculations, the surface areas, pore diameter and pore volume of the respective samples were calculated.

4.2.7 Ash analysis

- **Ash formation**

An empty dish was heated in the furnace to (550 ± 10) °C for at least 60 min. The dish was then removed from the furnace. It was allowed to cool on a heat resistant plate for 5 to 10 min and then transferred to a desiccator without desiccant and allowed cooling to ambient temperature. When the dish was cooled, weighed to the nearest 0.1 mg and recorded the mass. Then known mass of material was placed over the empty dish and put in the muffle furnace after weighing. The temperature was first raised to 110^{o}C and waited for enough time until sample was fully dried. The percentage moisture content was calculated. Then temperature was increased to 550^{o}C and gave a minimum time of 120 minutes. After this the dish was removed and placed in the desiccator for 5-10 minutes. Weighed the burnt (ash) material with the dish and ash on dry basis was determined by the following formula;

$$A_d = \frac{(m_3 - m_1)}{(m_2 - m_1)} \times 100 \times \frac{100}{(100 - M_{ad})} \qquad [4.1]$$

Where

m_3= Mass of ash plus dish

m_2= Mass of dish plus test sample

m_1= Mass of an empty dish

M_{ad}= %age moisture contents of the test sample

- **Furnace method for ash fused beads and XRF for ash characterisation**

The following procedure was adopted to characterize the ash compositions.

‘Weigh 0.5g ± 0.0005g of standard or sample ash (ground to pass 100 µm) into a Pt/Au crucible, add 5.0g ± 0.005g of flux, and 0.05g lithium bromide.’

Mixed these dry ingredients and placed in the dish. Heat the mixture in a furnace at 1250^{o}C with continuous swirling after 3, 6 and 9 minutes. After 9 minutes, the empty casting mould was placed in the furnace to preheat it before placing the molten mixture in it. Then after 3 minutes, the molten sample was poured into the casting mould ensuring the lip of the fusion dish just touches the surface for complete transfer. This casting mould was then placed in the heat sink for about 5 minutes. The molten mixture started solidifying forming a disc that was removed from the casting mould with gentle tapping. If there were any cracking

or crystallisation observed, the whole process was repeated with different proportions having higher amount of flux to 7.5g ± 0.005g as mentioned in the established procedure.

The XRF technique utilizes the X-ray beam to remove the inner orbital electron of the specific element that makes the element unstable. Specific photon energy of specific intensity is released when the outer orbital electron is shifted to the inner orbit to fill the gap of missing electron. The intensity of the photon and number of photons of specific fluorescent radiation were utilized to detect and quantify the elements in the ash. It was found that crop residue biomass samples showed higher mass fraction of silica with the major contribution in the Rice husk samples and remaining elements with varying proportions in the different biomass.

4.2.8 Scanning electron microscopy

A Carl Zeiss EVO MA15 Scanning Electron Microscope was used to study the surface morphology of the raw and post explosion residue samples from modified $1m^3$ vessel. Solid dust sample was placed on the stub using double sided sticking carbon tab. These stubs after placing dust are brushed to remove the weakly attached dust particles. To prevent the excessive charging on the solid particles, the sample stubs were placed in Emscope SC coating unit for gold coating before projecting the electron beam onto the sample for SEM imaging. These gold coated stubs at the different samples were then placed into the unit sample holder using small screws. After this, a high vacuum was created by lowering the pressure to <10mbar and an electron beam was focussed onto the sample. After adjusting the resolution and brightness for the specific working distance, the static images were captured for different magnifications focussing different areas of sample. The dust holder was then moved for the next sample stubs and the surface morphological study was performed for the other sample. This process was continued until all the samples images were captured and saved for different magnifications using specific settings. SEM images for post explosion residue in comparison to the raw sample help to study the mechanism of flame propagation.

4.3 Sieving & Milling

An analytical Sieve Shaker was used to separate the particles on the basis of their sizes. Different mesh # sieves were arranged in descending order from

bottom to top i.e. smaller mesh size sieve was at the top and highest mesh size sieve was at the bottom above pan. This stack of sieves was then fixed on the Analytical sieve shaker vibrating surface with the tightening screws. A mixture of biomass was placed on the top most sieve leaving 1/3rd space for free movements of particles. The suitable vibrating speed and time of sieving was set for the distribution of the respective mixture into varying size fractions. After this sieving time, different sized fractions were collected on each sieve with the size smaller than the pore size of the upper sieve and larger than the pore size of the lower sieve on which it resides.

The milling was performed prior to sieving for the as received selected biomass samples on a Shredder unit cutting mill in the Geography Department to reduce the size lower than 500 µm. Some samples were further milled in the ultrafine grinder to less than 63 µm.

Different raw and treated biomass samples were prepared for different size ranged fractions as shown in the table 4.2 below, with different colours scheme, to be tested on the modified Hartmann tube and the 1m^3 vessel. The complete concentration profile for different size range fractions on the modified 1m^3 vessel could not be drawn due to limited amount of dust samples.

Table 4.2: Sieved sizes of the selected samples tested on the modified Hartmann tube or/and modified 1m³ vessel

Substances	Size fractions used 'µm'								
	<63	**63-75**	**63-150**	**63-500**	**75-150**	**150-300**	**300-500**	**<500**	**<1000**
Bagasse (B)									
Rice husk (RH)									
Wheat straw (WS)									
Yellow pine wood (YPW)									
Steam exploded wood (BP)									
Corn cob (CC)									
Peanut shell (PS)									
Pine wood pellet (Blz)									
HW sawdust (Dfl)									
CWW 1 (Dk 1)									
CWW 2 (Dk 2)									
SPF raw									
SPF torrefied									

Hartmann tube
ISO 1m³
Tested on both

4.4 Explosibility test using the modified Hartmann tube

There are a number of systematic approaches for the determination of the explosibility parameters like Hartmann, 20L sphere and 1m³ vessel. The modified Hartmann tube as developed by Huescar Medina et al. (2013) and refined further in this work as the most appropriate approach for biomass dust that are difficult to characterize on the standard ISO 1m³ vessel due to dispersion issue. The modified Hartmann is 322mm long and 61mm inside diameter vertical tube, closed from the bottom as shown in Figure 4.2 and 4.3 as schematic diagram. The confinement was provided by covering the top end with a special Aluminium foil (99% purity) of 0.020mm thickness fixed with a locking ring. The three thermocouples at distances 50mm, 100mm and 150mm from the electrodes were fixed to measure the time of arrival of the flame. A pressure transducer was located at the top before venting to record the pressure. The continuous arc was activated by the electrical spark box. The

injection pressure of air was lifted up to 7 barg as it gives the good repeatability results. It was reliably used for the measurements of the minimum explosible concentration after setting a reasonable criterion of detection of flame to 100mbar pressure or/and 100mm distance from ignition point. The results obtained were comparable with the standard ISO $1m^3$ vessel with little repeatability errors.

4.4.1 Repeatability of the tests and the explosion criteria

As shown in Figure 4.4, the pressure of the air without any dust goes to maximum 0.36bar using a pre-set of 7bar dispersion pressure through the small reservoir of 50ml in the pressure line. Aluminium foil used as a venting disc was confirmed to have consistent bursting pressure for a number of repeat tests. As Figure 4.11, displays the three repeat tests of the same concentration in comparison to air giving a consistent rise in pressure with an average bursting pressure of 1.53 bar of the venting disc. Explosion criteria was based on the resemblance with the criteria of the lean flammability limit of gases and flame detachment. High speed video photography showed that the detachment of flame was supported with a clear pressure rise of 100 mbar and detection of flame by thermocouples to 100 mm distance. So, it was considered to use the explosion criteria as flame propagation to at least 100 mm distance or/and the pressure rise to 100 mbar or above due to explosion.

Figure 4.2: Modified Hartmann dust explosion tube

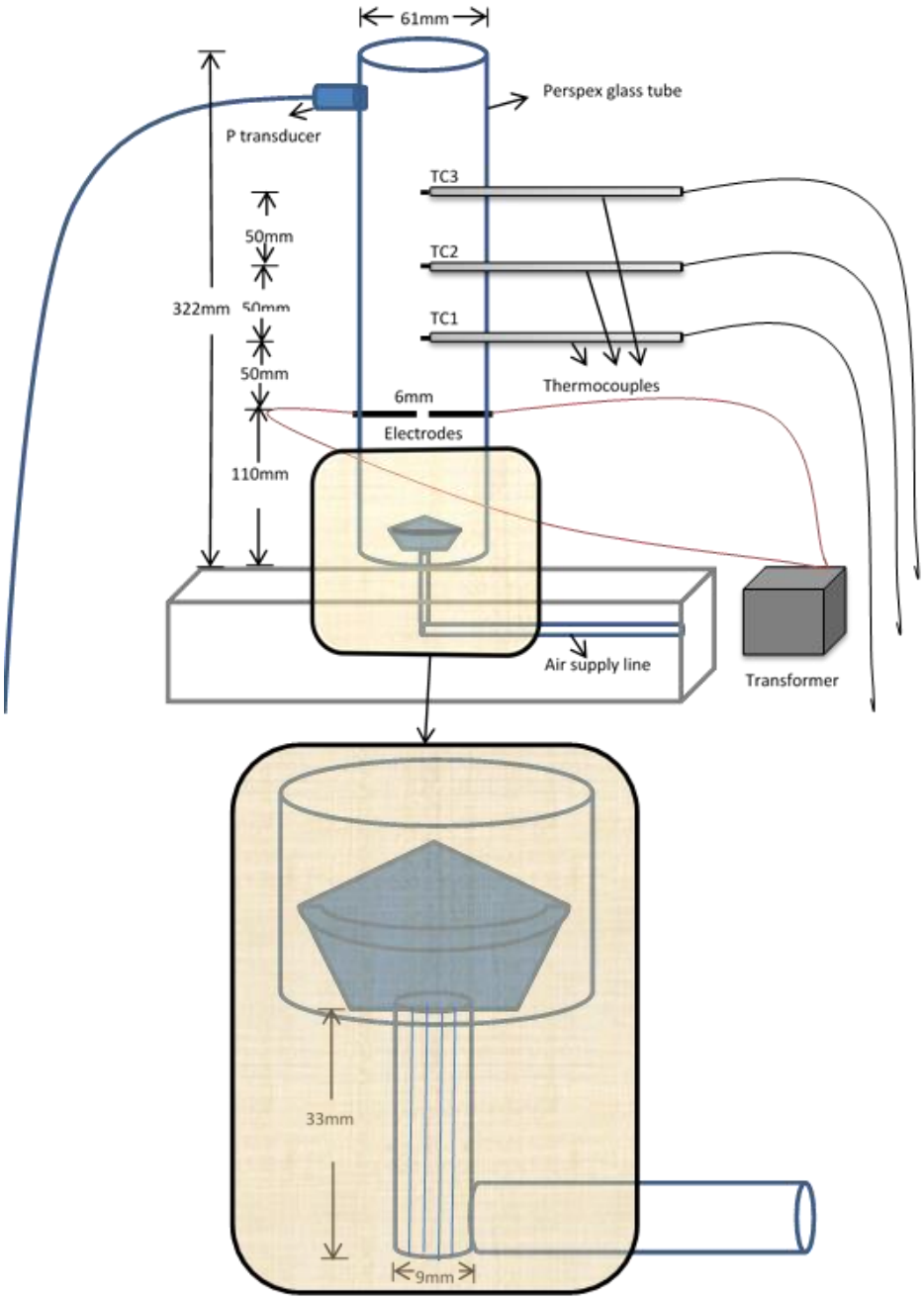

Figure 4.3: Schematic diagram of modified Hartmann dust explosion tube

The reactivity of the dust was measured with the rate of pressure rise from the Pressure-time trace and flame speeds using a linear array of three thermocouples above the spark. For the three repeated tests, the rate of pressure rise results were measured in the last 2ms interval of the pressure time curve as shown in Figure 4.4 giving the consistent results.

Flame propagation was detected from the variation of voltage signals of the linear thermocouples array above the spark. The time of the flame arrival to these thermocouples was recorded and plotted against thermocouple distance from spark as shown in Figure 4.5. The slope of this plot was considered as the flame speed and an average of the three repeat tests was recognised as the corresponding flame speed of the respective concentration. For rich concentration, this flame speed was recognised to be for the post explosion event after the diffusion of air (See Appendix J).

A detailed procedure for the flammability testing of material is explained below;

1 Make sure that the modified Hartmann unit is operated inside the fume cupboard.
2 Turn on the modified Hartmann unit and clean the Hartmann tube if necessary.
3 Secure the venting disc (Aluminium foil) with the locking ring at the top of the modified Hartmann tube.
4 Open the mushroom shaped cup for two anti-clockwise turns.
5 Distribute the weighed sample on the mushroom shaped cup uniformly.
6 Lock the Hartmann tube with the bayonet fitting with screws tightening.
7 Make the connections of electrodes to power supply.
8 Adjust the dispersion pressure to 7 bar using compressed air line/cylinder regulator and bleed valve on Hartmann unit.
9 Earth the thermocouples and close the door of the fume cupboard.
10 Start acquisition of data through the data logger and activate the spark by pressing the arc button using remote handset that results dispersion of dust through the pre-existing constant arc.
11 After the test, close the air flow and turn off the Hartmann unit.
12 Disconnect spark electrodes from transformer and earthed wires
13 Unlock the Hartmann tube and remove the venting cover.
14 Clean the Hartmann tube thoroughly and repeat the procedure again for next test.
15 Each concentration is repeated three times and the successive concentration is decreased until a lean limit is obtained with 0% explosion probability (no explosion) for the three repeat tests.

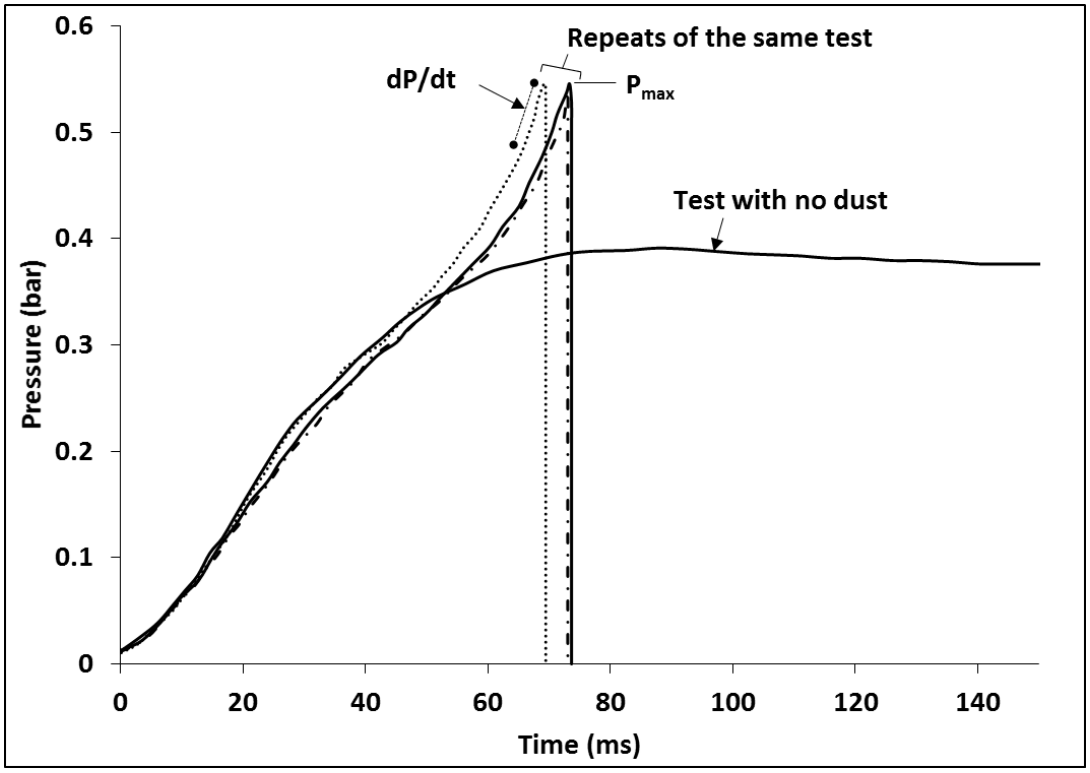

Figure 4.4: Pressure-time trace of ignition of dust in comparison to air

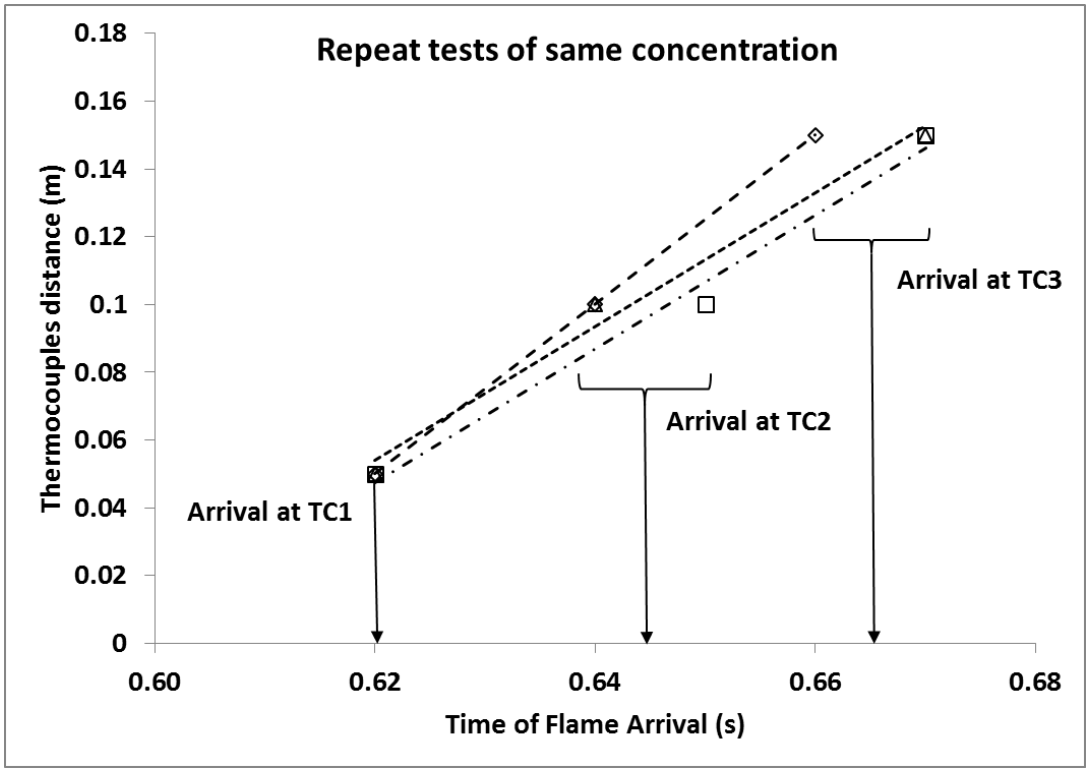

Figure 4.5: Thermocouple distance vs. time of flame arrival for flame speed measurements

4.4.2 Time sequence for ignition delay

The dispersion of the dust cloud with the existence of the pre-spark ignition results in the combustion of the stratified mixture of the dust cloud as revealed by photographic analysis of flame propagation. So, the dust concentration at the time of ignition might not be the same as that of the nominal dust concentration.

Ignition with suitable ignition delay provides sufficient time for dispersion and distribution of the particles in the tube prior to ignition. The timing sequence for the ignition delay (ID) was controlled by a digital timer regulating the time duration for the activation of the spark after the dispersion of air as shown in Figure 4.6. This modified Hartmann tube with the ignition delay was first tested for a standard Propane gas with known lower flammability limit. Then, it was employed for the standard dusts of known minimum explosible concentration (MEC) from the other reliable units.

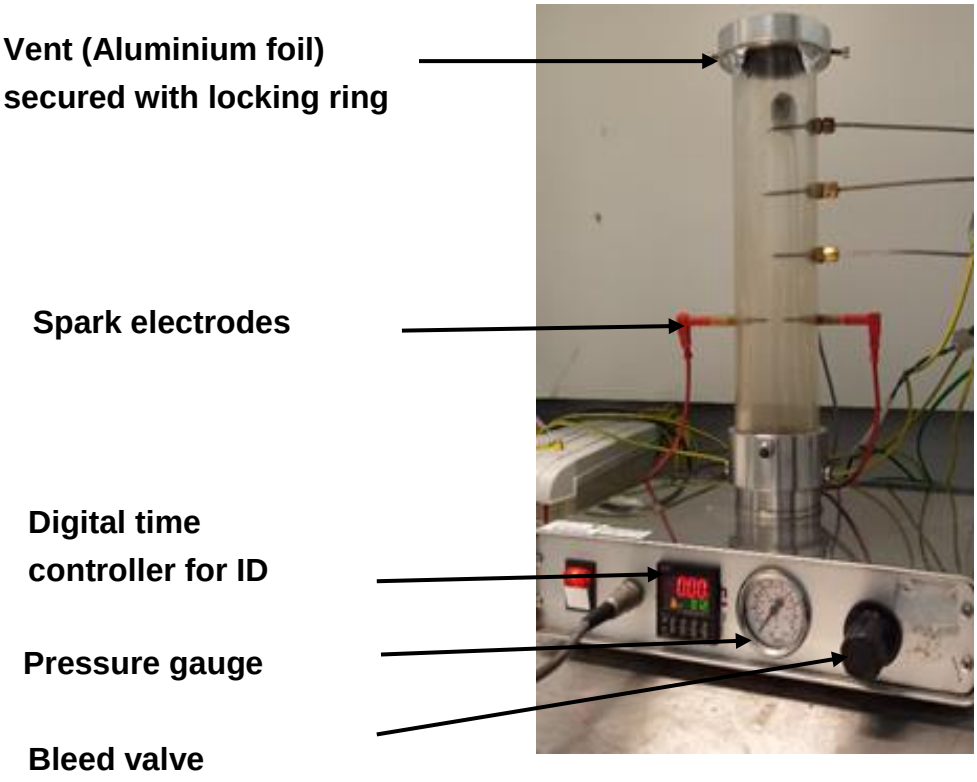

Figure 4.6: Modified Hartmann dust explosion tube

4.5 Explosibility tests on the modified 1 m^3 vessel

The explosibility parameters for the selected biomass dusts and their particle dependence was also tested on a modified ISO 1m^3 explosion vessel as shown in Figure 4.7. The standard dust injection system uses a 'C' ring disperser inside the explosion vessel. A pre-weighed quantity of dust is placed in the external 5L dust pot. This pot is then pressurised to 20bar to pneumatically drive the dust to the main vessel. The main vessel is maintained under vacuum to 933 mbar so that the addition of the air dust mixture from the dust pot is at atmospheric pressure prior to ignition. The dust pot is connected to the main vessel via a delivery pipe having a fast acting pneumatic gate valve. Opening of this valve allows the dust air mixture to disperse through the C ring disperser in the vessel. After an optimum ignition delay of 0.6s for C-ring disperser, the strong chemical ignitor activates the spark. A suitable timing of the valve (valve off timing) results the timely closing of the fast acting gate valve to avoid the leaking of pressure going to dust pot. The dust cloud propagates the flame causing a build-up of pressure. After the explosion, it is allowed to cool and dilute suitably before purging (See Appendix F for tick sheet procedure). The instrumentation diagrams for the main control unit and dust explosion rig are shown in Appendix B and C.

The dust containing fibrous particles that occur in woody and plant biomass after milling [73] would not pass through standard C ring disperser. The 'C' ring will only allow small spherical type particles to pass. Nut shell dusts are biomasses that do operate with the standard C ring dust injector [18], as nut particles are fractured in milling in a similar way to coal. For woody biomass and plant based biomass, a new disperser was required and a spherical grid injector was developed and calibrated, similar to an explosion suppressant injector. This would disperse the woody and plant biomass milled to <63µm, but would not disperse larger particle sizes.

Different designs of other dispersers are shown in the existing literature of standards but no detail is provided on their calibration. At Leeds University, calibration of these dispersers was performed based on determining optimum ignition delay and valve off timing of the disperser giving the same explosibility characteristics with the same mass burning as that of the standard C ring using standard dusts. The ignition delay for the spherical disperser with the 10L dust injection pot was calibrated against the standard C ring disperser using cornflour to have an ignition delay (between start of

injection and ignition) of 0.5s, compared with the standard C ring delay of 0.6s. Similarly the hemispherical cup was also calibrated for an optimum ignition delay of 0.5s and a valve off timing 0.64s using standard corn flour and a Colombian coal sample. These modified ISO vessel dust injection systems were used in the present work.

A further problem with woody and plant pulverised biomass was the low bulk density, which resulted in the standard 5L external dust injection pot being too small to hold a sufficient mass of biomass powder. To overcome this, the existing 5L pot used with the ISO 1 m^3 dust explosion vessel was extended to 10L volume with a 5L pot extension. The 10L external pot was calibrated to give the same flame speed and K_{st} as the 5L dust injection pot with the C ring disperser using cornflour as a reference dust [82]. The air pressure in the external vessel was reduced from 20 bar for the 5L vessel to 10 bar for the 10L vessel, so that the total mass of external air to disperse the dust remained the same [82].

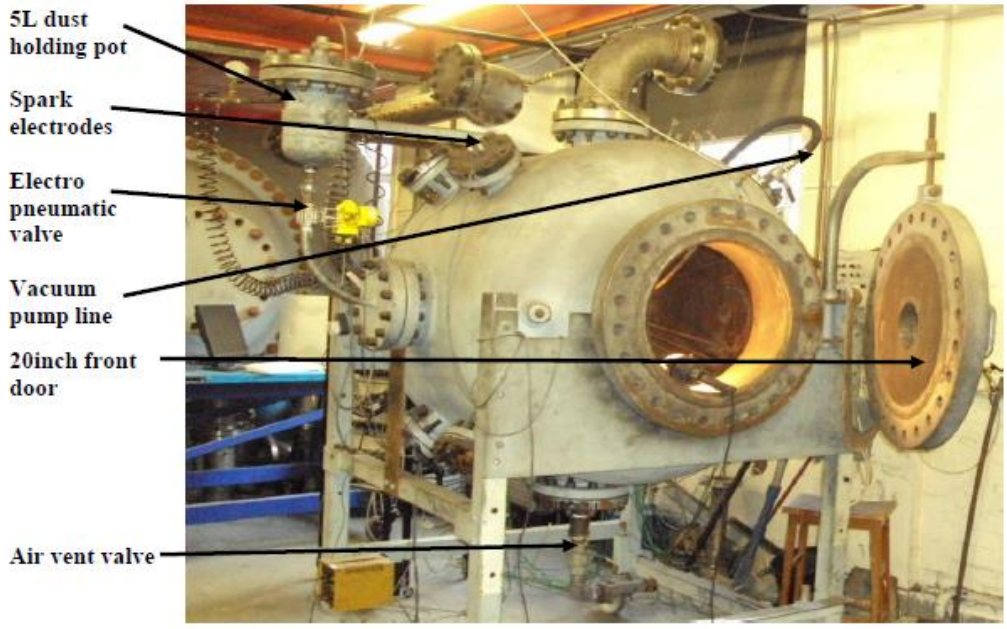

Figure 4.7: Standard ISO 1m^3 dust explosion vessel

4.5.1 Deflagration index and flame speed measurements

The ISO 1 m^3 dust explosion vessel was modified to enable the flame speed to be determined using a linear array of mineral insulated exposed junction type K thermocouples as shown in Figure 4.8. These measured the time of flame arrival as the time of the first measureable temperature rise. The dead time was minimal due to the size of the thermocouple exposed junction, 0.5mm, and for a flame speed of 1 m/s this is a 0.5ms uncertainty in flame arrival time which is the same for each thermocouple and hence not an error in the determination of flame speed. The thermal lag in the thermocouple response is irrelevant as the aim was not to measure the flame temperature, but the time of flame arrival. Three linear thermocouple arrays were used to determine the flame speed in three directions at 90^o to each other. If the three flame speeds are similar than a spherical flame propagation is achieved and this was then a valid measurement of the spherical flame speed (See Appendices D and E).

It was demonstrated for turbulent gas flames in the present experimental equipment that repeat measurements of flame speed and burning velocity can be made with a 95% confidence of +/- 8%. For dust explosions they showed that the spherical flame speed repeatability was a 95% confidence of 16% of the mean value. The greater data variability was due to the extra variability of the dust dispersion in addition to the randomness of turbulence.

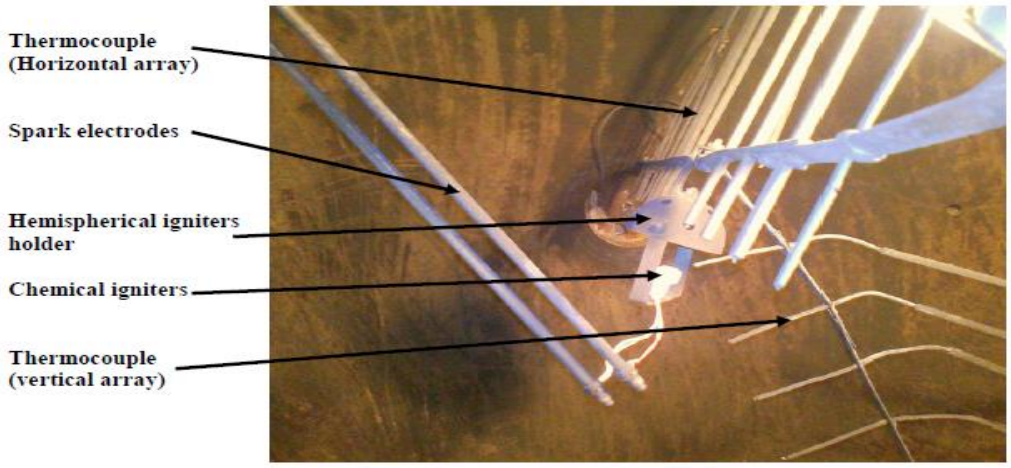

Figure 4.8: Array of thermocouples and igniter

The thermocouple arrays were all in the first half of flame travel where the pressure rise is low. In a spherical vessel when the flame is half way across the vessel the volume burnt is 1/8 but the mass burnt is about 1/50 or 2% and the pressure rise is proportional to the mass burnt. Thus the flame speed in this work and the burning velocities derived from this were at constant pressure [110]. Also shown in Figure 4.9 is an example plot of the flame arrival time vs. distance for the three arrays of type K thermocouples. Figure 4.16 shows that the flame propagation was reasonably symmetrical, which means that the flame propagation was reasonably spherical. Average of the slope for these arrays of thermocouples was considered as the flame speed of the respective concentration.

Two Keller type-PAA/11 piezo-resistive pressure transducers were mounted in the explosion vessel to record the explosion pressure history and one pressure transducer was placed in the 10L dust pot. The response time of these pressure transducers was less than 1ms and their factory calibration accuracy was certified at <1%. The error in the determination of the deflagration index, K_{st} ($=dP/dt_{max}V^{1/3}$), was also < 1%.

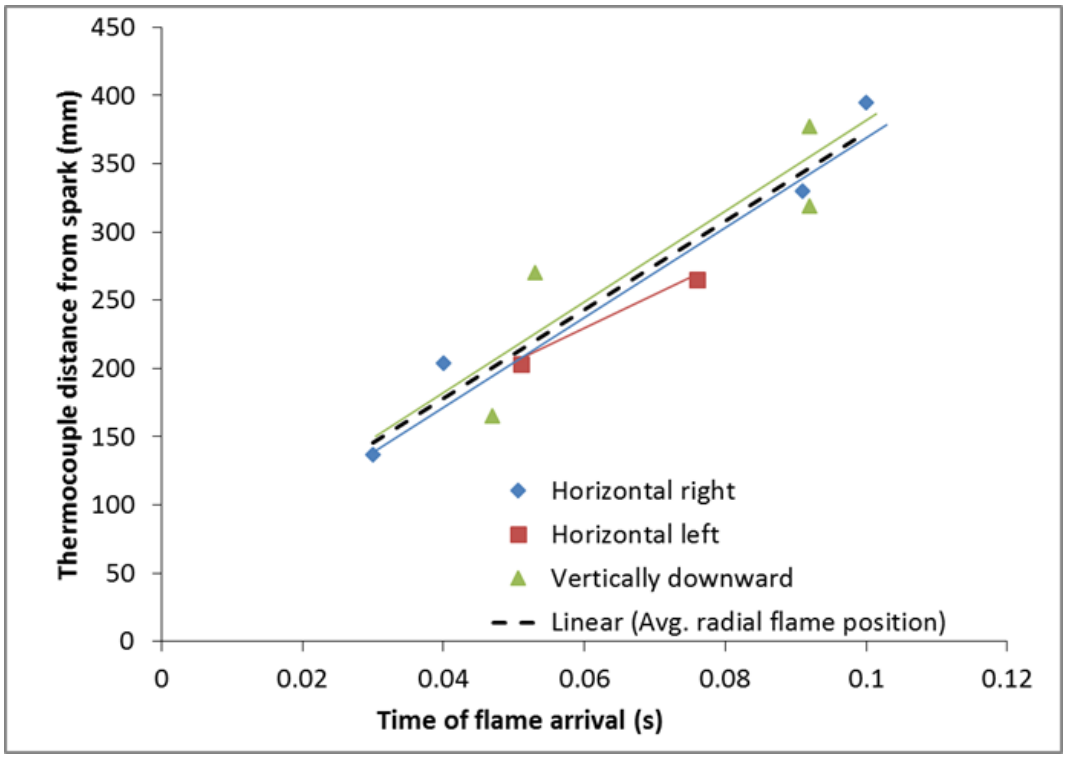

Figure 4.9: An example of flame speed measurement

The main cause of variation in the measurement of K_{st} was the variability of turbulence and the randomness of the dust dispersion. Sattar et al. (2014) showed from repeat tests using cornflour dust that the 95% confidence interval for the measured K_{st} was 12% of the mean value. This was better than the 16% confidence of the measurement of flame speed, as the rate of pressure rise is a mean measurement that essentially surface averages the flame propagation. The flame speed measurements were carried out on three radial lines and hence would show more variability than the rate of pressure rise repeatability.

Figure 4.10 shows, for the present fibrous type agricultural waste biomass, an example of the pressure trace and rate of pressure rise measurements. The pressure time plot was converted to rate of pressure rise after applying some degree of smoothing. This was then changed to normalised the rate of pressure rise independent to the size of the vessel using the expression as;

$$Deflagration\ index, K_{st} = \frac{dP}{dt}\ (V)^{1/3}$$

Figure 4.11 shows an example of the repeat tests of the same concentration as part of this research work. It can be noted that the percentage error of pressure and rate of pressure rise was less than 10% in accordance with the standard [104]. It shows the good repeatability and this was checked routinely during the research work.

A feature of the biomass dust explosions was that only about half of the dust was burnt. At the end of the experiment when the vessel was opened there was a large quantity of unburnt powder on the floor of the vessel. This indicates that all the dust placed in the external pot does not all take part in the explosion and so there is uncertainty over the concentration of the dust that the flame propagated through. At the end of each dust explosion the debris was collected using a standard vacuum dust extractor into a bag filter. The bag filter was weighed before and after the extraction to determine the mass of dust that was not burnt. Analysis of this large quantity of explosion debris showed that it was mainly the original dust [18, 82, 110]. This showed that the concentration injected was not the concentration that the flame propagated through. The measured weight of unburnt dust enabled the mass of dust that burnt in the test to be determined and from this, the burnt dust equivalence ratio could be determined.

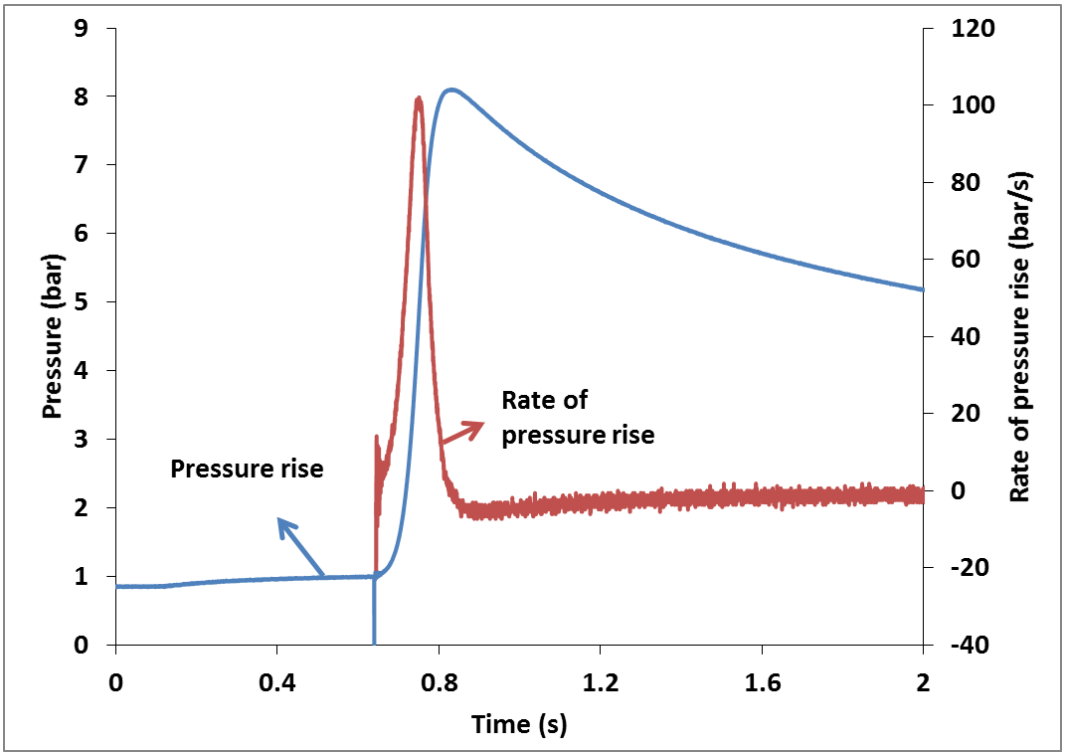

Figure 4.10: An example of pressure-time history and rate of pressure rise

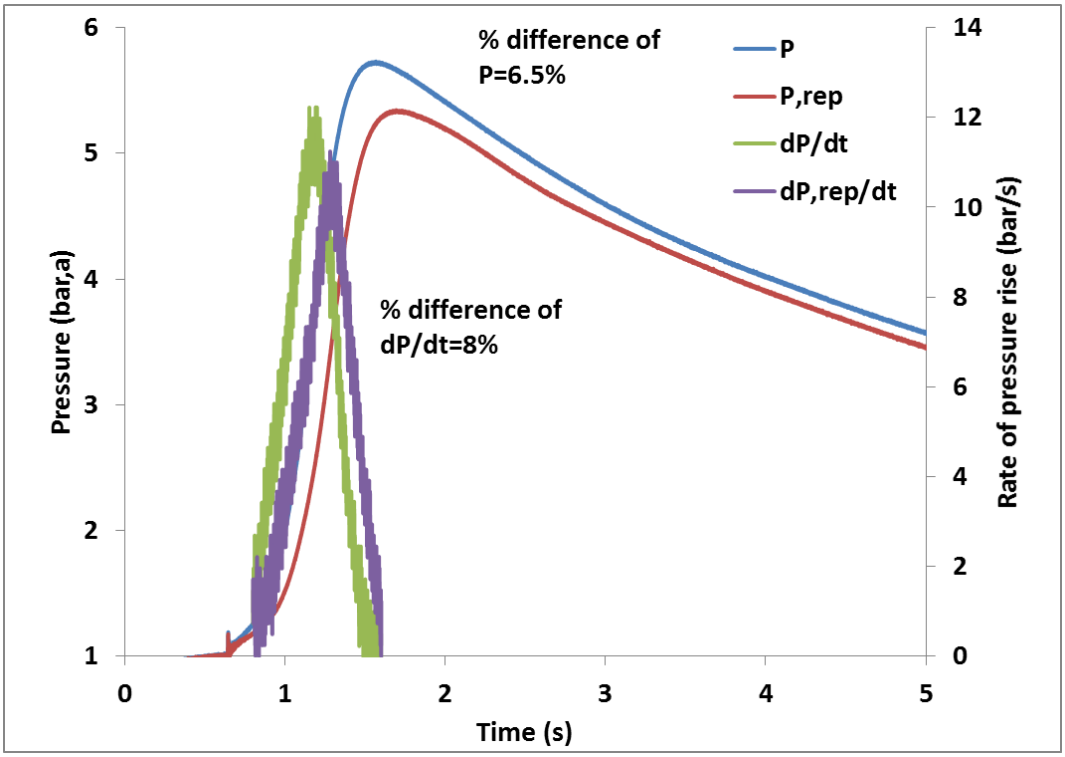

Figure 4.11: An example of pressure-time history and rate of pressure rise

The weight of dust remaining after the explosion included the ash from the biomass dust that did burn. As the ash fraction of the dust was known, the weight remaining could be corrected for this, using Eqs. 4.2. This then allows

the equivalence ratio of the dust that did burn to be determined using Eq. 4.3.

$$Actual\ burnt\ mass = \frac{(Injected\ mass - Vessel\ residue)}{1 - Ash\ fraction} \quad [4.2]$$

$$Burnt\ equivalence\ ratio = \frac{Stoichiometric\ Air\ to\ Fuel\ by\ mass}{Actual\ Air\ to\ Fuel\ by\ mass} \quad [4.3]$$

The accuracy of this correction for the unburnt mass of injected biomass is poor as it is difficult to ensure that all the unburnt biomass was collected, the weighing of the unburnt biomass in the filtered collection bags had <1% error. To account for uncollected unburnt material 5% was added to the collected mass as a reasonable estimate of the amount left in crevices inside the vessel or lost during purging. Repeat tests indicate that the measurement of the unburnt mass had a repeatability of 5% of the measured value. The dust that did not burn was analysed in the same way as the raw dust and this showed that it was predominantly unburnt original dust.

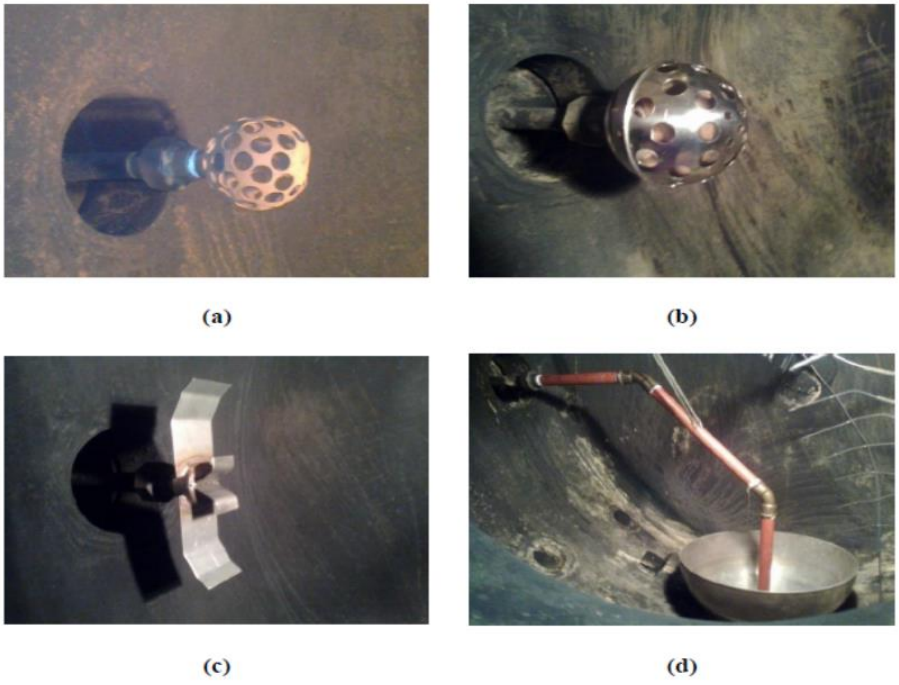

Figure 4.12: Types of dispersers a) & b) Spherical dispersers c) Rebound nozzle d) Hemispherical dispersing cup

The source of this unburnt dust was the explosion induced wind entraining the relatively large dust particles ahead of the flame and eventually carrying them onto the wall where they were compressed by the pressure rise. After the pressure fell due to heat losses at the end of the explosion, this wall dust fell onto the floor of the vessel, where it was collected after the explosion [18]. There was some evidence of partial pyrolysis of the outer layer of this dust, but this was a small effect and only made a small change in the composition of the residue dust from the original dust [91].

There are two approaches for the dispersion of dust. One is placing the dust outside in the external dust pot and pressurizing it with air. The air pressure results the flow of dust from the dust pot to the disperser that is inside the main vessel with the opening of the pneumatic valve in the delivery pipe connecting the pot with the disperser as shown in Figure 4.7. In the second approach, the dust is placed inside the main vessel in a round cup (hemispherical disperser) and a puff of air produces the transverse motion that results in the generation of dust cloud. This disperser was suitable for the testing of coarse size fractions of dust; designed and fabricated by another Ph.D. student (**David Slatter**). This hemispherical cup with drilled pipe was further calibrated in this work before testing it for coarse particle sized fractions.

One of the modifications in the hemispherical cup is to place the cover with tiny holes that will help to distribute the dust uniformly. However it was experienced that the size of the holes are not enough to disperse all the dust and a sufficient amount of dust does not participate in the propagation of the flame. The increase in the size of the holes/ increasing the number of holes to provide enough flow area for the dust also failed to effectively disperse the dust. Finally it was hemi-cup without any cover with a drilled pipe which resulted in good uniform dispersion giving even propagation of the flame. The re-design for the hemispherical disperser is shown below in Figure 4.13.

For the testing of the gaseous mixture, the partial pressure technique was used. The main vessel was evacuated first and the barometer was used for producing the specified mixture of gases that balanced by the addition of air to achieve the total pressure of atmospheric pressure. For the ignition of gaseous mixture, a spark igniter was recommended and found to be suitable to avoid buoyancy effects due to the strong chemical igniter.

Figure 4.13: Re-design of the hemispherical disperser

4.5.2 Calibration of the drilled pipe hemisphere dispersers

Dispersion of the coarse fraction of solid dust using the hemispherical cup with a drilled pipe required more force of the dispersion air to lift the particles transversely for dispersion. It was found that dispersion pressure of 20 bar instead of 10 bar for 10L dust pot resulted in a higher mass dispersion and burning comparable to the standard C ring disperser. The main vessel was maintained at further low vacuum for this new settings so that the addition of air from the external pot results in the pressure being atmospheric just before ignition. Standard C ring disperser with the optimum ignition delay of 0.6s was found to have turbulence factor in the range of 4.0-5.5 [110, 156, 157]. Turbulence factor was measured with 10% Methane using the following formula as;

$$Turbulence\ factor = \frac{Kg_{,turbulence}}{Kg_{,laminar}} \qquad [4.4]$$

The turbulence factor for different designed dispersers were measured for different ignition delays as shown in Figure 4.14. It was found that the calibrated spherical grid disperser had a maximum comparable turbulence factor for 0.5s ignition delays whereas for drilled pipe hemisphere a wide range of ignition delays (0.5-0.7) were found to give turbulence factor comparable to the standard C ring and literature results. It was decided to base the calibration on standard corn flour dust explosibility results for optimum ignition delay for the drilled pipe hemisphere.

Standard corn flour dust was tested for the most reactive concentration of 750g/m^3 on different ignition delays using the drilled pipe hemisphere. Explosibility characteristics in terms of deflagration index (normalized rate of

pressure rise), maximum to initial pressure ratio and percentage mass burnt was compared with the results of the standard C ring disperser as shown in Figure 4.15. It was noticed that decreasing the ignition delay from 0.7s to 0.5s showed a good comparison with the standard C ring disperser. Based on this, 0.5s ignition delay was found to be reasonable.

As shown in Figure 4.16, pressure traces using standard C ring and drilled pipe hemisphere for most reactive concentration of corn flour. Similar trends of rise and decay of pressure after reaching maximum for the calibrated settings of drilled pipe hemisphere was analogous with standard C ring disperser.

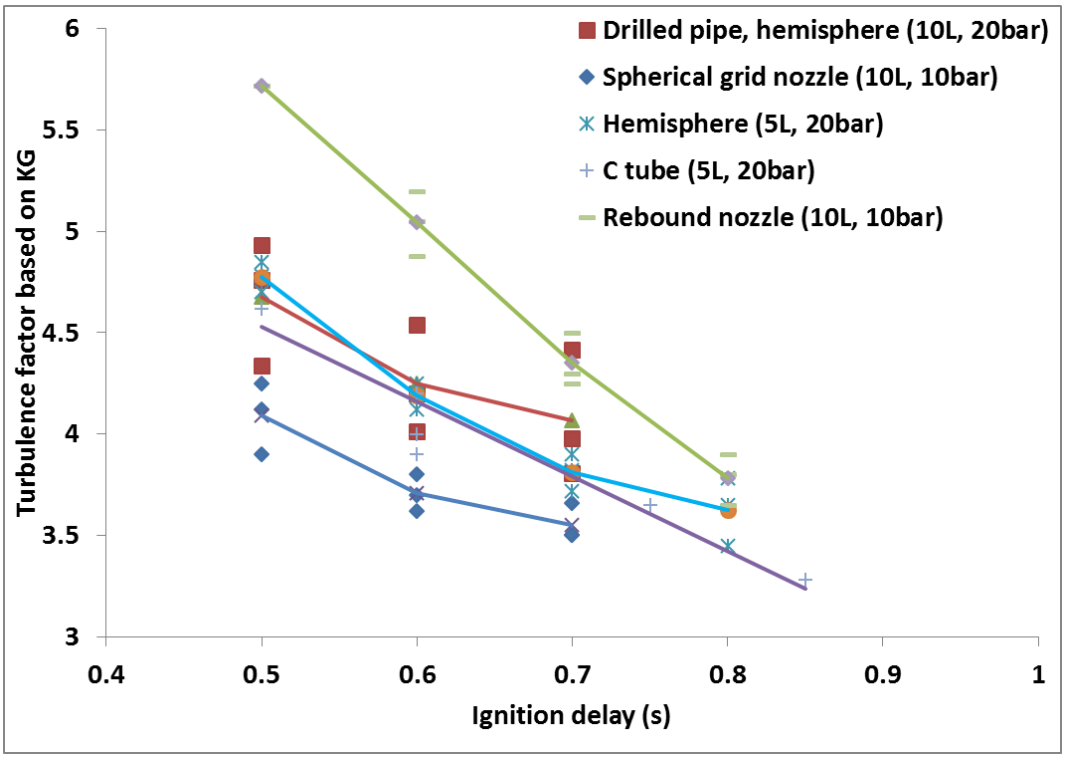

Figure 4.14: Turbulence factor for different designed dispersers for different ignition delays

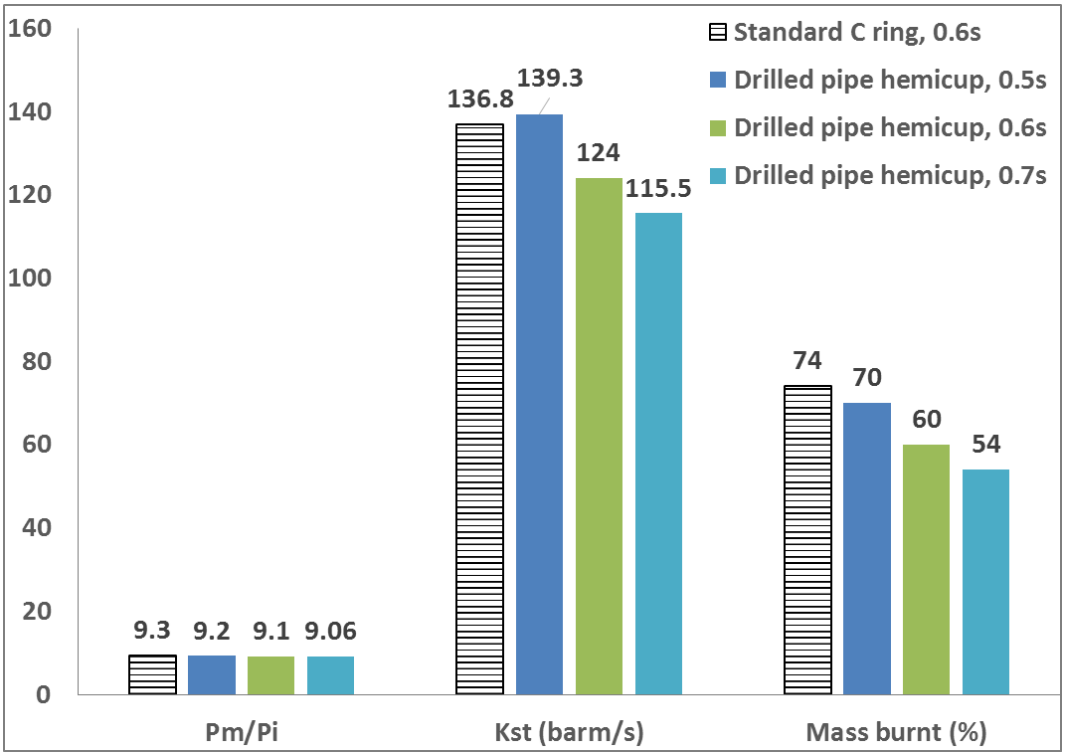

Figure 4.15: Explosibility characteristics of corn flour using drilled pipe hemisphere for different ignition delays in comparison to standard C ring disperser

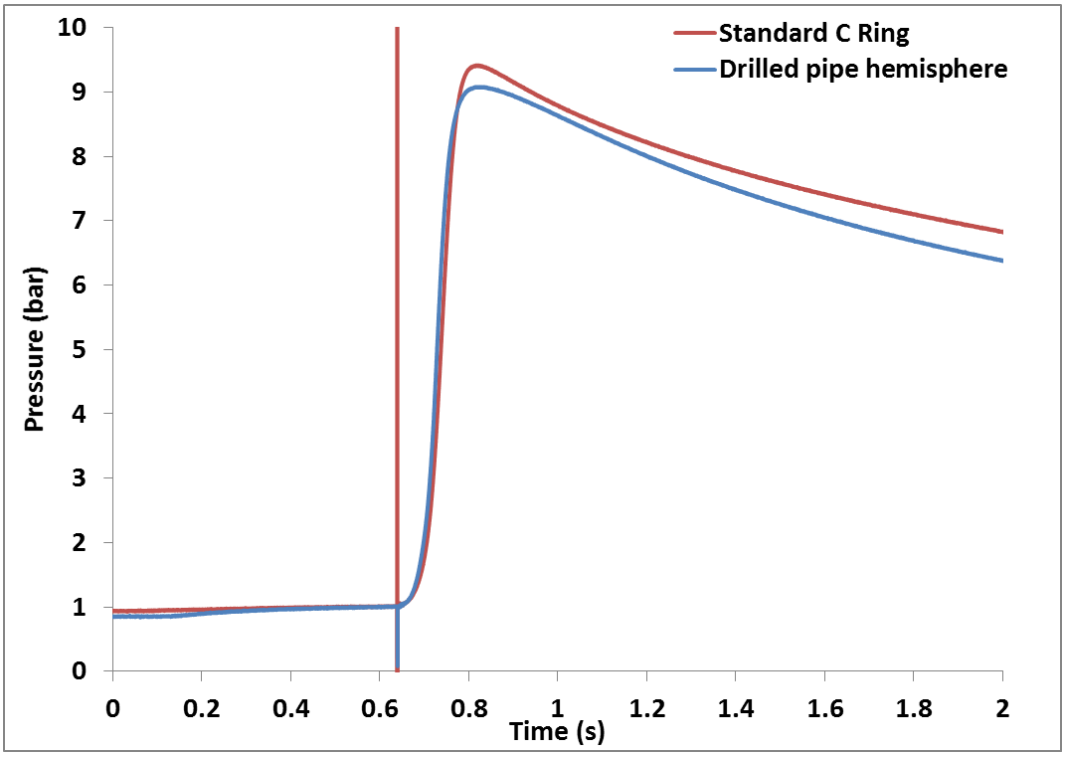

Figure 4.16: Comparison of pressure trace of corn flour for drilled pipe hemispherical disperser in comparison to standard C ring

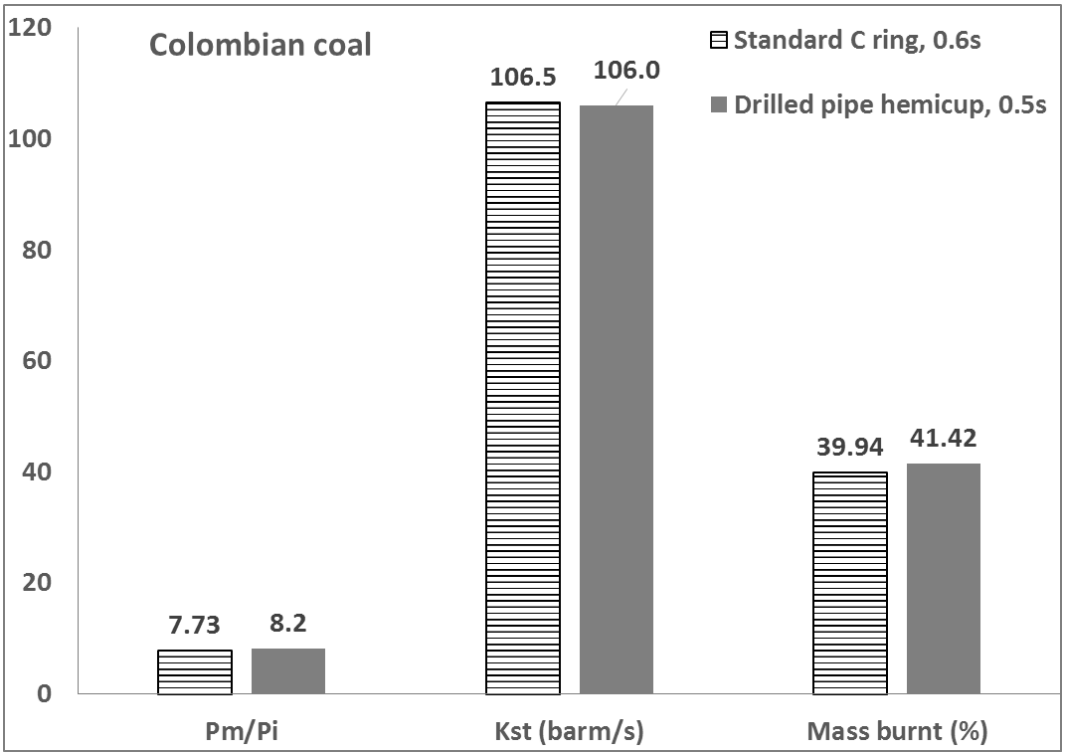

Figure 4.17: Explosibility characteristics of Colombian coal for the most reactive concentration using calibrated ignition delay of drilled pipe hemisphere in comparison to standard C ring

Later, one of the fine Colombian coal sample was also tested for the most reactive concentration at the same calibrated ignition delay of 0.5s and compared with the standard C ring. It also showed a very good comparison with the standard C ring disperser as shown in Figure 4.17 and thus 0.5s was selected as the optimum ignition delay for drilled pipe hemisphere with turbulence factor of 4.7.

4.5.3 Pressure loss and dust layer thickness

Pressure time history of the burnt dust cloud was recorded using two piezo-resistive pressure transducers in the main vessel. The higher the rate of pressure rise means the fast propagation of the flame. Pressure time history for fine bagasse dust was plotted in comparison to 10% turbulent Methane as shown in Figure 4.18. Burning of fine bagasse dust in comparison to Methane gas was slower due to the time lag in releasing enough volatile. This time lag was found to increase with coarse size fractions due to less exposed surface. Flame propagation quenches after touching with the walls that acts to absorb the heat. As shown in Figure 4.18, the pressure starts to decay after reaching to the maximum. As it was explained before that during propagation of flame, a proportionate mass was pushed against the wall. This mass after hitting the wall forms a thin or thick layer on the wall leading

to mass drops down in the vessel depending on the concentration and type of dust. This layer acts as an insulating medium and lowers the decay of pressure. In contrast to dust explosion, pressure decay for gaseous mixture was much faster due to quick cooling after direct contact with vessel wall without the existence of this insulating layer. This pressure loss after reaching to the maximum can be computed for 10% drop of maximum pressure as demonstrated in Figure 4.18.

Also this rate of pressure loss is a strong function of dust layer thickness and maximum flame temperature. After reaching the maximum explosion pressure with maximum mass burning, the maximum flame temperature remains almost constant. After further increase in concentration, the rate of pressure loss solely depends on the dust layer thickness with smaller decay rate for higher dust layer thickness.

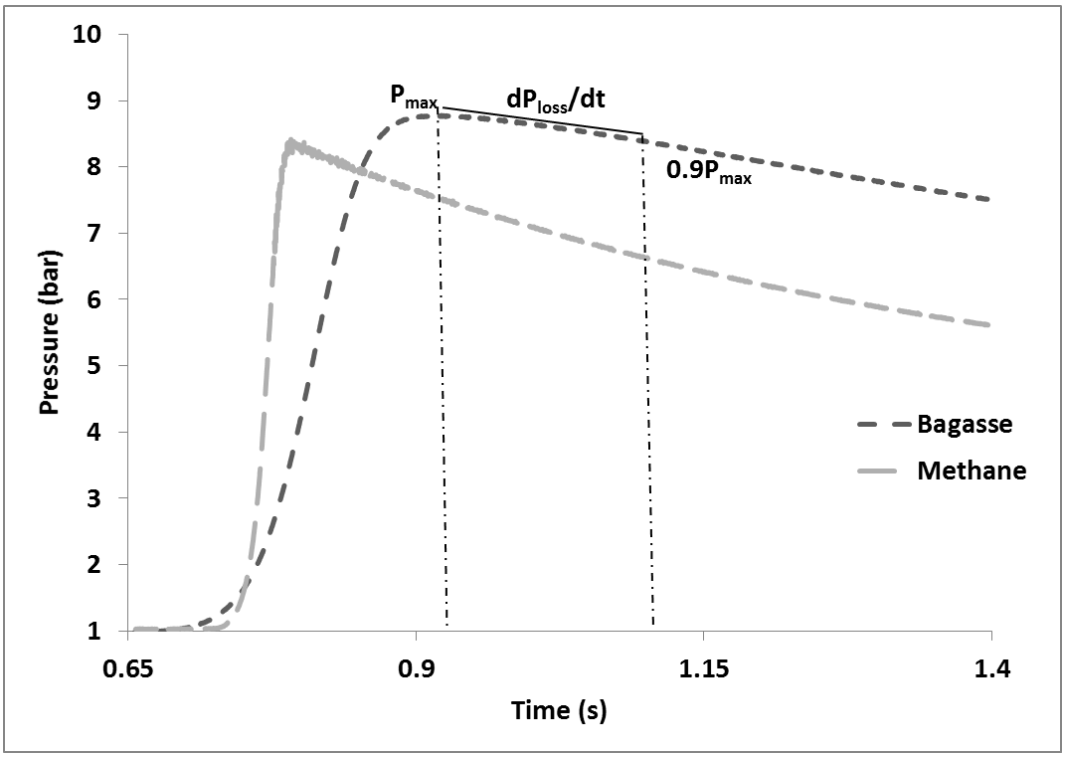

Figure 4.18: Pressure time history of fine bagasse dust in comparison to methane and rate of pressure loss determination

4.6 Comparison of 1m^3 vessel and modified Hartmann tube for the measurement of minimum explosible concentration

The minimum explosible concentration (MEC) or lean explosion limit (LEL) is important in dust and gas explosion safety [97, 158]. For leaner concentrations than the MEC, the mixture is not flammable and explosion protection measures are not required. How close to the limits it is safe to operate, without explosion protection, is usually separately regulated and operation at 25% of the limits is quite a common requirement in the UK HSE guidance [24]. The MEC for dusts should be measured to the same accuracy with the same definition of the lean limit as for gas/air explosions [97] and currently this is not the case [158]. For gases the LEL has historically been defined as the lowest concentration at which an explosion can occur [159, 160] and the same criteria has historically been applied to dust MEC determination [73], which is a literal interpretation of the term MEC, the minimum concentration at which an explosion can occur. The majority of the LEL data in the literature was measured as the leanest mixture that did propagate a flame. Indeed the reference LEL data in the European standard [97] is for this definition of LEL, the leanest mixture that did propagate a flame [97, 161]. However, in recent European standards these definition of LEL and MEC have not been used [97, 161] and have been changed to the mixture that will not ignite at a specified interval from the mixture that did ignite, although this is not mentioned in the EU closed vessel explosion LEL method [97].

In the tube method the LEL should be determined with a resolution of 10% of the LEL for gaseous concentrations >2% or 0.2% for concentrations below this [97], which is an increased error. The value for the last ignition should be reported and the concentration gap that was tested with no ignition should be within 10% of the last positive ignition. The standard essentially sets the LEL at up to 10% below the concentration that had a measured flame that propagated. In equivalence ratio, Ø, terms hydrocarbon–air mixtures have a lean limit that is about Ø=0.5 and so the resolution of this limit is Ø<0.05. Most reported LEL for gases resolve the lean limit better than this and normally report to 0.01Ø. In dust concentration terms the <0.05Ø resolution for a pure hydrocarbon dust such as polyethylene is < 4 g/m^3 and for a cellulose or biomass type dust with a stoichiometric A/F ratio of 6/1 by mass (200 g/m^3) it would be a resolution of the MEC to <10 g/m^3.

The resolution for the determination of the MEC for dust is very coarse in the European dust explosion MEC standard [158]. The requirement is to test the

dust air mixture with the following concentrations of dust: for <500 g/m^3 each successive concentration tested is 50% of the previous one and above 500 g/m^3 the concentration is increased in 250 g/m^3 increments [158]. This means that for most dusts the only concentration tested in the near limit mixture region are 1000, 750, 500, 250, 125, 60, 30, 15 and 7.5 g/m^3. The principle is that if for example there is an explosion with >0.3 pressure rise at 60 g/m^3 and there is no explosion with >0.3 bar pressure rise at 30 g/m^3, then the MEC is 30 g/m^3 and there is no requirement to test intermediate concentrations and hence determine the actual MEC. This is why in tabulations of dust MEC there are so many dusts with MEC of 15, 30, 60 or 125 g/m^3 [73].

For a pure hydrocarbon dust such as polyethylene, the stoichiometric concentration is 80 g/m^3 and the lean limit would be expected to be 40 g/m^3 if the dust behaved like a gas, but the reported value is [68] 30 g/m^3, 0.37Ø due to the above methodology being used, whereas the actual limit is likely to be closer to 40 g/m^3, 0.5Ø. In the worst case with say an actual limit of 55 g/m^3 reported as 30 g/m^3 the error is 25 g/m^3 or a (25/80) 31% error. For cellulosic dusts such as biomass a typical stoichiometric A/F is 6/1 [24] on a dry ash free basis (daf) which is 200 g/m^3. An actual lean limit of 55 g/m^3, 0.27Ø, would be reported as 30 g/m^3, 0.15Ø. This is the origin of some of the ultra-lean MEC reported for dusts [68, 73], which are in reality simply inaccurate measurements allowed by the European standard [158].

It is not reasonable to adopt a different safety standard for dusts than for gases and this work aims to show that the modified Hartmann dust explosion equipment can give a better accuracy on the MEC determination than using the standard 1 m^3 method. This is because it is easier and lower cost to do more tests with greater resolution of the MEC. Also the MEC from modified Hartmann tube [162] is similar to that for the vertical tube LEL European standard method [97].

As shown in table 4.3, the comparison of MEC in terms of g/m^3 for different dusts was presented. MEC for a number of dusts were also converted to equivalence ratio as shown in table 4.4. It was observed that modified Hartmann tube resulted in much leaner MEC compared to other experimental methods that again focus on importance of ignition delay for the modified Hartmann tube.

Table 4.3: Comparison of MEC measurements in g/m^3

Dust	Hartmann [163, 164]	1 m^3 or 20 L [73]	1 m^3 [68]
Sugar	45	60	60
Milk Powder	50	60	60
Aluminium	30 6 µm 40 17 µm	30 22-29 µm 6 < 10 µm 60 41 µm	30 29 µm
Cellulose	55	60 51 µm	60 33 µm
Wheat Starch	45	60 20 µm	30
Lycopodium This work	22 22		30 14 (burnt)
Polypropylene	30 – 35	30 25 µm	30
Polyethylene This work	30 15 63 µm	30 <10 µm	30 <10 µm
Sulphur	20	30 20 µm	30
Peat	100	60-125	125

Table 4.4: MEC for gases, vapours and dusts in terms of Ø

Gas/Dust	A/F Ø=1	daf. g/m^3 Ø=1	MEC Ø	Method
Methane	17.2	70	0.46	EU Tube [97]
Propane	15.7	76	0.43	Tube [165]
Ethylene	14.8	90	0.38	EU Tube [97]
Polyethylene	14.8	81	0.25	Hartmann [164]
			0.37	1 m^3 [73]
n-Hexane	15.2	79	0.46	EU Tube [97]
1,3,5 TMB 70 ^{0}C			0.50	EU Tube [97]
Hydrogen	34.5	34.8	0.12	Tube [165]
CO	3.45	350	0.41	Tube [166]
Ethanol	9.0	133	0.48	Tube [165]
PMA	7.27	165	0.18	1 m^3 [73]
PMMA	8.26	145	0.21	Hartmann [163]
PET	7.18	167	0.24	Hartmann [163]
Cellulose	5.12	234	0.24	Hartmann [163]
Wood	5.24	229	0.20	Hartmann [164]
Torrefied Wood	7.17	167	0.20	Hartmann [87]
Torrefied	6.61	181	0.17	Hartmann [87]
Norway Spruce	8.70	138	0.22	
Wood 95 µm	5.63	213	0.14	1 m^3 [167]
Bark 57 µm	6.03	199	0.14	1 m^3 [167]
Forest Residue 102 µm	4.78	251	0.22	1 m^3 [167]
Bagasse	6.45	186	0.27	Hartmann [17]
Rice Husks	6.24	192	0.35	Hartmann [17]
Wheat Straw	6.03	199	0.55	Hartmann [17]
Corn Cob	5.34	225	0.22	Hartmann Unpublished work)
Peanut Shells	6.78	177	0.18	Hartmann (Unphublished work)
Lycopodium	10.4	115	0.18	Hartmann
			0.12	1 m^3
Corn flour	5.64	213	0.27	Hartmann
			0.34	1 m^3
Pine Wood Dust	6.39	189	0.2	Hartmann
			0.14	1 m^3
Walnut Shells	6.75	178	0.19	Hartmann
			0.24	1 m^3
Pistachio Nut Shells	6.22	193	0.20	Hartmann
			0.18	1 m^3
Colombian Coal	11.18	107	0.39	Hartmann
			0.43	1 m^3

4.7 Conclusions

Different analytical techniques necessary to explain the experimental results were explained briefly. Experimental methodologies of the modified Hartmann tube and modified ISO 1m^3 vessel for the determination of explosiblity indices and other characteristics were also explained. Modified Hartmann tube with ignition flammability criteria similar to gas lean flammability limit was developed giving the comparable results to that of the standard methods. The improvements in the existing methods to test the fibrous and high voluminous biomass dust were discussed. A small grid spherical disperser was calibrated previously for optimum settings but this still was not suitable for coarse size fractions greater than 63µm sieve size. A new drilled pipe hemispherical disperser was calibrated to test different sized fractions of biomass for this research work. A higher dispersion pressure (20bar with 10L volume) was found to be necessary to lift more mass for coarse size fractions resulting higher dispersion. Optimum calibration settings were determined using standard corn flour and fine Colombian coal sample. The measurement of MEC for dust needs to be improved so that it is as accurate as that for gases. It was shown that a closed vessel gas explosion, of similar size to the vertical cylinder used in the dust explosion Hartmann equipment, could determine the MEC with agreement with the European gas flammability standard. A 1 m^3 cylindrical vessel for gas explosions LEL determination did not give agreement with the accepted LEL and the error was at least 20% richer. Detailed work on determination of optimum ignition delay will be discussed in the experimental chapter.

Chapter 5 CHEMICAL CHARACTERISATION AND FLAME PROPGATION MODELS OF BIOMASS VOLATILE

The chemistry involved in the propagation of pulverised biomass flames is not well understood. All biomass fuels release volatiles at a much lower temperature than coal and the proportion of volatiles is much greater than for coal, typically 80% compared to 30%. Thus, the rate of release of volatiles from biomass fuels is much more important in the pulverised fuel flame propagation than it is for coal, where the rate of char oxidation is more important. The rate of release of volatiles from dry biomass follows three stages: the first stage for typically 10% of the volatiles occurs over 200 – 300^{o}C, the second stage of about 70% of the total volatile mass occurs over the temperature range 300 – 400^{o}C. Finally, there is a slow loss of volatiles, accounting for remaining 20% of volatiles, over the temperature range 400 – 900^{o}C. Stagg's quick approximation method was used to determine the kinetics for the rate of volatile yield. Biomass samples were found to have lower activation energies and higher rate of release of volatiles in comparison with coal samples, up to 300 – 400^{o}C. Similar release rates were found for the 3rd stage of volatile release. The release of volatiles at low temperatures potentially makes the pulverised biomass fuel more reactive and one consequence is shown in the measurement of minimum explosible concentration, MEC. A good correlation was found between activation energies and the MEC, determined on the modified Hartmann equipment. There is currently little understanding of the composition of the volatiles released at low temperatures from biomass, as most publications are for pyrolysis conditions at high temperature. It is possible that the volatiles are a mixture of mainly H_2, CO and CH_4 and the likely proportions of these were calculated from the elemental and thermo-gravimetric analysis. This was done for a range of biomasses and this showed that the most important volatile gas is likely to be CO and that CH_4 yield is very low. This means that the conventional model used in coal combustion of char plus methane combustion is not applicable to biomass combustion.

5.1 Introduction

Pulverised biomass combustion in existing pulverised coal power stations is one of the most cost effective routes to greenhouse gas (GHG) reductions in electric power supply. In 2014 5.8% of the UK's supplied electricity was generated from pulverised biomass mainly used in existing coal fired power stations [6]. This was a 25.7% increase on 2013 and in 2014 was 19.69 Mtoe [6]. It was the fastest

growing renewable electricity source between 2013 and 2014. In spite of its growing use, the mechanism of combustion of pulverised biomass has received relatively little study. The properties of biomass are quite different from those of coal and these will result in different burning mechanism. Perhaps the greatest difference between the two fuels is the much higher proportion of volatile matter in biomass. The rate at which volatiles are released from biomass and the global kinetics of this volatile release are studied in the present work, with the aim that the global kinetics can be incorporated into CFD modelling of biomass combustion.

Biomass fuels have a lower bulk density, higher volatile content, lower calorific value and higher moisture content than coal and a greater fire and explosion risk [22, 168]. Woody biomass fuels have a more variable composition than coal [1, 9, 10, 42, 73, 78, 83] and they are also more difficult to mill due to their fibrous structure.

A wide range of biomass sources from wood to agricultural wastes are studied in the present work, some of which were supplied in pellet form but were crushed to extract the original pulverised biomass. The agricultural biomass was milled and sieved in the laboratory. A characteristic of biomass is its fibrous structure, which makes biomass difficult to mill in equipment designed for the milling of brittle coal.

Thermally treating the biomass by heating at around 260–320^{o}C, is a process known as torrefaction. This causes (among other changes) the biomass to become brittle and easier to mill. An alternative thermal treatment process that also destroys the fibrous structure is “steam-explosion” treatment which involves heating to similar temperatures with hot steam at high pressure and then releasing this pressure so that the water absorbed in the biomass ‘explodes’ out shattering the biomass. Steam exploded biomass is often referred to as ‘black pellets’ as the final fuel pellets are black. Both types of thermally treated biomass were included in the present study for comparison. The parent wood was yellow pine and this is also included in the study [169].

The high volatile content of biomass and thermally treated biomass and its ease of release make biomass more reactive than coal. One measure of this increased reactivity is the lean flammability limit or minimum explosible concentration (MEC) [78] and this was the method used in the present work using the modified Hartmann dust explosion

equipment. This equipment was modified to enable the flame propagation speed (another reactivity parameter) to be determined.

The high reactivity of biomass is also shown in the large number of explosion and fire incidents in pulverised biomass production, storage and utilisation in power plants. Many biomass fire/explosion incidents have occurred in the past and are still happening [78, 170]. The detailed investigations of these biofuels need to be assessed properly before their adoption and retrofitting of the plants [42, 73]. The present work gives both reactivity information in the form of the rate of volatile release and the MEC.

Biomasses are more reactive and have different chemical characterisation than coal [9, 83]. They have higher volatile yield and lower fixed carbon content compared to coals [1, 10]. The adoption of biomass as a partial or complete replacement for coal requires the measurement of the chemical and physical properties and the chemistry involved in their conversion. Particle size and the heating rates greatly affect the rate of release of volatiles due to the thermal inertia of the particles. The rate of release of volatiles is a critical parameter for the stability of the pulverised fuel flames on burners.

It has been observed that decreasing the particle size and increasing the heating rate results in an increase in the rate of release of volatiles up to a critical point [1, 10]. It was observed that biofuels of coarse particle size range of 300-500 µm were still explosible in contrast to coals of similar particle size [17, 19, 171, 172]. Woody biomasses showed a decrease in the MEC with a decrease in particles size. However, the ash derived crop residues when milled enriched the finer fraction with more ash contents. The enhanced yield of ash in the finer fraction acts as an inert and counterbalances the effect of particle size on the lean flammability limit (LFL) [17].

The minimum explosible concentrations of the biomasses are found to be much leaner than for coal and even hydrocarbon gases in terms of equivalence ratio [17-19, 22, 23, 87, 110]. Most of the data on the MEC in the literature are expressed in terms of g/m^3, which when converted to equivalence ratio helps to compare the results with equivalent LEL data for other fuels [24]. Most hydrocarbon fuels have their lean flammability limits at half of their stoichiometric concentration. Oxygenated fuels such as biomass were found to have their MEC

much leaner than the LEL for gaseous hydrocarbons [17-19, 22-24, 87, 110]. It was also observed that coal and biomass fuels have no upper flammability limit. Deguingand & Galant [93] employed weak spark ignition for the determination of the upper flammable limit and found apparent upper flammable limit of coal dust to be ~ 4 kg/m^3, which is more an ignitability limit rather than a flammability limit because of the weak ignition source. Wolanski [95] found that increasing the concentration reduces the flame temperature below its limit value and also observed that the dusts do not have upper flammability limit.

The kinetics for volatile yield and their chemical characterisation will help to understand the mechanism of flame propagation in pulverised biomass. A range of biomass samples including woody and agricultural biomass were investigated for the release of volatiles using thermal gravimetric analysis (TGA) and their devolatilisation kinetics were derived using Stagg's [173-175] quick approximation method. Two different models, as developed by Staggs [173-175], were applied for the kinetic study of these biomasses: Series Reaction Model and Competitive Reaction Model.

5.2 Research materials

Second generation biomass crop residues including sugarcane bagasse, rice husk, wheat straw, corn cobs and peanut shells were sourced from Pakistan. They were collected from the local mills of the respective crops and milled locally to less than 1 mm prior to export to UK. Other woody biomass such as yellow pine and its steam exploded black pellets were supplied by Zilkha biomass energy for this research work. Other woody biomass that were the feedstocks of boiler as Hardwood (HW) sawdust, Pine wood pellet, Construction waste wood (CWW) for two different batches were supplied by local power plants. All these fuel samples were further milled and sieved to study the reactivity and explosion hazards associated with these biomass in association with particle size dependence.

5.3 Determination of the stoichiometric A/F

A consequence of the variable composition of biomass is that the stoichiometric A/F by mass for biomass is variable. This has important consequences for burner control of excess air. In the literature on biomass combustion, particularly that relating to the explosion hazards, pulverized biomass concentrations are always expressed in units of g/m^3 and until the work of Andrews and Phylaktou [24] there was no

conversion of concentration into equivalence ratio or the mixture concentration relative to the stoichiometric concentration. In contrast all publications on combustion for gas/air mixtures express the mixture concentration in terms of equivalence ratio. The stoichiometric A/F can be computed by carbon, hydrogen and oxygen balance from the elemental composition of the biomass. The stoichiometric A/F can be converted to g/m^3 at ambient volumetric conditions using the density of air as 1200 g/m^3 and the conversion from the stoichiometric A/F is given in Eq. 5.1.

Concentration g_{fuel}/m^3_{air} = 1200 / $A/F_{stoichiometric}$
[5.1]

For example for a typical wood with a stoichiometric A/F of 6 the concentration is 200 g/m^3. In contrast, a pure hydrocarbon (gas, liquid or solid) has a stoichiometric A/F of about 15 and a concentration of 80 g/m^3.The stoichiometric A/F of the selected samples were calculated by carbon, hydrogen and oxygen balance utilizing the elemental H/C (y) O/C (z), N/C (w) and S/C (k). The stoichiometric F/A is given by Eq. 5.2.

$$CH_yO_zN_wS_k + aO_2 \rightarrow bCO_2 + cH_2O + dNO_2 + eSO_2$$

$$Stoichiometric\ \left(\frac{F}{A}\right) = \frac{(12 + y + 16z + 14w + 32k)}{\left[\left(1 + \frac{y}{4}\right) - \frac{z}{2} + w + k\right] \cdot 137.9} \qquad [5.2]$$

The stoichiometric actual A/F can be calculated from the stoichiometric A/F on a daf basis using Eq. 5.3.

$$\text{Actual}(\ A/F) = Stoichiometric(\ A/F)[1 - (x_w + x_a)] \qquad [5.3]$$

Where x_w and x_a are the mass fractions of the moisture and ash contents in the sample respectively.

5.4 Chemical characterisation

The chemical characterisations of selected biomass samples are shown in Table 5.1. This includes the elemental analysis, the proximate analysis, the calorific value and the stoichiometric A/F on a daf and actual basis. Biomass samples were found to have lower carbon contents in the range of 46-57% compared to coals that have much higher values. Similarly %hydrogen content of most of the biomass were measured to be higher except CWW2 compared to coal samples. Important feature of this renewable biofuel is that they have negligible

amount of nitrogen and sulphur as shown in table 5.1; that are problematic for combustion due to the release of hazardous NO_x and SO_x. Also these biomass fuels showed higher oxygen contents due to inherent oxygen in their structures and for that reason, described as oxygenated fuels.

Proximate analysis showed higher volatile and lower fixed carbon contents compared to coal samples. Moisture and ash contents vary depending on the type of biomass. For example, agricultural crop residues were found to have higher moisture and ash contents compared to woody biomass which have less inert as shown in table 5.1. Three agricultural waste bagasse, rice husk and wheat straw were again analysed for the finer fractions that showed an interesting feature of enriching ash in that fraction. This was due to brittle nature of ash that mills along with the biomass and enrich the finer fraction during sieving. For this reason, these finer fraction showed higher proportion of ash in the proximate analysis changing the other proportions accordingly.

Due to the presence of inherent oxygen, biofuels have lower stoichiometric air to fuel (A/F) ratio than coals. Studied biomass samples showed stoichiometric A/F on dry ash free basis range from 5.4 to 7.5. This stoichiometric A/F ratio were also changed to actual stoichiometric ratio after incorporating %ash and moisture contents.

Heating values of these biofuels especially crop residues were less due to high moisture and ash contents. They have less energy density due to their voluminous nature in contrast to coals having higher heating contents.

Similarly the bulk and true particle density were also presented in table 5.2 for the selected biomass samples. Utilizing these values of densities, the porosity of these solid fuels were also calculated. Results showed a wide difference of actual particle and bulk densities with high porosities. A possible reason for this is the highly irregular fibrous structure leaving intra-particle spaces in packing. BET surface area results were also included in table 5.2 showing variation from 0.84-1.96 m^2/g. Surface area of the steam treated sample increased compared to untreated raw pine wood due to generation of more fine sized particles.

Figure 5.1 shows the H/C ratio against O/C for different biomasses and coals. Proportions of these components of biomass vary from one biomass to another and as they have quite different H/C and O/C ratio the variability of biomass is mainly due to the variability of the constituent components of biomass. Also included in Figure 5.1 is the composition of the main constituents of biomass: cellulose, hemicellulose and lignin (based on chemical formulae of $C_6H_{10}O_5$, $C_5H_{10}O_5$ and a mixture of $C_9H_{10}O_2$, $C_{10}H_{12}O_3$, $C_{11}H_{14}O_4$ for lignin respectively [176, 177]).

The stoichiometric A/F_{daf} are shown as a function of H/C in Figure 5.2 and this shows the wide variation with biomass composition. Also shown is that the stoichiometric A/F of hemicellulose is 3.15 and 9.56 for Lignin and these cover the entire spectrum of biomass compositions. This again shows that biomass composition variability is controlled by the varying cellulose, hemicellulose and lignin proportions.

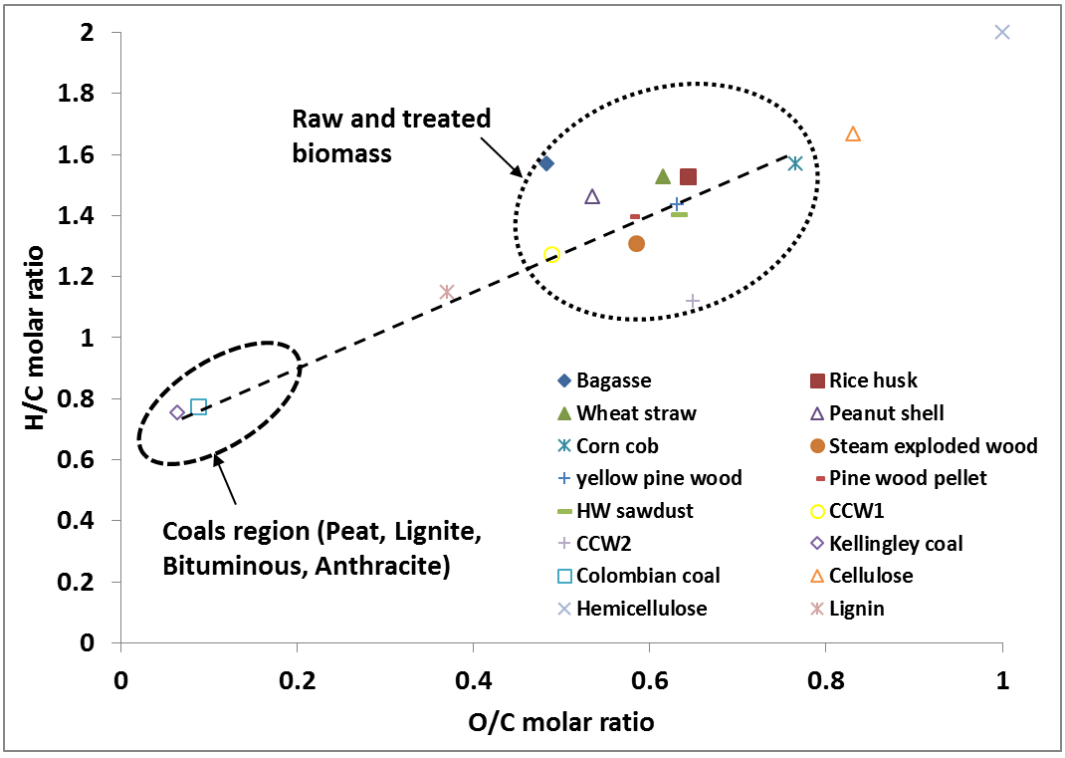

Figure 5.1 Atomic H/C vs. O/C molar ratios of biomass and coal samples in comparison to pure Cellulose, Hemicellulose and Lignin

Table 5.1: Chemical Characterisation of the selected biomass and coal samples

Biomass	C	H	N	S	O	VM	FC	H_2O	Ash	Calorific value, CV MJ/kg		Stoich A/F daf.	Stoich A/F actual
	% mass dry basis					% mass daf. basis		% mass ar basis		actual	daf	g/g	
Bagasse (B)	43.6	5.7	1.0	0.1	28.0	92.3	7.7	7.2	20.1	15.6	21.5	7.5	5.4
B<63µm	38.2	4.9	0.9	0.1	30.8	86.7	13.3	6.8	23.4	-		6.4	4.4
Rice Husk (RH)	40.2	5.1	0.9	0.0	34.4	83.7	16.4	7.7	17.9	15.2	20.4	6.2	4.5
RH<63µm	32.5	4.5	1.1	0.2	28.3	83.1	16.9	6.6	31.2	-		6.1	3.8
Wheat Straw (WS)	38.2	4.9	1.0	0.1	31.3	86.2	13.8	6.8	22.8	14.5	20.6	6.4	4.5
WS<63µm	23.9	3.1	0.5	0.0	21.2	82.7	17.3	4.0	49.2	-		6.0	2.8
Corn Cobs (CC)	41.6	5.4	1.0	0.1	42.4	82.5	17.6	7.1	8.8	14.8	17.6	5.4	4.5
Peanut Shell (PS)	49.1	6.0	1.4	0.0	35.0	78.1	21.9	7.0	8	18.2	21.4	6.9	5.9
Steam exploded wood (BP)	51.3	5.6	0.4	0	39.9	78.6	21.4	4.4	2.7	20.4	22.0	6.3	5.8
Yellow pine (YPW)	50.1	6.0	0	0	42.1	83.4	16.5	5.4	1.7	20.0	21.5	6.1	5.7
Pine wood pellet (Blz)	50.3	5.9	0.5	0	38.8	84.6	15.4	6.7	4.3	19.2	21.6	6.4	5.7
HW Sawdust (Dfl)	49.5	5.8	0.4	0	41.8	85.6	14.4	6.0	2.4	19.4	21.2	6	5.5
CWW1 (Dk 1)	48.8	5.2	0.6	0..0	31.8	89.9	10.1	4.9	13	18.3	22.3	7	5.7
CWW2 (Dk 2)	49.4	4.6	0.4	0.2	42.8	94.1	5.9	6.7	2.4	19.1	21.0	5.6	5.1
Kellingley Coal (K Coal)	66.1	4.2	2.4	2.3	5.6	36.9	63.3	1.7	19.1	25.0	31.6	11.6	9.2
Colombian Coal (C Coal)	68.8	4.4	2.2	0.7	8.1	41.3	58.6	3.2	15.3	26.4	32.4	11.2	9.1

Table 5.2: Bulk and particle densities with the porosity of biomass samples

	B	RH	WS	CC	PS	BP	YPW	Blz	Dfl	Dk 1	Dk 2
Bulk density (Kg/m^3)	204	382	318	284	320	437	229	199	210	240	196
True density (Kg/m^3)	1671	2203	1702	-	-	1752	1678	1757	1784	1675	1695
Porosity (%)	88	83	81	-	-	75	86	89	88	86	88
BET surface area (m^2/g)	0.96	-	1.96	-	-	1.6	1.55	0.84	1.46	-	-

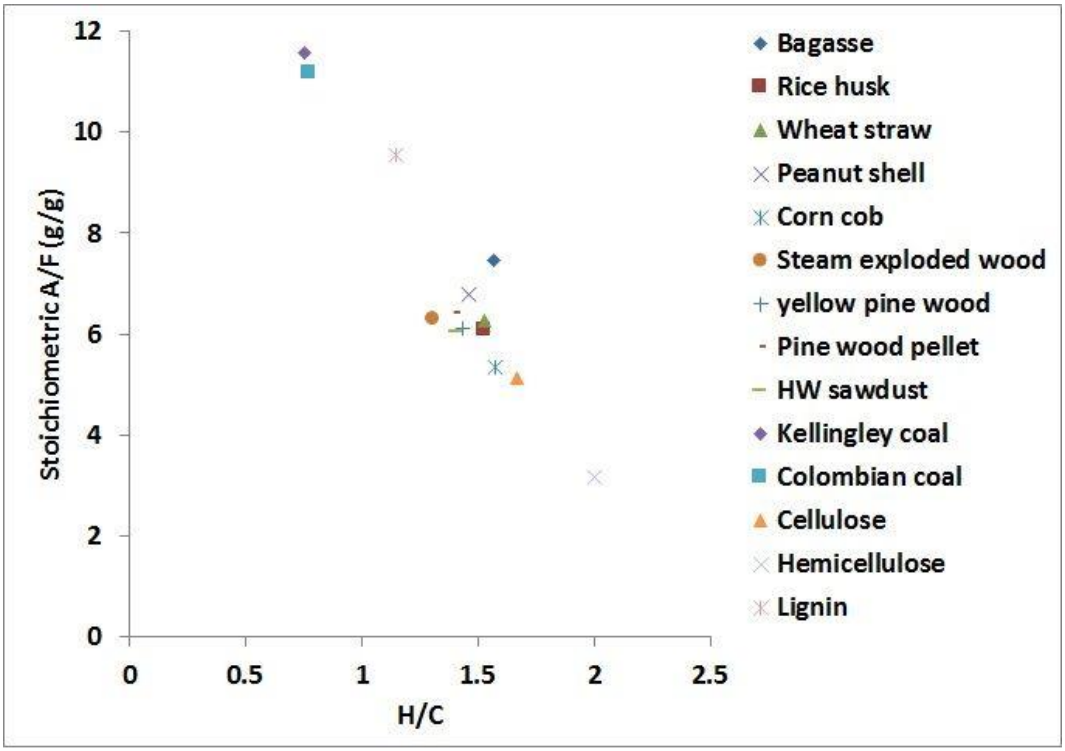

Figure 5.2 Molar H/C v stoichiometric A/F by mass of selected biomasses

Besides analytical methods, Sheng and Azevedo (2002) proposed a model based on extended CPD to measure the proportions of Cellulose, hemicellulose and lignin contents [176]. The proposed correlations were based on H/C, O/C and VM for large number of biomass samples with correlation coefficient roughly 90% using eq. 5.4 and 5.5. The proportions of hemicellulose was determined by the difference method after deducting the percentage mass of cellulose and lignin from total of 100.

$$Cellulose = -1019.07 + 293.810\left(\frac{O}{C}\right) - 187.639\left(\frac{O}{C}\right)^2 + 65.1426(HC) - 19.3025\left(\frac{H}{C}\right)^2 + 21.7448(VM) - 0.132123(VM)^2 \quad [5.4]$$

$$Lignin = 612.099 + 195.366\left(\frac{O}{C}\right) - 156.535\left(\frac{O}{C}\right)^2 + 511.357(HC) - 177.025\left(\frac{H}{C}\right)^2 - 24.3224(VM) + 0.145306(VM)^2 \quad [5.5]$$

It was assumed in this work that based on elemental and TGA analysis, these components proportions can be estimated based on simple pyrolysis decomposition of biomass into these components as;

$$CH_xO_y \text{ (Biomass)} \rightarrow a \text{ Cellulose} + b \text{ Hemicellulose} + c \text{ Lignin}$$

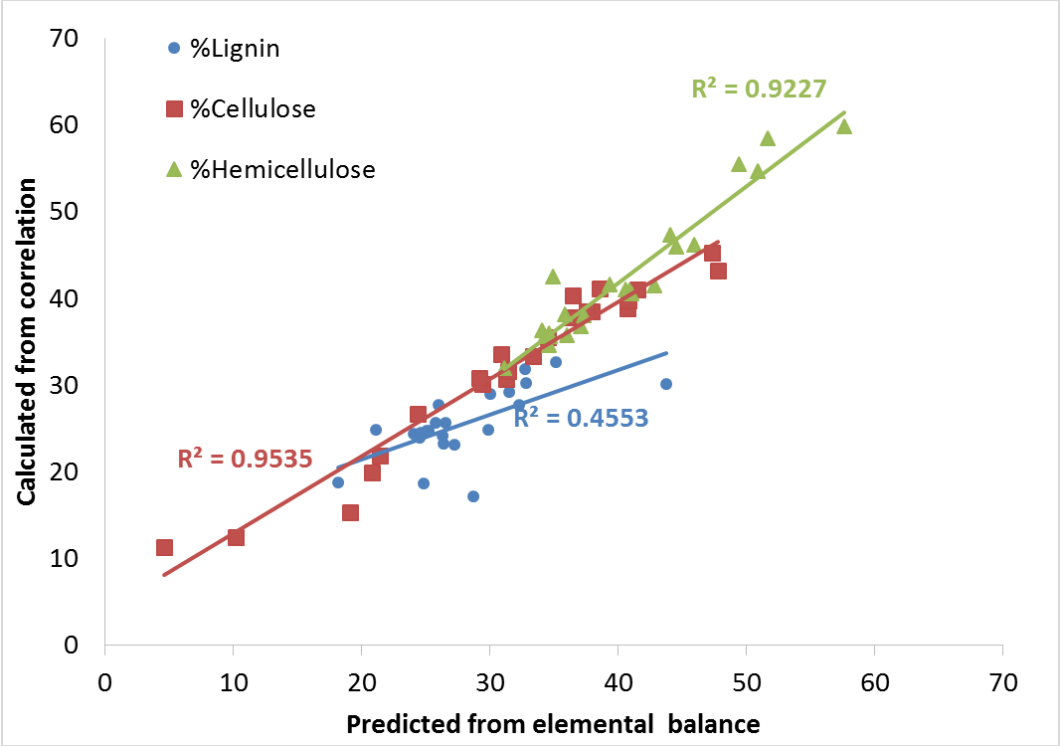

Figure 5.3: Chemical components based on elemental balance and correlations for a number of biomass samples

These components can also be expressed as CHO if there elemental compositions are known. However for different biomass materials, the elemental molar ratios exist for a range for these components especially for hemicellulose and lignin with multiple compounds structure.

An iteration procedure was followed using solver method in Excel to estimate the percentages of cellulose, hemicellulose and lignin contents after converging the molar ratios within the existing range of their molar ratios. A good comparison was found for estimation of % cellulose and % hemicellulose contents using the correlations (Eq. 5.4 and 5.5) in comparison to the predicted using elemental balance. The % lignin contents were dispersed widely with poor correlation coefficient as shown in Figure 5.3.

Also it was found from pyrolysis experiments that these chemical species in pure form release for specific temperature ranges: Hemicellulose for 220-315^{o}C, Cellulose for 315-400^{o}C and Lignin for >400^{o}C [178]. However for biomass samples with complex overlapping structure and presence of ash cause hindrance for the release of these components [179]. Based on actual variation of daf TGA plots for different biomass samples, these chemical components were measured with their temperature ranges. However these are just the estimation assuming the free and independent release of these

component without any influence from other component that is not true in reality. The calorific values in Table 5.1 are reduced for biomass with a high water and ash content such as agricultural waste material. If the water is removed and a process to remove the ash is used, such as acid water washing, then the higher calorific value on a daf results, which is also shown in Table 5.1. The increase in CV for agricultural waste biomass on a daf basis is considerable and for these high ash fuels, acid washing to remove ash components such as potassium will be essential; as the reduction in flame temperature from the low CV will make good heat transfer in boilers difficult. It is known that the CV_{daf} of biomass is correlated to the elemental analysis and Eq. 5.6 [180] is a common relationship used for this.

$$CV_{higher} = 1.87\%C^2 - 144\% - 2820\%H + 63.8\%C \times \%H + 129\%N + 20147 \quad [5.6]$$

A consequence of Eq. 5.6 is that a high oxygen content of biomass, which reduces the % of all the other components, reduces the CV. Lignin has the lowest oxygen content at 21.3% with hemicellulose the highest at 55.0% and cellulose at 49.8%. A high CV_{daf} thus occurs for biomass with high lignin content and a low CV occurs for biomass with high hemicellulose content.

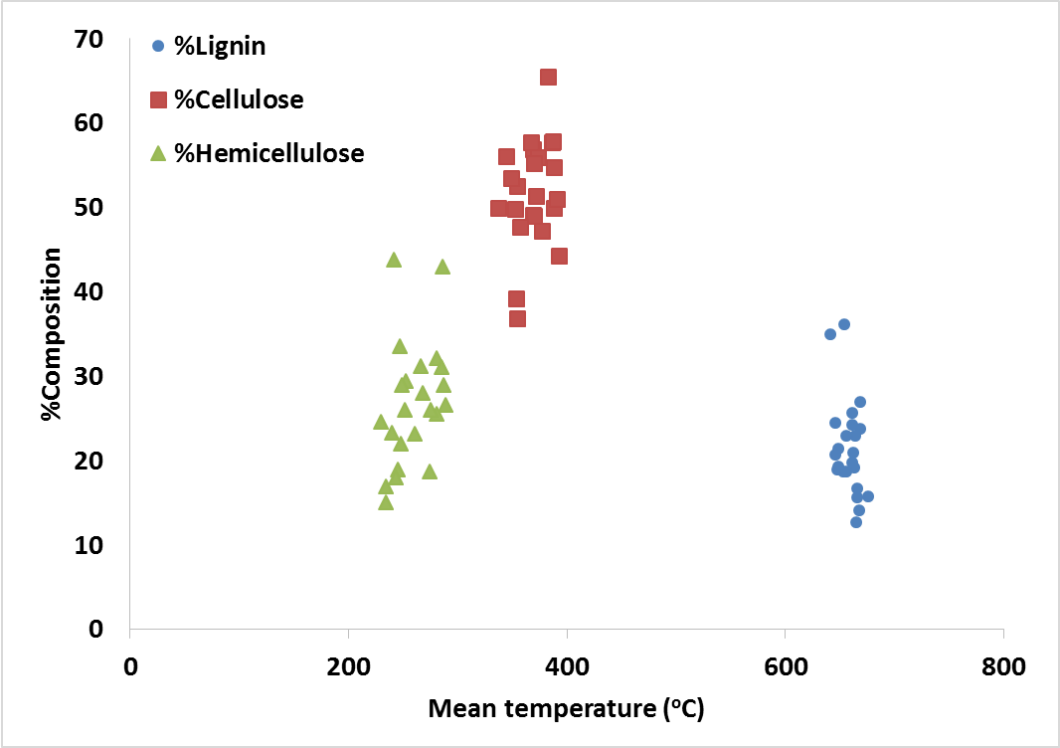

Figure 5.4: % Chemical components based on TGA plots vs. average temperature of number of biomass samples

5.5 Volatile matter determination

Figure 5.5 shows that the normalised TGA release of volatiles was similar for all biomass and yet had significant differences, which are shown more clearly in the rate of mass loss plots in Figure 5.6. The release of volatiles for the coal samples was found to occur at a much higher temperature compared to biomass samples, as shown in Figures. 5.5 and 5.6. Biomass samples release 80-90% of their volatiles in the temperature range of 350-450^{o}C, whereas for coal samples the release of volatiles was only about 30%. Figure 5.6 shows that the peak rate of release of volatiles from biomass is higher than for coal and occurs at lower temperatures. Also for some biomass samples, there were two sharp peaks observed showing the decomposition of hollo-cellulose at lower temperature with subsequent lignin decomposition at higher temperature. Decomposition of these components depends on their overlapping structure and level of ash contents in the sample [178, 181].

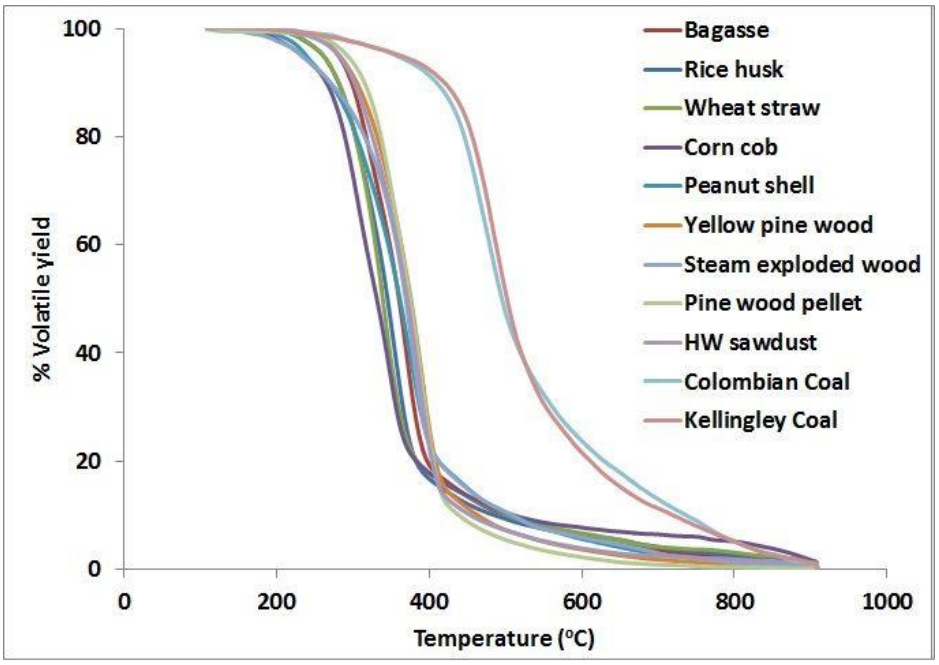

Figure 5.5 % yield of volatiles vs. temperature for biomass samples in comparison to coals

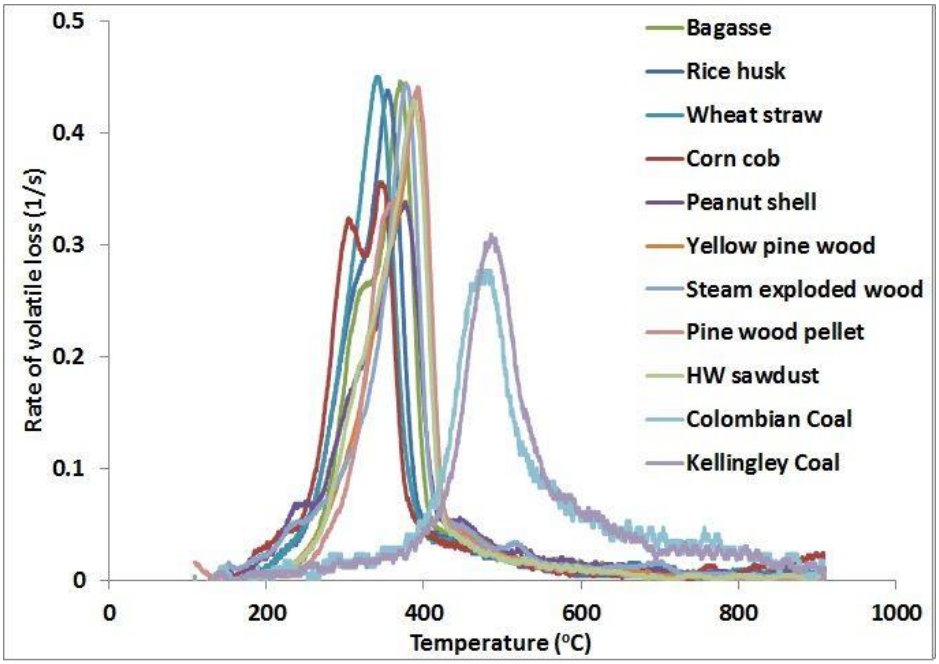

Figure 5.6 Rate of volatile loss vs. temperature for biomass samples in comparison to coals

Similarly the combustion of char for biomass samples was quicker than the coal materials as shown in Figure 5.7. This was due to higher volatile yield in biomass leaving behind more porous structure having higher surface area. This active surface of biomass has fast combustion reaction due to more diffusion and interaction with oxygen. Crop residue biomass samples despite of having higher ash were containing more reactive char than the woody biomass due to more porous and soft structure compared with woody biomass samples. Effect of pre-treatment like steam explosion increased the reactivity of char for the yellow pine wood sample. Rate of char combustion have greater influence on the reactivity of coal as they have higher char yield compared to biomass samples. Colombian coal showed much higher reactivity of char than Kellingley coal with fast burning rate as shown in Figure 5.7.

5.6 Correlations of biomass volatile fraction

Table 5.1 shows that on a raw particulate basis the volatile fraction (VF) of all the biomass studied varied from 60.7 – 85.5% on an as received basis and on a dry ash free (daf) basis it varied from 78.1 – 94.1%. Although all biomass have a high VF there is significant difference in the VF for different biomass. The use of the daf VF was because the water and ash content were variable and considered to have little influence on the volatile release.

Table 5.3: TGA peak volatile rate and corresponding temperature of biomass and coal samples

Samples	Max. volatile yield rate (10^{-3}) (1/s)	Temperature (°C)
Bagasse (B)	446	369.9
Rice husk (RH)	437	353
Wheat straw (WS)	450	341.4
Corn cob (CC)	354	344
Peanut shell (PS)	338	376
Yellow pine wood (YPW)	436	389
Steam exploded wood (BP)	444	375
Pine wood pellet (Blz)	441	391
Hardwood sawdust (Dfl)	429	386
Kellingley Coal (K Coal)	309	485
Colombian Coal (C Coal)	270	483.6

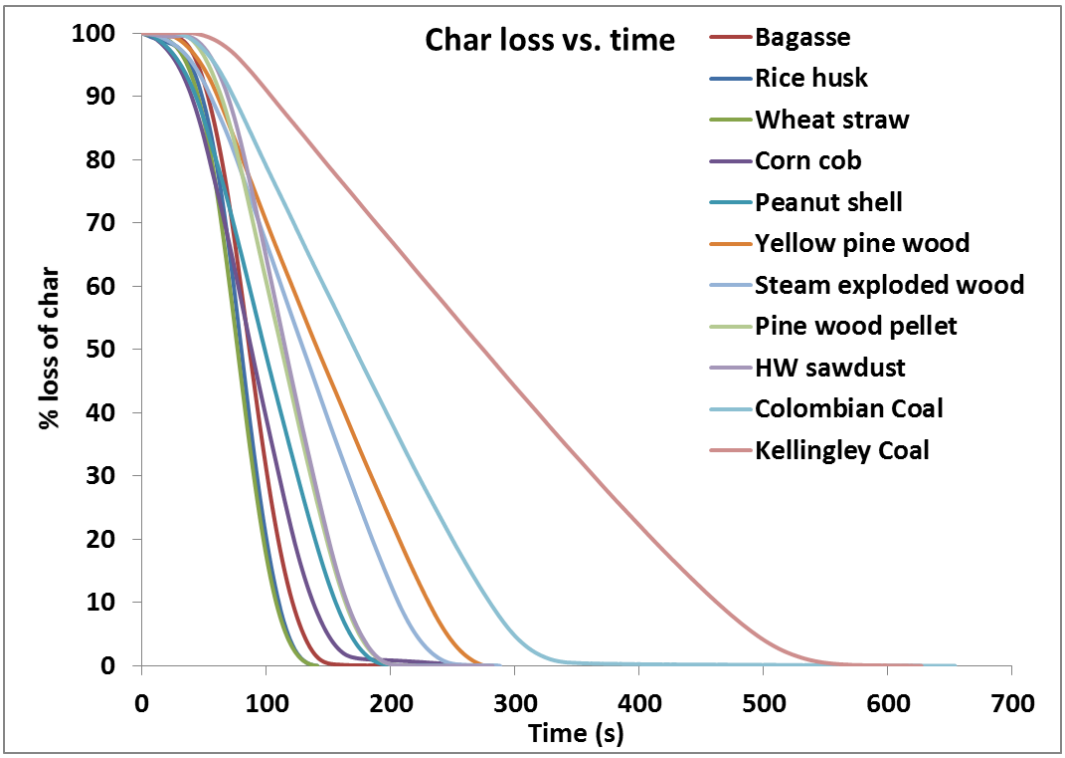

Figure 5.7 % loss of char vs. time of biomass and coal samples

Figure 5.8 shows the data of the volatile fraction against H/C molar ratio of the biomass and coal samples. It shows that biomass samples with higher H/C ratio produce higher volatile fraction in contrast to coal samples. The data scatter for biomass is large and could not be correlated. Figure 5.9 shows the volatile fraction plotted as a function of the O/C molar ratio. This again shows that biomass samples have higher volatile fraction and O/C compared to coal samples. For biomass samples, the O/C is the dominant factor in the volatile fraction this would imply that CO was the main component of the volatile gases. Pyrolysis of biomass samples also showed the major proportions of CO that increase further for fast/flash pyrolysis employing higher heating rate and higher temperature [151, 182]. The measured CV and the volatile fraction are reasonably well correlated, as shown in Figure 5.10. As the volatile fraction of biomass increases Figure 5.9 shows that the oxygen content also increases. A limiting condition of 100% volatiles that are all CO is shown in Figure 5.10 to be not far below the extrapolated line. There would be some hydrocarbons as well, but CO is likely to dominate the volatile gas composition.

5.7 Computation of volatile composition by elemental balance

If the composition of the volatiles is assumed to be exclusively CO, CH_4 and H_2 then the relative amounts can be computed from the elemental and TGA proximate analysis. The results of this computation are shown in Table 5.4 for two different assumptions. The first computation assumes that under very rapid heating in flames all the biomass becomes volatile and the mean composition of the released gases is the same as the biomass elemental composition. The second computation assumes that the fixed carbon determined by TGA does not appear in the gas phase and hence the mean carbon content of the volatiles is reduced from that in the biomass.

The results are shown in Table 5.4 where there are negative amounts for a gas, this indicates that an elemental balance could not be achieved and hence there must be other gases present than the three assumed. However, there are only a few cases of negative values and so in most cases the simple three gas assumption may be valid.

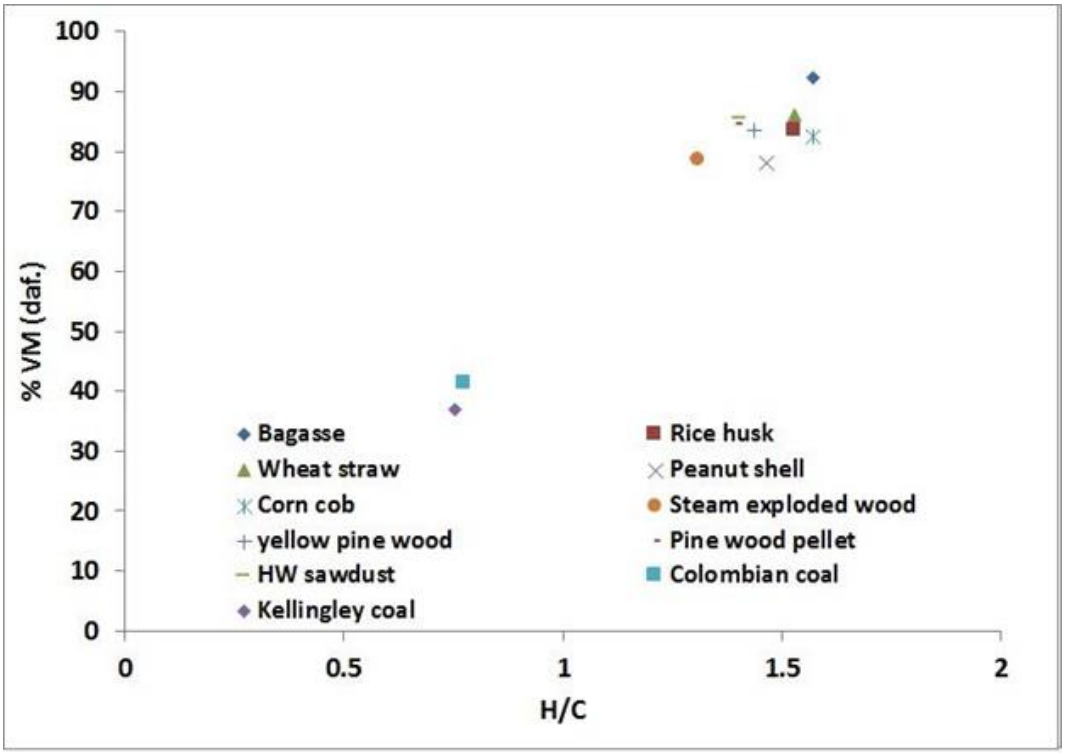

Figure 5.8 Correlation of %VM (daf) with molar H/C of selected biomass and coal samples

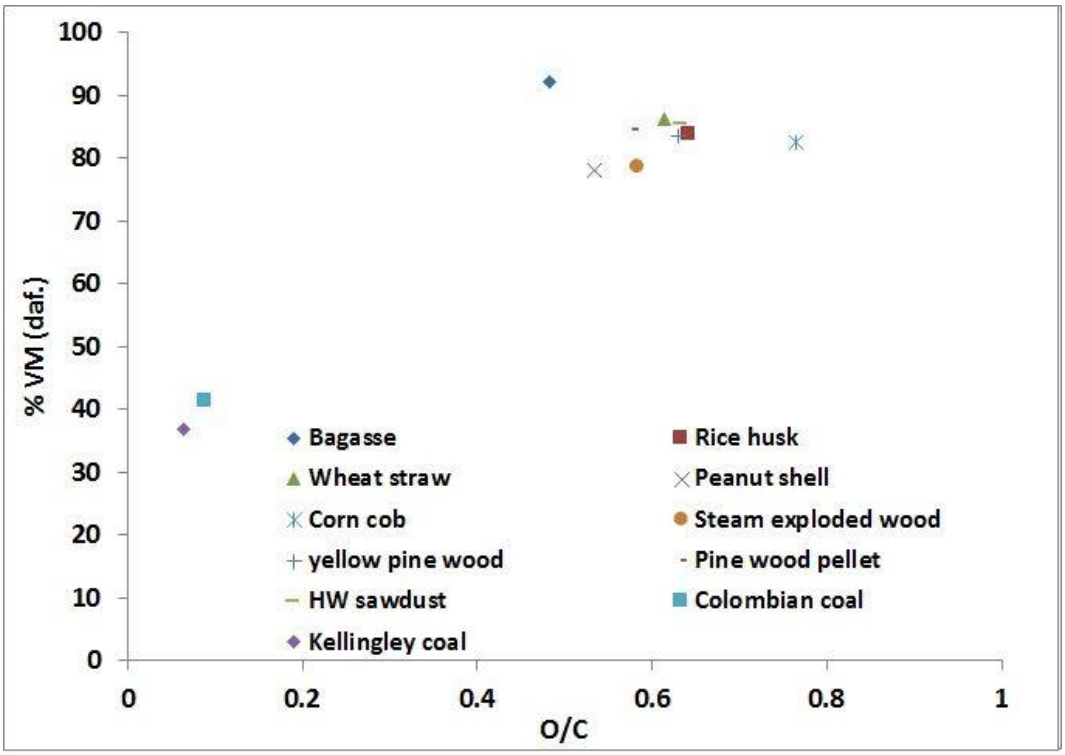

Figure 5.9 Correlation of %VM (daf) with molar O/C of selected biomass and coal samples

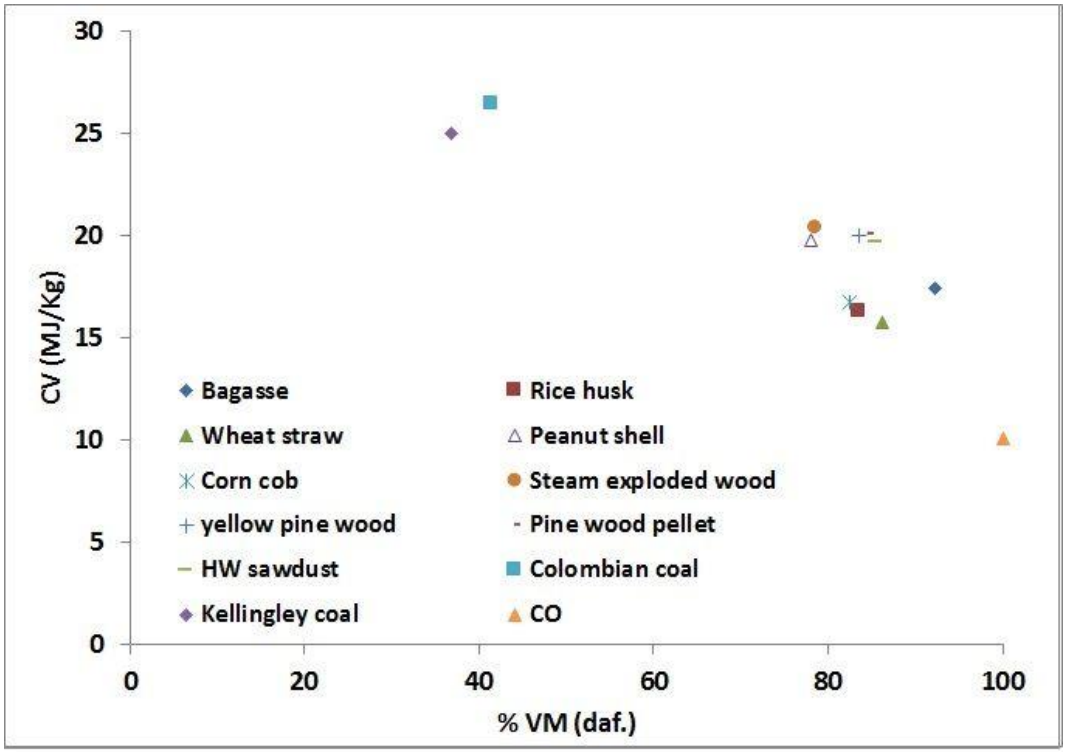

Figure 5.10 Correlation of CV with the % volatile matter of selected biomass and coal samples

Table 5.4 shows that if the mean composition of the biomass volatiles is the same as the solid biomass (daf) then CO varies between 63 – 83% by mass and CH_4 varies between 15 and 39% with little hydrogen. However, for coal the assumption results in impossible amounts of methane, high hydrogen and low CO. Thus, as is well known, this model is not realistic for coal but it could be for biomass. If the fixed carbon is not turned into volatile with rapid flame heating, then the predictions are much more sensible for coal with 56% CO and 49% CH_4. In modelling of coal combustion the volatiles are often assumed to be methane. For biomass the predicted CO is increased from the previous case to 70 – 100% roughly and lower CH_4 is predicted in the range 0-30%. Some hydrogen is also predicted for some biomass. Both cases could be reasonable for biomass. The low level of char in biomass combustion in explosions and furnaces indicates that assuming the mean composition of the volatiles is the same as that of the biomass, may be reasonable and some CFD models of biomass combustion make this assumption.

Table 5.4: Computation of the volatile composition based on elemental balance and the assumption of CO, CH_4 and H_2 as the only gases in the volatiles

Biomass	Including FC with the Volatiles					Volatile excluding FC				
	Formula	Stoich. A/F	CO %	CH_4 %	H_2 %	Formula	Stoich. A/F	CO %	CH_4 %	H_2 %
Rice Husk (RH)	$CH_{1.53}O_{0.64}$	6.15	76%	24%	0%	$CH_{2.10}O_{0.97}$	4.85	92%	2%	7%
Bagasse (B)	$CH_{1.57}O_{0.48}$	7.46	63%	39%	-2%	$CH_{1.73}O_{0.57}$	6.96	70%	30%	0%
Wheat Straw (WS)	$CH_{1.53}O_{0.61}$	6.35	74%	26%	0%	$CH_{1.95}O_{0.85}$	5.29	87%	8%	5%
Corn Cobs (CC)	$CH_{1.57}O_{0.77}$	5.40	83%	15%	2%	$CH_{2.35}O_{1.25}$	3.87	101%	-12%	10%
Peanut Shell (PS)	$CH_{1.46}O_{0.53}$	6.88	68%	34%	-2%	$CH_{2.56}O_{1.15}$	4.46	98%	-7%	10%
Steam exploded wood (BP)	$CH_{1.31}O_{0.58}$	6.31	72%	29%	-2%	$CH_{1.46}O_{0.66}$	5.91	77%	22%	0%
Yellow pine wood	$CH_{1.44}O_{0.63}$	6.12	75%	25%	0%	$CH_{1.86}O_{0.86}$	5.18	87%	8%	5%
Pinewood pellet (BLZ)	$CH_{1.40}O_{0.58}$	6.45	72%	30%	-1%	$CH_{2.03}O_{0.95}$	4.84	91%	2%	6%
Hardwood sawdust (DFL)	$CH_{1.41}O_{0.63}$	6.06	75%	25%	0%	$CH_{1.97}O_{0.93}$	4.90	90%	4%	6%
Kellingley Coal (K Coal)	$CH_{0.75}O_{0.06}$	11.59	13%	109%	-22%	$CH_{1.39}O_{0.39}$	8.07	56%	49%	-5%
Colombian Coal (C Coal)	$CH_{0.77}O_{0.09}$	11.18	17%	103%	-20%	$CH_{1.37}O_{0.40}$	8.01	56%	49%	-5%

Table 5.5: Ash Characterisation of the selected three crop residues using X-ray fluorescent method

	Al_2O_3	BaO	CaO	Fe_2O_3	K_2O	MgO	MnO	P_2O_5	SiO_2	SrO	TiO_2	Others
	% mass											
WS_{ash}	10.5	0.04	5.4	0.6	9.5	2.2	0.2	0.7	59	0.05	0.9	11
RH_{ash}	1.3	0	2.3	0.9	2.1	0.4	0	0.6	87	0.01	0.01	5
B_{ash}	9.1	0.1	9.4	3.5	5.2	3.1	0.6	1.7	48	0.2	0.7	19

Ashes of three crop residues bagasse, rice husk and wheat straw were analysed using X-ray fluorescence technique. The results showed as % proportion of mass in the respective sample. The siliceous contents were measured to be in higher proportions in all these sample and especially in rice husk. The reason of these higher siliceous minerals was found to be due to admixture of soil during their collection. After silica oxide, the next higher proportions were found to be Alumina, potassium oxide and calcium oxide with rest of the mineral oxide in negligible amounts. Presence of these minerals cause powerful corrosive action and are very problematic. However, some of these metallic oxide like Alumina and Magnesium oxide act to catalyse the combustion of biomass. These biomass samples especially agricultural wastes need to be processed for the reduction of these ash minerals before their application.

5.8 Stagg's quick approximation method for kinetic data from TGA

Stagg's [173-175] quick approximation method was used to determine the kinetic data for the rate of volatile's yield from a solid that is applicable for low temperature TGA analysis. Two different models were developed: the Series Reaction Model and the Competitive Reaction Model. The model assumption, for both the series and competitive reaction models, were a first order reaction, as in Eq. 5.7, and $T_c/\Delta T_c >> 1$, where T_c is the characteristic temperature (temperature for 50% of the mass fraction i.e. c=0.5) and ΔT_c= Characteristic temperature range.

$$Rate\ Constant\ 'k' = Ae^{\left(\frac{-T_A}{T_S}\right)} \quad [5.7]$$

Where T_A is the activation temperature, A is pre-exponential factor and T_S is the solid material temperature

$$T_A = -\frac{T_C^2}{c.\Delta T_C.\log(c)} \quad [5.8]$$

$$A = \frac{\left(H \times Exp\left(\frac{T_A}{T_c}\right)\right)}{c \times \Delta T_c} \quad [5.9]$$

Here 'H' is heating rate.

T_c and ΔT_c are adjusted until the integral of the residual error approaches zero using GRG non-linear solving method in the 'Solver' option in Microsoft Excel.

5.8.1 Series reaction model

Figure 5.5 shows that the rate of release of volatiles from dry biomass follows three stages: the first stage occurs over 200– 300ºC and accounts for typically 10% of the volatile loss. The second stage is the rapid mass loss of about 70% of the total volatile mass over the temperature range 300 – 400ºC. Finally, there is a slow loss of volatiles accounting for about 20% of the volatile loss over the temperature range 400 – 900ºC. These three stages were present in the coal samples but at much higher temperatures. In this proposed simple model, the rate of release of volatiles was split into two stages and the first stage combines the initial first and second stages. Cellulose and hemicellulose in the biomass break down in the lower temperature range release the primary volatiles. In the later stage, some remaining contents of cellulose and hemicellulose decompose, possibly to tar, but it is mainly hard lignin that partially decomposes, depending on the heating rate and temperature. This later volatile loss is due to the higher decomposition temperature of lignin.

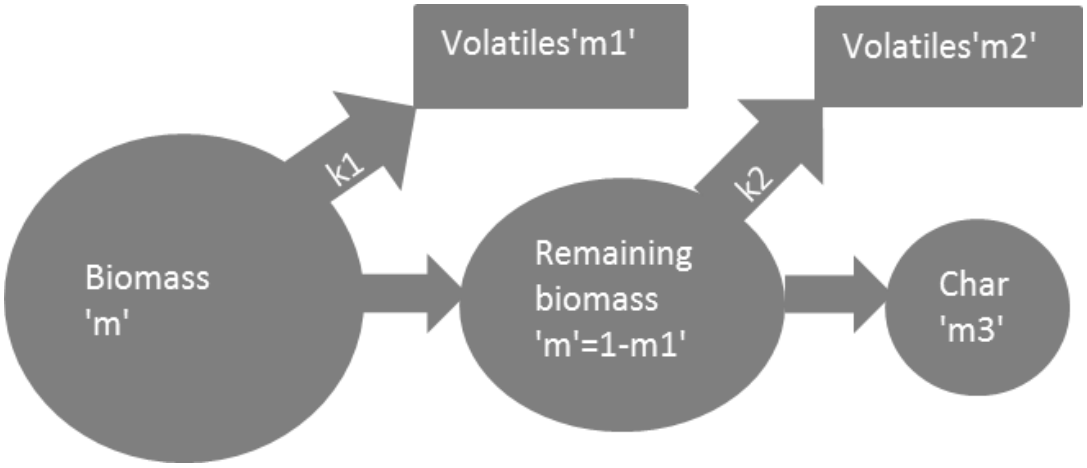

Figure 5.11 Series Model for rate of volatile release

Table 5.6: Predicted Kinetics for two phases in TGA volatile's loss in series reaction model

Materials	Activation energy 'E' (KJ/mol)		Activation energy (MJ/kg)		Rate Constant 'k' (s^{-1})		MEC
	1st phase	2nd phase	1st phase	2nd phase	1st phase	2nd phase	Eq. ratio
Bagasse	87.0	38.2	4.1	1.8	$1.7E+5e^{10468.8/T}$	$0.7e^{4593.4/T}$	0.27
Rice husk	83.1	38.9	3.4	1.6	$1.2E+5e^{9999.1/T}$	$0.7e^{4682.1/T}$	0.35
Wheat straw	93.3	36.8	3.9	1.6	$1.2E+6e^{11218/T}$	$0.7e^{4425.8/T}$	0.55
Corn cob	71.0	40.7	2.7	1.6	$1.5E+4e^{8545.6/T}$	$0.6e^{4902/T}$	0.22
Peanut shell	63.0	35.5	2.8	1.6	$1.5E+3e^{7578.4/T}$	$0.7e^{4269.7/T}$	0.18
Yellow pine wood (YPW)	88.4	32.4	3.8	1.4	$1.6E+5e^{10631.1/T}$	$0.8e^{3716.2/T}$	0.35
Steam exploded wood (BP)	68.2	35.3	3.0	1.6	$3.7E+3e^{8208.4/T}$	$0.7e^{4251.1/T}$	0.2
Pinewood pellet (BLZ)	98.5	31.9	4.3	1.4	$1.0E+6e^{11854.4/T}$	$0.8e^{3841.3/T}$	0.46
Hardwood sawdust (DFL)	85.7	34.2	3.6	1.4	$1.0E+5e^{10310.3/T}$	$0.8e^{4114.3/T}$	0.36
Colombian Coal	105.6	39.8	7.4	2.8	$2.6E+5e^{12703.6/T}$	$0.6e^{4790.9/T}$	0.39
Kellingley Coal	111.0	38.1	8.1	2.8	$5.6E+5e^{13352.3/T}$	$0.7e^{4586.4/T}$	-

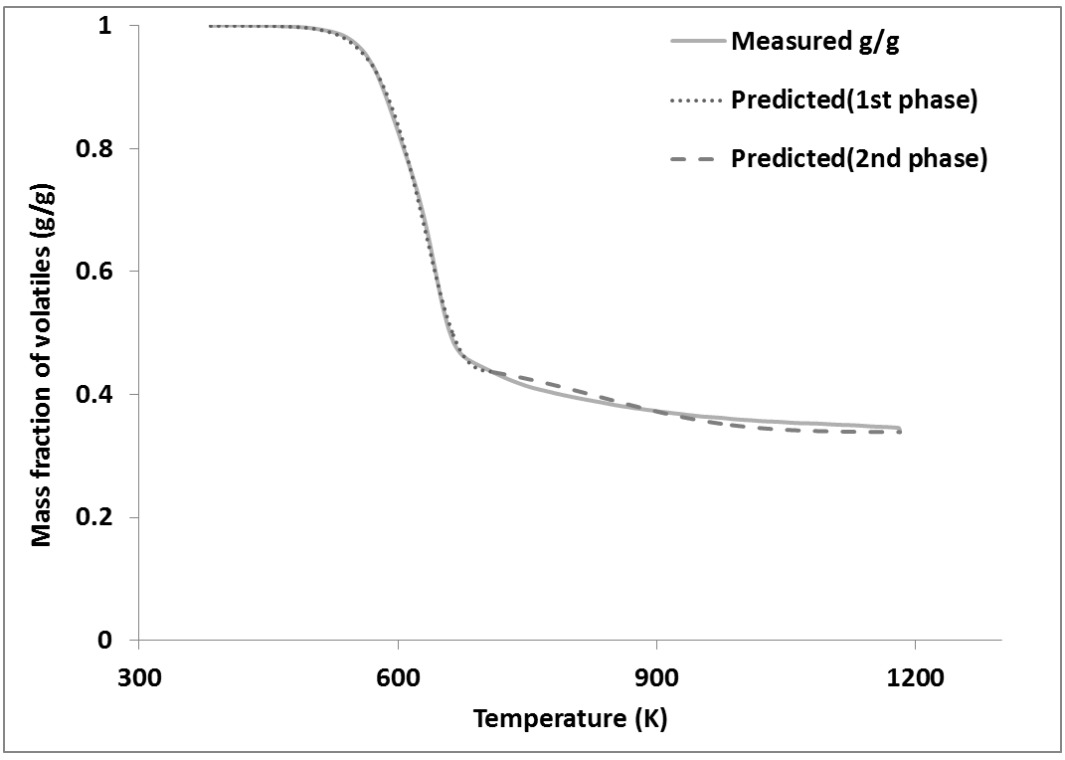

Figure 5.12 Predicted % yield of volatiles vs. temperature for two phases in comparison to experimental TGA result

With slow heating rate and low temperatures, there is some char residue left. It is possible that in propagating flames in pulverised biomass, where heating rates are much higher than in a TGA, that the fixed carbon will be less and the yield of CO will be higher.

The 'Series Reaction Model' mechanism is shown in Figure 5.11 and involves two routes to the release of volatiles: directly from the original biomass and via low temperature pyrolysis that produce material, such as tar, that subsequently decomposes to release volatiles. Kinetic equations for the release of volatile from these two phases are given by Eqs. 5.10 and 5.11. The production of char is given by Eq. 5.12.

$$\frac{dm}{dt} = -k_1\, m \qquad [5.10]$$

$$\frac{dm'}{dt} = -k_2\, m' \qquad [5.11]$$

$$m_3 = (m' - m_2) \qquad [5.12]$$

The rate of release of volatiles for the two phases was predicted using this model and compared with the experimental TGA results for slow heating rate of 25°C/min as shown in Figure 5.12, for one of the biomass in Figure 5.5. The fit to the data by the model was very good for the first two phases of the volatile release, showing that modelling them as one first order volatile release reaction was valid. The fit to the last stage of volatile release was not as good, but was reasonable. It is the good fit to the rapid volatile release phase that is important as this is the most important stage in flame propagation.

Activation energies and rate constants obtained from this Series Reaction model are given in Table 5.6 for all the biomass and the coal samples. The activation energies in Table 5.6 showed lower activation energy for biomass fuels than coal. Higher activation energies reflect higher energy requirements for the release of volatiles.

The lean limit MEC of the selected biomass samples as determined using the modified Hartmann explosion tube are compared with these activation energies in Table 5.6. Activation energies for the first phase showed a good correlation with the MEC as shown in Figure 5.13. Table 5.6 shows that activation energies for the second phase were approximately similar and hence the late release of volatiles is not contributing to the difference in the rate of volatile release and the MEC differences for different biomasses. This is to be expected as it is the

initial volatile release that is going to control the flame propagation rate and hence the MEC.

Figure 5.13 shows poor agreement with the trend for wheat straw (high MEC) and Bagasse (low MEC) for similar activation energy. One explanation for this could be differences in the ash content, but Table 5.1 shows that there is little difference in ash. Bagasse has more volatiles and a lower MEC than would be expected. It is possible that there are particle size differences with the pulverised bagasse being coarser than that for wheat straw in the modified Hartmann tests. All the biomasses were milled and sieved below 63 µm and the size distributions for the particles used in the MEC tests are shown in Table 5.7. Previous works by the authors [17-19, 21-23, 110, 169] have shown that particle size does affect the MEC. However, Table 5.7 shows that the size difference between bagasse and wheat straw were small. Hence, the reason for these two biomasses not following the trend of the other biomass in Figure 5.13 is not known and further work is required over a wider range of biomass samples.

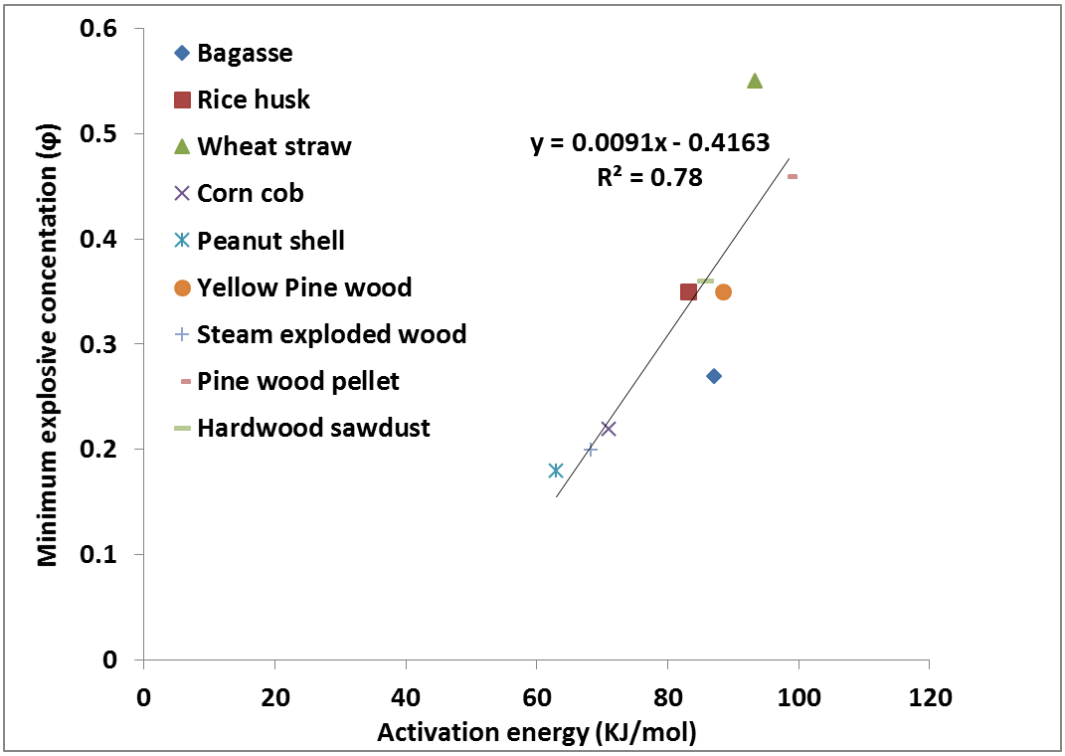

Figure 5.13 Correlation of MEC with activation energies based on the series reaction model for volatile's loss of biomass samples

Table 5.7 Particle size distribution in the MEC tests

Samples	d(0.1)	d(0.5)	d(0.9)	Surface mean diameter $d_{3,2}$	Volume mean diameter, $d_{4,3}$
	μm				
Bagasse (B)	24.3	125.6	356.0	70.2	201.5
Rice husk (RH)	13.6	191.6	563.8	33.5	247.7
Wheat Straw (WS)	18.8	126.1	441.5	78.0	213.4
Corn cob (CC)	45.0	372.6	777.8	98.1	394.1
Peanut shell (PS)	24.3	176.1	698.5	63.5	282.4
Steam exploded wood (BP)	13.0	54.8	162.3	30.3	75.9
Yellow pine wood (YPW)	30.7	198.3	629.6	77.2	287.1
Pine wood pellet (BLZ)	33.0	180.4	569.2	68.4	245.6
HW sawdust (DFL)	28.0	184.2	576.3	56.2	247.3
Colombian Coal (C Coal)	6.8	28.1	85.2	14.7	40.1
Kellingley Coal (K Coal)	5.0	25.5	65.3	12.0	30.9

In addition to the rate of volatile release activation energy on MEC as a reactivity parameter, its impact on flame propagation parameters was investigated. In the modified Hartmann equipment the concentration of biomass dust was varied to determine the peak reactivity concentration in terms of the rate of pressure rise prior to the bursting of the vent at the top of the vessel. The correlation of this with the volatile release activation energy is shown in Figure 5.14. This shows no correlation between the rate of pressure rise and the activation energy. This was unexpected as the rate of flame propagation is often modelled as the release of volatiles followed by combustion. It is likely that flame propagation is controlled by the rate of heating of the particles by conduction and radiation from the flame front. The release of volatiles is a consequence of this heating and not the cause of the heating.

Similarly the activation energies for the first main stage of volatile release were plotted against % inert as shown in Figure 5.15. There were two independent correlations further observed similar to the plot of % inert against MEC as will be discussed further in chapter 6. Increase in level of ash plus moisture content have more profound effect on woody biomass than on the crop residue sample and showed higher activation energies for sample having more inert. The activation energy requirement for the release

of volatiles play an important role for the propagation of flame and higher inert suppresses the reactivity of biomass.

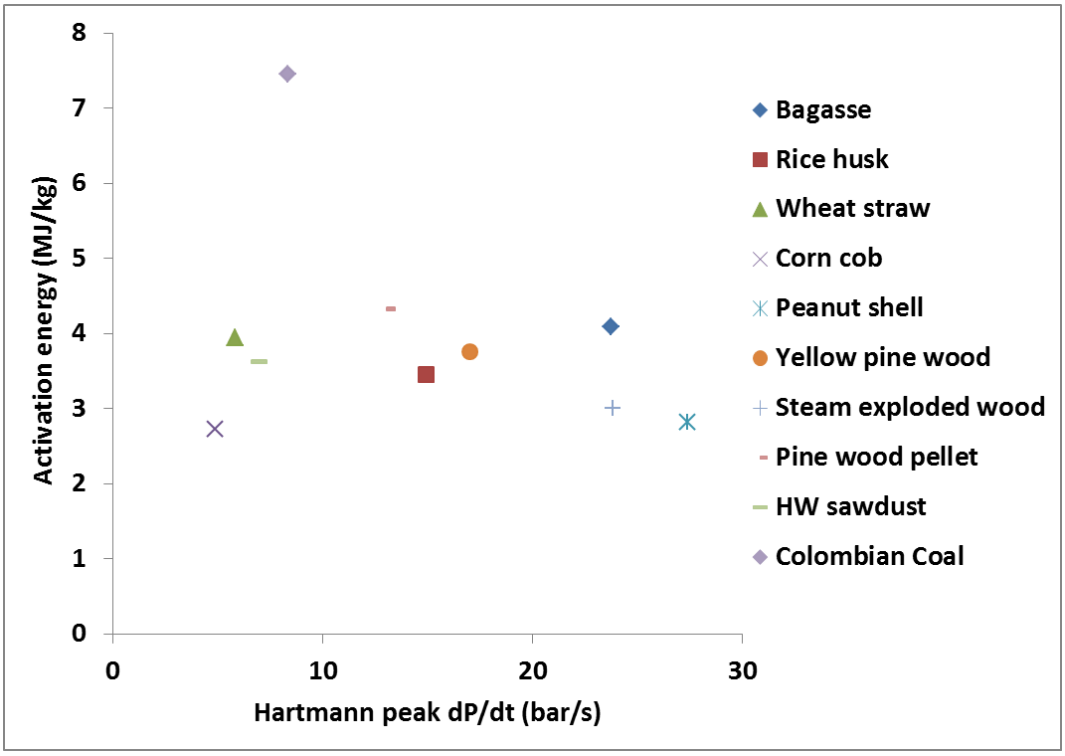

Figure 5.14 Correlation of the activation energy for volatile release with the initial rate of pressure rise in the modified Hartmann tube

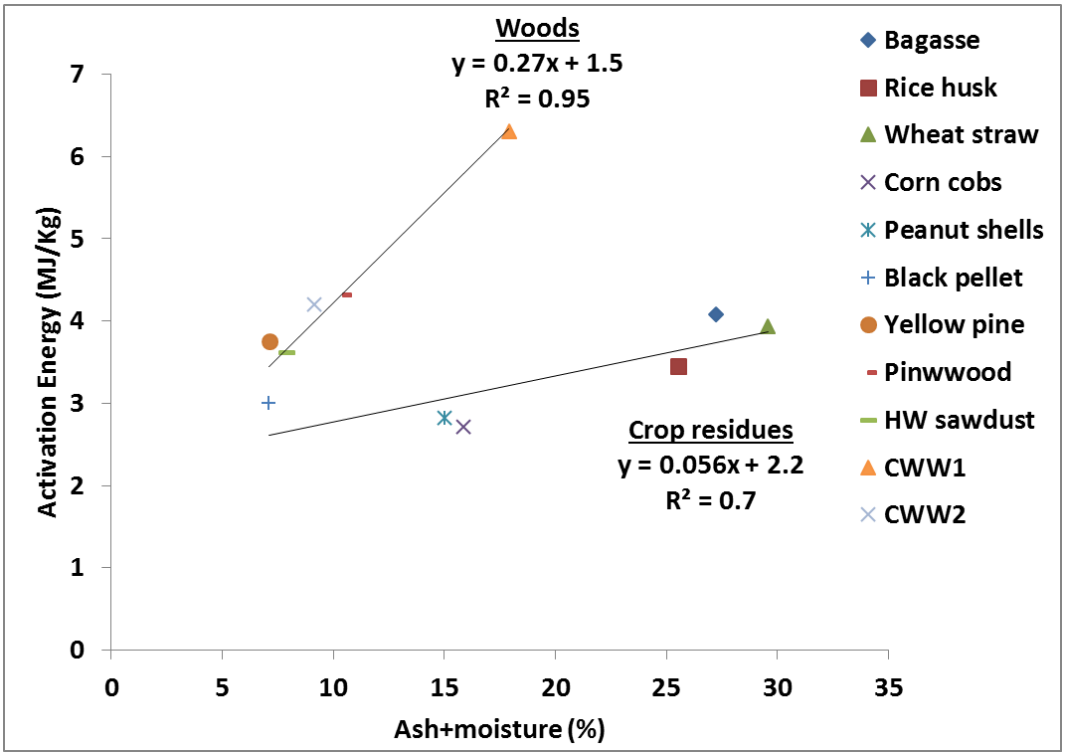

Figure 5.15 Effect of inert on activation energy for volatile yield of biomass

5.8.2 Competitive reaction model

In this reaction model, the slow heating rate in the TGA is assumed to result in the competitive reactions shown in Figure 5.16. The model assumes that heating results in the release of tars with some primary volatiles that form secondary volatiles with the build-up of some char. This model has no direct production of volatiles from the original biomass, which is a key feature of the Series Reaction model. This model may be more applicable for crop residues with higher ash contents that retard the release of volatiles [181]. Even at higher heating rate, the release of volatiles slows down under the influence of ash. The net effect is the release of volatile matter with some residual char contents mainly composed of ash.

The kinetic equations for the release of volatile for these phases are given below;

$$\frac{dm_1}{dt} = -k_1 m_1 \qquad [5.13]$$

$$\frac{dm_2}{dt} = -(k_2 + k_3) m_2 \qquad [5.14]$$

$$\frac{dm_3}{dt} = k_3 m_2 \qquad [5.15]$$

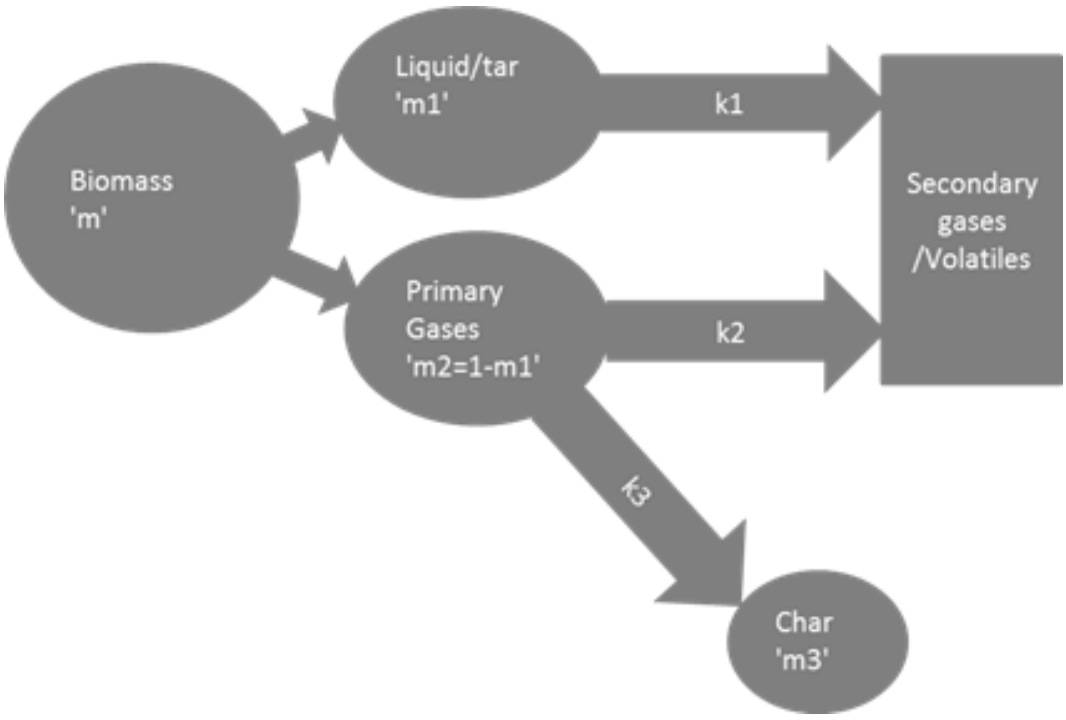

Figure 5.16 Competitive Reaction Model for rate of volatile release with the build-up of char

Table 5.8 Predicted kinetics for TGA volatile's loss in competitive reaction model

	Activation energy 'E' 'KJ/mol' (MJ/kg)			Rate Constant 'k' (s^{-1})		
Materials	**m_1**	**m_2**	**m_3**	**k_1**	**k_2**	**k_3**
Bagasse	40 (1.9)	89 (4.2)	65.6 (3.1)	$1.0e^{4.0E+4/T}$	$1.7E+5e^{8.9E+4/T}$	$1.0E+3e^{6.5E+4/T}$
Rice husk	41.1 (1.7)	84.3 (3.5)	34 (1.4)	$1.0e^{4.1E+4/T}$	$1.2E+5e^{8.4E+4/T}$	$1.8e^{3.4E+4/T}$
Wheat straw	39.2 (1.7)	94.5 (4.0)	32.6 (1.4)	$1.0e^{3.9E+4/T}$	$1.1E+6e^{9.4E+4/T}$	$1.9e^{3.2E+4/T}$
Corn cob	39.8 (1.5)	72.4 (2.8)	32.6 (1.3)	$1.0e^{3.9E+4/T}$	$1.4E+5e^{7.2E+4/T}$	$1.8e^{3.2E+4/T}$
Peanut shell	40.3 (1.8)	60.9 (2.7)	35 (1.6)	$1.0e^{4.0E+4/T}$	$6.2E+2e^{6.0E+4/T}$	$1.7e^{3.5E+4/T}$
Yellow pine wood (YPW)	38.4 (1.6)	86.4 (3.7)	38.5 (1.6)	$1.0e^{3.8E+4/T}$	$7.9E+4e^{8.6E+4/T}$	$1.8e^{3.8E+4/T}$
Steam exploded wood (BP)	41.8 (1.8)	65.6 (2.9)	36.7 (1.6)	$1.0e^{4.2E+4/T}$	$1.5E+3e^{6.6E+4/T}$	$1.8e^{3.7E+4/T}$
Pinewood pellet (BLZ)	36 (1.6)	100.6 (4.4)	38.4 (1.7)	$1..0e^{3.6E+4/T}$	$1.2E+6e^{1.0E+5/T}$	$1.8e^{3.8E+4/T}$
Hardwood sawdust (DFL)	39.2 (1.7)	84.4 (3.6)	38.4 (1.6)	$1.0e^{3.9E+4/T}$	$6.0E+4e^{8.4E+4/T}$	$1.8e^{3.8E+4/T}$
Colombian Coal	62.4 (4.4)	332.6 (23.5)	80.2 (5.7)	$80.8e^{6.2E+4/T}$	$148.4e^{3.3E+5/T}$	$1.0e^{8.0E+4/T}$
Kellingley Coal	30.9 (2.2)	182 (13.2)	83.4 (6.1)	$0.16e^{3E+4/T}$	$1.0E+10e^{1.8E+5/T}$	$5.1E+3e^{8.3E+4/T}$

An example of the data fit for the competitive reaction model to the TGA results is shown for pine wood in Figs. 5.17 and 5.18. The fit to the volatile release is better for the competitive reaction model. The kinetic data derived from the competitive reaction model fits to the TGA data for all the biomass and coal samples is shown in Table 5.8. However, the final stage of the volatile loss is not the critical contribution to the flame propagation and Table 5.8 shows that the kinetics of this stage are similar for biomass for K_1 and K_3 but are significantly different for K_2. This implies that the dominant route in first two stages of the volatile loss is as good as for the series reaction model in Figure 5.12. However, the fit to the final stage of this model to volatiles is the same as for the series model, direct evolution of gases from the biomass with subsequent pyrolysis of these gases. The route via tar and char was not a major difference between the biomass.

The dominance of the direct release of volatiles from the biomass in the three stage process is shown for pine wood in Figure 5.19. This shows that the added complexity of the competitive reaction model is not justified and the series reaction model is adequate for modelling the volatile release and for correlation of the MEC. The correlation of the MEC data with the volatile release kinetic fit to the TGA data for the competitive reaction model is shown in Figure 5.20.

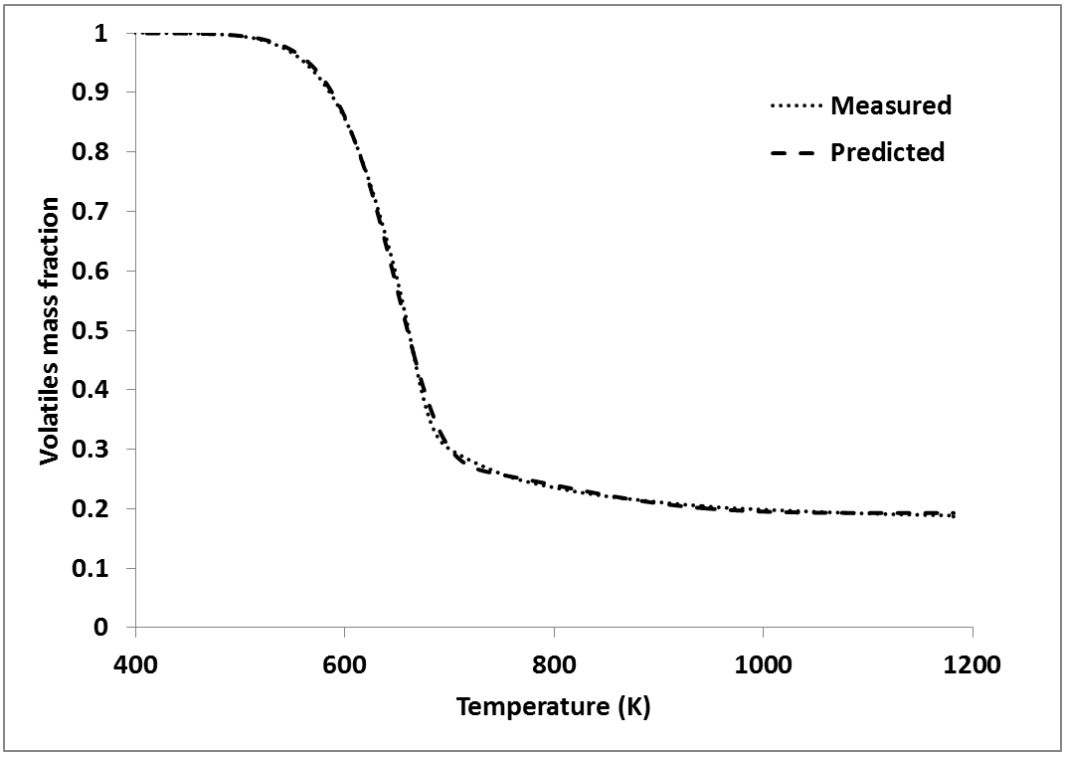

Figure 5.17 Fit of the competitive reaction model for the % yield of volatiles from pine wood as a function of temperature in comparison to TGA experimental result

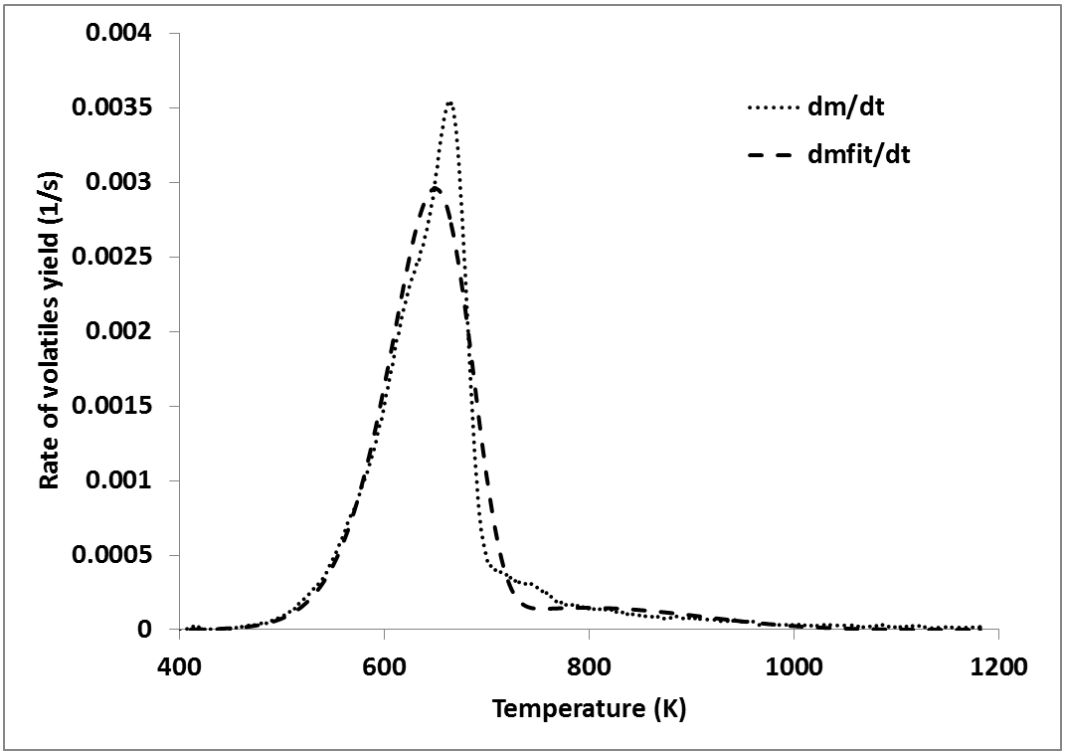

Figure 5.18 Comparison of the data fit by the competitive reaction model with the experimental results for rate of volatile yield

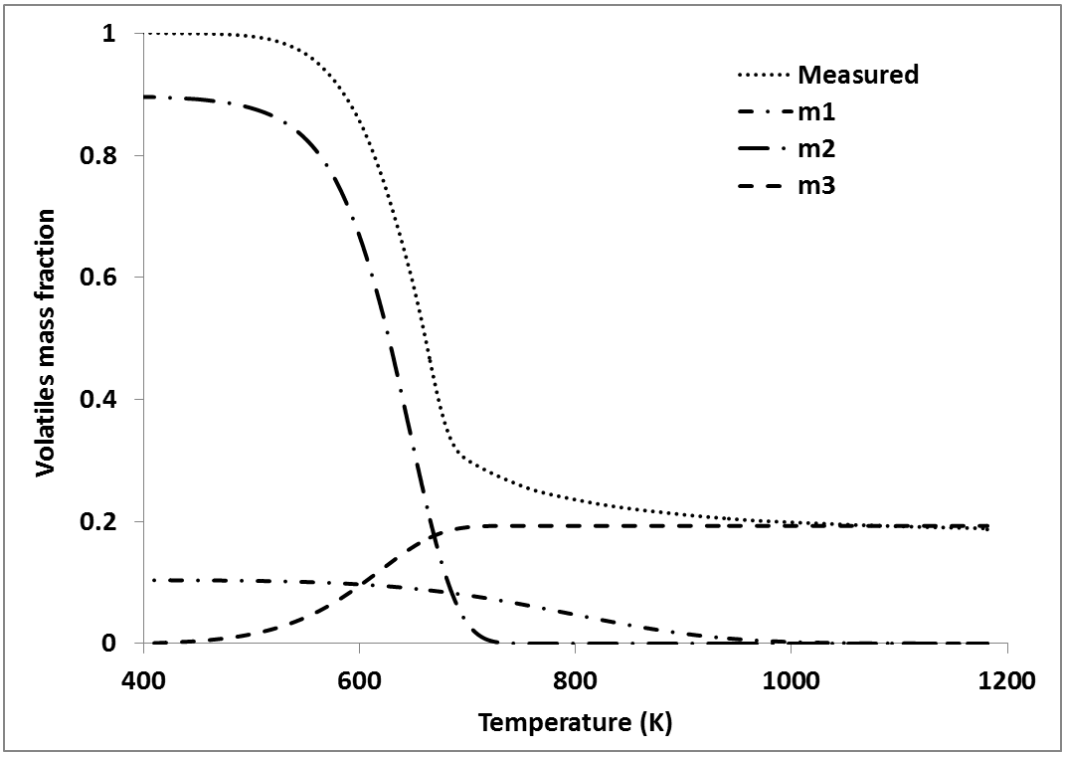

Figure 5.19 Competitive reaction model showing the three routes to volatile release and char and tar formation

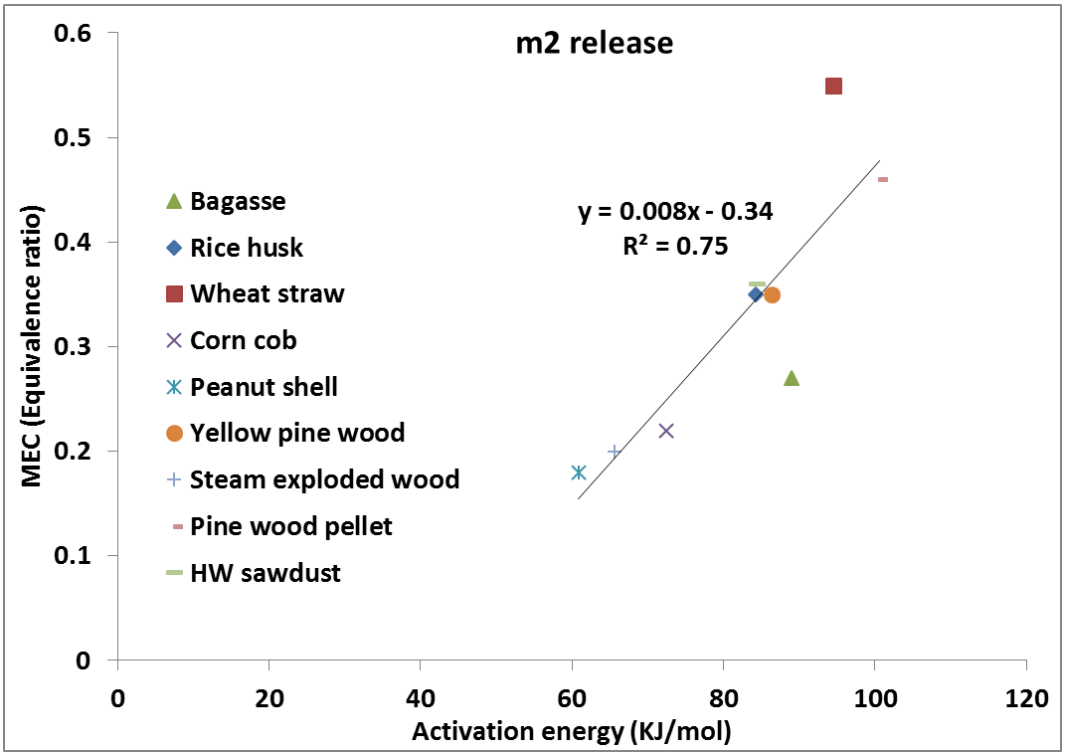

Figure 5.20 Correlation of MEC with the direct biomass volatile release from the competitive reaction model

This is very similar to the results in Figure 5.13 and the results for wheat straw and bagasse being well of the correlating line are also present.

Thermally-treated biomass, known as steam exploded biomass or a black pellet, that has more fines with regular shaped particles like coal, was found to have lower activation energy for volatile release as compared to most of the biomass samples. This was because the prime action of the thermal treatment is to break up the fibres in biomass to yield finer particles which facilitate the easier evolution of volatiles.

5.9 Conclusions

1. Biomass composition by elemental and proximate analysis is extremely variable and this leads to significant variability in the stoichiometic A/F by mass.

2. If CO, CH_4 and H_2 were assumed to be the only gases released during low temperature heating of biomass then it could be shown through CHO balance that CO was the most important gas. It is possible that for biomass with rapid heating, a greater proportion of volatiles will be released and the limiting condition of no fixed carbon in flame combustion was used to show that this would decrease the

CO and increase the CH_4 yields, but this model would not be appropriate for coal.

3. Correlations for the volatile proportion of biomass were investigated and the H/C and CV were the best correlators, athough there was significant data scatter.

4. Two kinetic models based on TGA analysis showed that biomass fuels were more reactive than coal due to the lower energy required to release the volatiles.

5. For the series reaction model, the activation energies of the biomass samples were lower than the coal samples due to the fast release of volatiles.

6. The competitive reaction model also predicted low activation energies for biomass samples.

7. The low energy required to release the volatiles in biomass fuels was considered to be due to the soft and porous structure of the agricultural biomass.

8. MEC data showed that biomasses that release volatiles more easily have leaner MEC and hence are more reactive. However, there were some anomalous results for bagasse and wheat straw that did not fit this trend with no obvious reason for the difference.

9. There was no correlation between the initial rate of pressure rise in the modified Hartmann explosions and the volatile release activation energy. This indicates that it is the heating of the particles by conduction and radiation that controls the rate of propagation. The release of volatiles is a consequence of this heating and not the cause.

Chapter 6 MODIFIED HARTMANN RESULTS FOR EXPLOSIBILITY CHARACTERISTICS

This chapter includes the tests performed on the modified Hartmann dust explosion tube. Different size fractions dusts were employed on the modified Hartmann tube at zero ignition delay to study the effect of particle size on the lean flammability limits. High ash crop residues showed little higher lean limit for the finer fraction than the next coarse fraction. This was due to high brittle ash milled to a finer size; sharing greater proportion of the finer fraction. Also TGA analysis of the finest fraction crop residue revealed that it contains higher ash contents than the other samples. With very coarse fraction, it was found that they either did not ignite or ignited with a higher lean flammability limit. The reason for this was the reduction in release of volatiles in the available time leading to heterogeneous reaction of the solid air mixture delaying the development of sustainable flame that ultimately quenches after touching with the wall.

The effect of ignition delay on the flame propagation of fine fractions of biomass was also presented. The ignition delay with the modified Hartmann tube was achieved by commissioning an electronic circuit activating with the pressing of the arc button. Initially propane gas was tested to study the effect of ignition delay on the lean flammability limit. Then it was tested with standard polyethylene, Lycopodium, corn flour, walnut shell and pistachio nut shell.

The modified Hartmann tube was also used for the measurements of aerosol combustion as aerosols were supposed to behave in a similar way to the fine dusts. The experimental methodology was changed a number of times for injection and dispersion of aerosols. Low boiling diesel and glycerol were used to study the aerosol combustion behaviour. Flame propagation of stoichiometric and lean concentrations of diesel was also studied and compared photographically using high speed camera.

6.1 Explosibility results of agricultural waste pulverised biomass and particle size effect

6.1.1 Agricultural waste pulverised biomass: MEC and flame speed

The reactivity, in terms of the maximum rate of pressure rise before the vent bursts for the three crop residues is shown in Figure 6.1 as a function of the equivalence ratio Ø. A critical feature of the burner operation and its safety assessment is to know the worst case most reactive mixture Ø, as explosion

protection measures require them to be designed for the most reactive mixture. Thus determining and understanding the mixture condition where this occurs is important and has been neglected in the literature.

Figure 6.1 shows that maximum reactivity for most of the sized fractions were at an equivalence ratio ($Ø_{daf}$) of 1.3-1.5. For wheat straw dusts with particle size <63µm and 63-75µm, the peak reactivity was Ødaf=1.4 and for rice husk dusts of the same size range, the peak reactivity was similar at $Ø_{daf}$=1.5. Similarly for bagasse of the same size range, the peak reactivity was $Ø_{daf}$= 1.25. Most hydrocarbon gases have a peak reactivity at Ø=1.05. For rice husk and wheat straw dusts the reactivity was higher for 63-75µm dusts and this was because of the increase in ash content as the dust was milled finer. For bagasse, this did not occur and the <63µm dust was the most reactive, probably due to the lower ash content of this fine dust.

Figure 6.2 shows that there was a reasonable correlation (R^2=0.8) between the rate of pressure rise prior to the vent bursting and the flame speed for the tested biomass. However, the correlation between different biomass in terms of the relative reactivity was not good. The rate of pressure rise showed that rice husk dust and bagasse dust had similar peak reactivity, which was roughly twice that of wheat straw dust. The pressure rise measures the mean mass burning rate and hence takes into account the shape of the flame. The flame speed measurements are made on the centreline of the vessel and this may not be the mean flame speed.

There are no previous measurements to our knowledge on this type of agricultural waste biomass with <63µm particle size, but the present results indicate that there could be fire and explosion hazards associated with these agricultural waste materials due to their high volatile content that enhances their reactivity. As shown in their chemical characterisation, the main reason that wheat straw could be less reactive is that for the fine powders the volatile matter is very low at 39% compared with 52% and 61% for rice husks and bagasse respectively. Wheat straw also had the highest ash content in the <63µm dust and this will reduce the dust reactivity.

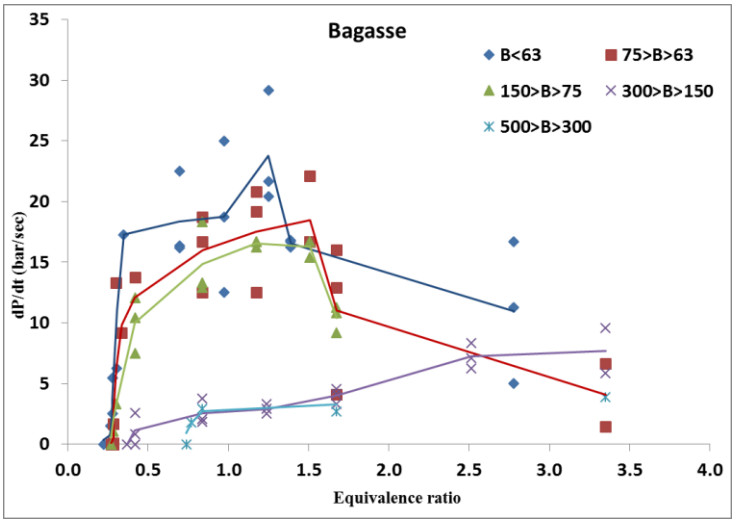

Figure 6.1 Rate of pressure rise (dP/dt) as a function of equivalence ratio and particle size

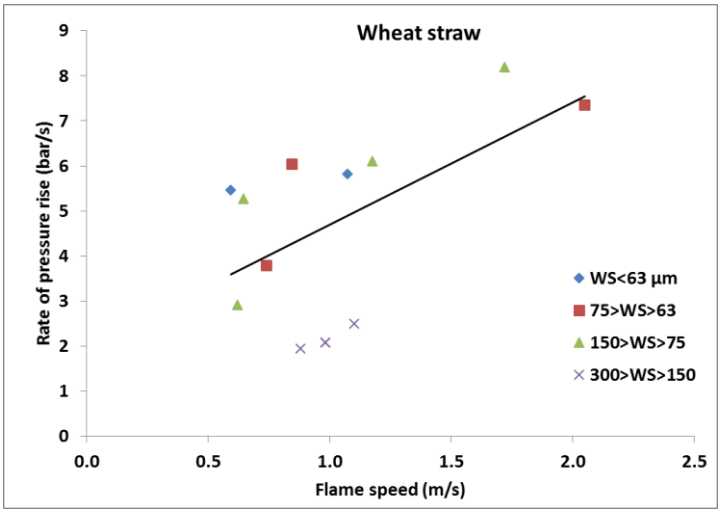

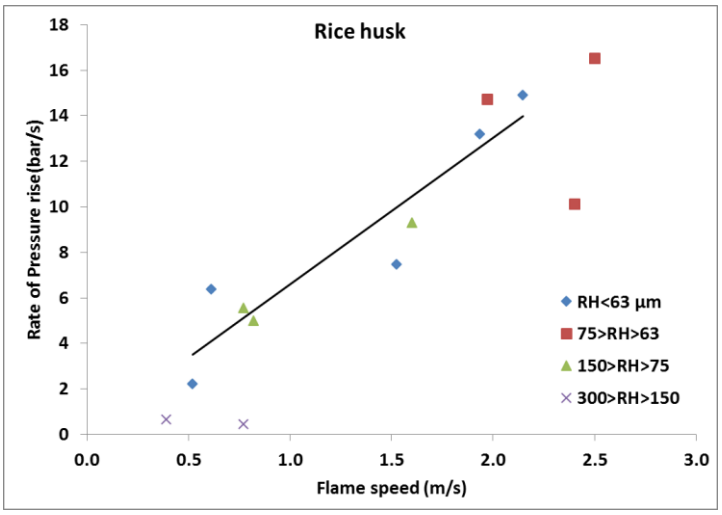

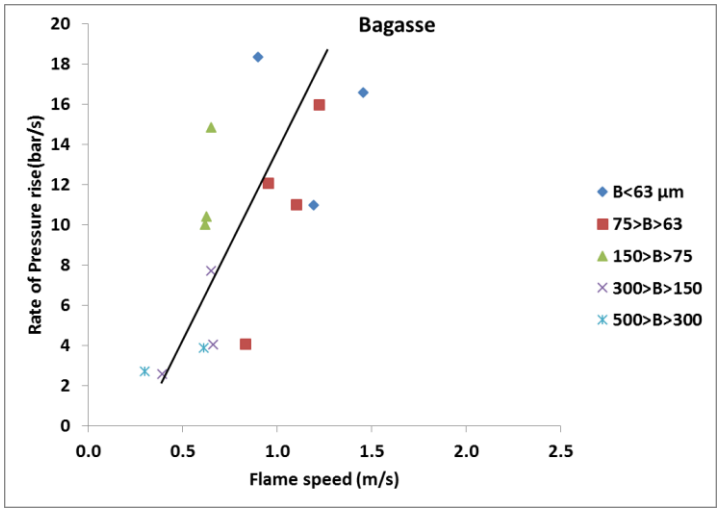

Figure 6.2 Rate of pressure rise (dP/dt) vs. flame speed for different sized fractions of crop residues

6.1.2 Explosibility characteristics of varying size fractions Corn cobs and peanut shells

Corn cobs and peanut shell agricultural wastes were split into different size range fractions like <63 µm, 63<PS<150 µm, 150<PS<300 µm and 300<PS<500 µm to study the effect of particle size on the reactivity of these crop wastes. Modified Hartmann experimental results showed increase in sensitivity of explosion with decreasing particle size. For example for peanut shell dust, it was found that lean limit in terms of equivalence ratio was 0.18Ø for the finer fraction of size<63 µm, 0.22Ø for the fraction of size 63<PS<150 µm and 0.33Ø for the fraction of size 150<PS<300 µm as shown in Figure 6.3. The coarser fraction of size 300<PS<500 µm was found to be non-explosible. The most reactive mixture was found to change with the particle size. Finer fractions were found to have worst concentration of 1.25Ø whereas for coarse fraction, it exceeded to around 1.8Ø in terms of equivalence ratio. Peak flame speed was determined to be 2 to 3.2 m/s for coarser to finer size fractions.

As shown in Figure 6.3, corn cob dust showed roughly same lean limit of 0.2Ø for size fractions <63 µm and 63<CC<150 µm, and reactivity decreased for coarser fractions. Lean limit was found to be 0.34Ø for the size fraction 150<CC<300 µm and around 0.7Ø for 300<CC<500µm size range.

The most reactive mixture was found to be at equivalence ratio around 1.4 closer to stoichiometric concentration for the finer fraction. For coarse size fractions, the most reactive concentration could not be measured even at equivalence ratio of 2.8. The flame speed was determined to be in the range 0.75 to 2.3m/s.

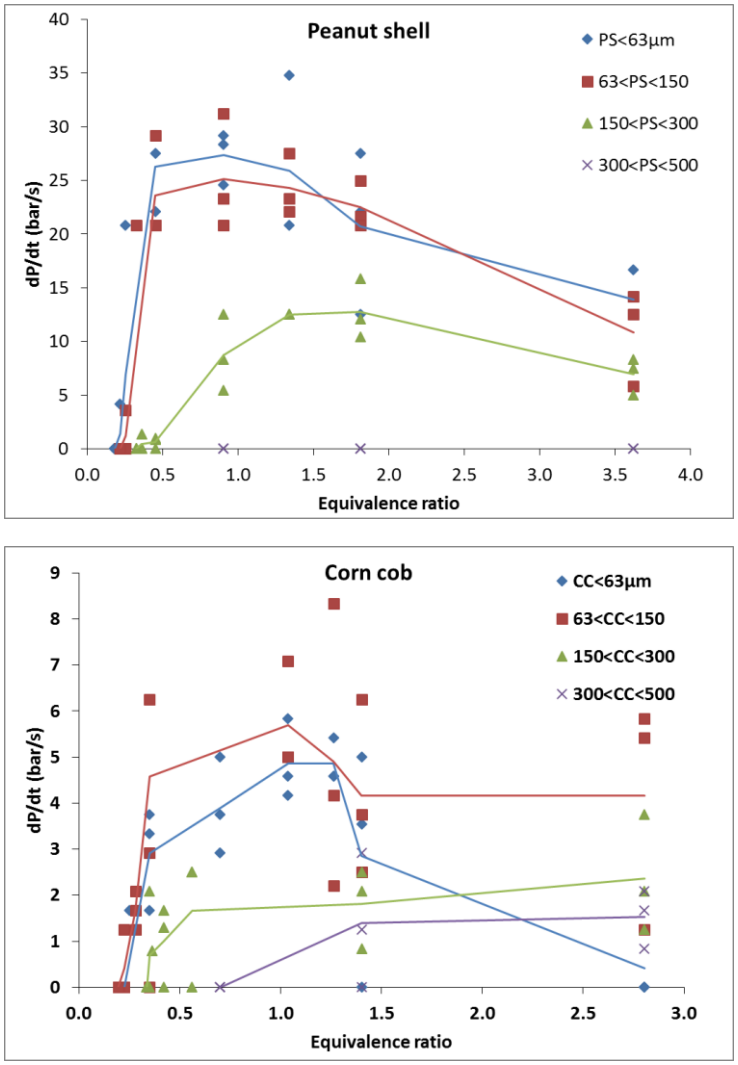

Figure 6.3 Rate of pressure rise for different sized fractions of peanut shell and corn cob

Minimum explosible concentration was defined as the last leaner concentration that ignites in the excess amount of air. Extra safe condition represents the last concentration that does not ignite and is followed in this work as MEC. In the modified Hartmann tube measurements, the probability of the explosion could be determined. As shown in Figure 6.4, the probability of explosion against the MEC were plotted. For example, MEC for 0% explosion probability meant no explosion for three repeated tests whereas the concentration for 100% explosion probability meant the explosion for all the three repeated tests. Sometimes, it is desirable to quote the concentration for 0% explosion probability as the lean limit for extra safe working conditions. Explosion probability based on 0%, 50% and 100% for all the agricultural residues were plotted as shown in Figure 6.4.

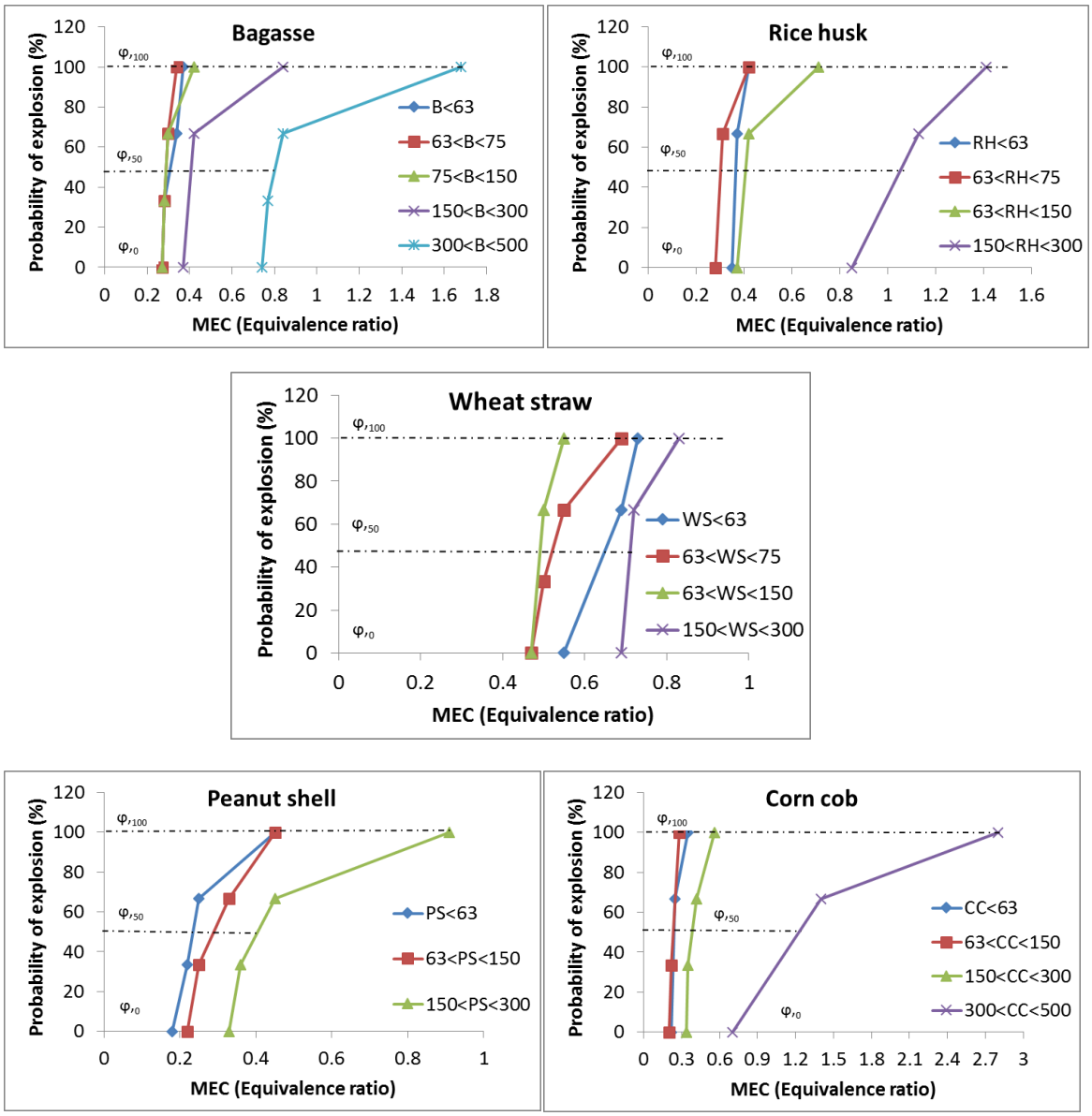

Figure 6.4 Probability of explosion vs. Equivalence ratio of selected biomass residues

6.2 Explosibility characteristics and size dependence on the flame propagation of woody biomass

Four woody biomass that were the feedstock of the boiler in the local mill in the UK were tested for their exposibility characteristics. These woody biomass were supplied in the form of pellets that were milled and sieved to three different size range fractions to study the role of fine and coarse particle in the flame propagation. Sieved sizes were classified as <63µm, 63-500µm and <500µm. SEM images of these sieved woody samples showed fibrous and porous structure (See Appendix H).

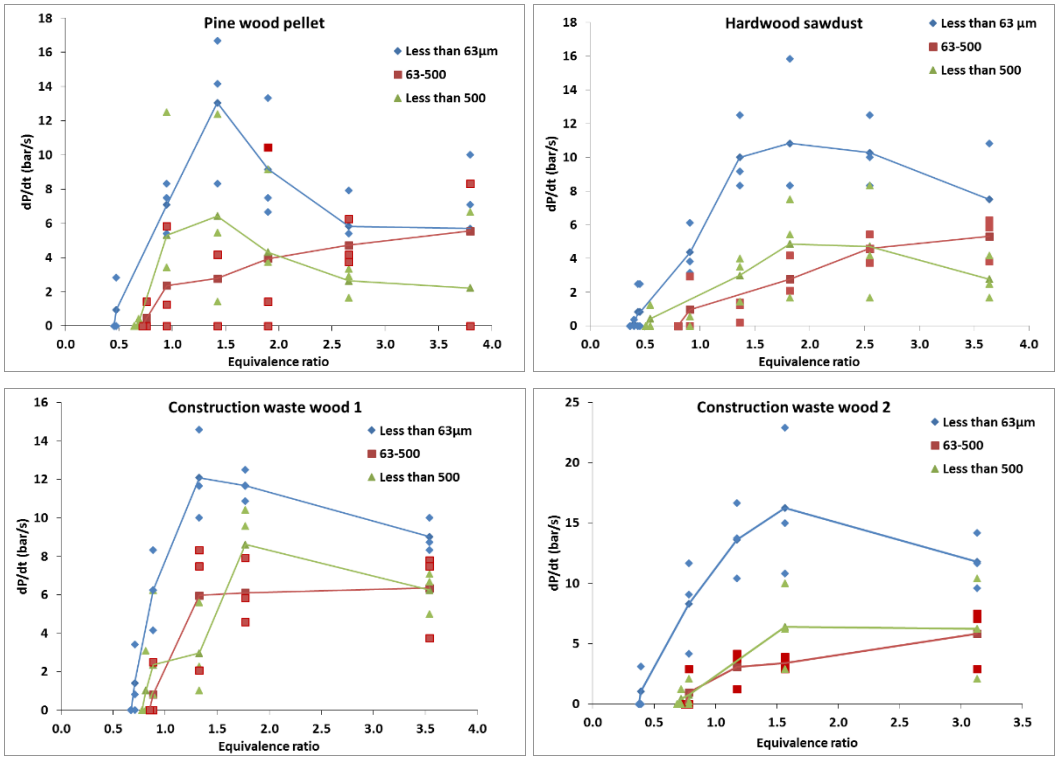

Figure 6.5 Size dependence of wood on flame propagation

The reactivity in terms of the maximum rate of pressure rise before the vent bursts for each wood samples is shown in Figure 6.5 as a function of the equivalence ratio. Pine wood pellet and HW sawdust as shown in Figure 6.5 a) and b) showed the lean limit of the finer fraction at an equivalence ratio of 0.46Ø and 0.36Ø respectively. For coarser fraction with no fines (63-500µm), lean limits were exceeded to 0.72Ø and 0.8Ø for pine wood and HW sawdust respectively. However, the fraction involving fine and coarse particles, were found to be in between of finer and coarse fraction in terms of their lean limits. It was also found that the most reactive concentration was a function of fine particles as the fraction<63µm with more fines, have worst concentration near to stoichiometric concentration whereas the fraction with least fine 63-500µm had the higher most reactive concentration. The most reactive concentration for pine wood pellet sample was found to be 1.42Ø for <63 and <500µ size fractions and even higher than 3.80Ø for 63-500 size fraction. For HW sawdust sample, the most reactive concentration was found to be 1.82Ø for <63µm size fraction and higher than 3.5Ø for 63-500 and <500µm size range fractions.

For construction wood waste batch 1 sample as shown in Figure 6.5 c), the lean limit and most reactive concentration of the leaner size fraction (<63µm) were determined to be 0.67Ø and 1.33Ø in terms of equivalence ratio respectively. For the coarser size fraction (63-500µm), the lean limit was

determined to be 0.85Ø and the most reactive concentration was observed to be even higher than 3.54Ø in terms of equivalence ratio. For the fraction of size (<500µm) containing mixture of fine and coarse particles, the lean limit and most reactive concentration were determined to be 0.78Ø and 1.8Ø respectively.

Similarly for the second batch, the lean limits of the size fractions <63, 63-500, <500µm were determined to be 0.38Ø, 0.75Ø and 0.69Ø respectively. The most reactive concentrations for size fractions <63 and <500µm were determined to be same (1.56Ø in terms of equivalence ratio) and for size fraction 63-500µm, the most reactive concentration was found to be higher than 3.0Ø equivalence ratio.

From these results, it was summarized that the finer sized fractions have the lean limit lower than the coarser fractions. The fractions comprising of fine and coarse particles (<500µm) were leaner than 63-500µm fraction that shows the strong influence of fine particles on the sensitivity of ignition. The most reactive concentration was observed to shift to a more rich concentration with the increase in the size of the particles. It was concluded that careful consideration should be taken in the handling of these boiler feed-stocks and generation of fine particles due to wearing and tearing in the handling of wood pellets can cause the explosibility threats to the working environment.

6.2.1 MEC as a function of average particle size

Combustion of solid fuel is strongly dependent on the size range of the fractions. A fraction with coarse particles requires longer time for pyrolysis and enough generation of volatile to sustain the flame propagation. Fine particles turn to volatiles instantaneously facilitating the combustion. A detailed study of the effect of particle size on the propagation of flame for agricultural waste residues and woody samples was carried out as explained above. MEC in terms of equivalence ratio were plotted (using the analysis of as received sample) against the average particle sizes for varying size range fractions for agricultural waste and woody biomass as shown in Figure 6.6 and 6.7 respectively. It was observed that for most of the agricultural wastes, the lean limits become independent of particle size below the average particle size of 80µm. However, for some agricultural wastes, carrying more ash contents in the finer fractions, showed higher lean limits. This was due to counterbalance effect of inert in increasing the lean limits of the finer size

fraction. Also there was a sharp increase of lean limit for average particle size above 220µm.

However for woody biomass carrying less inert, lean limits decrease gradually with the decrease of particle size making it more reactive than the coarse size fractions. These woody samples showed gradual change of lean limits for even very higher average particle size of 250µm. After this size, trend in the change of MEC started to change sharply depending on the woody sample.

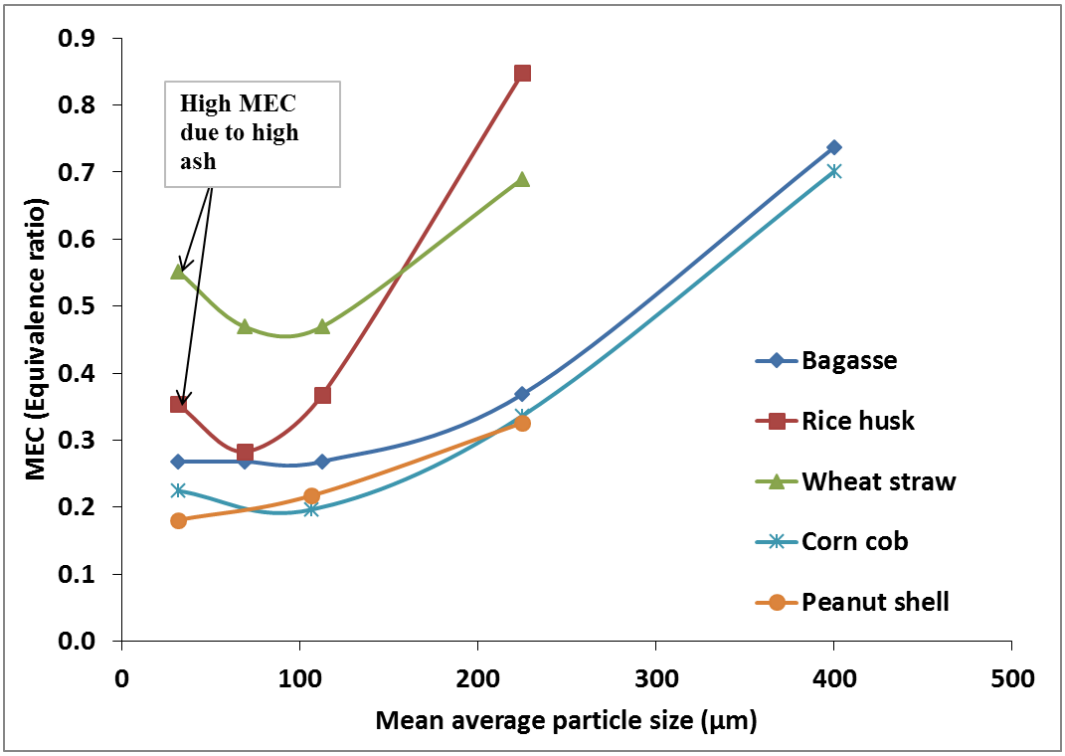

Figure 6.6 Effect of average particle size on minimum explosible concentration of agricultural waste biomass

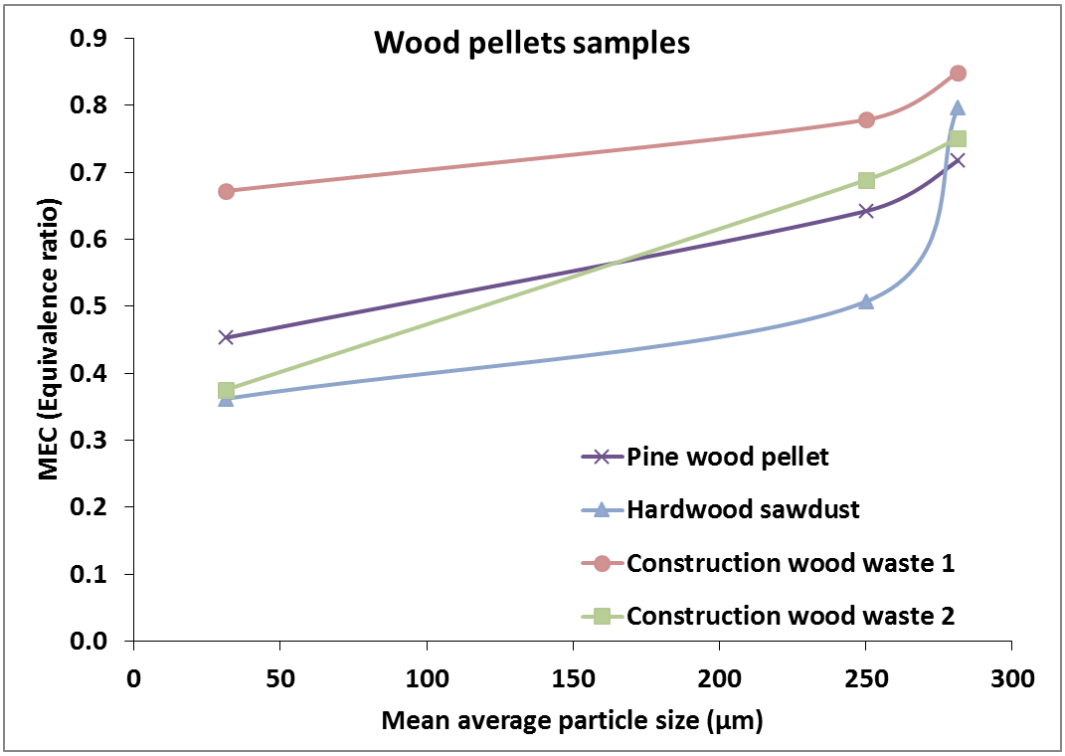

Figure 6.7: Effect of average particle size on minimum explosible concentration of woody biomass samples

6.3 Effect of steam explosion pre-treatment on the reactivity of pine wood

Thermal treatment processes such as torrefaction aim to break up the fibrous nature of woody biomass and make it more brittle so that it can be more easily milled alongside coal or on its own in the same mills as used for coal. The intention would be for these thermal treatment processes to be based at the source of the biomass alongside the palletisation plant. They have the advantage of nearly zero water in the biomass, a higher pellet density and less tendency for the pellet to fracture and form dust clouds in transport. The net result will be a higher energy carrying capacity for ships of fixed volume capacity and hence cheaper transport costs of the fuel. At present it is not clear whether the potential advantages of torrefied biomass outweighs the increased cost of manufacture, for power generation.

Biomass materials have low bulk density, fibrous in nature and have low heating values [2, 3]. The cost of transporting raw biomass from source to the power generation plant for milling is too high. Thermal pre-treatment of the biomass potentially can reduce these transport costs. Torrefaction is one of the advanced and attractive pre-treatment that gives the following benefits [4, 5]. Torrefied biomass are more compact (Higher bulk density), have a

higher heating value and are more easily pulverised as the biomass fibres are broken up by the thermal treatment. Torrefaction results in a significant loss of volatiles from the biomass depending on the torrefaction conditions; these are usually recycled to provide the heat for the torrefaction process. Thermally treated biomass materials are often referred to as bio coal as they are closer in properties to coal than to the original biomass.

An alternative thermal treatment to torrefaction is ‘steam explosion’. This is a commercial process at the pilot plant stage, that treats the woody biomass with pressurised hot water (1.2-1.7MPa, 170-250^{o}C) for a short time (up to 10 mins.) and then releases the pressure to flash vaporise the water and this process inside the woody biomass structure shatters the particles into finer fractions [6, 7]. These steam exploded biomass materials are transformed into pellets known as ‘Steam exploded pellets’ for the easiness of transportation. They are often referred to as ‘black pellets’ due to their black colour.

The new structure of biomass has similar properties to that of torrefied biomass. The steam exploded biomass process has potentially a lower energy consumption than that of torrefied biomass with a lower loss of volatiles. The steam exploded process is intended to have a lower tar formation and less cracking of the raw biomass material. The resultant pellets potentially have a higher proportion of the original biomass energy than for torrefied biomass. The steam exploded biomass treatment and palletisation process produces a pellet with an externally sealed outer surface due to the treatment process. This leaves them less sensitive to absorb water than for torrefied biomass. The biomass fibres in the pellets are destroyed and the pellets are easily pulverised, which are similar to the benefits of torrefied biomass. Steam exploded biomass is potentially a lower cost product than torrefied biomass and is potentially a better product in terms of energy content as a proportion of the original biomass energy on a daf basis.

The steam exploded sample as shown in Figure 6.8 and 6.9 have an MEC leaner than its raw material making it more reactive. The lean limits in term of equivalence ratio for steam exploded and raw sample were found to be 0.20Ø and 0.39Ø respectively. However, the most reactive concentration for both of these materials was found to be at the same equivalence ratio of 1.32Ø based on both rate of pressure rise and flame speed, as shown in Figure 6.8 and 6.9. The maximum flame speeds was determined to be about

2.5 m/s for both of these materials reflecting the same rate of flame propagation.

It was concluded that steam exploded biomass, in spite of losing some volatiles in the thermal process, was more reactive due to opening of active sites as a result of transformation of the structure by the volatile outgassing and the breakup of the fibrous structure of the biomass.

The surface morphology was investigated using SEM imaging, as shown in Figure 6.10. The raw biomass had fibrous particles with wide variation in the particle size distribution, whereas the steam exploded sample had less variation in the particle size distribution. Both samples were milled and sieved to less than 63 µm, but the steam exploded biomass showed a greater fine fraction than the raw biomass as shown in particle size distribution (Appendix I). The leaner MEC for the steam exploded sample was due to the increase in the exposed surface area that resulted from the thermal treatment and the reduction in particle size, which increased the rate of heating of the biomass particles. This gave a faster release of volatiles which was responsible for the leaner MEC.

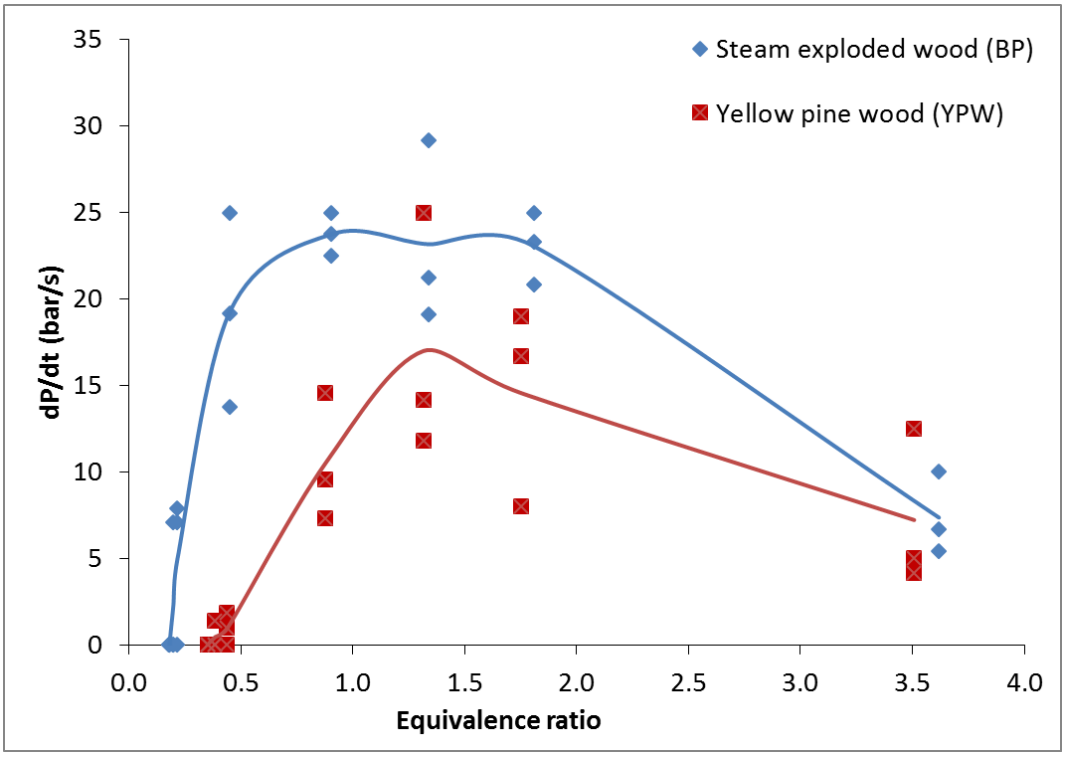

Figure 6.8 Rate of pressure rise of raw pine in comparison to its steam exploded

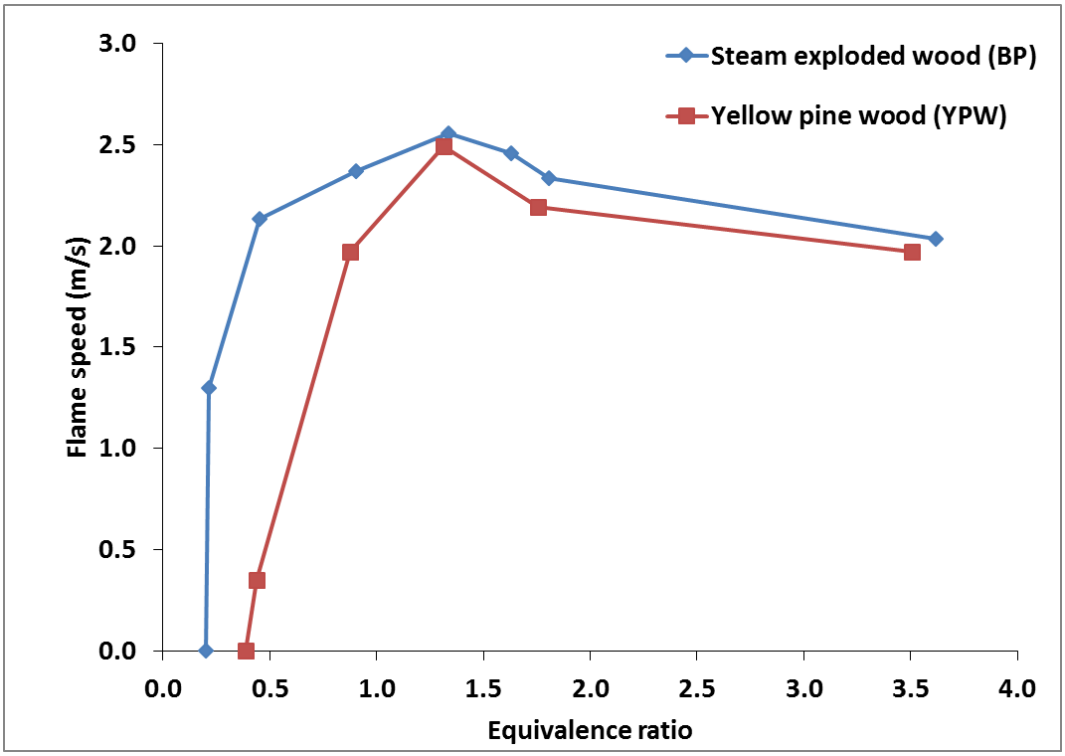

Figure 6.9: Linear flame speed of steam exploded pine in comparison to its raw

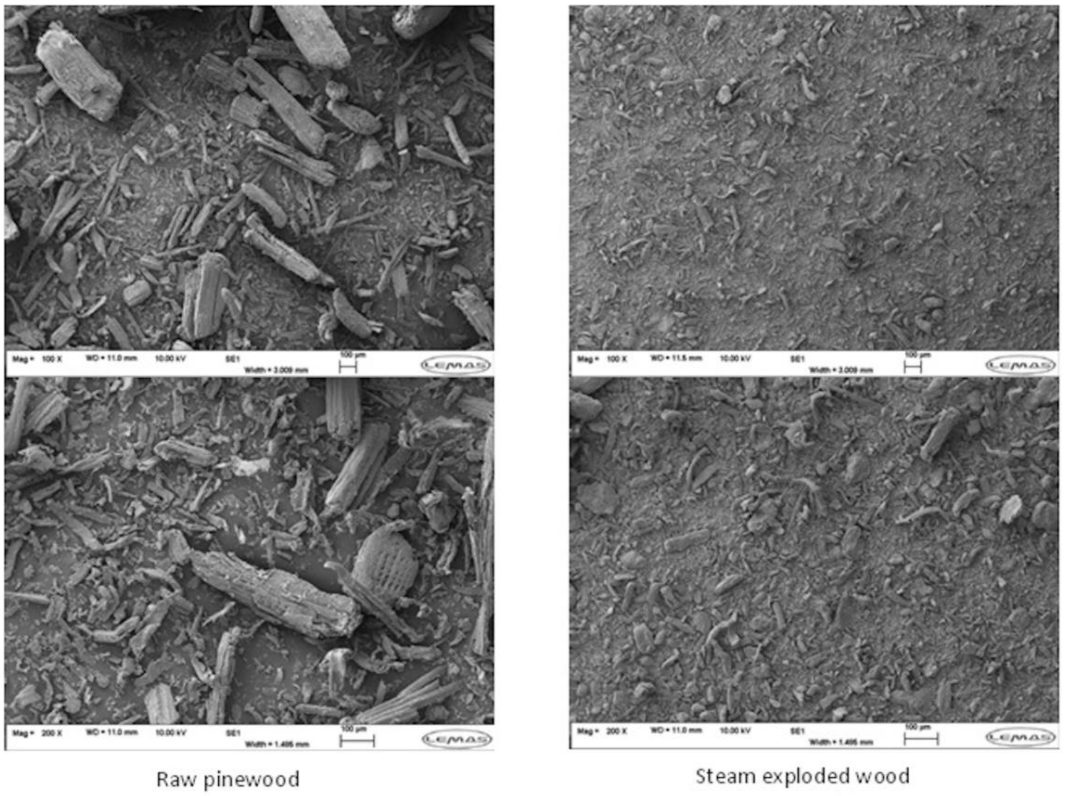

Figure 6.10: SEM images of raw pine wood in comparison to its steam treated sample

6.4 Effect of inerts (ash+moisture on the reactivity of biofuels

Presence of inerts in the form of moisture and ash contents resist in the fast propagation of flame. This result in the delay in the formation of a combustible mixture due to evolution of volatiles. As the moisture is the final combustion product and the ash is the residual inert mass after combustion, so the existence of these inerts in the sample would suppress the combustion. To study the effect of inert on the lean flammability limits, %ash+moisture of selected agricultural residues in combination with other biomass and woody biomass samples were plotted against their corresponding MEC as measured using modified Modified Hartmann tube as shown in Figure 6.11. For three agricultural waste having higher ash contents, separate analysis of <63µm were used to calculate the actual MEC that are different from the values quoted before due to different actual air to fuel ratio due to the higher ash contents in the finer fraction. The higher MEC of woody biomass compared to agricultural wastes show a separate correlation with greater influence of inert on the lean flammability limit. Biomass nut shells showed a consistent low inert and therefore negligible variation of lean limits however agricultural wastes showed a clear variation of MEC with % inert. Despite the higher inerts, these agricultural waste showed low MEC compared to wood samples.

Relative results for varying size fractions of the selected biomass samples using the modified Hartmann tube give a good idea of dependence of particle size on the reactivity. However, the absolute values for explosibility characteristics need to be determined using standard ISO 1m^3. Some dusts are not explosible on the modified Hartmann tube due to the weak ignition source but this does not mean that they are non-explosible until they are tested on ISO vessel. Similarly, the pre-existing spark sometimes ignites the underdeveloped dust cloud yielding inaccurate explosibility results. So, to avoid the hazards of marginal explosible dusts, it was better to use lean flammability limits as the concentration for 0% explosion probability.

Figure 6.12 showed the range of lean limits for different biomass samples based on non-ignited and last weakly ignited concentration. It was found that selected biomass samples have their lean flammability range from 0.2 to 0.7 in terms of equivalence ratio. Similarly the difference in lean explosibility limits based on ignited and non-ignited concentration for various size range fractions was presented in table 6.1.

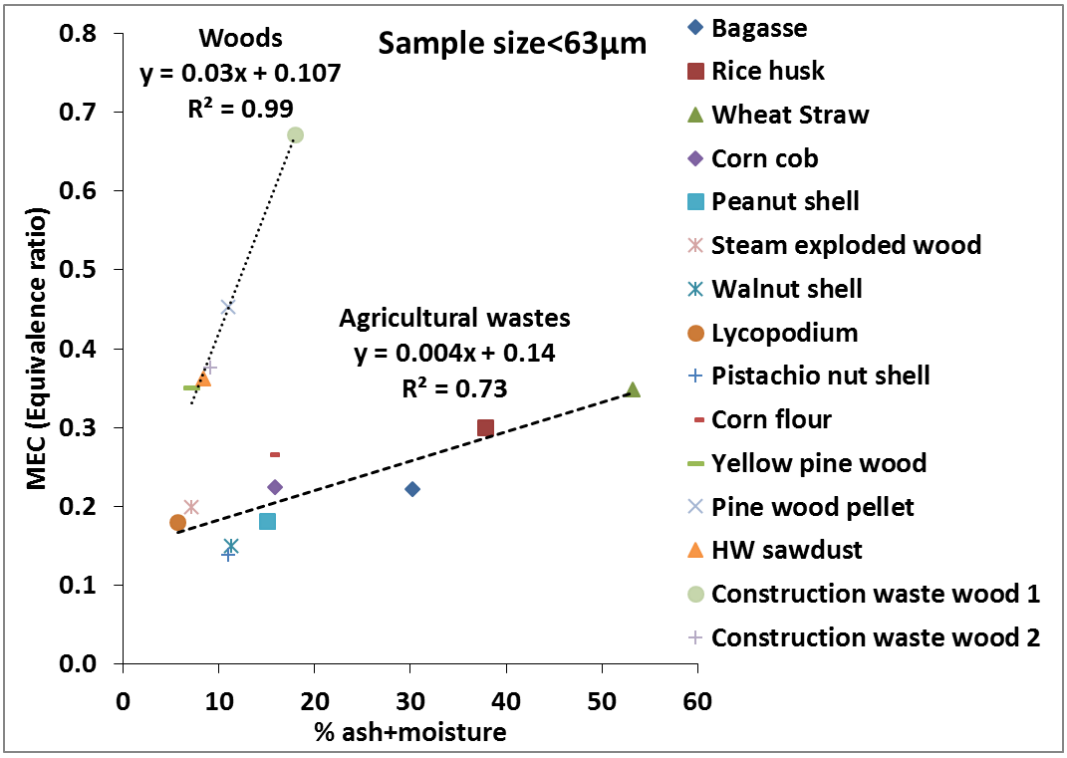

Figure 6.11 Effect of inert on minimum explosible concentration of biomass

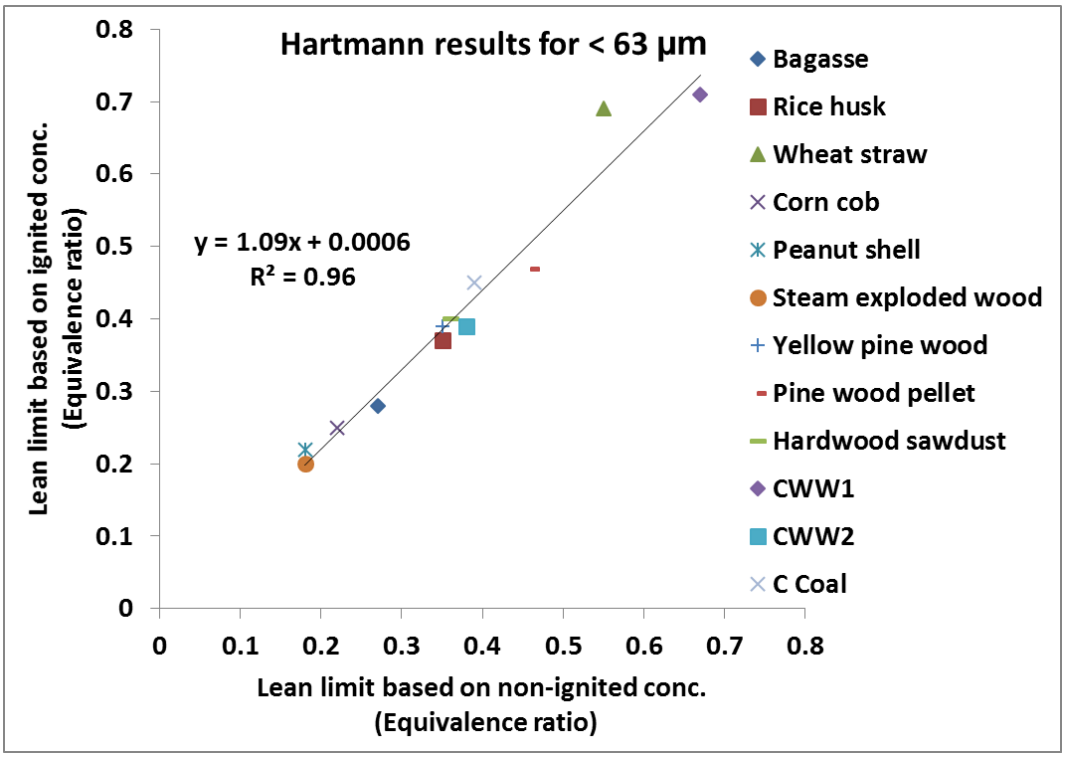

Figure 6.12 Lean flammability limits based on ignited and non-ignited concentrations

Table 6.1: MEC based on ignited and non-ignited concentration for different size range fractions

Samples	Avg. size 'µm'	MEC (Equivalence ratio)	
		Conc. that did not ignite	Last conc. ignited
Bagasse (B)			
B<63	31.5	0.27	0.28
63<B<75	69	0.27	0.28
75<B<150	112.5	0.27	0.28
150<B<300	225	0.37	0.42
300<B<500	400	0.74	0.77
Rice husk (RH)			
RH<63	31.5	0.35	0.37
63<RH<75	69	0.28	0.31
63<RH<150	106.5	0.37	0.42
150<RH<300	225	0.85	1.13
300<RH<500	400	-	-
Wheat straw (WS)			
WS<63	31.5	0.55	0.69
63<WS<75	69	0.47	0.5
75<WS<150	112.5	0.47	0.5
150<WS<300	225	0.69	0.72
300<WS<500	400	-	-
Corn cob (CC)			
CC<63	31.5	0.22	0.25
63<CC<150	106.5	0.2	0.22
150<CC<300	225	0.34	0.35
300<CC<500	400	0.7	1.4
Peanut shell (PS)			
PS<63	31.5	0.18	0.22
63<PS<150	106.5	0.22	0.25
150<PS<300	225	0.33	0.36
300<PS<500	400	0.91	1.81
Pine wood pellet (Blz)			
Blz<63	31.5	0.46	0.47
Blz<500	250	0.65	0.68
63<Blz<500	281.5	0.72	0.76
Hardwood sawdust (Dfl)			
Dfl<63	31.5	0.36	0.4
Dfl<500	250	0.51	0.55
63<Dfl<500	281.5	0.8	0.84
Construction wood waste 1 (CWW1)			
Dk 1<63	31.5	0.67	0.71
Dk 1<500	250	0.78	0.81
63<Dk 1<500	281.5	0.85	0.88
Construction wood waste 2 (CWW2)			
Dk 2<63	31.5	0.38	0.39
Dk 2<500	250	0.69	0.72
63<Dk 2<500	281.5	0.75	0.78

6.5 Measurement of flame speed using high speed photography

A high resolution photographic camera was used to study the propagation of the flame using the modified Hartmann tube. A frame rate of 5000 fps was selected to visualize the development and propagation of the flame, frame by frame. For flame speed calculations, the initial time was taken for the appearance of the spark and the final time was taken for 100mm propagation of flame as detected from second thermocouple above spark. The relative variation of time was recorded and the flame speed was calculated by dividing the travelled distance of 100mm with the time taken as shown in Figures 6.13-18 for different samples.

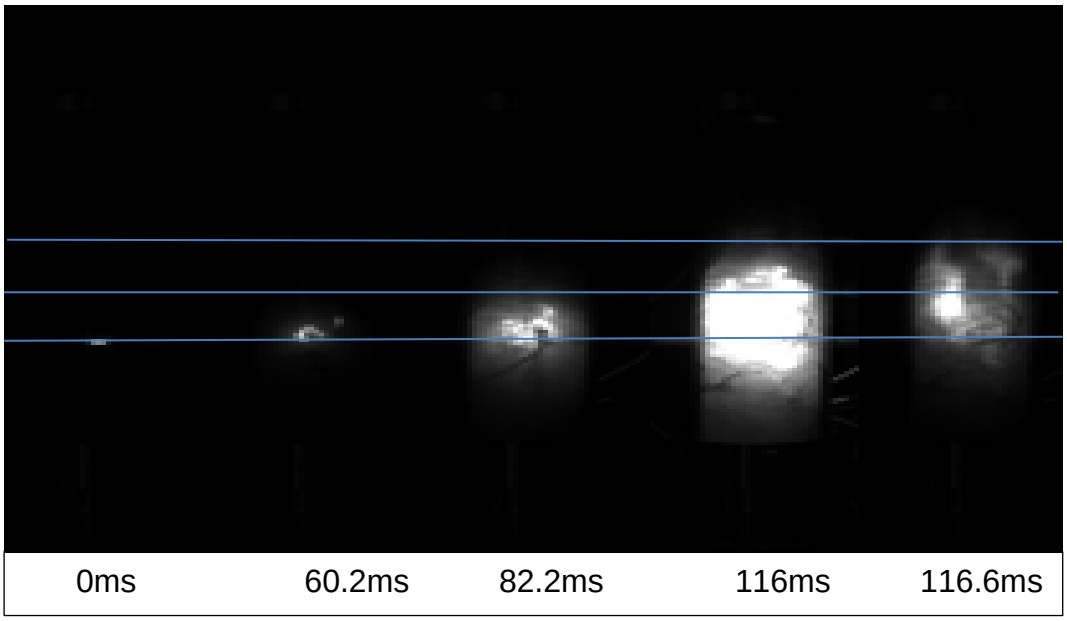

Figure 6.13: Flame speed measurement of bagasse (<63µm) at 0ms ignition delay

Flame speed=100 / (116.6-60.2) = 1.77m/s

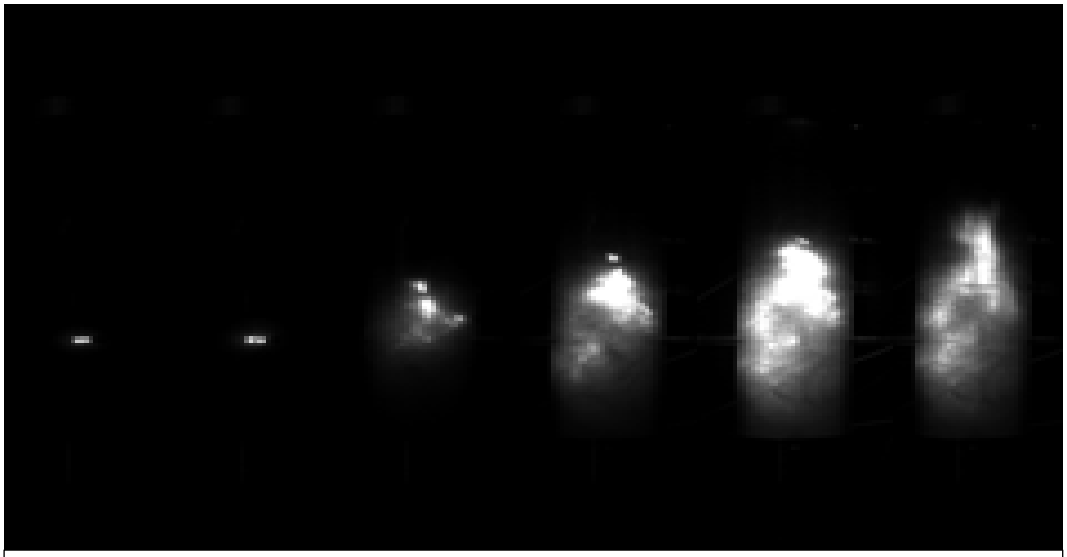

Figure 6.14: Flame speed measurement of hard wood sawdust (<63µm) at 0ms ignition delay

Flame speed =100 / (83.4-5) =1.27m/s

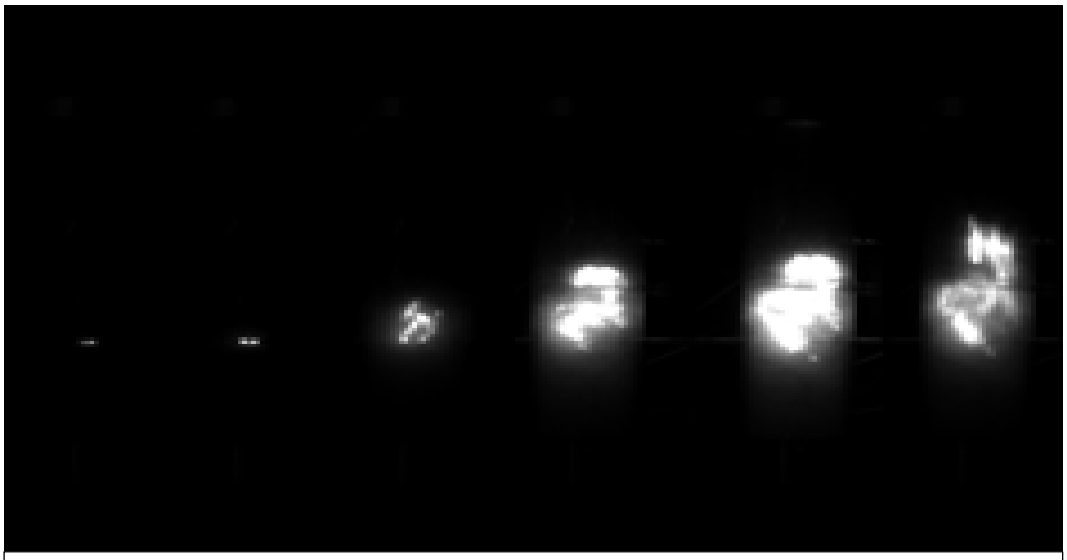

Figure 6.15: Flame speed measurement of pinewood pellet (<63µm) at 0ms ignition delay

Flame speed =100 / (85.2-4) =1.23m/s

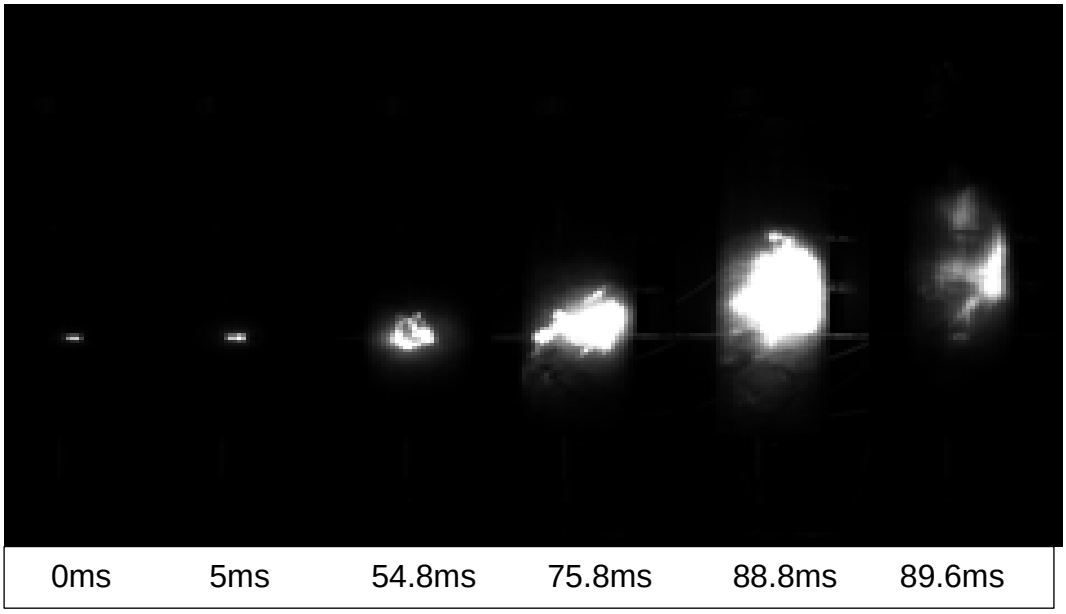

Figure 6. 16: Flame speed measurement of steam exploded wood (<63µm) at 0ms ignition delay

Flame speed =100 / (89.6-5) =1.18m/s

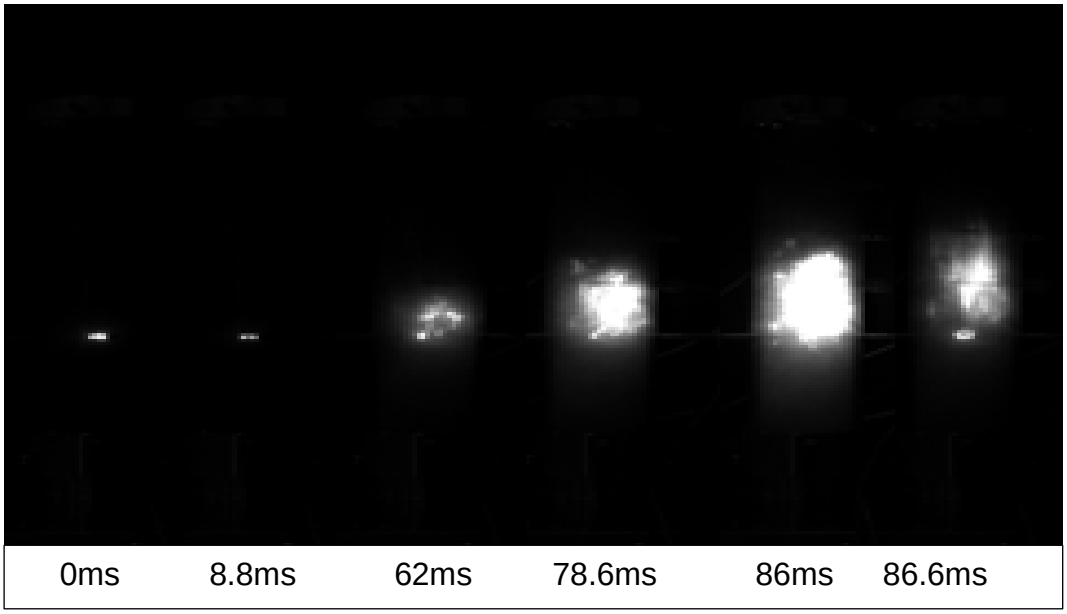

Figure 6.17: Flame speed measurement of yellow pine wood (<63µm) at 0ms ignition delay

Flame speed=100 / (86.6-8.8) =1.28m/s

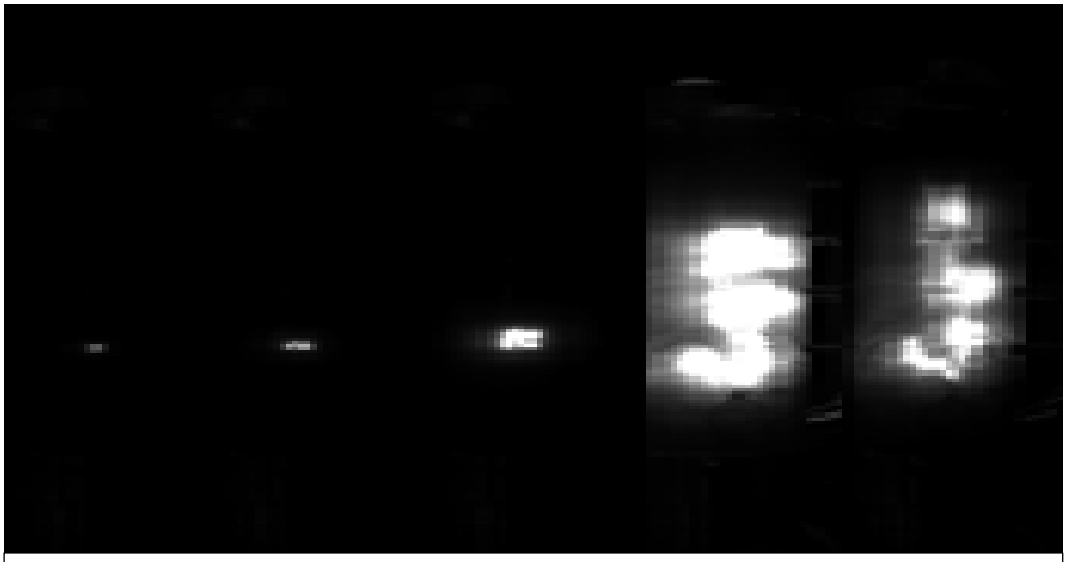

Figure 6.18: Flame speed measurement of Colombian coal (<63µm) at 0ms ignition delay

Flame speed=100 / (119-27) =1.08m/s

6.6 Ignition delay for the modified Hartmann tube

At zero ignition delay, the pre-existing spark in the dispersion process ignites the under-developed dust cloud and the lean limits determined at this condition are not consistent. There should be enough time for the dust cloud to establish before the activation of the spark for the accurate determination of the MEC for the dust.

To calibrate the modified Hartmann tube for the optimum ignition delay, it was first tested with Propane gas, a heavier gas which showed ~ 130 sec diffusion time, without any air push from the base to the spark (11cm). This concentration of the Propane was varied from 23ml to 17ml with a fixed longest ignition delay of 4 s. It was observed that all the volumes of propane ignited apart from the experiment using 17ml did not and this was confirmed by repeating this ten times. This fixed volume was admitted to THE modified Hartmann tube with a step ignition delay of 200ms starting from 100ms. The results showed that at the lower ignition delay, there was improper distribution of this volume of Propane in the modified Hartmann tube and it showed explosion due to rich localized concentration near the spark. The higher the ignition delay resulted the reduction in the intensity of the explosion with low dP/dt. This was because at higher ignition delay, the propane gas disperses in the tube with air and distribute uniformly in the entire column. A stage was reached when there is uniform local

concentration of the Propane in the entire column which is reported at an ignition delay of 4s. It was concluded that 1.7% of propane is the lower flammability limit as also reported in the German literature [183].

Based on these results, it was assumed that the modified Hartmann tube requires an optimum ignition delay for a fixed size range dust.

6.6.1 Tests with Propane

First the diffusion rate of propane was found with a free flow of propane movements without the air injection. The quantified propane gas (that is 3% of the volume of modified Hartmann tube) was slowly entered from base into the middle of the modified Hartmann tube using 50mL syringe through a septum. From the base, it diffused into the stationary atmospheric air in the upward direction. The ignition point is located at a height of 110mm from the base and was activated with a short time interval. The time was recorded for the delay in the ignition of the propane gas (Time taken to reach the spark point from the bottom of the modified Hartmann tube). This time delay of 130s is known as the time for the free diffusion of propane gas vertically upward in the air. Using this, the diffusion velocity was calculated as,

$$\text{Diffusion velocity of propane} = 110/130 = 0.85\text{mm/s}$$

As the diffusion time is very large, so it was assumed that even with air injection, it requires enough time for the proper mixing of propane and air to fill up the whole tube and form a uniform mixture. It was also noted that the initial pressure in the tube at the time of ignition is a function of the ignition delay.

$$\text{Initial pressure} = f(\text{ignition delay}) \qquad [6.1]$$

So a correction was applied on the calculation of the actual concentration of the propane burnt with a specified ignition delay. This was done using the following expression

$$P_i V_i = P_s V_s \qquad [6.2]$$

Where

P_i=Ignition pressure at the time of the spark (measured from the P-t graph)

V_i=Volume at the time of ignition (Volume of the modified Hartmann tube)

P_s= Standard pressure (1.013bar)

V_s = Standard corrected volume

So, volume at standard condition was found using the above equation and then the concentration of the propane was calculated using the following expression

$$Actual\ \%\ of\ Propane = \frac{Volume\ of\ Propane\ injected}{Standard\ corrected\ volume} \quad [6.3]$$

The different volumes of propane were tested in the modified Hartmann tube with a pre-existing spark until a lean limit is obtained. The lean limit of propane at no ignition delay was found to be 0.8% with an injection volume of 11ml. The pressure at ignition time with no ignition delay was observed to be higher than the atmospheric pressure that is corrected for the standard condition. Different volumes of propane, each with an increasing ignition delay were injected in the modified Hartmann tube (assuming no leakage of propane due to higher density and low diffusion rate) that lower the ignition pressure. A suitable ignition delay was needed for the uniform mixture to be formed before ignition. The injected volume varied from 10ml to 17ml with the variation in the lean limit found to be a strong function of the ignition delay.

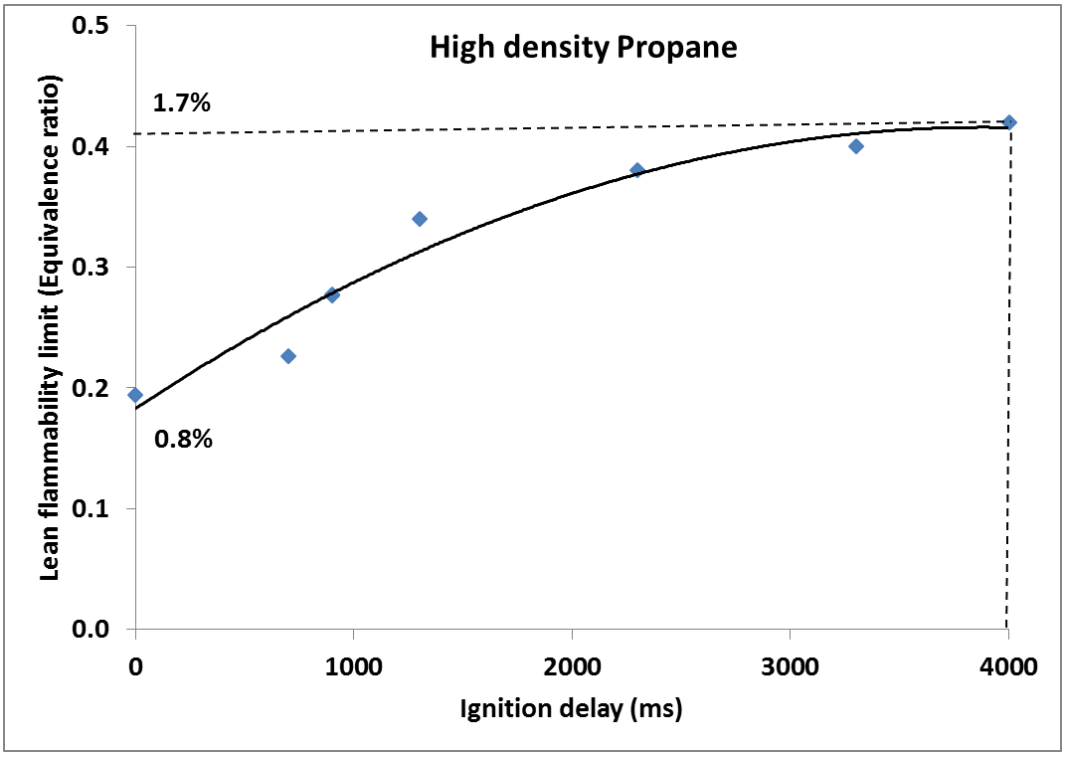

Figure 6.19 Effect of ignition delay on LFL of high density Propane

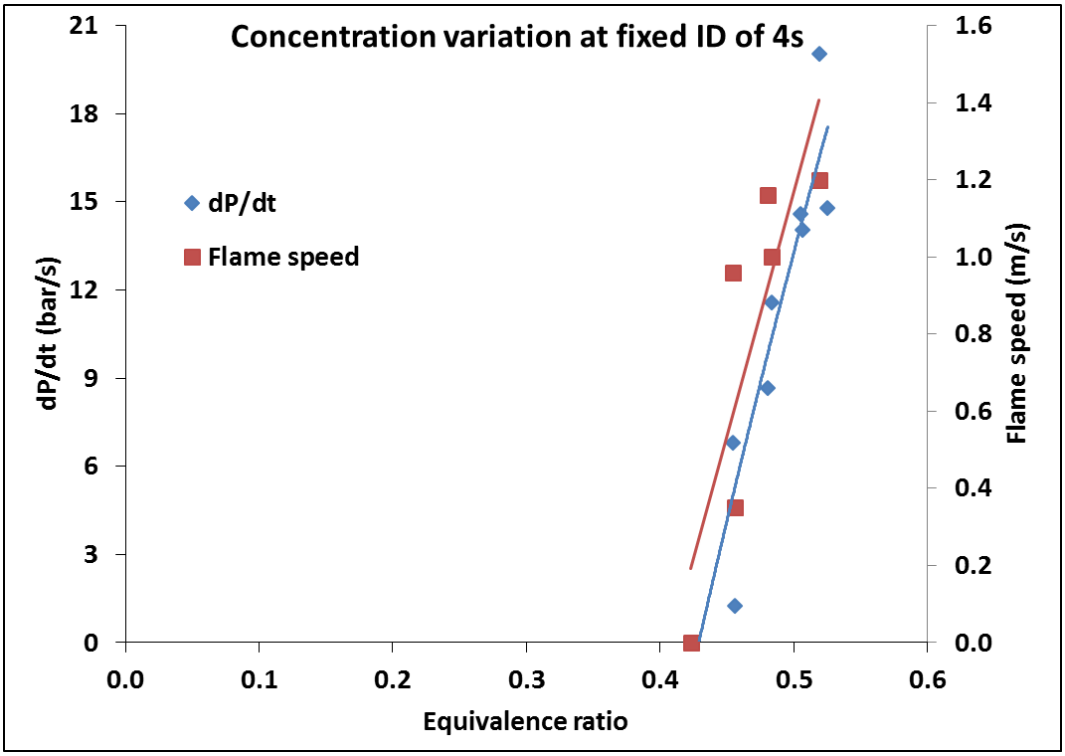

Figure 6.20 Concentration variation for fixed ignition delay of 4s

It was revealed that the lower volume of propane from 11ml to 16ml was igniting with the lower ignition delay (Lean limit, 0.8% at 0ms with injected volume of 11ml, 0.92% at 700ms with injected volume of 12ml, 1.1% & 1.15% at 900ms with injected volumes of 13ml & 14ml respectively, 1.37% at 1300ms with injected volume of 15ml and same 1.37% at 2300ms at injected volume of 16ml) and do not ignite with the increasing ignition delay. As, it can be seen in Figure 6.19, that increasing the ignition delay will increase the lean flammability limit for the different injected volumes. It means that for an injected volume, insufficient low ignition delay will ignite the local rich mixture of propane that is not distributed in the whole 1L modified Hartmann tube. So, an optimum ignition delay was necessary in the formation of unified mixture of propane with air for testing of its flammability limits.

An arbitrary ignition delay of 4000 ms was selected and the same procedure was repeated as shown in Figure 6.20. It was observed that at this ignition delay, the lean limit of propane was measured to be 1.7% (injected volume of 17ml). Also higher injected volume than 17ml were igniting with ignition delays of 4000, 5000 and even at 6000 ms. So, on this basis, it was decided that the 4s ignition delay is the highest ignition delay for the proper diffusion and mixing of 17ml injected volume of propane for 1L modified Hartmann tube. This means that a higher injected volume than 17mL is sufficient to

form an ignitable mixture even if given sufficient delay time for its mixing and diffusion. It was confirmed by repeating the tests ten times at the ignition delay of 4s with the injection volume of 17ml, that this concentration of propane 1.7% is the actual lean limit of propane as also supported by German standard of gas flammability limits [183].

6.6.2 Polyethylene results at different ignition delays (0, 50, 100, 120 & 150ms)

The test performed on the modified Hartmann tube at no ignition delay showed that the minimum explosible concentration of the high molecular weight (53-75 microns) Polyethylene was 7.4g/m^3 (equivalence ratio=0.09) as shown in Figure 6.21. The minimum explosible concentration for an ignition delay of 50ms was found to be around 14.8g/m^3 (equivalence ratio=0.18). Also the peak rate of pressure rise for 50ms ignition delay was higher than that at no ignition delay but as the concentration is approached towards the minimum explosible concentration, the rate of pressure rise for 50ms fell below than the rate of pressure rise at no ignition delay. This high peak rate of pressure rise was probably due to the higher turbulence level. For the higher ignition delay of 100 and 120ms, the minimum explosible concentration was measured to be same 14.7 g/m^3 but the peak rate of pressure rise dropped significantly. This might be due to turbulence decay of some proportion of mass. For further high ignition delay of 150ms, minimum explosible concentration was increased to 29.6g/m^3 (Equivalence=0.37) with small rate of pressure rise. This very higher ignition delay resulted in a higher turbulence decay and most of the particles were believed to be burnt during the settling stage.

The reported values of the Polyethylene dust has a lower flammability limit of 20 g/m^3 (Equivalence ratio=0.25). As our criteria for minimum explosible concentration was based on the concentration with 0% ignition probability for the three consecutive tests. So, based on this, the optimum ignition delay was measured to be 50-120ms for Polyethylene dust (See Appendix K).

Figure 6.22 shows the position of the spark on the pressure time plot of Polyethylene dust for different ignition delay timings. It was observed that for no ignition delay, the spark activates before dispersion of the dust and the dust cloud propagates in the tube through the pre-existing spark. It was observed that for 50 ms ignition delay, the spark appears in the underdeveloped dust cloud propagating in the tube having high turbulence with more steep peak. It was found that for 100 and 120 ms, spark appears

after the dust cloud is almost fully dispersed at the reflection point of the pressure time curve and the later rise of pressure was due to explosion. It was noted with further increase of the ignition delay (to 150 ms) that the pressure drops slightly after achieving the maximum before the appearance of spark. It was concluded that a suitable ignition delay was necessary for the determination of the flammability characteristics however, the ignition delay is a function of physical properties of the dust and especially particle size. For the higher particle size, it takes longer to evolve enough volatiles to sustain flame propagation as will be demonstrated later. Flame propagation of fine sized pine wood and thermally treated pine was also studied photographically for ignition delay (See Appendix L) that showed more luminous flame for an ignition delay of 120ms.

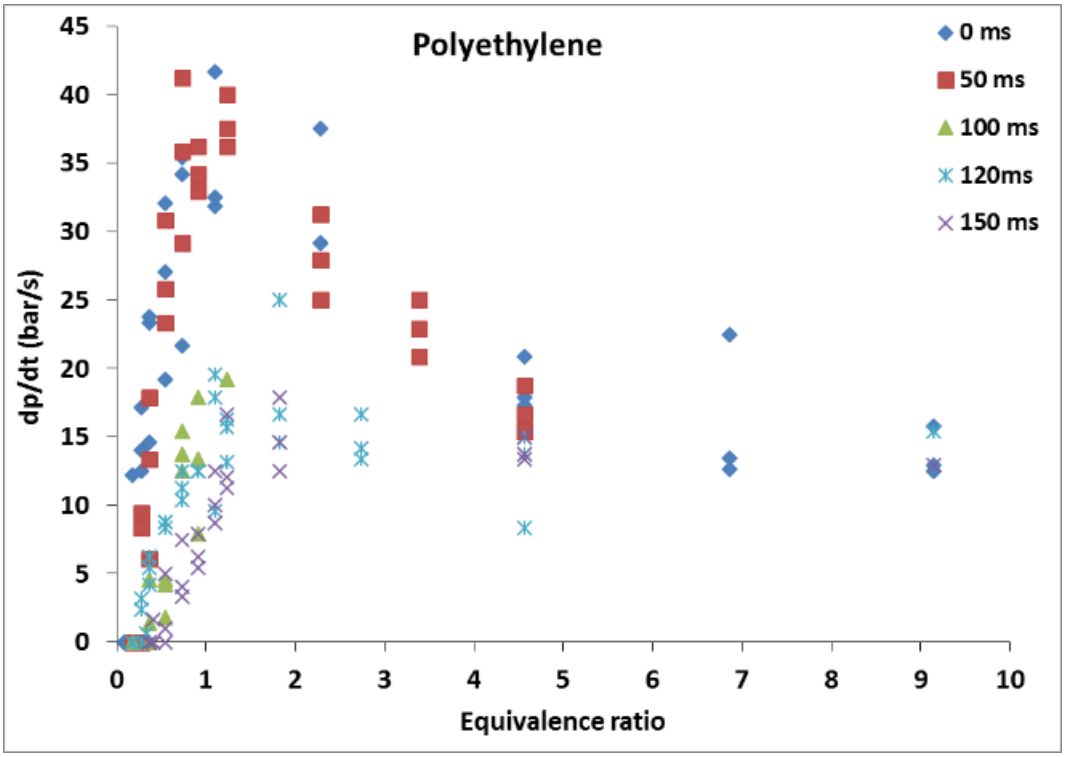

Figure 6.21 Effect of ignition delay on the lean limit of Polyethylene dust

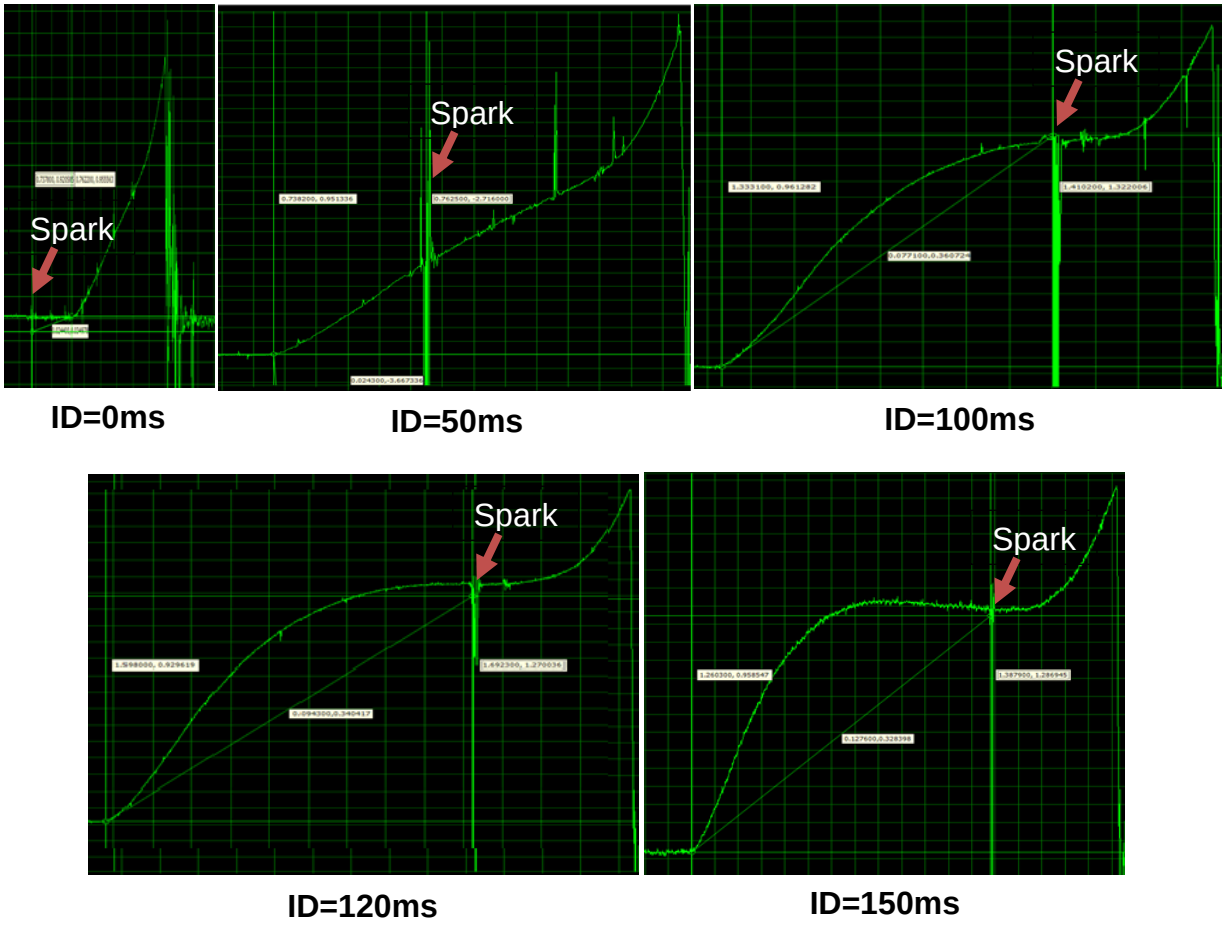

Figure 6.22 Position of spark on Pressure time curve for varying ignition delays

Different biomass samples were tested for different ignition delays on the modified Hartmann tube as shown in Figure 6.23. Most biomass samples showed slightly higher minimum explosible concentration at 50ms except Lycopodium compared to 0ms ignition delay. For further higher ignition delay, polyethylene and walnut shell showed consistent lean limit till 120ms independent on ignition delay, however lycopodium, pistachio nut shells and corn flour were measured to explode at much higher concentration giving higher minimum explosible concentrations. So, based on these results, it was concluded that lean flammability concentrations are very lean for 0ms ignition delay due to burning of the stratified mixture as was also revealed by flame propagation of Propane. MEC increased to a slightly higher concentration at 50ms for most of the dust. This ignition delay of 50ms showed the higher turbulence level as shown in Figure 6.21 for polyethylene and Figure 6.22 through spark position. For higher ignition delays, different dusts reacted differently depended on their physical properties (Figure 6.23). As some CFD modelling work on the modified Hartmann tube also revealed the optimum ignition delay in the range 60-120ms for combustion of uniform

dust cloud [184-186], so it was concluded that optimum ignition delay for modified Hartmann tube is 50ms or above but smaller than 120ms as there will be decaying of turbulence after this ignition delay.

6.7 Particle distribution of fine and coarse sized fractions in the modified Hartmann tube for 0 and 120ms ignition delays

Distribution of fine and coarse sized fractions of bagasse were also analysed as shown below. Fine <63µm and coarse 150-300µm samples of bagasse were ignited at 0 and 120ms ignition delays. For 0ms ignition delay, pre-existing spark can be observed before the dispersion of dust in the tube. The fine size fraction of bagasse was dispersed uniformly and ignited with less time delay due to instantaneous release of volatiles as shown in Figure 6.24 and 6.25. Similarly this instantaneous burning showed a more glaring flame for the fine size fraction. It was found that for 0ms, the underdeveloped dust cloud was igniting. For coarse size fraction of bagasse, there was an irregular flame with more stratified burning as shown in Figure 6.26 and 6.27. Bigger particles were observed to glare independently due to local burning of volatiles. Bigger particles travelling faster resulted more delay for combustion at 0ms as the volatiles consumed locally without building up flame (Figure 6.26). The developed cloud at 120ms, showed less delay time and the appearance of the spark resulted the evolution and burning of this cumulative volatiles (Figure 6.27).

Turbulent flame speeds for fine and coarse size bagasse dust at 0 ms and 120 ms ignition delays were measured using frame to frame analysis in the photographic study as shown in Figures 6.24-27.

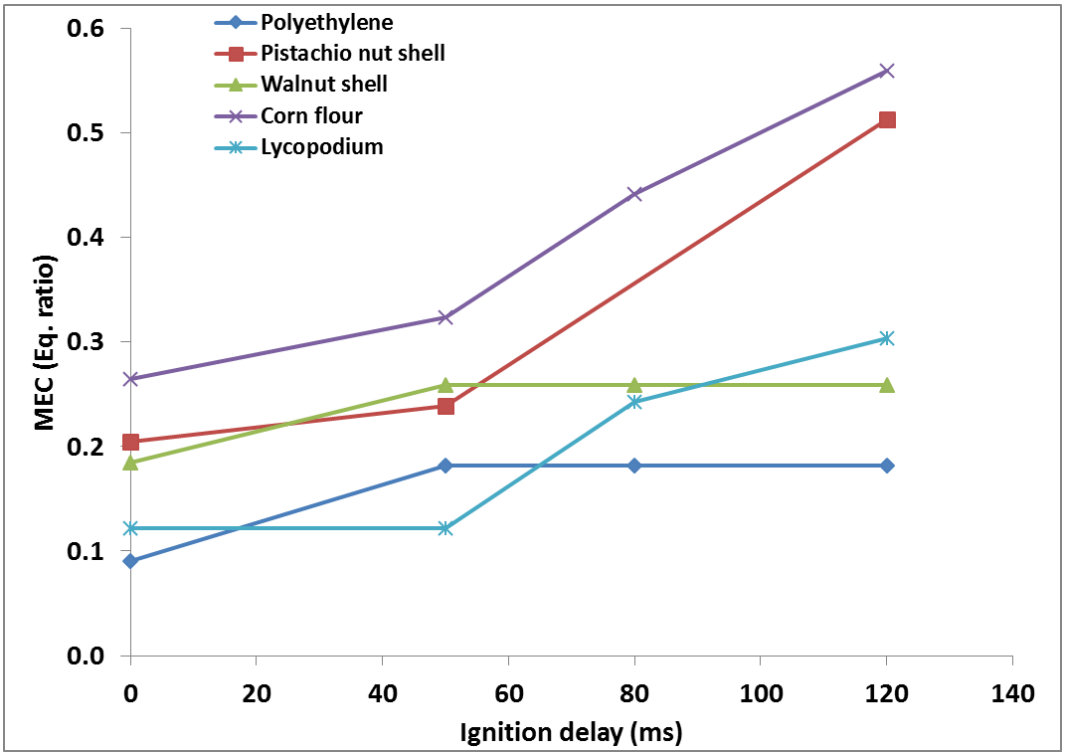

Figure 6.23: MEC vs. ignition delay for different biomass dust

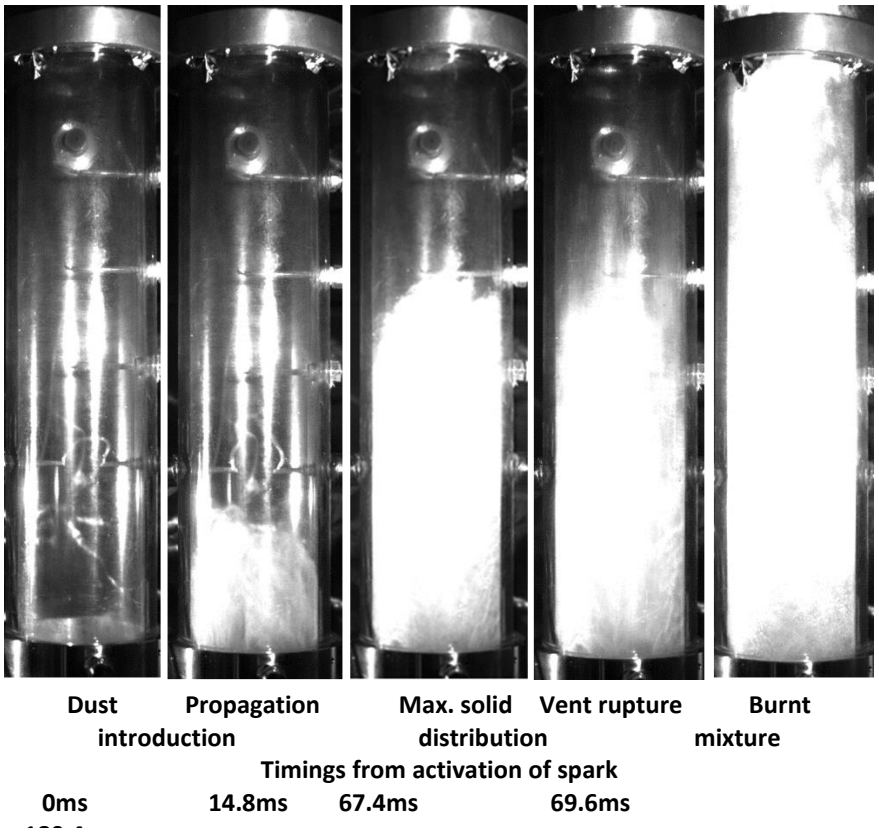

Figure 6.24: Distribution of fine sized bagasse particles in the modified Hartmann tube at 0ms ignition delay

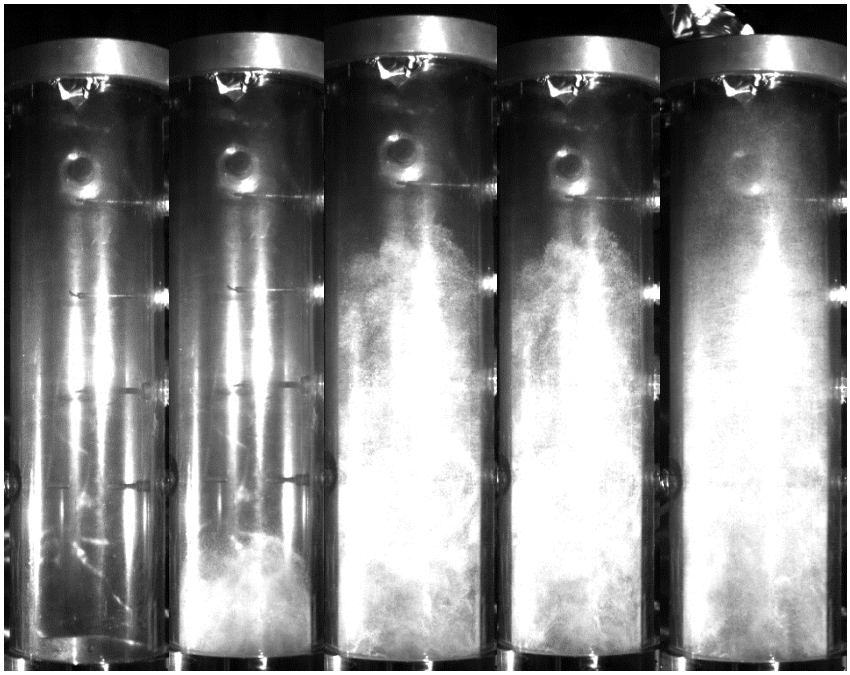

Figure 6.25: Distribution of fine sized bagasse particles in the modified Hartmann tube at 120ms ignition delay

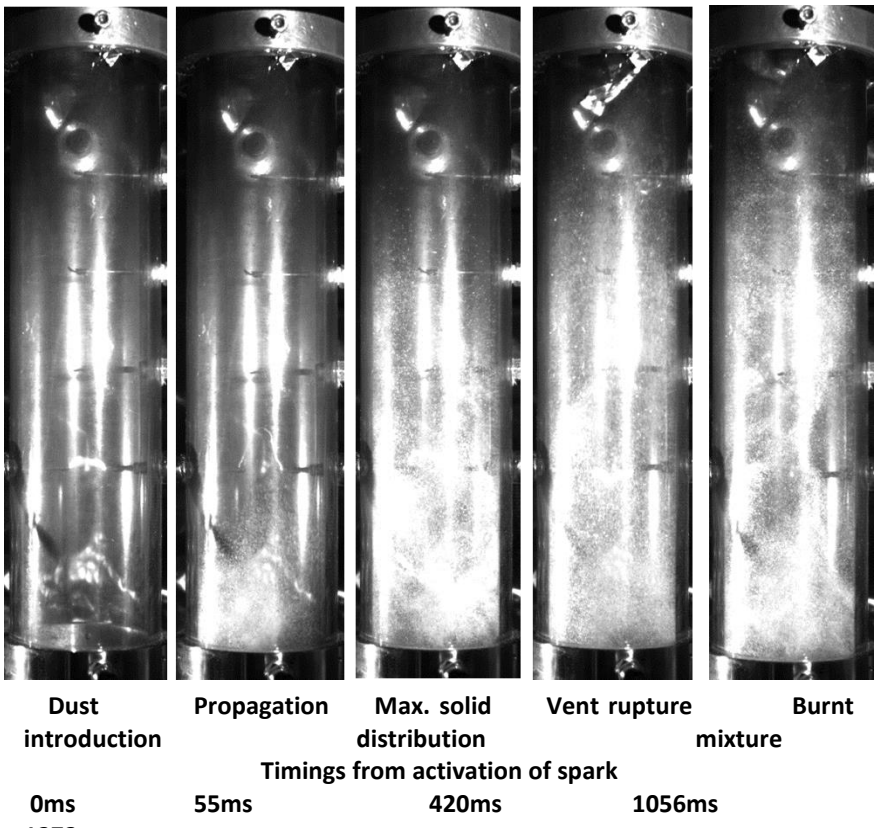

Figure 6.26: Distribution of coarse sized bagasse particles in the modified Hartmann tube at 0ms ignition delay

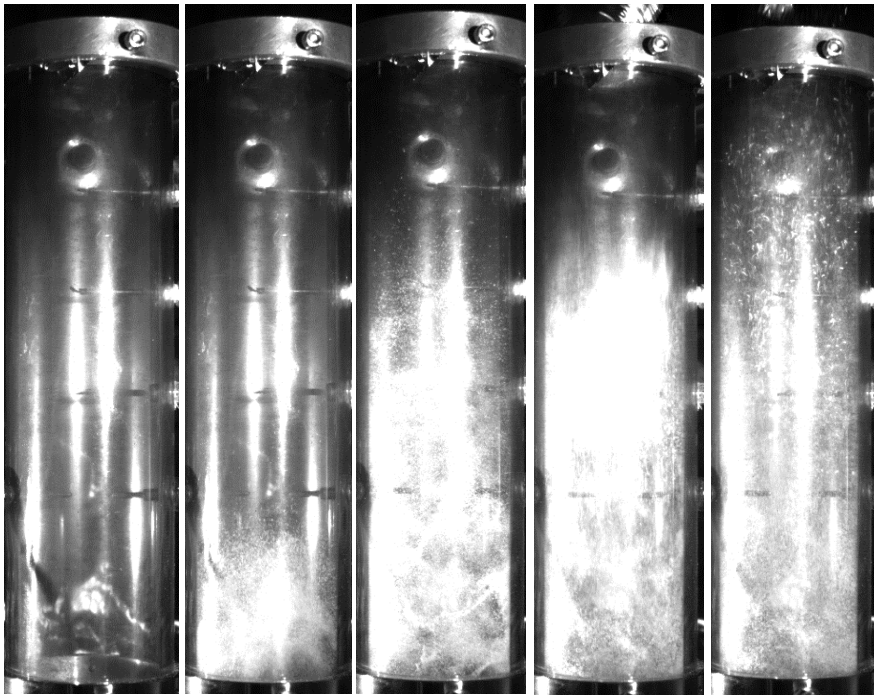

Figure 6.27: Distribution of coarse sized bagasse particles in the modified Hartmann tube at 120ms ignition delay

6.8 Aerosol combustion in the modified Hartmann tube

The modified Hartmann tube for dust explosions was also used to investigate flame propagation in liquid aerosols as there is no developed methodologies so far for the measurements of explosibility properties of aerosols. It was considered that this equipment could be modified for use with liquid fuels, as there is no agreed methodology for measuring flame propagation properties of liquid aerosols. The 7 barg air pressure generates a sonic flow of the air and it was considered that if this impinged on a small liquid pool of aerosol in the dispersion cup of the modified Hartmann tube, then it would easily atomise the fuel in the same way that air blast atomisation works. However, when this was experimented with the air jets, if simply smeared the liquid over the surface of the mushroom shaped cup and did not atomise the liquid.

It was decided that the sonic air flow had to pass through the liquid and direct it vertically to generate the shear mechanism that occurs in air blast atomisation. Consequently the mushroom shaped cup at the base of the modified Hartmann tube that directs the air onto the dust, was removed and the liquid for the test was inserted directly into the air jet supply tube. This tube had a 90^{o} bend downstream of the solenoid valve that controlled the

start of the air flow. The liquid sat at this bend and directed air blast dispersed it in the Hartmann Perspex tube in the form of tiny droplets.

The procedure for investigating liquid aerosol explosions discussed above, was shown to work provided that the amount of diesel necessary to be flammable was carefully calculated and injected into the test. The procedure was to calculate the stoichiometric quantity of diesel using a typical diesel H/C of 1.9 which gives a stoichiometric A/F of 14.3. The mass of air after injection of the compressed air and before the vent burst is 1L at 1.35 bara and at atmospheric temperature, taken as 293K, is 1.605g and thus 0.112 g of diesel is required. Using a diesel density of 820 kg/m3 this is 0.137×10^{-6} m^3 of diesel or 0.137 mL. An accurate digital pipette was used to inject this quantity and to vary the equivalence ratio. The result was a very violent explosion for initially cold liquid diesel. This explosion was more violent than any dust explosion for coal or biomass or food products carried out on dust explosions.

The results are shown in Figure 6.28 for the lean side of stoichiometric. If the aerosol behaved as a premixed gas then a lean limit at 0.45 of stoichiometric would be expected using the European definition of flammability. The explosion tests at 0ms ignition delay showed the lean flammability limit of diesel as low as 0.15 in terms of equivalence ratio. Later, the actual lean limit of around equivalence ratio 0.45 was tested for varying ignition delay. It was found that the actual lean concentration did not explode at 70ms ignition delay for three repeat tests and propagated a weak flame at 60ms. So, the optimum ignition delay for aerosol combustion was measured to be 70ms based on no explosion for the three repeated tests. This ignition delay is well in the range of optimum ignition delays of fine solid dusts.

Photographic studies shown in Figure 6.29 and 6.30, using high speed videos, revealed that the ignition of stoichiometric mixture of diesel is much stronger and luminous in comparison to the one near to lean concentration with the pre-existing spark. Also stoichiometric combustion of diesel aerosol propagated the flame quicker with vent rupture at less time delay compared to lean concentration. It was also found that for 0ms ignition delay, stratified mixture of diesel was burning with various zones of high and low luminosity that also support the use of optimum ignition delay for aerosol combustion.

Further work was proceeded at 70ms ignition delay that was supposed to be the optimum ignition delay. The concentration was increased starting with lean concentration of 0.45 in terms of equivalence ratio. Unfortunately, the

increasing concentration of diesel did not support explosion until an equivalence ratio of 1.5 ignited mildly. Probably this ignition delay was higher as there was direct air blast without mushroom shaped cup. It was considered that the ignition delay of 60ms might have been considered giving weak ignition of actual lean mixture. This work had to stop due to ongoing building construction but will be commenced in future.

A rich concentration was also tested that showed a delay in explosion for increasing concentration that was assumed due to cool flame mechanism (See Appendix L).

Specific proportion of coal diesel mixtures has proved to act as two in one fuel with high % volatile (See Appendix G) assisting efficient burning that will be studied later as future tasks.

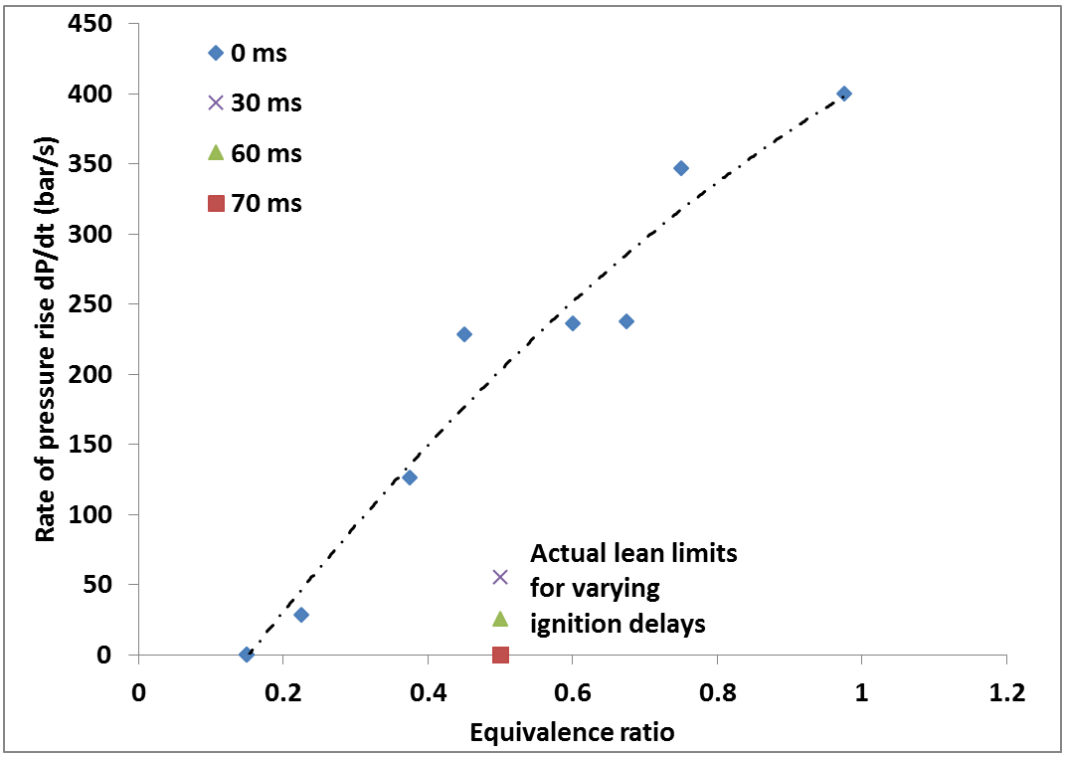

Figure 6.28: Reactivity of diesel aerosol for different ignition delays based on rate of pressure rise

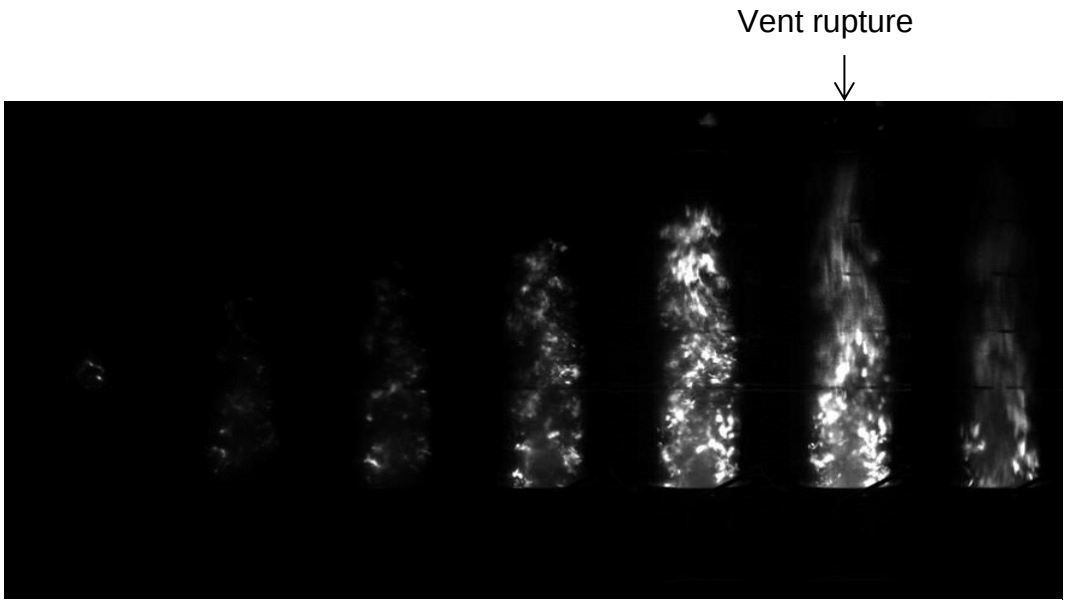

Figure 6.29: Flame propagation of stoichiometric concentration of diesel in modified Hartmann tube

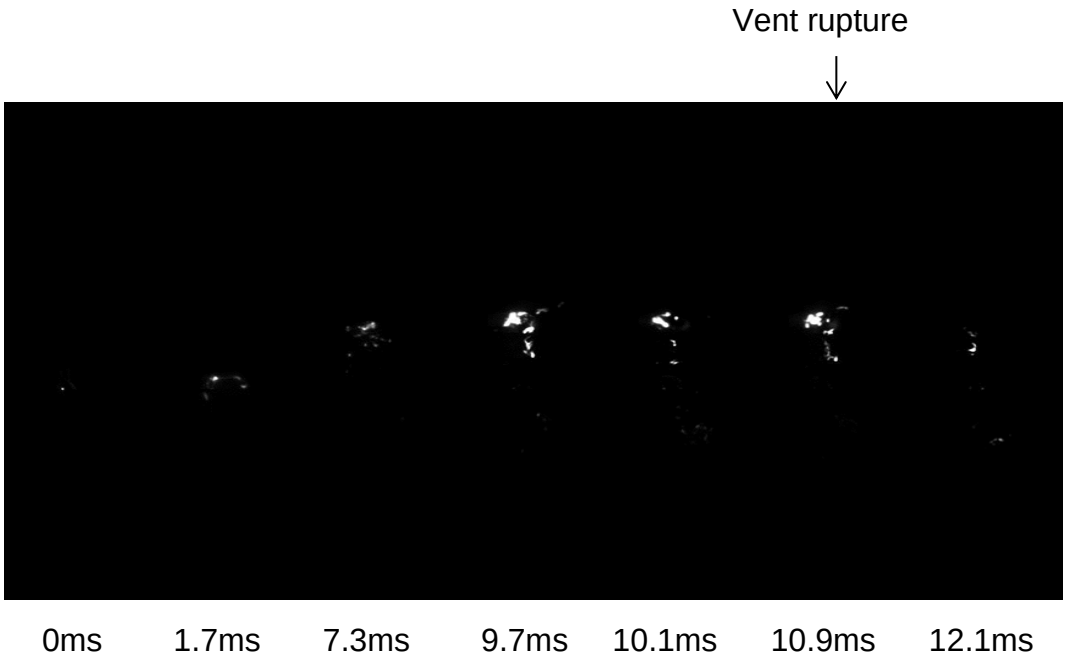

Figure 6.30: Flame propagation of lean concentration of diesel in modified Hartmann tube

6.9 Conclusion

From the experimental work on the modified Hartmann tube, it was concluded that particle size is an important parameter in the determination of the reactivity of solid biofuels. Based on the experimental results, it was concluded that the fine particles actively take part in combustion with instant release of volatiles in contrast to coarse particles. Flame propagated through the dust cloud of fine particles with less time lag. Peak reactivity was measured to be near stoichiometric concentration that shifts to rich concentration for coarse size fraction. The greater the size of the particles, the richer the concentration for peak reactivity. Increase in the particle size reduced the reactivity due to retardation of fast release of volatiles. The presence of fines with coarse particles facilitated the flame propagation. The presence of inert in the biomass especially for agricultural waste, counterbalance the effect of fine particles in enhancing the reactivity. Reactivity of solid fuels is also a strong function of ignition delay as the inappropriate ignition delay results the combustion of a stratified mixture of dust cloud. This work has demonstrated for the first time that an optimum ignition delay of 4s was necessary to achieve the actual lean flammability limit of propane. It was found using standard polyethylene dust along-with other biomass dusts, that an optimum ignition delay 50ms or above was suitable to ignite the dispersed cloud having higher turbulence. The distribution of particles and the ignition of fine particles in comparison to coarse was also monitored frame by frame using high speed camera that showed uniform and luminous flame propagation of fine and irregular and stratified local burning for coarse fraction. Aerosol fuels were also tested with some modification in the dispersion scheme of the modified Hartmann tube as there is no existing developed methodology for testing of aerosols flame propagation properties. Diesel propagated the flame with high rate of pressure rise but resulted the similar problem of stratified burning giving ultra-lean limit. Flame propagation was compared for stoichiometric and lean concentration showing efficient and luminous burning of stoichiometric mixture with higher time lag for lean mixture. More work is needed to study the flame propagation of aerosol with the determination of optimum ignition delay.

Chapter 7 EXPLOSIBILITY CHARACTERISTICS OF RAW AND TREATED BIOMASS SAMPLES USING MODIFIED 1m^3 VESSEL

Tests were performed on the modified ISO 1 m^3 vessel. Bagasse and wheat straw samples of very fine size of smaller than 63µm were tested using a small calibrated spherical grid disperser that was able to effectively disperse this size fraction. Rice husk crop residue with adequate amount was split into different sieve sizes to study the effect of particle size on the explosibility characteristics. Calibrated hemispherical cup with a drilled pipe was used to disperse the varying size fractions. Two more residues (corn cobs and peanut shells) for mixed fine and coarse sized particles with sieve size smaller than 500µm were tested using the same hemi-cup disperser. Steam exploded pine wood was also split into different sized fractions to study the effect of particle size along with the steam explosion treatment. Lastly, the very coarse fractions of SPF wood mixture and its torrefied sample of very coarse sieve size of smaller than 1000µm were tested. Experimental results showed that biomass residues have high fire and explosibility hazards in their handling. Sensitivity of explosion increased with the lowering of particle size. Post explosion samples were also analysed in detail that showed almost same characterisation of the fine fractions but a small variations in the coarse fractions chemical characterisation.

7.1 Explosibility characteristics of 2nd generation agricultural wastes sourced from Pakistan

Pakistan is a country with almost 2/3rd of its population involved in agricultural sectors. This agricultural sector accounts of around 21% of country's GDP [187] and around 20 % of their export [188]. The agricultural sector generates large amount of surplus residues that can be employed for rural developments. These dispersed residues are priceless fuel for small and medium sized power generation plants. The only investment needed on manpower to collect, transformed these residues into large bales and transported to a common point. Small power industries within 10 km radii for collecting of these residues as their feedstock are an efficient and economical power cycle. There are four major crop residues in the country that have the potential to fulfil more than 50% of country's energy demand based on 2014 energy requirement [189]. However, these biofuels have fire and explosibility hazards associated with them. Measurements of explosibility characteristics will help in proper designing of safety instruments to undercover these hazards for safe working environment.

7.1.1 Reactivity of fine samples of sugarcane bagasse and wheat straw

7.1.1.1 Turbulent flame speed and laminar burning velocity

The average flame speed for bagasse and wheat straw in comparison to the two coal samples is shown as a function of the burnt dust equivalence ratio in Figure 7.1. The range of mixtures investigated for wheat straw was less than that of bagasse because less wheat straw material was sent from the source in Pakistan. The maximum turbulent flame speeds were determined as 3.8m/s and 3.0m/s for bagasse and wheat straw dusts respectively, showing that bagasse was more reactive than wheat straw. The reason for this is the higher volatiles, higher hydrogen and lower oxygen content of bagasse compared with wheat straw, as shown in the chemical characterisation.

If the two biomasses are compared at the same burnt equivalence ratio, such as at Ø = 1 in Figure 7.1, then the flame speeds are the same at 3.0 m/s. Bagasse has an increase in reactivity relative to wheat straw only for rich burnt equivalence ratios. Figure 7.1 shows that selected samples have the comparative peak flame speed as Kellingley coal but lower than the flame speed of Colombian coal. The main reason was the higher ash contents in the biomass samples that acted as inert solid mass in suppressing the flame propagation. Colombian coal had the lowest ash content and the highest CV of all four fuels and this was part of the reason, it was most reactive. The similar flame speeds of the two biomass samples with Kellingley coal, in spite of the much lower CVs, indicates that the fuel CV is not the determining factor in the flame speed.

The peak flame speed for wheat straw dust was at an equivalence ratio of stoichiometric (Ø=1), but for bagasse dust and both coal samples it was at Ø ~2.0. This is difficult to explain as for wheat straw there was a clear reduction in the flame speed for burnt dust equivalence ratios >1, as expected for gas explosion flame speeds [110]. However, the wheat straw results are more unusual as most dusts continue to have high reactivity for rich mixtures as for bagasse and the two coal samples in this work [24, 73]. The occurrence of a high reactivity for rich dust/air mixtures was not commented on until this was pointed out by Andrews and Phylaktou (2010), as explosion results had never previously been expressed in equivalence ratio terms.

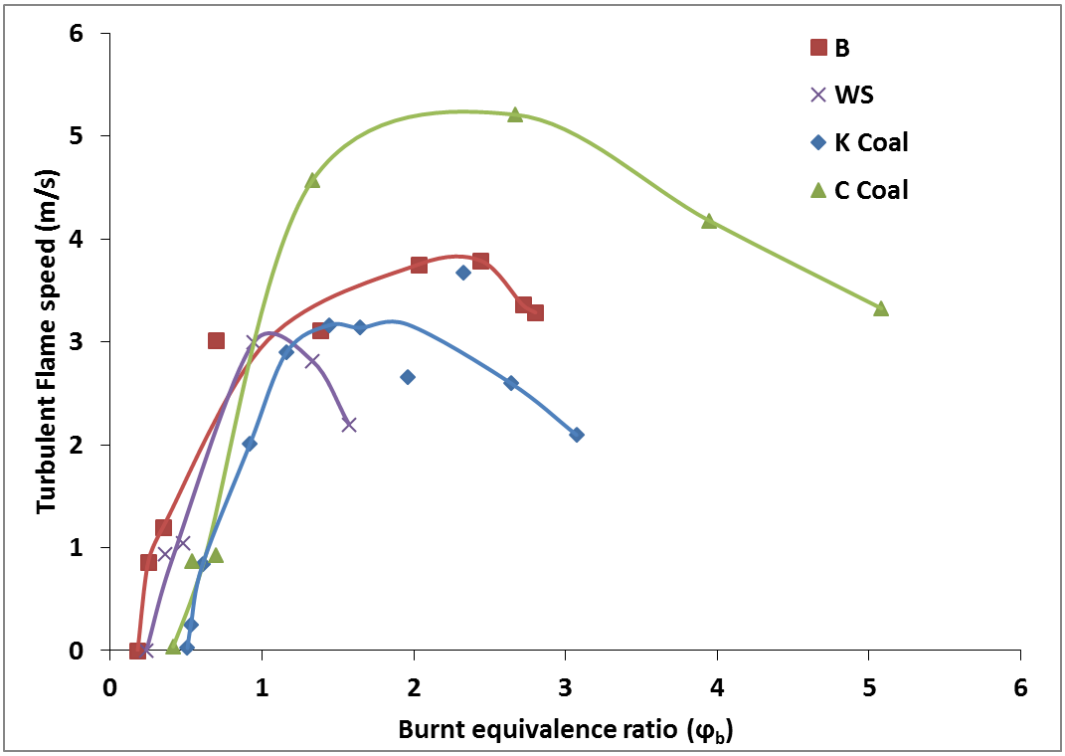

Figure 7.1 Flame speeds of Bagasse (B) and Wheat straw (WS) in comparison to Kellingley coal (K Coal) and Colombian coal (C Coal) as a function of the burnt equivalence ratio, Ø.

A possible explanation of this phenomenon is the action of the explosion induced wind ahead of the flame on dust particles that have a wide size distribution. This is the case in the present work and it was shown above that the size range for both agricultural dusts ranged up to 400 µm for $d_{90\%}$ with some particles larger than this. The flame speeds of about 3 m/s will have an unburnt gas velocity ahead of the flame of about 2.7 m/s, due to the expansion of the burnt gases. This gas velocity will entrain the particles ahead of the flame. The fine size particles will travel with the gas velocity ahead of the flame and eventually some will be compressed on the wall. These finer particles will propagate the initial flame front. However, the larger particles will lag the gas velocity due to drag effects and eventually these will be overtaken by the flame front. These large particles will then be flash heated by the burnt gases and as the mixture is rich, these large particles will be gasified releasing CO and hydrogen and the expansion of these gases on release will increase the pressure. High CO in the burnt gases for rich walnut shell dust explosion was measured by Sattar et al. (2012b). There is insufficient oxygen for these gasification gases to be burnt. The richer the mixture, the more large particles are gasified behind the flame front and hence the flame speed keeps increasing due to volume release and

expansion of gasification gases from the large particles. It is shown below that a consequence of this is that the peak pressure remains high for all the rich mixtures tested. However, the reason for the flame speeds to be reduced for wheat straw cannot be explained if this is the mechanism for bagasse. It will be shown below that the other reactivity parameter, K_{st}, does not support the reduction in reactivity for rich mixtures shown by the flame speed measurements for wheat straw.

The laminar burning velocity of the pulverised dust/air mixtures may be determined [110] from the turbulent flame speed. The laminar flame speed is first determined by using the calibrated turbulence factor (β= turbulent/laminar flame speed ratio) for the spherical flame injector, which was calibrated at β = 4.0 [82]. The laminar flame speed can then be used to determine the laminar burning velocity by dividing the flame speed by the constant pressure expansion ratio, E. In the present work this was taken as the measured P_m/P_i as advocated by Cashdollar (1996) [171]. These results are shown in Figure 7.2 and show very low laminar burning velocities that would be very difficult to measure without the turbulence in these experiments, as the flame would be strongly influenced by buoyancy, as for gas explosions with these low laminar burning velocities [190].

The low reactivity of the biomass and coal dusts relative to gases is easily seen by comparing the values of the turbulent flame speeds in Figure 7.1 with the laminar flame speeds of methane air, which has a peak value of about 3.0 m/s in large vessels, as used in the work [102]. The present turbulent flame speeds are only just higher than the laminar flame speeds for hydrocarbon-air gas explosions. With a turbulence factor of 4 for the calibrated small spherical disperser, this gives laminar flame speeds roughly ¼ those of hydrocarbon-air mixtures.

In pulverised coal burners, the air is preheated to about 600K using an exhaust heat exchanger and the laminar burning velocity increases as the square of temperature [191]. This gives a factor of 4 increase in the burning velocity at 600K compared with 300K. Thus the turbulent flame speeds in Figure 7.1 will be close to the laminar flame speeds at 600K.

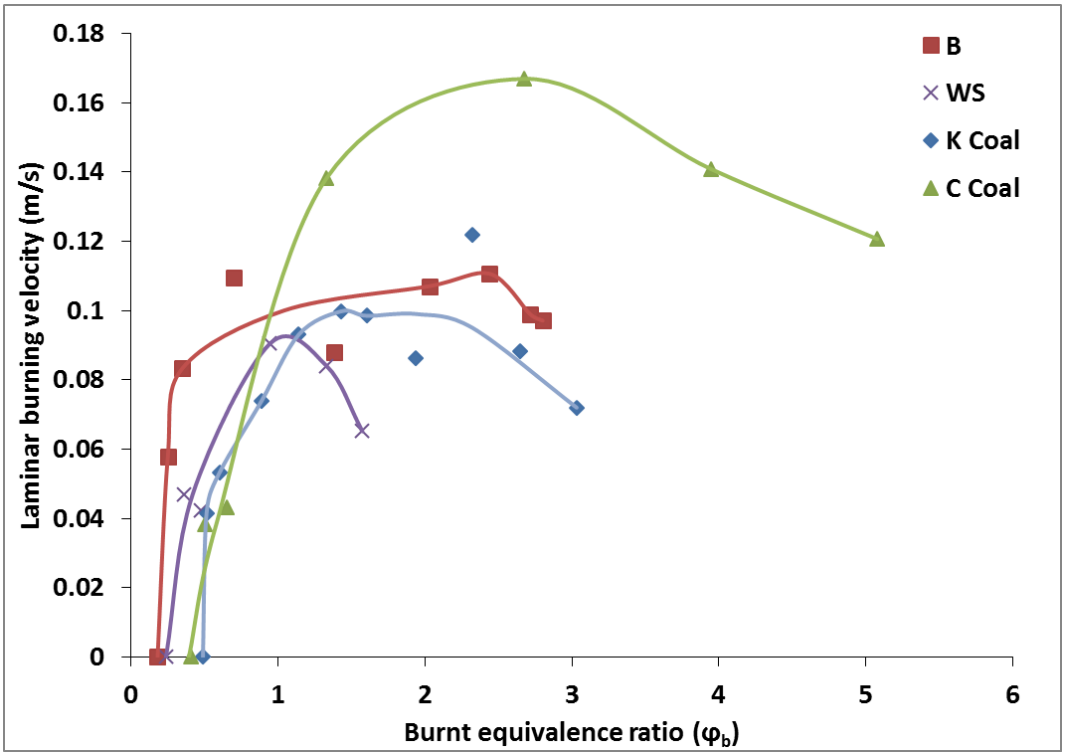

Figure 7.2 Variation of the laminar burning velocity with $Ø_{burnt}$ of bagasse (B), wheat straw (WS), Kellingley coal (K Coal) and Colombian coal (C Coal)

7.1.1.2 Heat Release Rate per Flame Area, MW/m²

The maximum heat release rate of these crop residue dusts was determined using Eq. 7.1 [168].

$$HRR\left(\frac{MW}{m^2}\right) = \frac{\left(S_{ft.}\rho_{u.}GCV\right)}{E\left(1+{}^{A}/_{F}\right)} \qquad [7.1]$$

Where S_{ft}= Turbulent flame speed (m/s), ρ_u= density of air (kg/m^3), GCV= Gross calorific value (MJ/kg), E= Expansion Ratio and A/F=Air to fuel ratio by mass.

The expansion factor E, is the unburnt gas to burnt gas density ratio at the constant pressure of the flame speed measurements. However, dust flame temperature and density are not easy to calculate with ash and water present and the constant volume expansion ratio is often used for E, which is measured by P_{max}/P_o values [171].

The HRR results are shown in Figure 7.3 which shows that the HRR increases with burnt gas equivalence ratio and continues to increase in the rich region. This is mainly driven by the flame speed measurements in Figure 7.1 which continue to go faster for rich mixtures. There is no decrease in the flame speed or HRR in the rich region as would occur for rich gaseous mixtures. For 20% excess air, the heat release rate for the biomass fuels

was 1.5 MW/m^2 for bagasse and 1.7 MW/m^2 for wheat straw, compared with 2.5 – 4 MW/m^2 for the two coal samples. For the stoichiometric $Ø_{burnt}$, the biomass HRR was about half of that of coal for the same turbulence level. This difference in HRR/m^2 arises from differences in the turbulent flame speed, expansion ratio, stoichiometric A/F and CV in Eq. 7.1. The lower CV and stoichiometric A/F for biomass compared to coal roughly cancels out in Eq. 7.1 and the main differences in HRR were due to flame speed and expansion ratio differences.

The peak heat release rate for the biomass fuels was 3.8 MW/m^2 for bagasse and 2.3 MW/m^2 for wheat straw, compared with 6.5 – 7 MW/m^2 for the two coal samples. However, the peak heat release for both coal samples occurred at a leaner mixture than for the biomass samples. This is likely to be due to the lower volatile fraction and the lower release of gasification products for rich mixtures with coal. Coal has to gasify carbon or char which requires a high residence time, whereas biomass is predominantly gasified volatiles from the particles, as chemical characterisation shows a much lower fixed carbon in biomass particles.

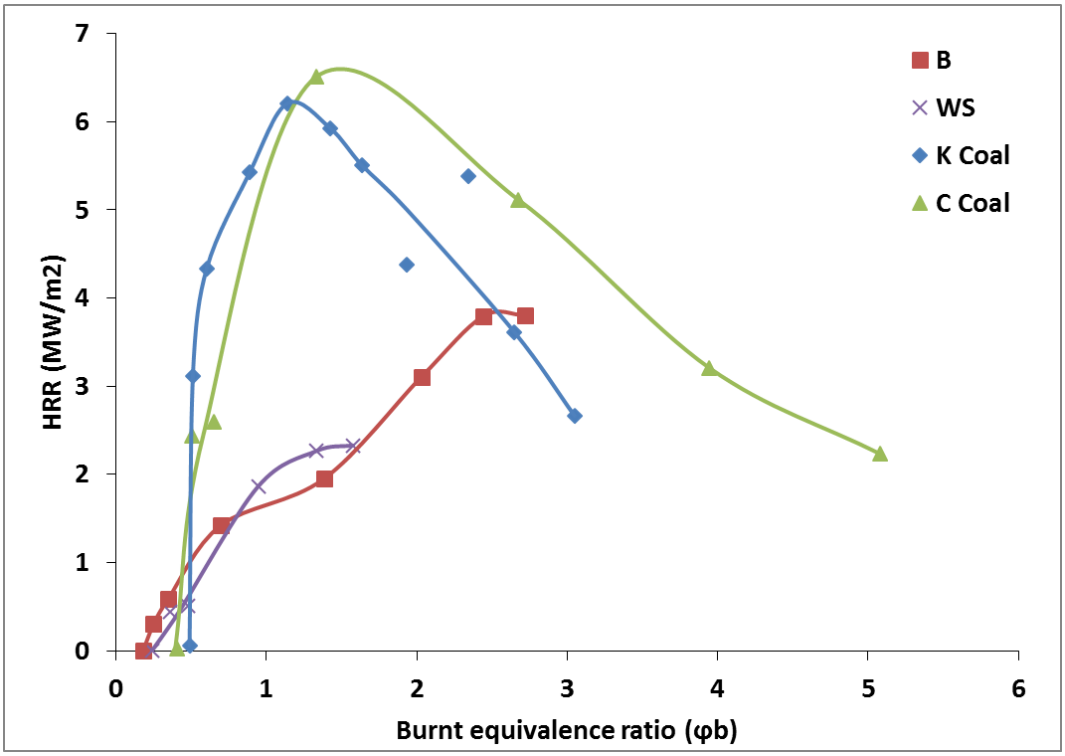

Figure 7.3 Heat release rate as a function of burnt equivalence ratio for crop residue dusts

The values of HRR in Figure 7.3 are in the range of existing coal furnaces with 20% excess air, where 1-5 MW/m^2 is typical [9, 192] which are lower HRR than the current peak HRR measurements for the two coal samples, but similar to their values for 20% excess air. Thus, it may be concluded that the turbulence conditions and turbulence flame propagation rates in the ISO 1 m^3 vessel are comparable with those for conventional coal plants for the same equivalence ratio. Although the two biomass results have a lower HRR than coal but their values are within the range that current coal combustion plants operate. Hence, biomass should be capable of being using as an alternative fuel without major changes to the coal combustion equipment. The lower HRR for biomass will result in pulverised flames with a longer flame and this has been observed on pulverised coal power plants retrofitted for biomass combustion (personal communication Drax power station).

7.1.1.3 Minimum Explosible Concentration (MEC)

The lean flammability limit, LEL, or minimum explosible concentration, MEC, for dusts in the ISO 1 m^3 spherical explosion vessel has been conventionally determined on the basis of the injected concentration. When about 50% of the mixture does not burn it is clear that the injected concentration is not the appropriate concentration to base the MEC. Also the ISO procedures for MEC determination only require the following concentrations to be tested: ….1000, 750, 500, 250, 125, 60, 30 and 15 g/m^3. The MEC is defined as the dust concentration that does not explode. Thus, if say 60 g/m^3 explodes and 30 g/m^3 does not then the MEC is 30 g/m^3 and there is no requirement in the standards to test intermediate concentrations. This is why tables of MEC for dusts have lots of materials with MEC of 60 or 30 g/m^3 [73]. This is a poor accuracy procedure and it is not sensible to have such a crude method for the determination of MEC for dusts.

In the tube method for the determination of gas/air flammability limits, the LEL should be determined with a resolution of 10% of the LEL for gaseous concentrations >2% or 0.2% for concentrations below this [97]. The concentration gap that was tested with no ignition should be within 10% of the last positive ignition. The standard essentially sets the LEL at up to 10% below the concentration that had a measured flame propagation. In equivalence ratio, Ø, terms where for hydrocarbon –air mixtures the lean limit is about Ø = 0.5, the resolution of this limit is Ø < 0.05. Most reported LEL for gases resolve the lean limit better than this and normally report to 0.01Ø. In dust concentration terms the 0.05Ø resolution for a pure hydrocarbon dust

such as polyethylene is 4 g/m^3 and for a cellulose or biomass type dust with a stoichiometric A/F ratio of 6/1 by mass (200 g/m^3) it would be a resolution of the MEC to 10 g/m^3, with normally better resolution than this [97]. This is a much better resolution of the MEC then is required in the legislated dust explosion MEC procedures. In the present work the MEC was determined as the leanest mixture that just did not explode.

The determination of the mixture concentration at the lean flammability limit is difficult in the ISO 1 m^3 vessel as in addition to the unburnt injected dust there is additional unburnt material due to the convective rise of the flame kernel near the lean limit [190], which leads to a combustion inefficiency loss of particulate material. The procedure of deducting the mass of residue from the injected mass would result in an extremely lean concentration at the MEC. Sattar et al. (2012a, b) introduced a procedure where the fraction of the dust that burnt at the maximum reactivity was assumed to be the fraction that burnt at all mixtures if there was no buoyancy. This procedure was used in the present work and on this basis it was found that bagasse dust had a lean limit at the burnt equivalence ratio of 0.22Ø and wheat straw dust had MEC of 0.29Ø, as shown in Figs. 7.1 and 7.3. The leaner MEC for bagasse is a further indication that bagasse was more reactive than wheat straw. These lean limits are in good agreement with other woody biomass dusts and are much lower than for the coal and hydrocarbon dusts [91].

The MEC for bagasse and wheat straw were also determined before using the modified Hartmann equipment [17]. This gave the lean limit as 0.22Ø for bagasse and 0.35Ø for wheat straw (for <63µm samples). For materials with a low ash and water content, such as corn cobs and peanut shells, the MEC was close to 0.2Ø, as found in the present work for bagasse and wheat straw. The MEC for bagasse and wheat straw for the modified Hartmann equipment was correlated with other results as a function of water and ash inert mass in the dusts [17]. The present MEC results for bagasse and wheat straw are compatible with those previously measured on the modified Hartmann equipment. For dusts, such as the present agricultural residues with high ash content, Bartknecht (1993) has shown that the lean flammability limits for gases and low reactivity dusts are sensitive to the ignition energy, with high ignition energy giving a leaner MEC [113]. However, more work is required on a more reliable method of determining the MEC as both the current methods have experimental errors [193].

7.1.1.4 Deflagration Parameter, K_{st}

The deflagration parameter, $K_{st} = dP/dt_{max}V^{1/3}$, is shown in Figure 7.4 (a) as a function of the burnt equivalence ratio. Figure 7.4 (a) shows that K_{st} was higher for bagasse dust in comparison to wheat straw dust, in agreement with the flame speed results. The bagasse K_{st} results were still increasing at $Ø_{burnt}$ of 2.5, whereas the flame speed in Figure 7.1 had levelled out at $Ø_{burnt}$ = 2.5. Thus it is not clear whether the maximum reactivity $Ø_{burnt}$ had reached its maximum value. For wheat straw dust Figure 7.4 (a) shows that K_{st} was very similar to that of bagasse up to an $Ø_{burnt}$ of 1, but that for richer mixtures K_{st} was lower for wheat straw than bagasse and reached a peak K_{st} of 82 at $Ø_{burnt}$ of 1.5. At this $Ø_{burnt}$ bagasse had a K_{st} of 90 and was still increasing to its maximum of 103 at $Ø_{burnt}$ of 2.7.

However, the limited amounts of pulverised wheat straw dust restricted to operate with richer mixtures and confirm that a K_{st} of 82 was the maximum value. Similarly the comparison with coals has the same trend as that of flame speed. Wheat straw dust had a similar K_{st} to Kellingley coal. The peak K_{st} for bagasse and Colombian coal were at the same burnt equivalence ratio, but Columbian coal had a significantly higher peak K_{st} at 129 compared to 103 bar m/s for bagasse.

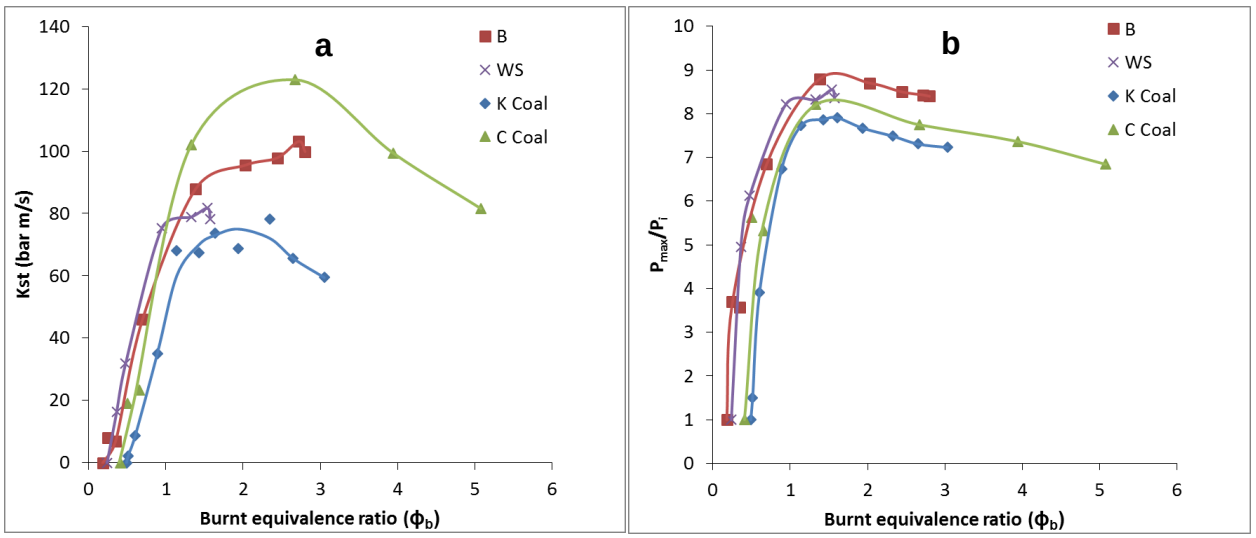

Figure 7.4 Reactivity of the selected residues in comparison to Kellingley coal (K Coal) and Colombian coal (C Coal) (a) K_{st} vs. burnt equivalence ratio (b) Pm/Pi vs. burnt equivalence ratio

The ratio of the maximum pressure to the initial pressure is shown in Figure 7.4 (b) as a function of the burnt equivalence ratio. This is the measured expansion ratio for constant volume combustion that has been used in the laminar burning velocity determinations discussed above. The ratio was slightly higher at 8.8 for bagasse dust than wheat straw dust, where the peak was 8.5. However, for both dusts the peak pressure occurred at the same $Ø_{burnt}$ of 1.5. The higher peak pressure rise indicates that bagasse had a higher flame temperature than wheat straw and this would be expected as chemical characterisation shows that the measured calorific value and volatile content was higher for bagasse and the ash content lower. Both these agricultural residues and coals have a good comparison for Pm/Pi; however there was more mass burning and higher Pm/Pi for agricultural residues in comparison to coals.

The turbulent flame speed and K_{st} are both parameters that measure the mixture reactivity and should be linearly correlated [24]. K_{st} is shown as a function of the measured turbulent flame speed in Figure 7.5. The level of agreement is relatively poor, but there is a correlation (R^2=0.85-0.95). For wheat straw for example there are three data points with K_{st} 75 – 82 bar m/s, but with a wider variation of the turbulence flame speed of 2.2 - 3 m/s.

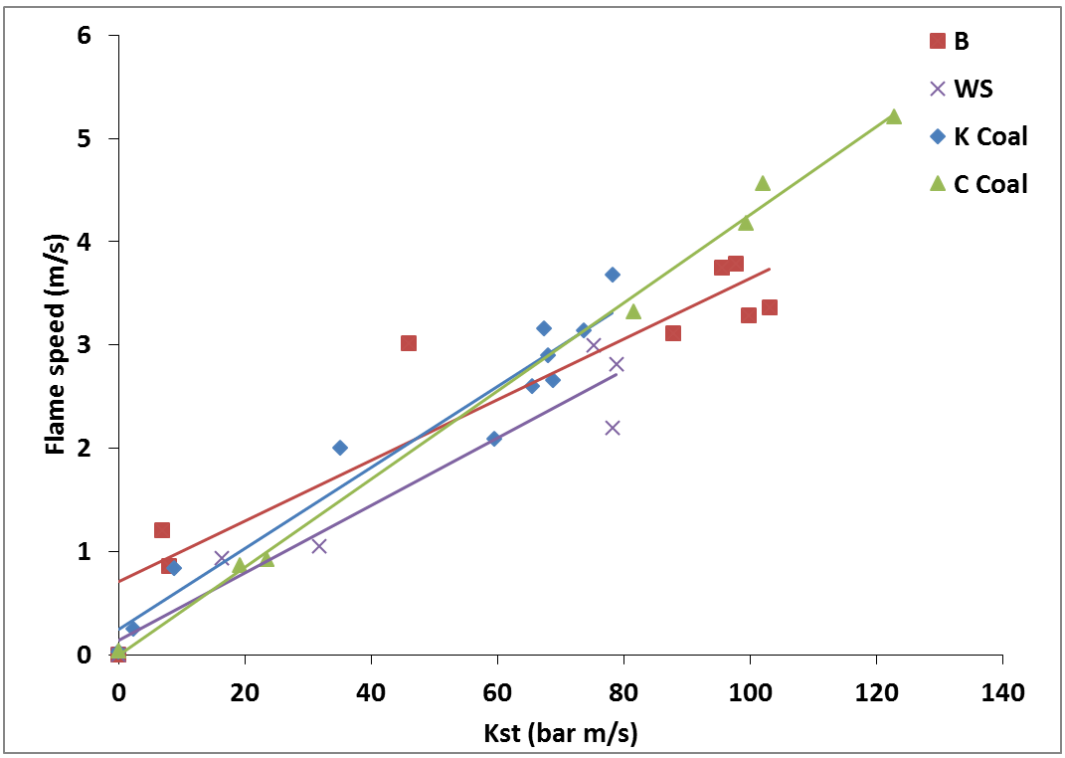

Figure 7.5 Correlation of Kst and turbulent flame speed of bagasse (B), wheat straw (WS), Kellingley coal (K Coal) and Colombian coal (C Coal)

A curious feature of the bagasse results was that for mixtures richer than $Ø_{burnt}$ of 1.5, P_m/P_i decreased as $Ø_{burnt}$ increased whereas K_{st} continued to increase. The peak flame temperature was at $Ø_{burnt}$ = 1.5 as that was where the peak pressure occurred. The model given above can explain these results. This is that large particles lag behind the flame front and are pyrolysed in the burnt gases and this heating reduces the burnt gas temperature and the pressure falls. The rich mixture has no oxygen and thus gasifies the large particles releasing CO and H_2. The sudden volume expansion of these pyrolysed large particles results in an increase in the peak rate of pressure rise and hence in K_{st}. The increased mass into the burnt gases without heat release cools the burnt gases and the peak pressure falls.

7.1.1.5 Particle Size Distribution and SEM Analysis

Although all the particles in the present work were sieved below 63µm the laser scatter method of particle sizing showed that there was still a significantly wide size distribution, as shown in the volume size distribution in Figure 7.6. Both figures compare the raw biomass size distribution with that of the residue left after the explosions. The bagasse particle size was slightly lower than wheat straw, which would be a further reason for the reactivity to be higher. There were reduced fines in the biomass residues, but this difference was insufficient to conclude that the flame had propagated only in the fines. The mean size distributions for10%, 50% and 90% of the size distribution are shown in Table 7.1. The size distribution for the two coal samples are also shown in Table 7.1 and these shows that coals were much finer fractions than all the biomass samples.

The size distributions in Figure 7.6 and Table 7.1 show that in spite of sieving to <63µm the biomass particles were relatively coarse and only the coal particles were substantially below the 63µm sieve size. This implies that the biomass particles were long cylinders with a diameter <63µm but a length greater than this, whereas the coal particles were more cubic. SEM analysis of the biomass particles, as shown in Figure 7.7 for the raw biomass and the residues, show that there were many large particles that were long cylinders. The laser light scattering particle size method interprets these as spheres of equivalent light scatter. The SEM analysis in Figure 7.7 shows little difference between the raw biomass and the biomass residue after the explosion. This also shows that the residue was predominantly the original material with a similar size distribution.

Table 7.1: Mean Size of the biomass (bagasse, wheat straw), their post explosion residues and coal samples

Sample	*d (10%)*	*d (50%)*	*d (90%)*	$d_{3,2}$	$d_{4,3}$
	µm				
Bagasse	24.3	125.6	356	70.2	201.5
Wheat straw	18.8	126.1	441.5	78.0	213.4
Bagasse residue	35.0	150.8	408.9	73.9	193.3
Wheat straw residue	35.6	154.9	464.5	72.0	209.0
Colombian Coal	6.8	28.1	85.2	14.7	40.1
Kellingley Coal	5.0	25.5	65.3	12.0	30.9

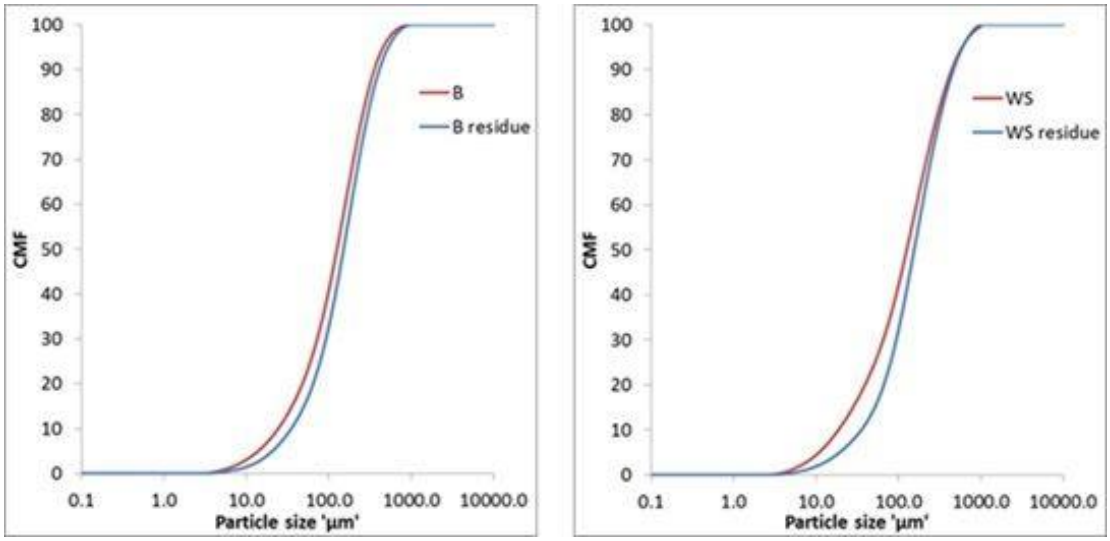

Figure 7.6 PSD of selected crops and their post explosion residues Left: Bagasse dust (B) & Right: Wheat straw dust (WS)

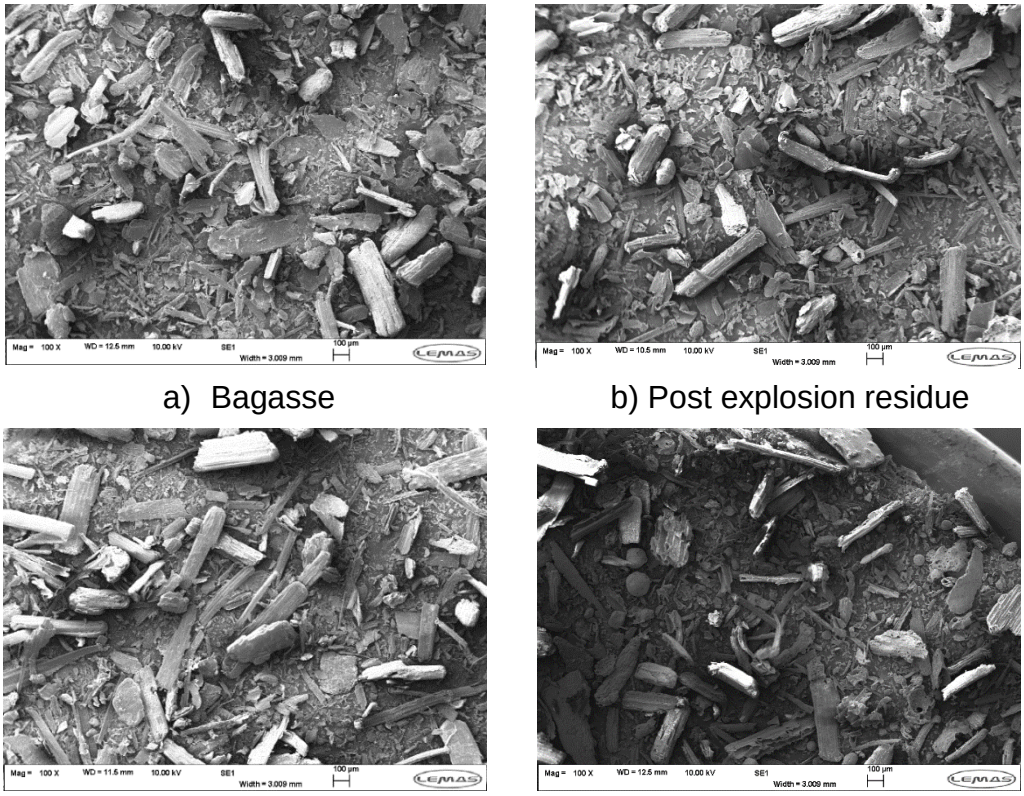

a) Bagasse b) Post explosion residue

c) Wheat straw d) Post explosion residue

Figure 7.7 Surface morphology comparison of crop residue samples and their post explosion residues

7.1.1.6 Elemental and Proximate analysis of post explosion residues in comparison to their raw

As shown in table 7.2, the chemical characterisation of the post explosion residues in comparison to raw samples were compared. It was found that post explosion residues have around same elemental proportions in terms of percentages with slight decrease of hydrogen contents. Also the TGA proximate analysis showed decrease of volatile due to corresponding increase of fixed carbon or ash in the post explosion residues. This slight variation of the chemical characterisation in the post explosion residues was due to the inclusion of ash/fixed carbon due to burnt mass proportion.

As a conclusion based on these results, lean flammability limits for these crop residues were lower at 0.2-0.3Ø compared with gaseous hydrocarbons. Peak turbulent flame speeds were 3-4m/s and K_{st} were 82 and 103 bar m/s. These reactivity parameters were similar to those for woody biomass and similar to two coal samples. These crop residues can be used for the generation of electricity in pulverised flame power plants after some pre-treatments.

Table 7.2: Chemical Characterisation of raw bagasse and wheat straw in comparison to post explosion residues

Biomass	Bagasse (B)	Post explosion residue B	Wheat straw (WS)	Post explosion residue WS
% C (dry)	43.6	45.0	38.2	31.3
% H (dry)	5.7	4.6	4.9	3.2
% N (dry)	1.0	0.9	1.0	0.8
% S (dry)	0.1	0.0	0.1	0.0
% O (dry)	28.0	31.4	31.3	23.1
% H2O	7.2	2.3	6.8	3.6
% VM (daf.)	92.3	78.4	86.2	73.5
% FC (daf.)	7.7	21.7	13.8	26.4
% Ash	20.1	17.6	22.8	40.1
CV (MJ/kg)	15.6	-	14.5	-
Stoich. A/F (g/g)	7.5	6.6	6.3	6.4
Actual stoich. conc. (g/m^3)	221.1	226.8	272.2	334.6

7.1.2 Explosibility characteristics of coarse fraction of corn cob and peanut shell<500µm

Two crop residues ‘Corn cob’ (CC) and ‘Peanut shell’ (PS) were investigated as they are typical of waste agricultural products in Pakistan. These agricultural residue samples were milled at source in Pakistan and it was this milled sample that was used in the explosions after sieving to <500µm. These coarse agricultural wastes were compared with fine milled <63µm coal samples and this is the main reason that these coals were comparatively more reactive as is shown in the results.

7.1.2.1 Chemical characterisation of post explosion residues of coarse corn cob and peanut shell in comparison to their raw samples

Table 7.2 shows the elemental and TGA analysis of the post explosion residues for the most reactive concentration, in comparison to their respective raw samples. For the corn cob residues the composition was very close to the original raw material for all parameters measured. In contrast the residues from the peanut shell dust explosions were significantly different. The biggest difference was the increase in ash, which is expected as the ash from the material that burns should accumulate with the residue alongside the material injected that did not burn. If only about 50% of the original material burns then the ash in the deposits should be about double that in the raw material and this occurs for the PS residues. The lack of an increase in ash for the CC is difficult to explain, apart from being a fly ash or measurement error. The PS residues had a significant decrease in volatiles and increase in fixed carbon together with a decrease in O content. This indicates some low temperature pyrolysis has occurred, with similar results to torrefaction. Why these two biomass behaved differently is not known. However, the post explosion residue is concluded to be predominantly the same as that of raw biomass.

Table 7.3: Chemical characterization of the post explosion residues in comparison to their raw corn cob and peanut shell samples

Biomass	Corn cobs (CC)	Post explosion residue CC	Peanut shell (PS)	Post explosion residue PS
% C (dry)	41.6	43.0	49.1	48.4
% H (dry)	5.4	5.4	6.0	5.2
% N (dry)	1.0	1.0	1.4	1.5
% S (dry)	0.1	0.0	0.0	0.0
% O (dry)	42.4	41.3	35.0	28.8
% H2O	7.1	6.2	7.0	5.8
% VM (dry)	74.7	72.1	71.4	61.8
% VM (daf.)	82.5	79.4	78.1	73.6
% FC (dry)	15.9	18.6	20.0	21.4
% FC (daf.)	17.6	20.6	21.9	25.5
% Ash	8.8	8.7	8.0	15.1
CV (MJ/kg)	16.7	17.2	19.7	19.2
Stoich. A/F (g/g)	5.4	5.5	6.8	7.3
Actual stoich. conc. (g/m^3)	264.2	256.4	204.6	207.8

7.1.2.2 Particle size distribution and surface morphological study of milled corn cob and peanut shell in comparison to their explosion residues

Table 7.4 shows the particle size distribution of the raw biomass (sieved to <500µm) and the post explosion residues. The two size distributions were very similar, again indicating that the residue was predominantly the original raw biomass. There was an increase in the proportion of fines and a decrease in the proportion of coarse material in the residues for both biomasses. However, for CC the surface average size decreased in the

residue whereas for the PS the surface averaged size increased in the residue, but the changes were relatively small.

Table 7.4 shows that the raw biomass size distributions as milled were relatively coarse with over 50% of the mass >373µm for CC and >176µm for PS. The distribution of sizes in the samples and residues are shown in the SEM images in Figure 7.8. There is no evidence in the size distribution or in the SEM images of the raw biomass and their residues, that only the fines burn in the explosion as also proved with minor difference of % fraction<100µm in table 7.4. The conclusion is that the fines and coarse material burn approximately with equal effectiveness and this was not expected. SEM in Figure7.8 of molten layers of the burnt mass showed the formation of some ceno-spheres so there was some pyrolysis of the biomass.

A physical model of the turbulent biomass flame front that fits the above evidence is that the explosion induced wind blows the dust ahead of the flame and eventually this dust is compressed into a layer on the walls. The flame then impinges on the wall and partially pyrolysis the outer layer, but the inner layer remains the original biomass with the original size distribution. After the explosion this residue falls off onto the floor of the vessel [18, 22, 194]. At the turbulent flame front the action of the explosion induced wind is for the fines to follow the gas flow and the coarse particles to lag behind and be enveloped in the products of reaction of the fines. The coarse material is then gasified in the hot combustion products of near stoichiometric burning of fines. This model explains why rich mixtures can burn with high pressure, as will be shown in the results. In these biomass samples there are sufficient fines for lean mixtures to burn and to give a relatively lean MEC. However, the temperature is still sufficient to ignite the coarse particles and for lean overall mixtures they can then burn as there is surplus oxygen. For rich overall equivalence ratios the coarse particles are gasified by heating in the products of rich combustion.

Table 7.4: Chemical characterization of the post explosion residues in comparison to their raw samples

Materials	**d (10%)**	**d (50%)**	**d (90%)**	**Surface weighted mean**	**Fines particles <100µm**
	µm				**% share**
Corn cob	45.0	372.6	777.8	98.1	19
Post explosion corn cob	48.4	239.6	668.3	92.1	22
Peanut shell	24.3	176.1	698.5	63.5	39
Post explosion peanut shell	32.4	180.9	648.6	75.3	35

7.1.2.3 K_{st} and P_m/P_i results

The K_{st}, P_m/P_i, S_T and U_L results as a function of $Ø_{burnt}$ are shown in Figs. 7.9-12 for the two biomass samples sieved to <500µm with comparison with two coals milled and sieved to <63µm. The coal samples had higher values of K_{st} mainly due to their much smaller particle size. Corn cobs were more reactive than peanut shells with higher K_{st} and S_T, but the higher P_m/P_i for CC resulted in the maximum laminar burning velocities being lower for CC. The increase in reactivity by the change in K_{st} for CC relative to PS was much larger than that based on the turbulent flame speeds. This was not expected and could be due to the measurement being based on the reactivity close to peak pressure in the explosion, whereas the flame speeds were measured in the initial near constant pressure flame propagation. The pressure rise in the explosions are shown in Figure 7.9 and show that despite of the low reactivity of the coarse biomass, the pressure rise was high and would be completely destructive if it occurred inside an enclosure such as pellet silo or pulveriser mill or pellet manufacturing plant. Also a peak pressure close to the theoretical maximum for gas explosions indicated that complete combustion of the fine and coarse biomass had occurred.

Figs. 7.9 and 12 show that the minimum explosible concentration (MEC) for CC and PS were 0.6 and $0.82Ø_{burnt}$ respectively. These lean limits were higher than the Kellingley ($Ø_{burnt}$=0.48) and Colombian coal samples ($Ø_{burnt}$=0.39). This difference was caused by the differences in the particles

size which was sieved to <63µm for the two coal samples and <500µm for the two biomass samples. Table 7.4 shows that PS were finer than CC and both had a very wide size distribution with 50% of the mass of size > 370µm for CC and 180µm for PS. The model that explains the present results, whereby large particles are pyrolysed in the burnt products of an initial flame front based on fine particle combustion, also can explain why the MEC is relatively rich for coarse biomass particles. If the MEC of the fine fraction is taken as that measured for biomass sieved to <63µm, which is about $0.2Ø_{burnt}$, then the overall mixture has to be rich enough at the limit to give $0.2Ø_{burnt}$ in the fine fraction. It will also be assumed that the fine fraction that burns can be taken as <100µm. For CC Table 7.4 shows that the fine fraction is 19% of the total mass and this would predict an MEC for the overall mixture of $0.62Ø_{burnt}$ which is very close to that measured. For PS the fine fraction was 39% and this would give the MEC as 0.5, which is much leaner than the measured MEC of 0.82Ø.

The pressure rise in Figure 7.10 is driven by the temperature of the burnt gases and a maximum pressure ratio of 7 for PS indicates about 2100K as the burnt gas temperature. The peak pressure for CC was higher at 8 indicating a burnt gas temperature of 2400K. This higher peak pressure for CC was unexpected as Table 7.3 shows that the GCV was much lower. For the two coal samples the Colombian coal had a 6% higher GCV than the Kellingley coal and there was a similarly higher peak pressure. The other unusual feature in Figure 7.10 is that the peak pressure for biomass occurs at $2.4Ø_{burnt}$ compared with $1.3Ø_{burnt}$ for coal. At $Ø_{burnt}=1$ both the biomass had the same peak pressure ratio of 5.5 and hence the same burnt gas temperature. The mechanism for large size particles to react behind the flame front for rich mixtures, as discussed above, postulates that the large particles are gasified in the rich overall mixture but with a temperature generated by near stoichiometric combustion in the fine particles that burn first. The release of gasified gases, CO and hydrogen, by the large particles will cause the pressure to increase in the chamber, not due to flame temperature increases but due to gas volume addition. If a simple assumption is made that all the mass of CC injected after $Ø_{burnt}=1$ was converted into CO with no change in the temperature at stoichiometric, then it may be shown, using the C content of the biomass in Table 7.3, that the 5.5 pressure ratio at $Ø_{burnt} = 1$ would increase to 7 at $Ø_{burnt} = 2.5$. This is the pressure found for PS but for CC it was 8. This difference is probably due to the assumption of constant flame temperature, which is the temperature

derived from the initial burning of the fines. As more mass is added, more fines occur and hence the temperature will rise and this is likely to account for the additional pressure ratio increase to 8 for the CC biomass.

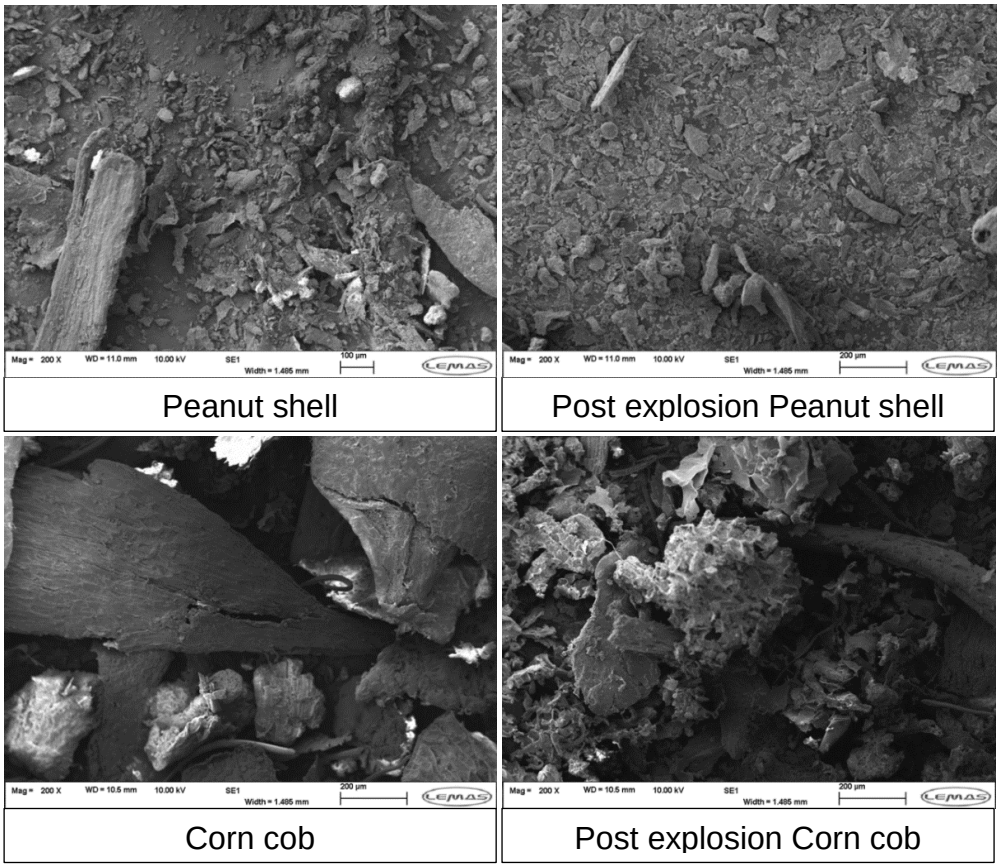

Figure 7.8: Scanning Electron Microscopy of the post explosion residues in comparison to their respective corn cob and peanut shell samples

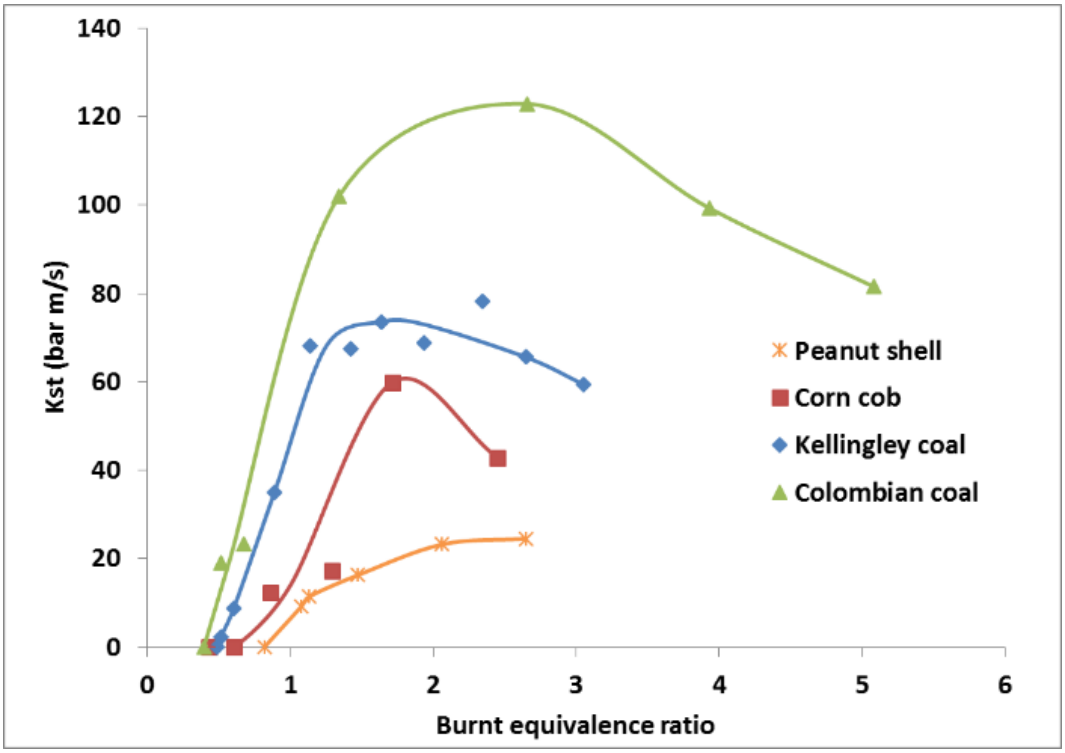

Figure 7.9: Kst v. $Ø_{burnt}$ of corn cob and peanut shell in comparison to Kellinglely coal and Colombian coal samples

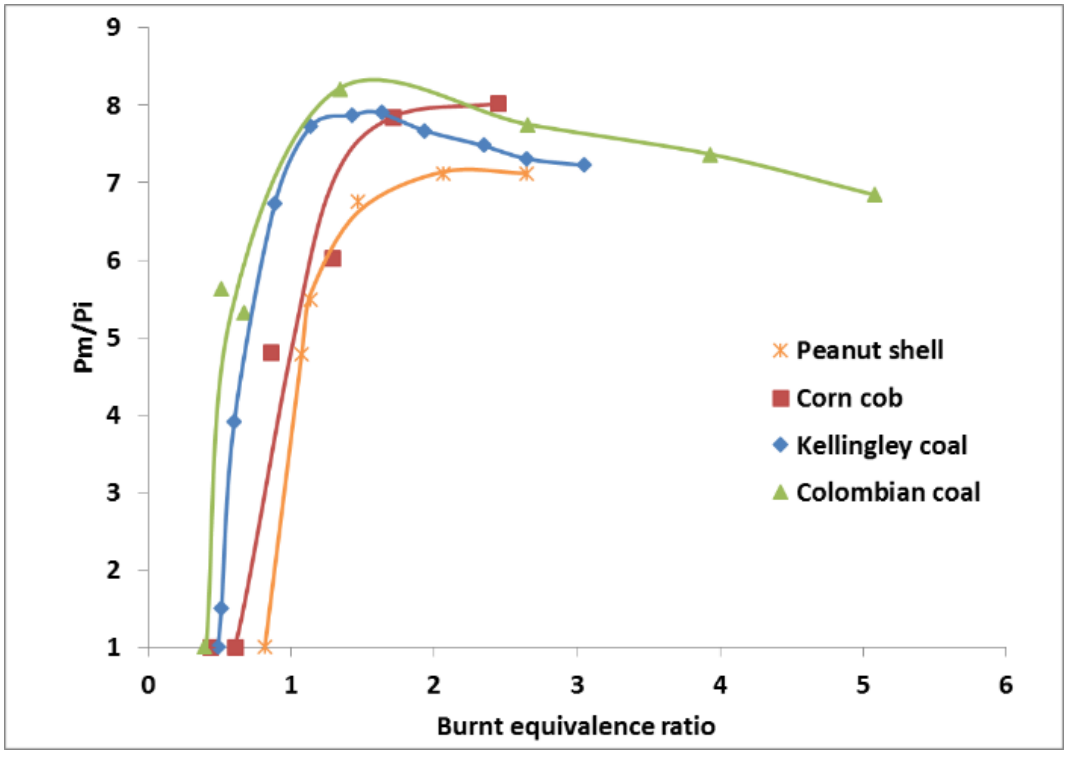

Figure 7.10: Pm/Pi v. $Ø_{burnt}$ for CC, PS and coal of corn cob and peanut shell in comparison to Kellinglely coal and Colombian coal samples

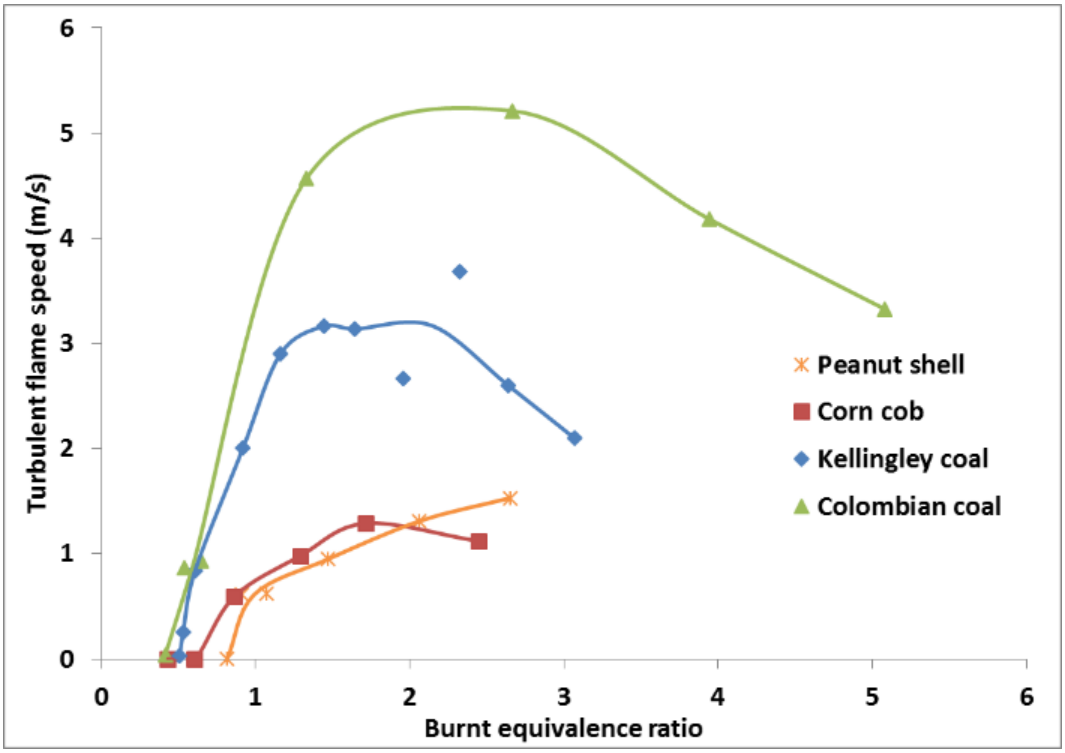

Figure 7.11: Turbulent flame speed, S_T v. $Ø_{burnt}$ of corn cob and peanut shell in comparison to Kellinglely coal and Colombian coal samples

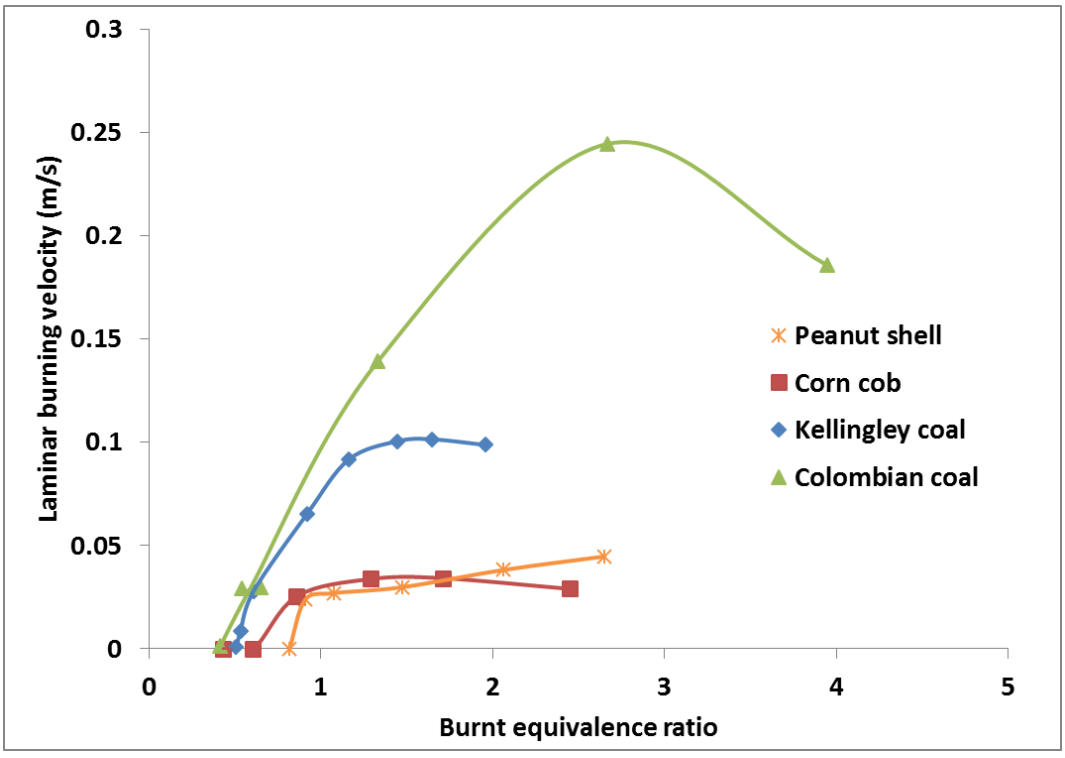

Figure 7. 12: Laminar burning velocity v $Ø_{burnt}$.of corn cob and peanut shell in comparison to Kellinglely coal and Colombian coal samples

7.2 Dependence of particle size on the explosibility characteristics of raw rice husk and steam exploded pine wood samples

7.2.1 Reactivity results of different sized fractions of rice husk agricultural waste

Rice crop is one of the top grown crops in Pakistan each year. According to Pakistan's federal committee on agriculture (FCA), a target of 7 million tons production of milled rice was set for the year 2015 due to sufficient water availability and normal weather condition [195]. US department of agriculture (USDA) estimated the rice production in Pakistan for 2013-2014 (November-October) to be 6.7 million tons and that production raised to 6.9 million tons for 2014-2015. However this rise of 3% was not confirmed by 'National Space Agency of Pakistan (SUPARCO) and United Nation's food and agricultural organization [195]. The production of milled rice for last five years is shown in Figure 7.13. This showed the increase of production each year except 2012 due to damage by flood. This crop along with its enormous residues has the potential of changing lifestyle for rural development [196].

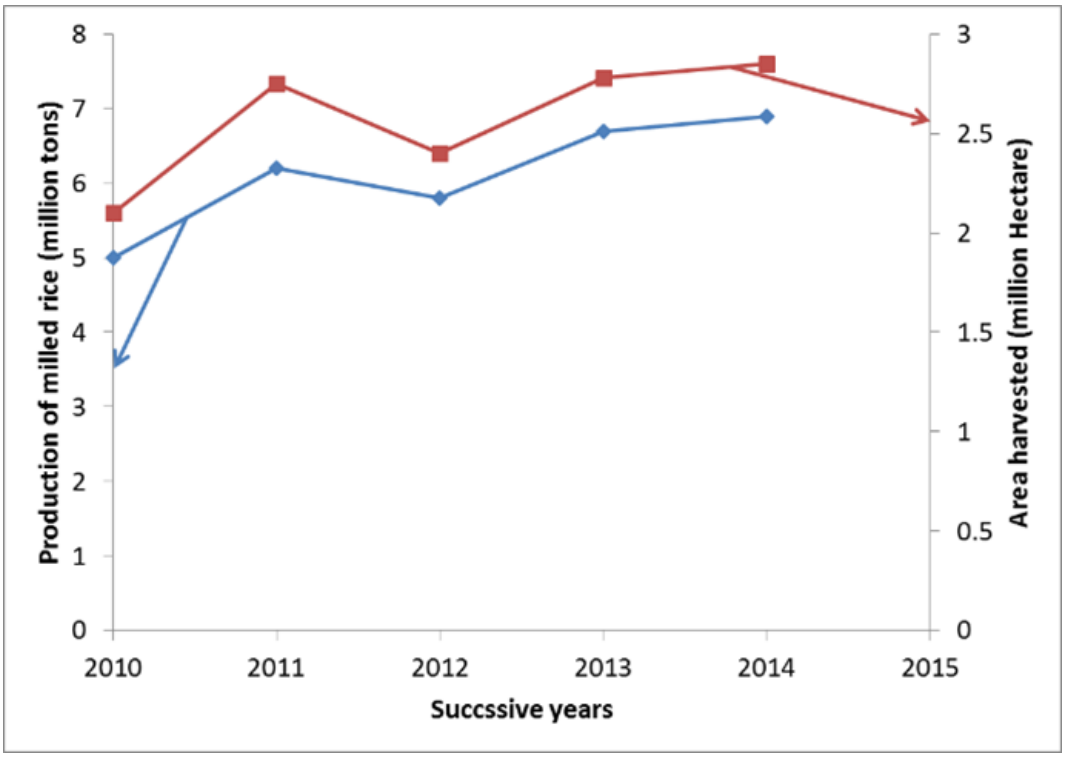

Figure 7.13: Production of milled Rice in Pakistan for the successive years [28]

Variation of particle sizes of these crop residues has strong influence on its burning characteristics. More fine particles with more expose surfaces facilitate the fast release of volatiles that were understood to play an important role in flame propagation. Utilization of these crop residues with coal or independently requires detailed investigation of its burning properties along with particle size dependence before their exploitation. This work aims to provide burning characteristic of rice husk crop residues for varying size range fractions.

7.2.1.1 Size specifications of the experimental materials

Excessively grown rice husk crop residue (RH) was imported from Pakistan for this experimental work. About 18 kg rice husk crop residue was first milled there in Pakistan before its transportation. After import to UK, it was milled further to less than 500 µm using Retch 100 ultrafine grinder and sieved into following size range fractions; less than 63 µm, 63-150 µm, 150-300 µm, 300-500 µm and less than 500 µm. It was noticed that proportion of fine fraction collected from sieving was small as compared to the coarse fraction, so some more milling of coarse fraction was performed using 80 micron sieve and sieved to get enough amount of fine fraction (<63 µm) for $1m^3$ testing.

Sieved fractions of different size ranges were analysed on Malvern Mastersizer 2000 for their actual sizes as shown in Figure 7.14. It can be observed based on particle size distribution that the actual particle size range for different sieved samples is much wider in contrast to their sieved sizes. This is due to the elongated particles of biomass able to pass axially through sieves. This area had not given enough attention and most of the models were developed considering biomass as fixed regular shape that is not true. It was noticed that the proportion of fine particles decreased with increasing sieved size. As for sieve size <63µm, the proportions of fines for actual size ≤63 µm is 20% that decreased to 11% for higher sieved size 63-150µm. For very high sieve size, there were still some fines but in negligible proportions. Sieved size sample of rice husk 0-500µm, showed the distribution for proportions of different sized particles. In this work, reactivity of different size range fractions of rice husk were compared and investigated for their flame propagation behavior. Reactivity were measured based on minimum explosible concentration (MEC), maximum rate of pressure rise (dP/dt, max), deflagration index (K_{st}) and turbulent and laminar flame speed. Tests could not be extended for very rich side due to limited sample's stock..

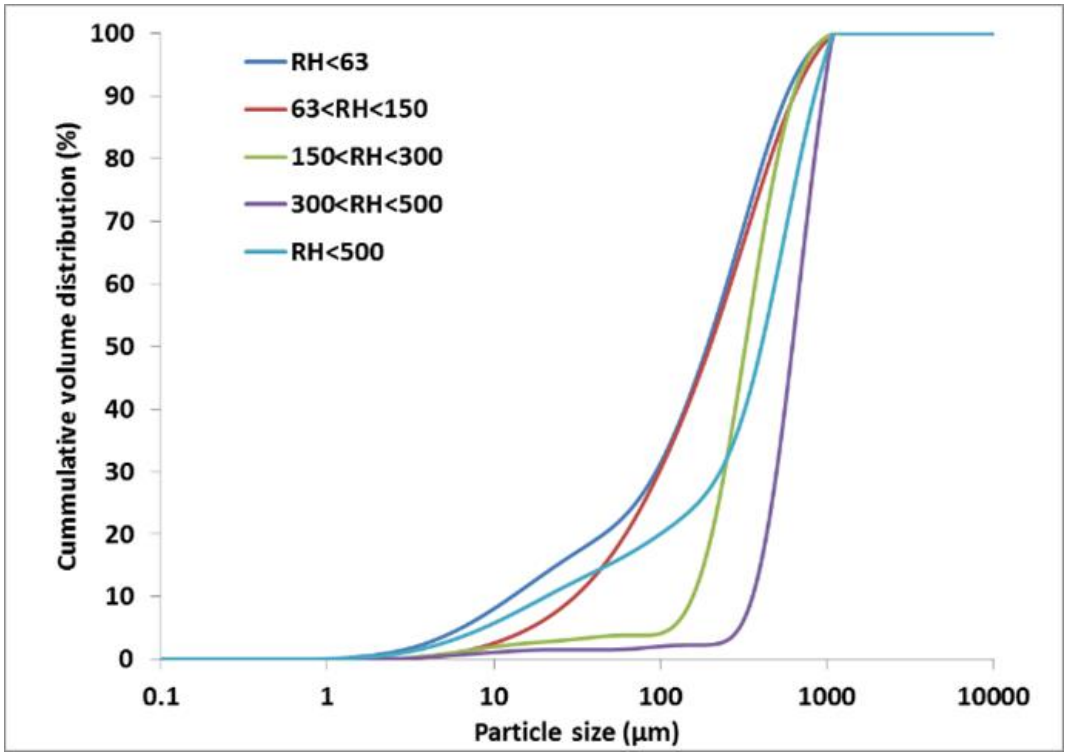

Figure 7.14: Particle size distribution of varying size fraction rice husk (RH)

7.2.1.2 Deflagration index vs. burnt equivalence ratio

Figure 7.15 showed deflagration index vs. burnt equivalence ratio for different sized fractions of selected rice husk residue. It was found that sized fraction with higher fines have higher peak deflagration index showing fast burning of particles. Also the peak deflagration index shifted to rich concentration for the coarse sized fraction.

Peak deflagration index was measured to be in the range of 33-83 bar m/s depending on the proportions of fine particles present. Very coarse fractions of size ranges 150-300 and 300-500 µm failed in propagation of flame. This is because of the delay in turning the coarse particles to volatiles to sustain the flame propagation.

7.2.1.3 Peak pressure relative to atmospheric pressure vs. burnt equivalence ratio

Maximum rise of explosion pressure relative to ambient were measured and displayed against burnt equivalence ratio in Figure 7.16. Peak pressure relative to atmospheric were measured to be in the range of 7.3-7.45 bar. It showed that very coarse fraction like 150-300 µm and 300-500 µm did not ignite however sized fraction containing enough fines such as 63-150 µm and smaller than 500 µm propagated the flame. So, the presence of fines

facilitated the flame to propagate and helped the burning of some proportions of coarse particles giving almost same peak rise of pressure but at higher equivalence ratio as compared to fine fractions.

7.2.1.4 Turbulent flame speed vs. burnt equivalence ratio

Flame speeds were measured from the plot of thermocouple distance vs. time of flame arrival for different concentrations. Fine fraction of sieved size <63 µm showed an average peak turbulent flame speed of 4.6 m/s whereas the sized fraction with less fines showed lower flame speed. It meant that the fines accelerated the flame due to their efficient burning. Coarse particles with longer delay in their burning resulted slow propagation of flame with less flame speed as shown in Figure 7.17.

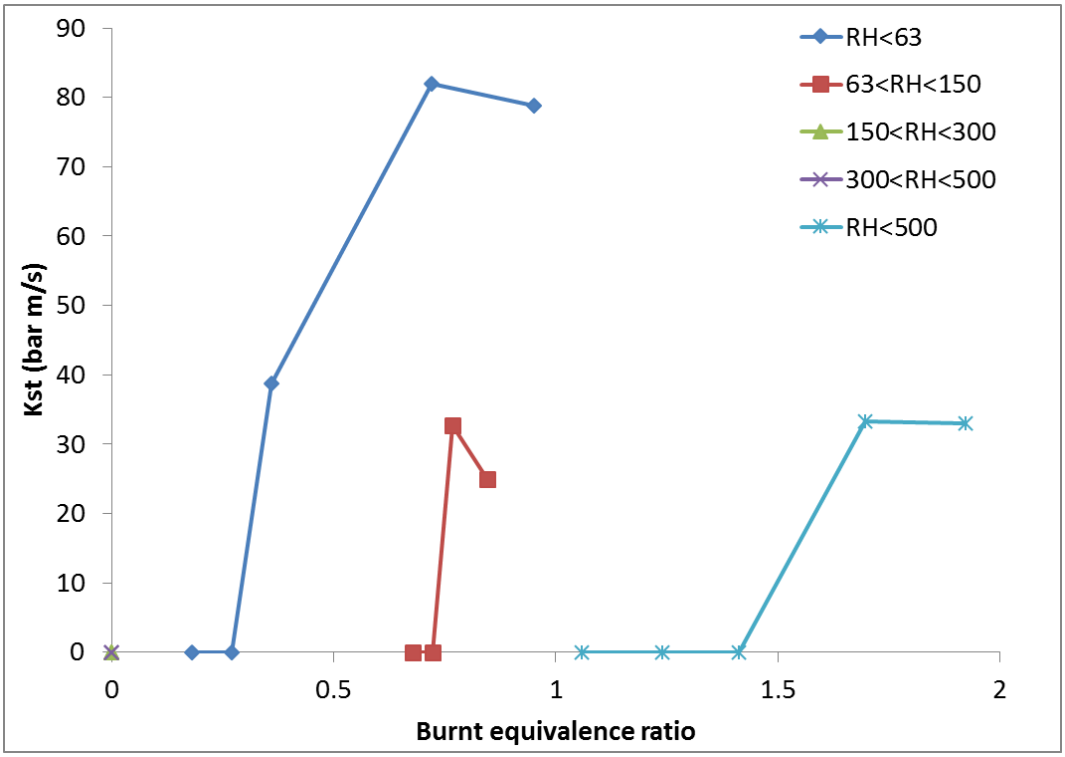

Figure 7.15: Kst vs. burnt equivalence ratio for different sized fractions of rice husk (RH)

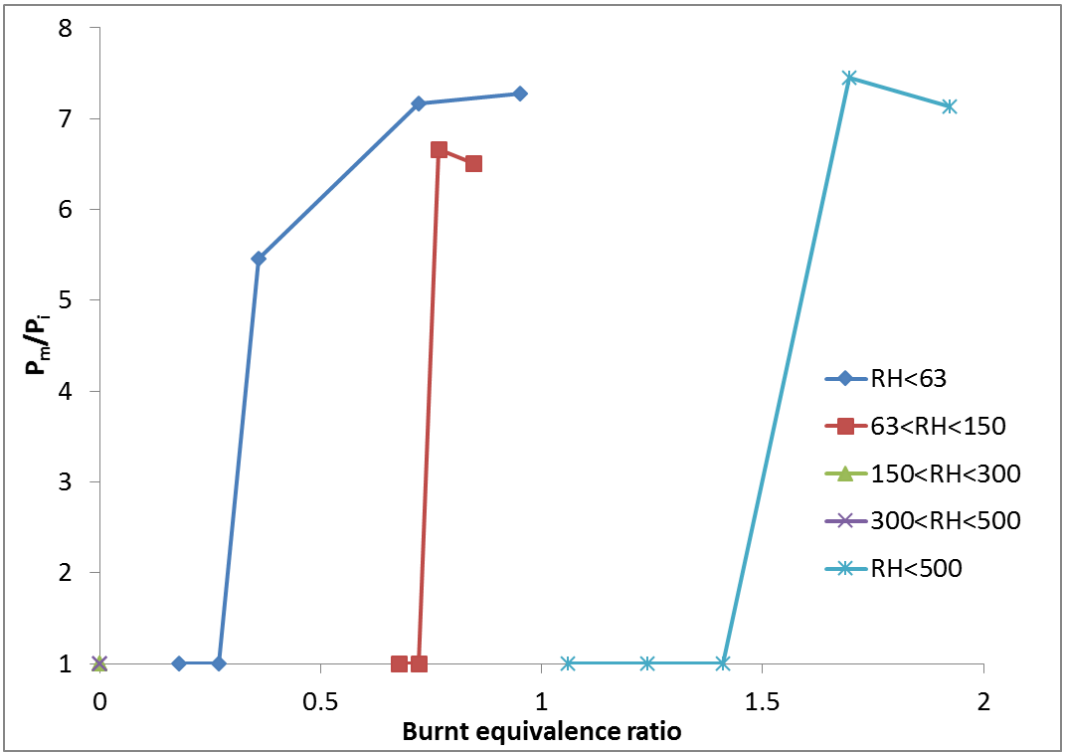

Figure 7.16: Pm/Pi vs. burnt equivalence ratio for different sized fractions of rice husk (RH)

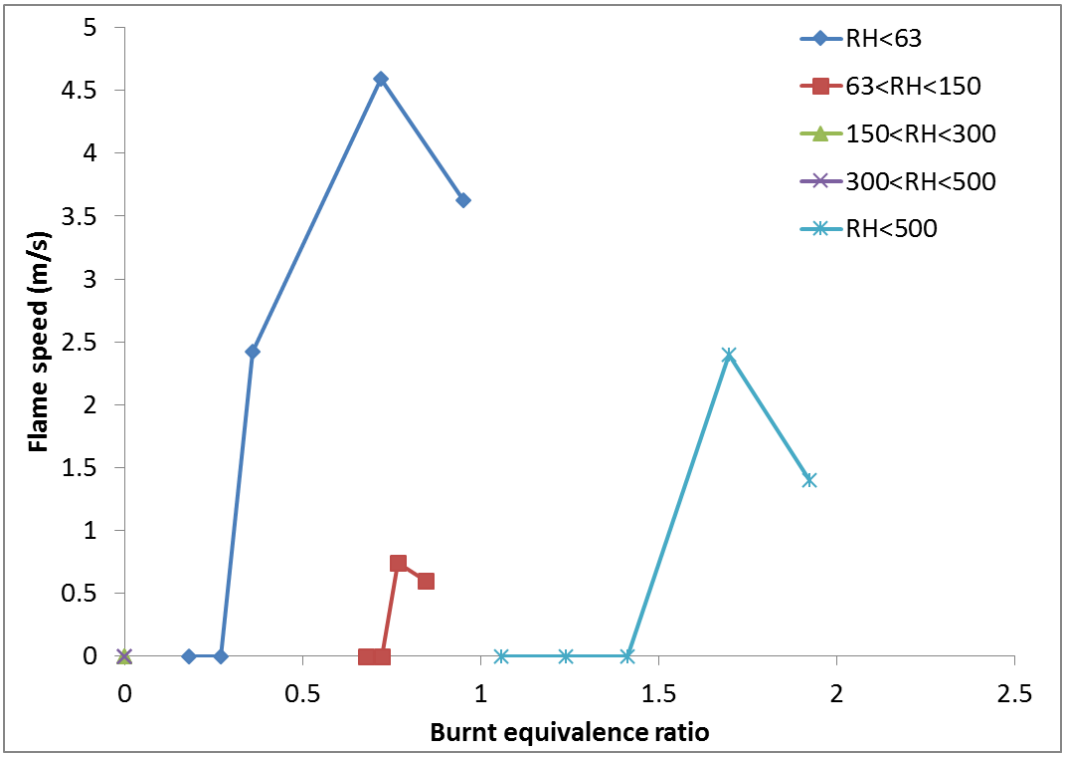

Figure 7.17: Flame speed vs. burnt equivalence ratio for different size fractions of rice husk (RH)

7.2.1.5 Analysis of rice husk post explosion residues

7.2.1.5.1 Ultimate and proximate analysis of post explosion residues

Table 7.5 showed the ultimate and TGA analysis of post explosion residues for the most reactive concentration of different sized fractions. Elemental analysis showed almost same composition for all the sized fractions as that of raw sample. However the TGA analysis showed drop in volatiles that was found to be higher for fine fraction in comparison to coarse. This was because of more release of volatiles from fines due to their more exposed surfaces. Similarly the ash contents were increased in the post explosion residues and there was significant increase of ash for the post explosion residue of fine fraction. This increase of ash in the finer fraction resulted the reduction in its calorific value. Stoichiometric air to fuel ratios were calculated to be almost same but actual stoichiometric concentration was much higher for the post explosion residue of fine fraction due to enhancement of ash.

Table 7.5: Chemical characterization of the post explosion residues in comparison to raw rice husk

Biomass	Raw rice husk	Post explosion Rice husk (RH) residues		
		RH<63µm	RH(63-150µm)	RH<500µm
% C (dry)	40.2	26.7	38.1	37.5
% H (dry)	5.1	3.5	4.9	4.2
% N (dry)	0.9	0.8	0.5	0.5
% S (dry)	0.0	0.0	0.0	0.0
% O (dry)	34.4	22.1	32.8	31.2
% H_2O	7.7	4.8	5.8	5.6
% VM (dry)	67.5	41.9	61.0	64.9
% VM (daf.)	83.7	78.8	80.0	88.6
% FC (dry)	13.2	11.3	15.2	8.5
% FC (daf.)	16.4	21.3	19.9	11.6
% Ash	17.9	44.6	22.3	25.2
CV (MJ/kg)	15.2	13.9	15.6	15.7
Stoich. A/F (g/g)	6.1	6.3	6.1	6
Actual stoich. conc. (g/m^3)	262.3	376.4	273.6	289.0

7.2.1.5.2 Particle size distribution

Cumulative plots for particle size distribution showed the increase in size for the fine fraction post explosion residue. This was due to formation of large fused ash layers in the sample. However, for the coarse fractions the trend were different as sized fraction (63-150 µm) showed increase in size of post explosion residue for 10% cumulative volume but almost same for 50 and 90% of the cumulative volume. Coarse fraction containing least fine (<500 µm) showed reverse trend with reduction in size of the post explosion residue as shown in Figure 7.18 that was due to partial burning of coarse particles leaving small sizes after the flame propagation.

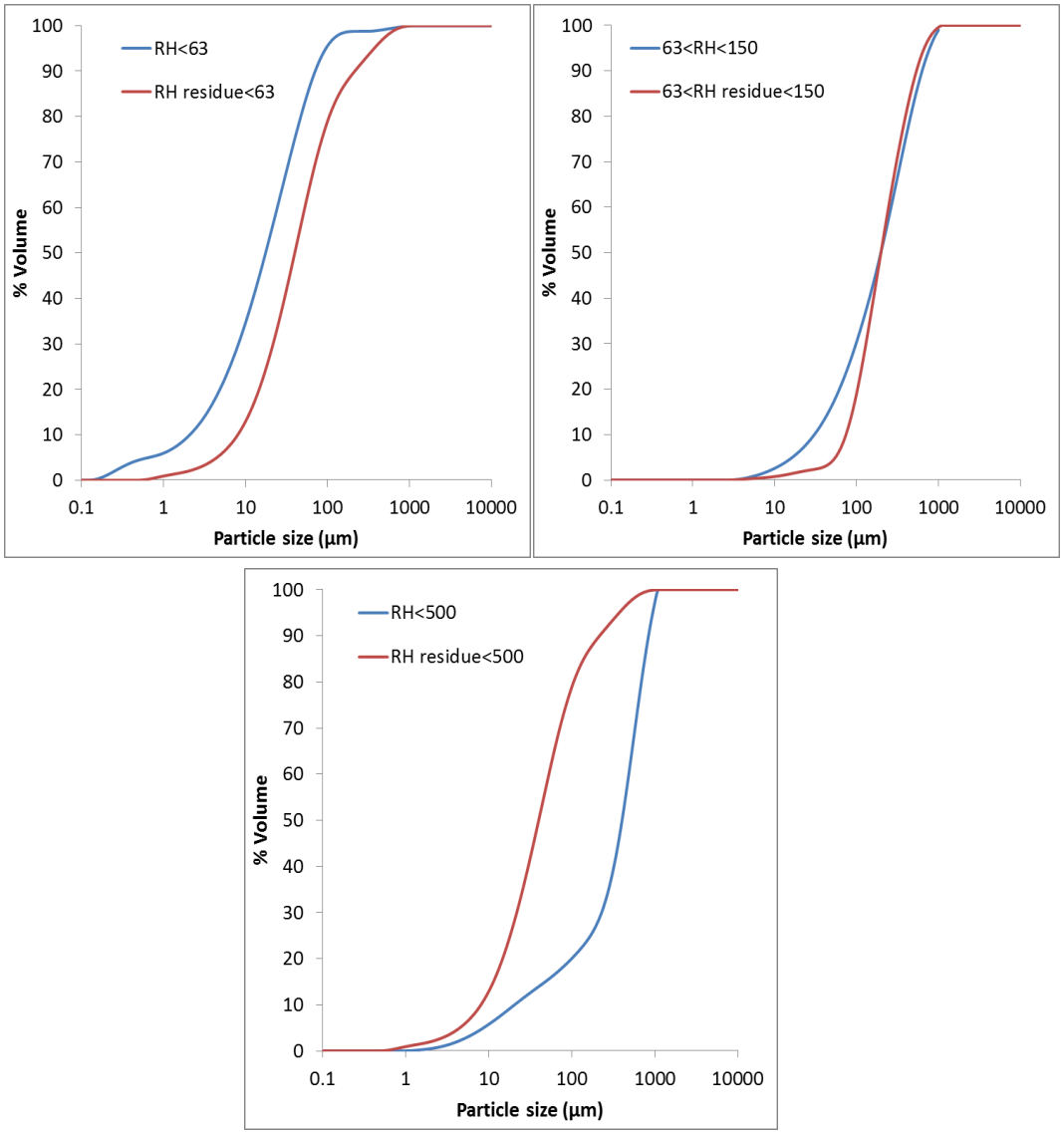

Figure 7.18: Cumulative analysis of different sized fractions of rice husk in comparison to respective post explosion residues

7.2.1.5.3 Surface morphological study

Scanning electron microscopy was performed as shown in Figure 7.19 on the rice husk and post explosion residues. Raw sample of rice husk was observed to have wide variation in particle sizes and shape. Also the particles were observed to be thin that resulted fast release of volatile. It was found that the post explosion residue for <63 µm sample had molten ash with formation of ceno-sphere indicating higher siliceous minerals in the ash contents as also found in ash characterisation. Most of the particles in <63 µm sample were burnt 100% in the propagation of flame in contrast to coarse fractions.

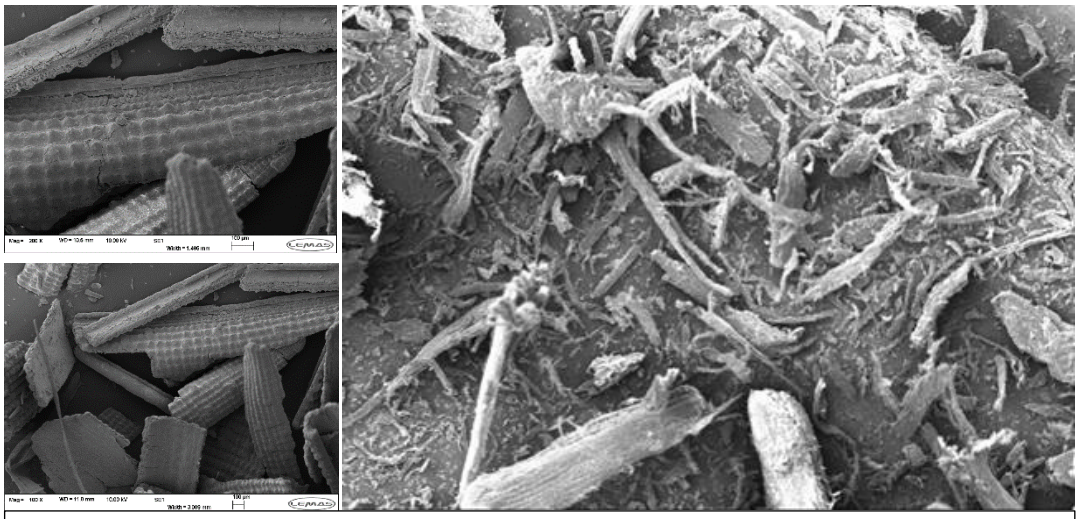

Raw Rice husk

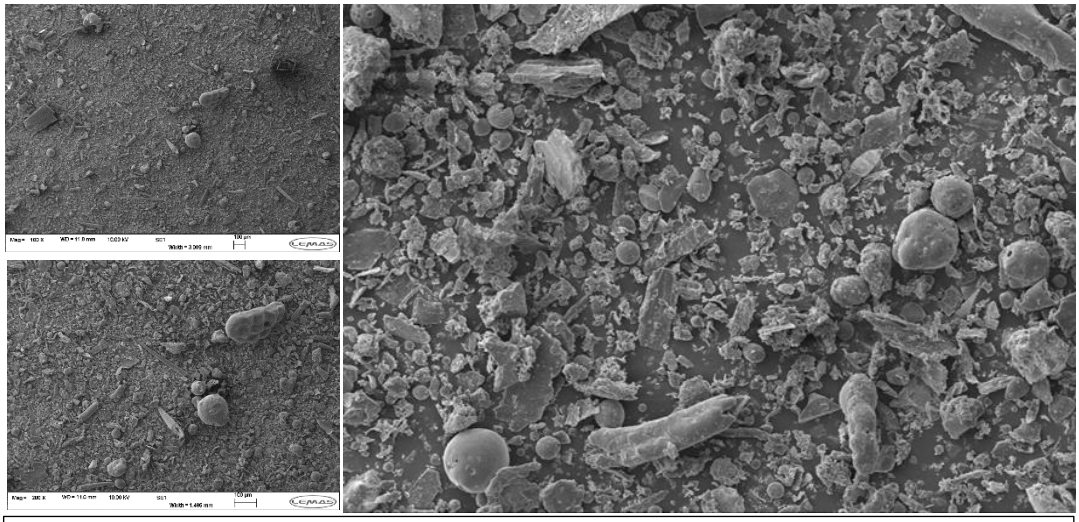

Post explosion residue

Figure 7.19: Scanning Electron Microscopy of Rice husk and its post explosion residue

7.2.1.5.4 Comparison of modified ISO 1 m³ explosion vessel and previous modified Hartmann tube results [17]

MEC of rice husk were presented against the average particle sizes for different size range fractions as shown in Figure 7.20. It was noticed that for fine fraction MEC was slightly lower in the current study of $1m^3$ measurements in comparison to modified Hartmann tube results. However for coarser fractions, the trend was opposite with more lean limits using modified $1m^3$ results. This difference was due to an error in the dispersion of dust with pre-existing spark in the modified Hartmann tube that result the burning of stratified mixture not reflecting the actual mixture feed. This issue

of modified Hartmann tube was high lighted before and an optimum ignition delay was recommended for the modified Hartmann dust explosion tube. Also the dispersion of dust in both units had different mechanism that might also have altered these results. It was still believed that modified Hartmann tube was a more suitable unit for the measurements of minimum explosible concentration.

In this work, different size range fractions of rice husk were tested using the modified ISO 1m^3 vessel with a calibrated hemispherical disperser. The objective was to study the flame propagation behaviour of fine and coarse size range fractions. The results showed that the fine fraction containing more fine actively participate 100% in the propagation of flame. However, the coarse fractions behaved differently with preferential burning of fine and partial burning of coarse particles with delay resulting less flame speed and rate of pressure rise. The pressure rise due to explosion were almost same showing almost same burning but the rate of burning for coarse fraction was slow in comparison to fine fractions. Size analysis of the raw and post explosion residues also showed different behaviour of coarse fraction with reduction in size of the post explosion residue in contrast to the fine fractions. The rice husk can be employed as a practical fuel with less milling required due to their ability to propagate the flame for even coarse size range.

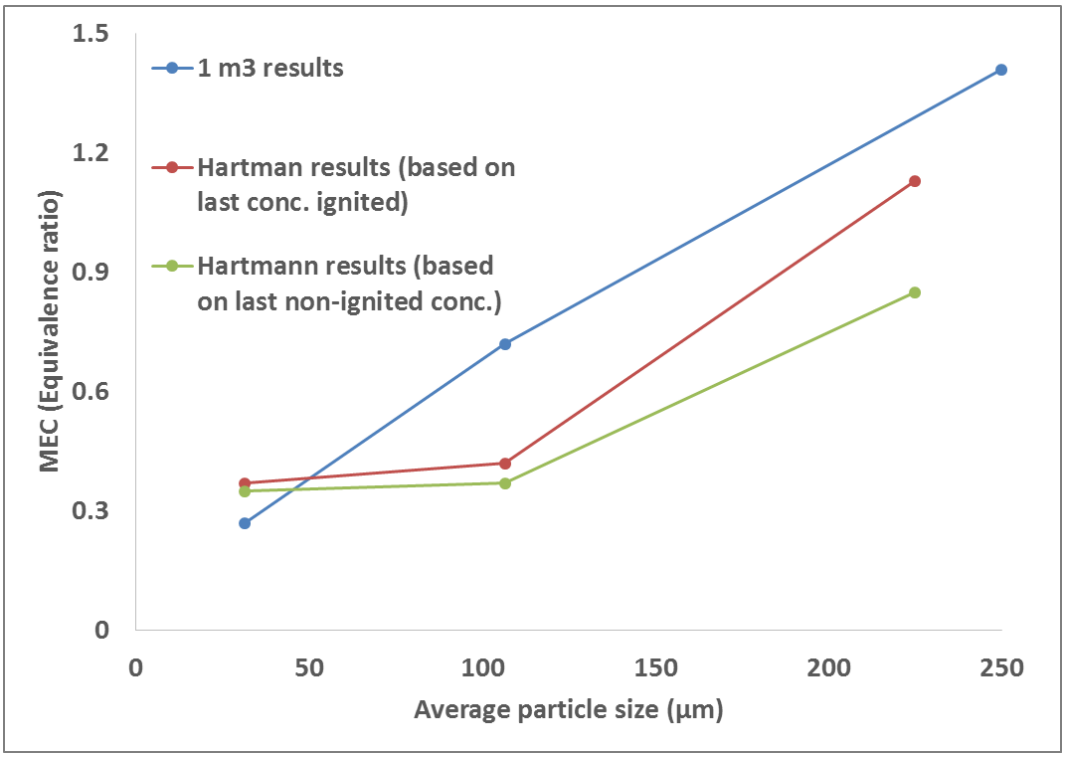

Figure 7.20: MEC comparison of different size fractions rice husk using modified 1 m^3 vessel and Hartmann tube measurements

However, the time lag in the combustion of coarse particles should be focused that might be reduced with some pre-treatment before their applications.

7.2.2 Reactivity results of different sized fractions of steam exploded pine wood

Some thermal pre-treatments such as ‘torrefaction’ and ‘steam explosion’ were applied that increased the brittleness of these biofuels leading to their easy milling. These thermal pre-treatments resulted in the shattering and altering of biomass structure causing small changes in their compositions [20, 197]. These thermally treated biomass samples are sometimes called ‘biocoal’ as they are in black color. The torrefied and steam exploded biomass were high quality fuels and pelletized for their easy transportation. The thermally treated fuel pellets mill in a similar way to coal and can be easily used to replace coal for the existing facilities. However, combustion characteristics of these treated biofuels need to be studied with particle size dependence as they don’t need to be milled as fine as coal due to high volatiles yield and their fast release making them more reactive. In this work, explosion characteristics of steam exploded pine wood were tested for different size range fractions to study the effect of particles size on the flame propagation behavior. Post explosion residues for different size range fractions were also analysed and compared with the steam exploded sample to study the flame propagation model.

7.2.2.1 Experimental materials

Raw pine wood sample after pre-treatment known as ‘Steam explosion’ were received in the form of pellets for this research work. Around 20 kg of these pellets were milled using Retch 100 ultrafine grinder to less than 500 µm and sieved for different size range fractions such as <63 µm, 63-150 µm, 150-300 µm and 300-500 µm.

Also particle size distributions of raw and steam exploded pine wood with different sieved sizes were presented in Figure 7.21. It was found that the fineness of raw pine wood was increased after steam explosion treatment. This increase in fineness of the steam exploded pine wood was due to shattering of structure and increase in the brittleness of the particles. Also the coarse particle size fraction of this steam exploded pine wood approached to the same particle size distribution as that of raw pine wood.

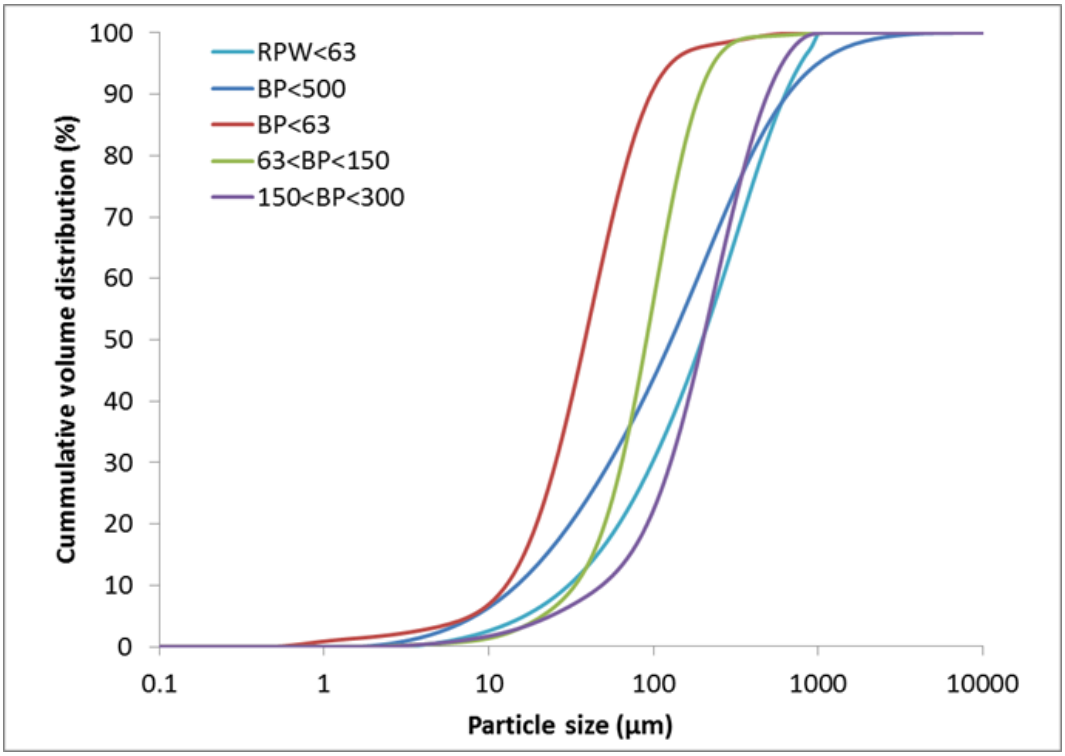

Figure 7.21: Particle size distribution of varying sized fraction steam explosion pine in comparison to its raw fine pine wood

7.2.2.2 Results and discussion

Reactivity's of different size ranged steam exploded fractions were measured in terms of rate of pressure rise, flame speed and maximum rise of pressure due to burning relative to ambient pressure. Complete concentration profile could not be obtained due to limited amounts of sized fractions.

7.2.2.2.1 Deflagration index vs. burnt equivalence ratio

Figure 7.22 showed the deflagration index (K_{st}) of different size ranged fractions of steam exploded pine wood against burnt equivalence ratio. It was found that fine particles had fast rate of propagation of flame with higher deflagration index compared to coarse sized fraction. Also it was found that the least reactive concentration was leaner than the coarse fractions. The coarse fraction with higher average particle size (300-500 µm) did not explode even for 1500 g/m^3 nominal concentration. Based on the trends of the coarse fraction, it can be assumed that coarse fraction required very rich concentration for their most reactive concentration.

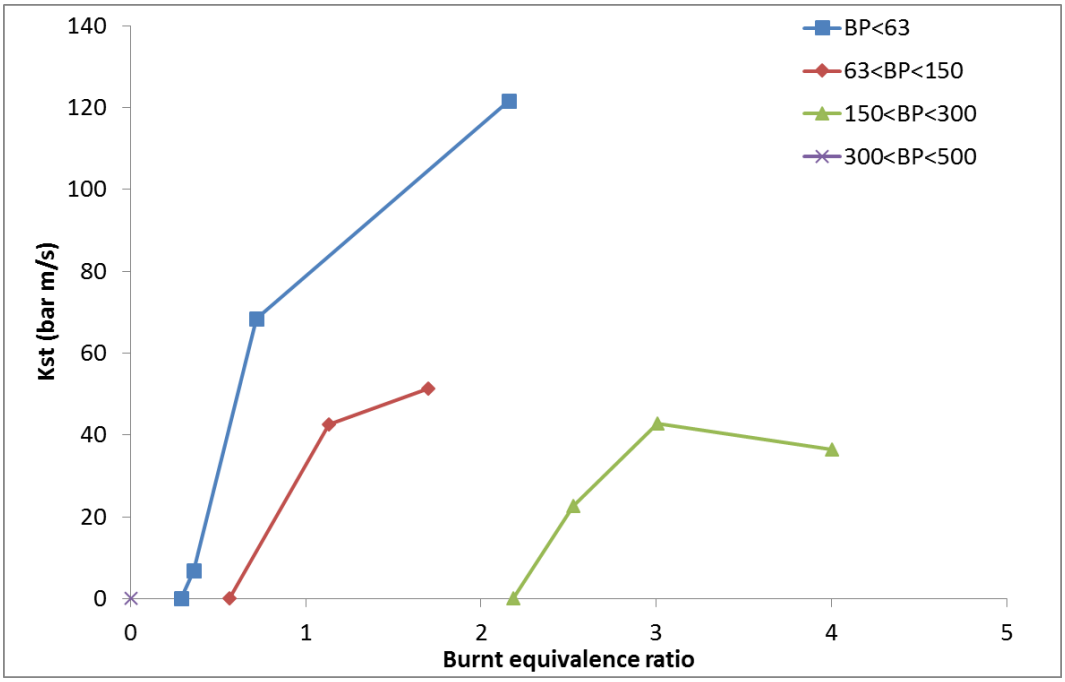

Figure 7.22: K_{st} vs. burnt equivalence ratio for different sized fractions steam exploded pine wood (BP)

Flame development and propagation was mainly due to release of volatiles that was with some delay due to thicker particle surface of the coarse particles. This enough release of volatiles for sustained development of flame needed higher amount of dust in the available time for the volatile release. Fine particles had more exposed surface area and they released higher volatiles yield efficiently resulting higher rate of pressure rise. Figure 7.22 showed the peak deflagration indices for the tested concentrations of these limited fractions to be in the range of 43-122 bar m/s with the higher value for the fine fraction. Very coarse fraction of size range 300-500 µm failed to ignite due to limited release of volatiles with existing concentration.

7.2.2.2.2 Peak pressure relative to atmospheric pressure vs. burnt equivalence ratio

Ratio of maximum pressure due to instantaneous burning relative to ambient pressure were plotted against burnt equivalence ratio for different sized fractions of steam exploded pine wood as shown in Figure 7.23. It was noticed that fine fractions were burning more with higher rise of pressure as compared to coarse fraction (150-300 µm) that was levelling at lower peak pressure ratio of around 7 bar. The finer fraction (< 63 µm) showed a peak pressure ratio of around 8.6 bar with a further rise for higher concentration that could not be tested due to limited amount of dust.

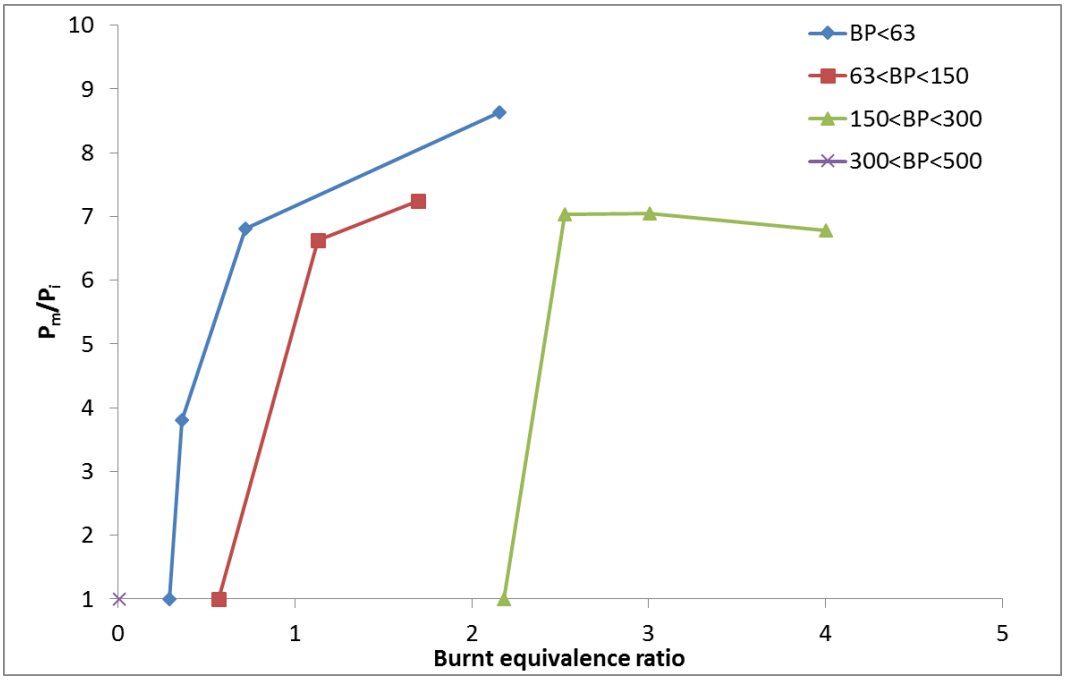

Figure 7.23: P_m/P_i vs. burnt equivalence ratio for different sized fractions steam exploded pine wood (BP)

Similarly, the size fraction having moderate size 63-150 µm giving the peak pressure ratio in between fine and coarse fractions. It meant that the presence of fines facilitated the propagation of the flame with higher mass burning. Very coarse fraction of size 300-500 µm could not be converted into enough gas for the flame propagation.

7.2.2.2.3 Turbulent flame speed vs. burnt equivalence ratio

Turbulent flame speed were also plotted for these different sized fractions against burnt equivalence ratio as shown in Figure 7.24. Flame speeds showed the same trend as deflagration index (K_{st}) for different burnt concentrations. Peaks flame speeds were measured to be in the range of 1.4-5.4 m/s with higher flame speed for the finer fraction. A greater proportion of fines resulted in the quick release of volatiles with their maximum rate of combustion. Increasing the sieved size showed a declined slope due to delay in the evolution of volatiles from the coarse particles for flame propagation. Also, less mass burning of coarse fractions showed a reduced flame speed until a very coarse sized fraction (300-500 µm) that could not support the propagation of flame.

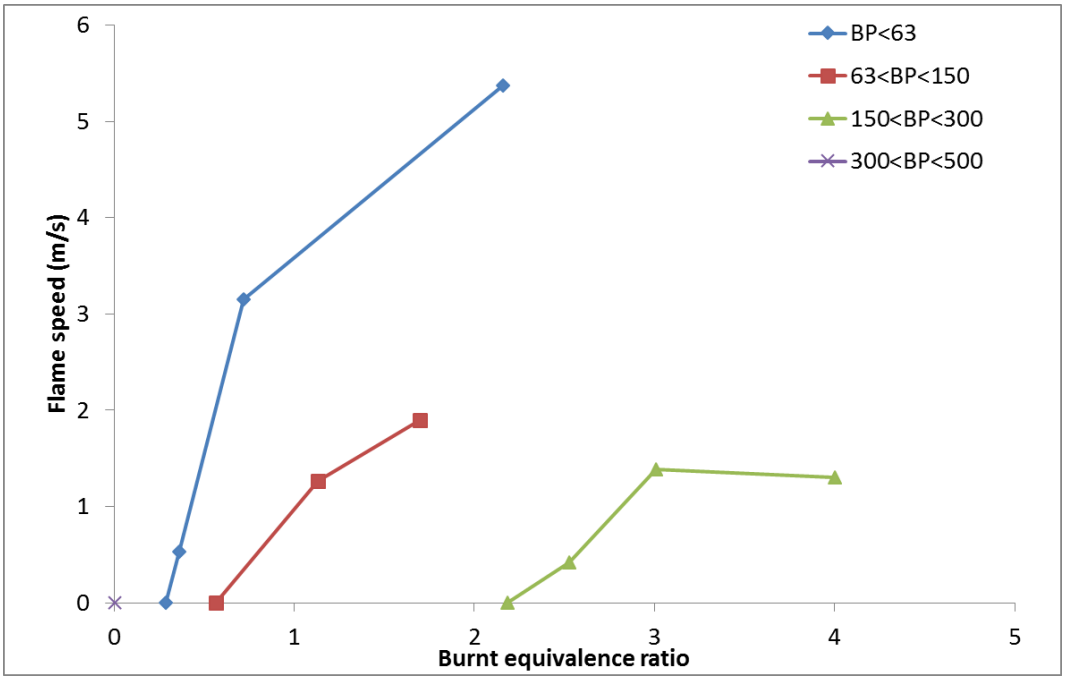

Figure 7.24: Turbulent flame speed vs. burnt equivalence ratio for different sized fractions steam exploded pine wood (BP)

7.2.2.3 Analysis of rice husk post explosion residues

7.2.2.3.1 Ultimate and proximate analysis of post explosion residues

Post explosion residues of the most reactive concentration from different sized range fractions were analysed and compared with raw steam exploded pine wood as shown in table 7.6. It was found that the residue samples had almost same elemental and TGA analysis with only the significant difference of ash and volatile contents. This addition of ash in the residue was due to burnt mass proportion forming combustion products of carbon dioxide and water. Carbon dioxide and some of the water vapours were discharged in the purging process leaving ash behind enriching the unburnt mass left in the vessel. It was found that more ash was found in the post explosion residue of finer fraction due to more mass burning whereas comparatively less ash was measured in the coarser fraction indicating less burning of coarse particles. The reduction of volatiles was due to relative enhancement of ash proportion in the residue samples as the highest increase of ash in the finer fraction resulted the maximum reduction of volatiles.

Table 7.6: Chemical characterization of the post explosion residues of different sized fractions in comparison to raw steam exploded pine

Biomass	Steam exploded pine wood (BP)	Post explosion residues of steam exploded pine wood		
		BP<63µm	BP(63-150µm)	BP(150-300µm)
% C (dry)	51.3	50.6	49.7	49.6
% H (dry)	5.6	5.5	5.6	5.7
% N (dry)	0.4	0.4	0.3	0.4
% S (dry)	0.0	0.0	0.0	0.0
% O (dry)	39.9	34.8	37.0	37.9
% H2O	4.4	4.8	4.7	5.8
% VM (dry)	76.4	67.5	71.2	71.9
% VM (daf.)	78.6	73.9	76.9	76.8
% FC (dry)	20.8	23.8	21.4	21.6
% FC (daf.)	21.4	26.1	23.1	23.2
% Ash	2.7	8.2	7.02	6.1
CV (MJ/kg)	19.5	19.6	19.3	19.3
Stoich. A/F (g/g)	6.3	6.8	6.5	6.4
Actual stoich. conc. (g/m^3)	205	202.8	209.1	212.8

7.2.2.3.2 Surface morphological study

Scanning electron microscope imaging were also compared for the finer samples of the raw pine wood with its steam exploded and the post explosion residue sample as shown in Figure 7.25. It was found that there were enrichment of fines in the steam exploded pine wood that actively participated in the flame propagation. The residue sample showed fused and molten ash with some of the mass unburnt that was exactly same as that of the original material. Also the elemental and TGA analysis revealed the same unburnt mass as the original. For the coarse fraction, there were formation of holes observed on the surface indicating the role of volatiles in

the flame propagation. However, the fine fractions contributed fully leaving inert behind for the most reactive concentration.

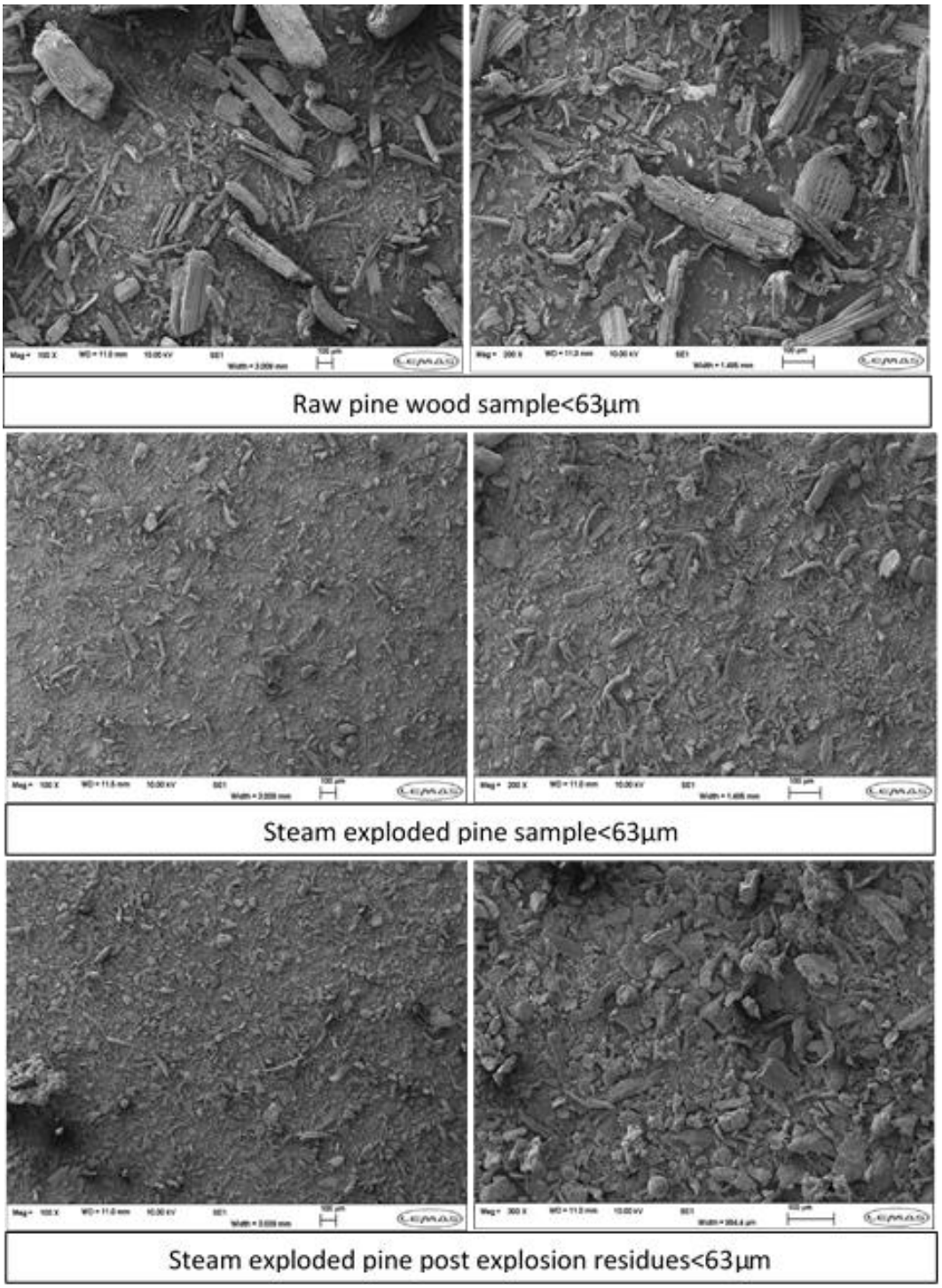

Figure 7.25: Scanning Electron Microscopy of raw pine, steam exploded pine and post explosion residue of steam exploded pine wood

7.2.2.4 Comparison of modified ISO 1 m^3 vessel and previous modified Hartmann tube results

MEC were close to each other based on modified Hartmann tube and 1 m^3 vessel measurements. Also it was noticed that the rate of pressure rise in 1 m^3 vessel was of the order of 6 as compared to Hartmann measurements. There was quick quenching in the Hartmann tube due to small diameter tube giving less rate of pressure rise compared to 1 m^3 vessel. Also it reflected that the most reactive concentration was at an equivalence ratio of around 1.8 based on both experimental techniques for extrapolated prediction of 1 m^3 vessel results.

Effect of average particle size on the minimum explosible concentration of the selected steam exploded pine wood on the modified 1 m^3 vessel was compared with other biomass samples based on previous modified Hartmann tube measurements as shown in Figure 7.27. It was found that steam exploded pine wood showed the leaner concentration (equivalence ratio of ~0.2)than the other raw biomass samples for the finer fraction of average particle of 31.5 µm. However with increasing particle size, the sensitivity of explosion reduced drastically than the raw biomass samples. Previous Hartmann results were based on pre-existing spark overestimating the lean limits and needs improvements in its methodology as explained in other work [193]. Detailed assessment of these renewable fuel based on explosibility characteristics were carried out before their employment for safe working environment.

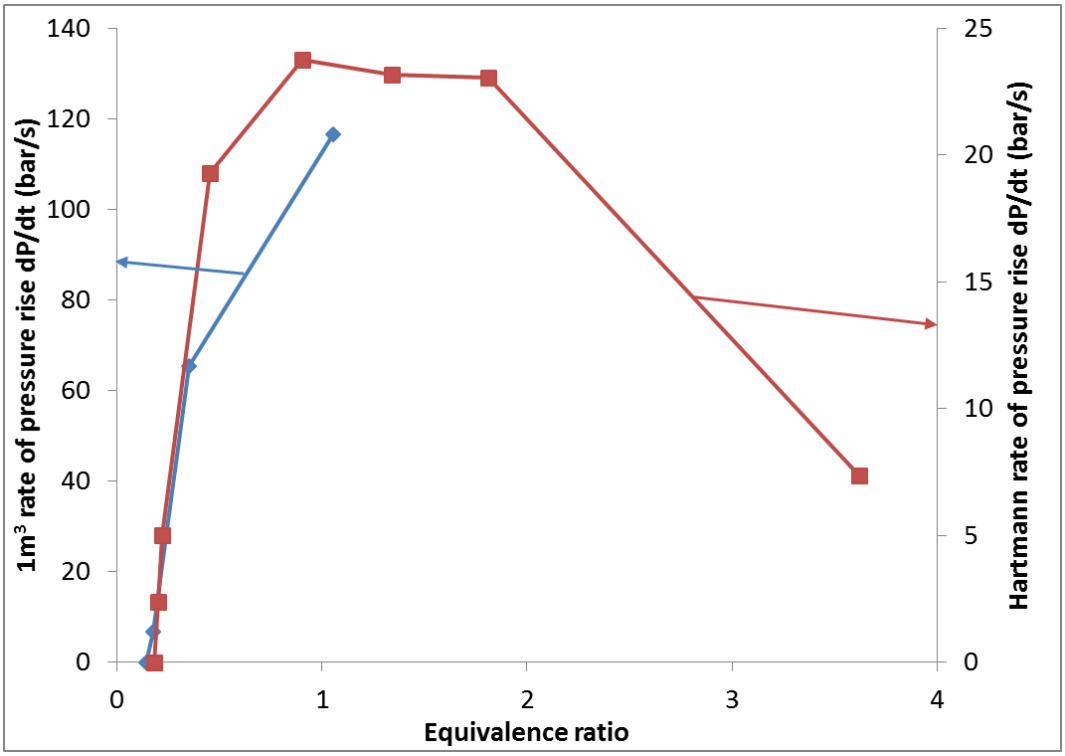

Figure 7.26: Comparison of rate of pressure rise from 1 m³ vessel and modified Hartmann tube measurements against equivalence ratio for fine fraction of steam exploded wood< 63 µm [169]

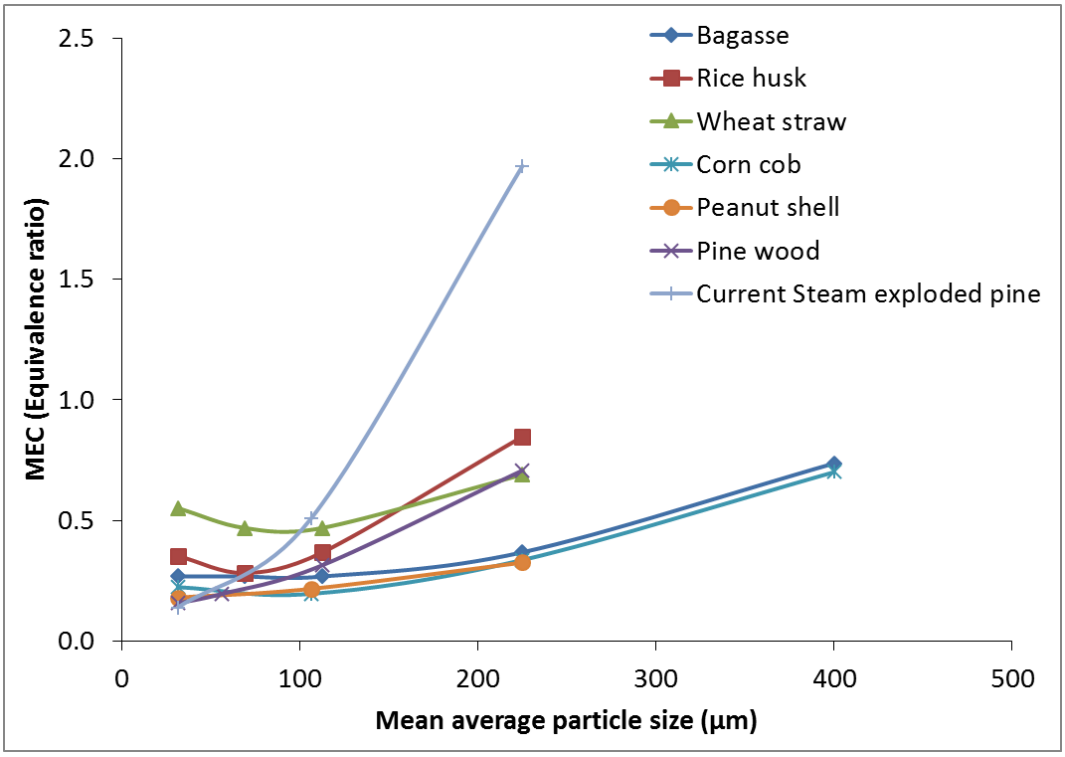

Figure 7.27: Effect of average particle size of selected biomass samples on the minimum explosible concentration (MEC) [17]

7.2.2.5 Conclusions

In this work, different size range fractions of steam exploded pine wood were tested to investigate the flame propagation behaviour and the effect of particle size. It was revealed that steam explosion treatment enhanced the proportions of fines compared to raw pine wood with more fibrous and elongated particles. Explosiblity results concluded that the finer fraction with more fines participated actively with greater mass burning and higher flame speed. Increasing the size of the fraction reduced the intensity of combustion with less flame speed and deflagration indices. Very coarse fraction containing no fines failed to propagate the flame due to delay in the burning of these coarse particles. Also the post explosion residues showed the same analysis as that of original steam exploded pine wood with the addition of ash due to burnt particles affecting the relative proportions of volatiles reduction. This work confirmed the severity of reaction with reduction in sizes and vice versa that need to be accessed fully before their adoption as fuel for the power generation plants.

7.3 Explosibility characteristics of coarse SPF wood mixture in comparison to its torrefied sample<1000µm

The raw biomass sample was a proportionate mixture of three woody biomass: Spruce (S), Pine (P) and Fir (F) that is referred to as the SPF sample with R referring to the raw sample and T to the torrefied sample. The torrefied biomass was manufactured in a pilot plant (Renewable fuel technology) with a 0.5 tonne per day production capacity of torrefied pulverised biomass, which was tested in the present work. This material was normally passed to a pellitizer process and sold into the thermal heating market as ‘biocoal’.

The torrefaction process that was used in this work [198] heats biomass by direct contact with hollow hot flat surfaces (trays), which at steady state operated at 303^{o}C on the top surface and 290^{o}C on the bottom surface. The biomass was injected cold into the torrefier and heat transferred from the trays by conduction, the biomass particles would be at a lower temperature than the trays for most of the residence time, but would reach equilibrium with the tray temperature before the torrefier exit. On the top side of the trays biomass is moved through the reactor by paddles, that are attached to a rotating shaft and this process gives uniform contact of the particles with the hot surface and a uniform torrefaction of each particle. The mean residence time of biomass particles inside the reactor was 7 minutes, which is typical

of other torrefaction processes [199]. Biomass moving through the reactor is traveling down the reactor from one tray to another, being slowly torrefied until it reaches the output chute. A gaseous by-product, torgas, is formed during the torrefaction process, which surrounds the biomass and prevents oxidation and this prevents explosion and self-ignition hazards. The torgas is removed from the torrefier, burnt with air and the hot exhaust gases flow through the hollow plates to deliver the heat required by the torrefaction process. Heat is recovered from the plate outlet gases in a counter current heat exchanger which preheats the combustion air and this recovers the latent heat of the water from the torgas burner. The torrefaction process requires no external energy input, apart from during start up.

The raw and torrefied biomass samples were of coarse particle size distribution of < 3 mm that were sieved to <1 mm for this research work.

7.3.1 Explosibility results

7.3.1.1 Deflagration index, K_{st} and P_m/P_i against burnt equivalence ratio

The K_{st} as a function of $Ø_{burnt}$ are shown in Figure 7.28 for SPFR and SPFT. The peak K_{st} was 24 and 36 bar m/s for raw and torrefied wood mixture respectively. Although the peak K_{st} occurred at a similar $Ø_{burnt}$ of 3.0 the torrefied SPF had higher K_{st} at all Ø and was much more reactive for $<Ø_{burnt}$ of 2.5. No lean mixture flame propagation for either raw or torrefied biomass were found. Thus biomass with coarse particle size, whether raw or torrefied, will only burn if the overall Ø of the mixture is rich and the highest reactivity, K_{st}, is for rich mixtures. This does not occur for gaseous mixtures and is unique to coarse dusts, particularly biomass dusts.

A mechanism for coarse biomass powders to burn in a propagating flame is proposed to explain these results, which is an extension of that used to explain why about half of the intial dust does not burn in the explosion [21, 22, 194]. The action of the wind, induced by the expanding spherical flame, on particles ahead of the flame with a variable size distribution is to blow the smallest particles close to the gas velocity with the larger particles lagging due to drag effects. The flame front is driven by the finer particles and the larger particles then lag behind and are heated to ignition by the hot burnt gases from the flame front. The mixture has to be very rich for the finer particles ahead of the flame to burn with only <20% of the total mass of particles in the size fraction that will burn easily. A flammable mixture of 20%

fine particles with $Ø_{MEC}$ of 0.4 needs $Ø_{burnt}$ of at least 2.0 for the overall mixture to burn. With this model the larger particles are gasified in the rich mixture of the hot burnt gases from the flame burning in the finer fraction. This releases CO [18] and H_2 which has insufficient oxygen to burn, but the volume release keeps the explosion pressure high for rich mixtures.

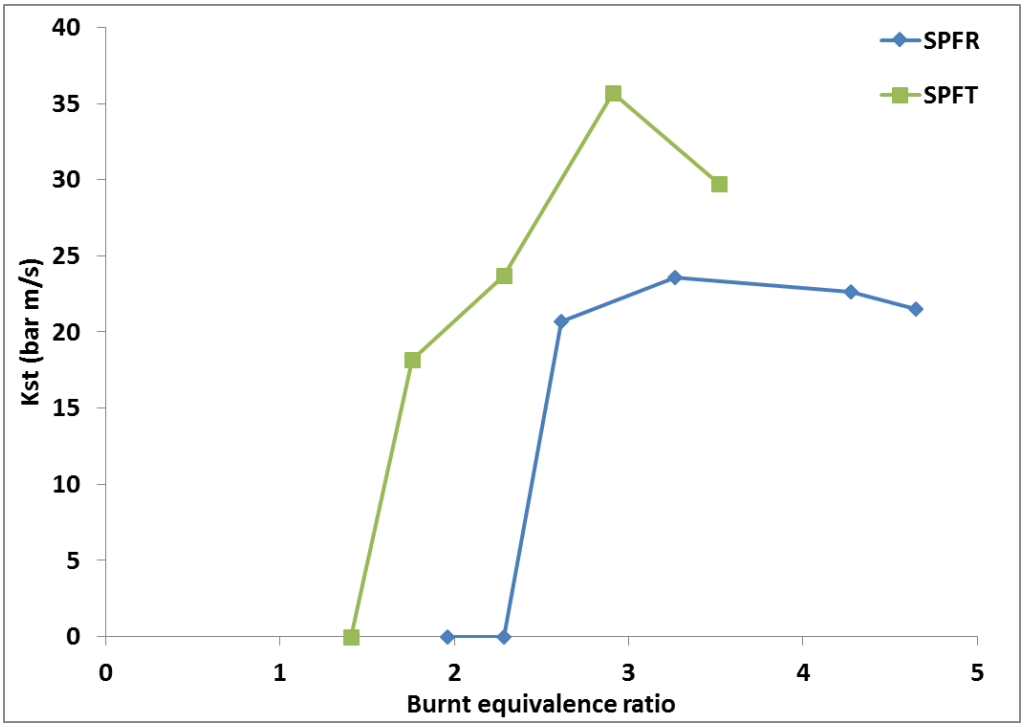

Figure 7.28: K_{st} v. $Ø_{burnt}$ for raw SPF in comparison with torrefied SPF

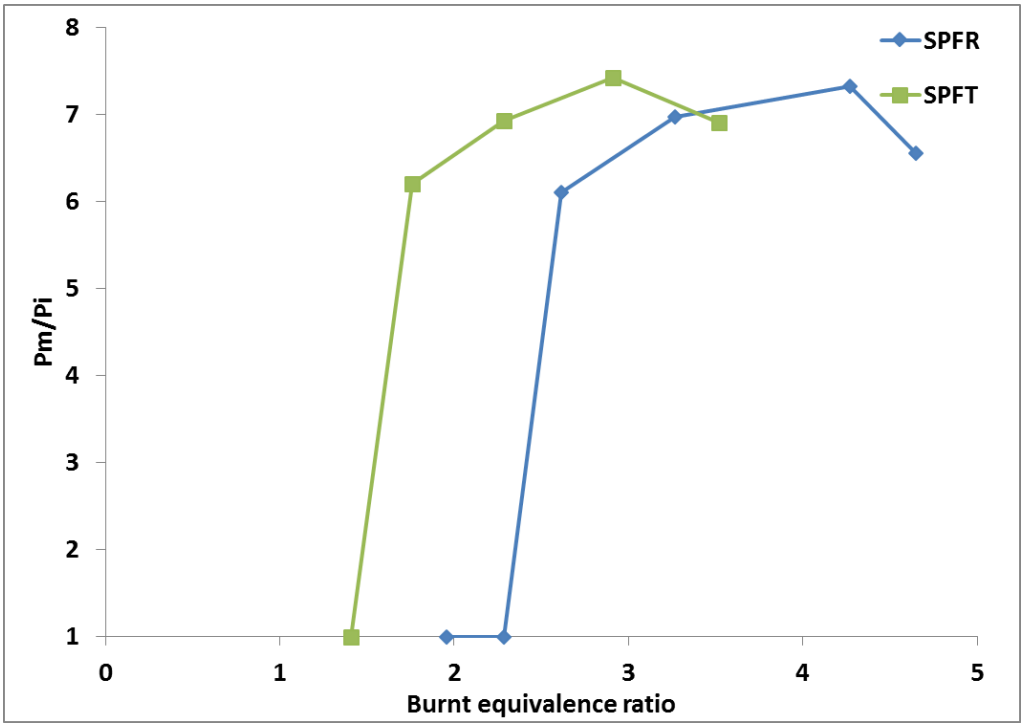

Figure 7.29 P_m/P_i v. $Ø_{burnt}$ for raw SPF in comparison with torrefied SPF

The maximum explosion pressure, P_m, to the intial pressure, P_i, is shown in Figure 7.29 as a function of $Ø_{burnt}$. This shows that at the maximum K_{st} Ø the peak pressure ratio was 7.4 for SPFT and 7.3 for SPFR. These are large pressure rises indicating that all the coarse mixture had burnt and also shows that despite of the low reactivity of these mixtures, as shown by their low K_{st}, the overpressure was high and would destroy any process plant enclosure used in the processing of this material. These pressure rises were lower than for fine particles of biomass, where for similar biomass composition P_m/P_i was about 8.5 [18, 22, 200, 201].

7.3.1.2 Flame speed and burning velocity measurements

The measured turbulent spherical flame speeds, S_T, for SPFR and SPFT are shown in Figure 7.30 as a function of $Ø_{burnt}$. These measurements of the mixture reactivity are very similar in their dependance on $Ø_{burnt}$ as for the K_{st} results in Figure 7.28. However, the two peak S_T for the raw and torrefied biomass were very similar at close to 1.0 m/s compared with a significant difference in K_{st} in Figure 7.28. This difference may be due to S_T being measured in the constant pressure period of the explosion and K_{st} is measured just before the peak pressure. Figure 7.30 also shows that for rich mixtures the flame speed remains high as the fuel concentration increases. This is considered to be explained by the model of the coarse biomass flame front with the flame driven by the finer particles in the mixture and the cosrse particles gasified behind the flame front. As more fuel is added, the Ø of the fine fraction flame increases and the temperature of this initial combustion increases this then results in more fast gasification of the coarse fraction and the gas volume release in the gasification reactions increases which causes the pressure to remain high even though for gases the pressure would fall for richer mixtures.

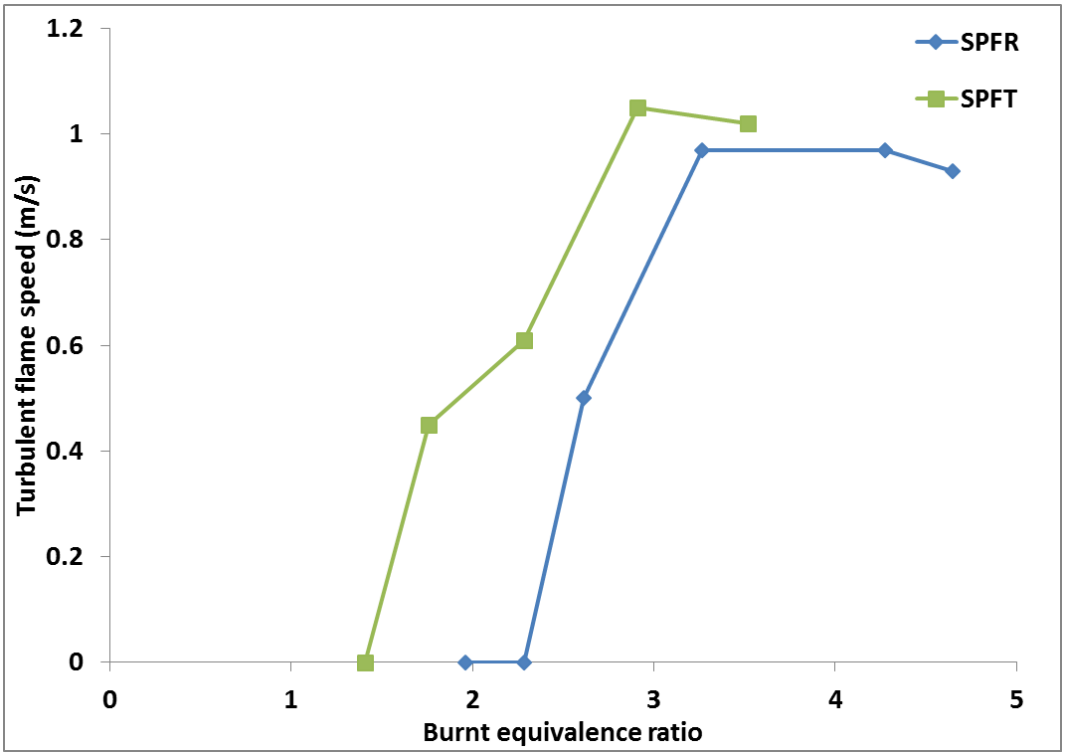

Figure 7.30 Turbulent flame speed vs. $Ø_{burnt}$ for raw SPF in comparison with torrefied SPF

7.3.1.3 Minimum explosible concentration, MEC

The MEC of the coarse SPF raw and torrified biomasses were determined from Figs. 7.28-7.30 to be 2.3 and 1.4 $Ø_{burnt}$ respectively. These lean flammability limits were much higher than other biomass for finer sieved fractions, where mixtures as lean as 0.2Ø were flammable [19, 87, 169, 202]. The explanation for the richer MEC with coarse biomass is that given above. The flame propagated in the fine fractions blown ahead of the flame by the explosion induced wind and the coarse particle drag leads to these particles burning behind the initial fine particle flame front and being gasified in the burnt gases. For the raw SPF particles Table 7.7 shows that the fine fraction is 11% of the total mass and the overall MEC is then 1.8Ø, which is close to the measured MEC. For the torrefied coarse SPF biomass the fine fraction is 15% and if the fine only MEC is 0.2Ø then the overall MEC is 1.3Ø, which is in good agreement with the measured MEC.

7.3.2 Analysis of post explosion residues

SEM images of the raw and torrefied biomass as shown in Figure 7.31 and 7.32 were compared with their respective post explosion residue of the most reactive concentration. Both fuels had a wide range of particle size and shapes. Post explosion residues revealed volatile release holes in the larger

particles, which increased the porosity of the particles. The SEM analysis of the residues showed the fused layer of ash from the burnt particles, but the particle size was very similar to the original raw or torrefied biomass.The particle size distributions are summarised in Table 7.7 and this shows that torrefaction reduced the particle size by 20% on a d_{10} basis and 18% on an surface mean diameter (SMD) and increased the proportion of fines (<100µm). The analysis of the residue after the explosion showed that for the torrefied material it was almost identical to the original dust in terms of the size distribution in Table 7.7 and the composition in Table 7.8. The increase in the ash in the residue was due to the ash of the burnt biomass as well as the unburnt biomass. For raw biomass there was a decrease in the particle size in the residue. The origin of this unburnt biomass was due to the action of the explosion induced wind ahead of the flame front in blowing particles away from the flame and eventually onto the vessel wall, where they fell onto the floor of the vessel at the end of the explosion. While on the wall they acted as an insulating layer that reduced the rate of vessel cooling, as shown by the reduction in the rate of pressure loss [194].

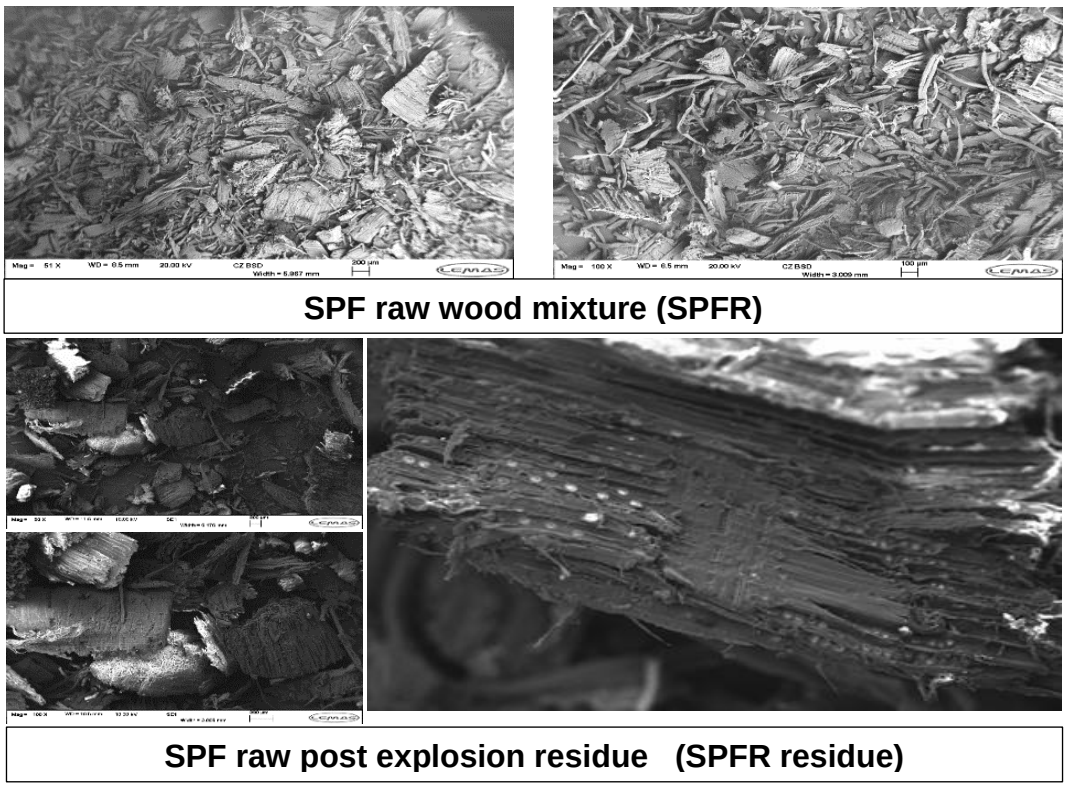

Figure 7.31: SEM images of SPFR and its post explosion residue

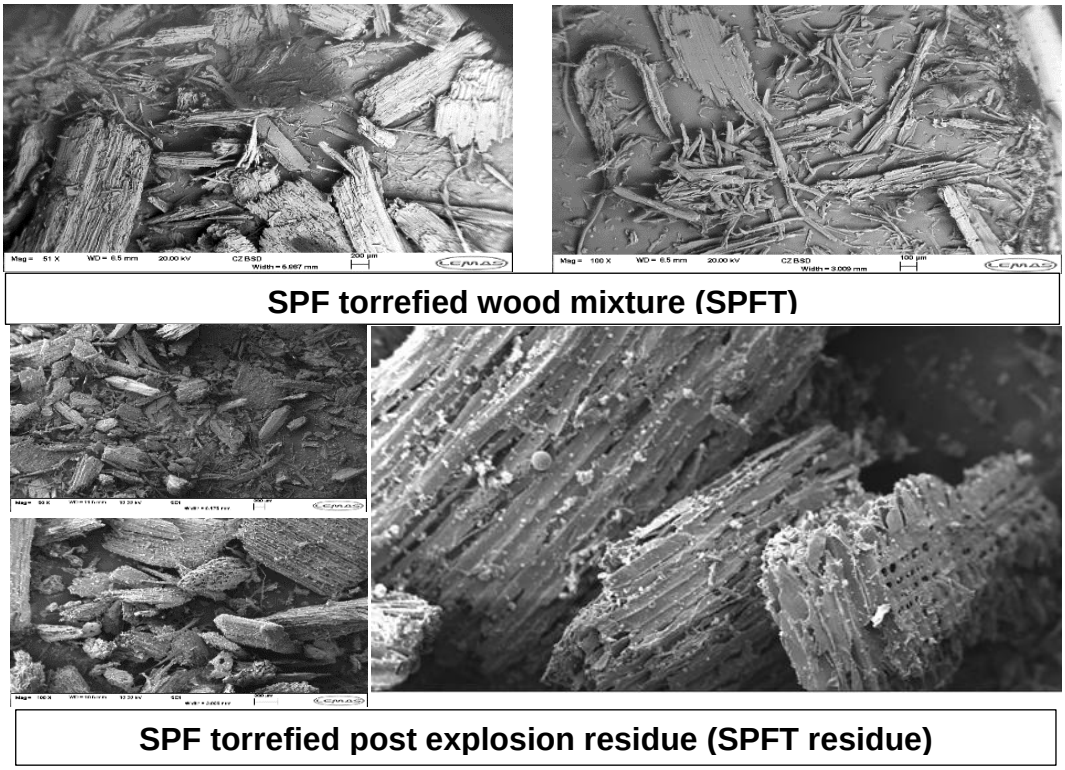

Figure 7.32: SEM images of SPFT and its post explosion residue

Table 7.7: Comparison of particle size distribution of SPF raw and torrefied wood mixture in comparison to their post explosion residues with sieve size<500

Biomass	d_{10}	d_{50}	d_{90}	d_{smd} or $d_{3,2}$	$d_{4,3}$	Fines particles <100µm
	µm					% share
SPFR	91	451	866	184	466	15
SPFR residue	69	288	747	124	351	17
SPFT	73	347	785	151	389	14
SPFT residue	78	343	781	164	388	14

Table 7.8: Properties of the raw and torrefied SPF samples and the explosion residues

Biomass	*%C*	*%H*	*%N*	*%O*	*%VM*	*%FC*	*%H_2O*	*%Ash*	*CV MJ/kg*	*CV MJ/kg*	*Stoich. A/F g/g*	*Stoich. g/m³*
	Dry basis				Dry basis		As rec.		daf.	actual	daf	actual
SPFR	49.0	6.8	1.1	40.3	79.6	17.6	7.8	2.6	19.9	17.8	6.4	187
SPFR residue	49.2	6.1	1.1	39.8	77.5	18.8	6.8	3.5	19.8	17.8	6.3	212
SPFT	52.8	6.7	1.1	40.3	77.7	18.8	4	3.2	21.7	20.1	7.05	183
SPFT residue	53.2	5.6	1.3	31.7	68.0	23.7	4.2	7.8	21.3	18.7	7.3	187

7.4 Overall analysis of pulverised biomass flame propagation

7.4.1 Explosion pressure rise for different size range fractions for same nominal concentration

For different size fractions of same dust ‘steam exploded wood (BP)’, it was found that fine fraction with particle size<63µm propagated the flame quickly with sharp rise of explosion pressure. For coarse fraction of size 63-150µm with same nominal concentration of 750g/m^3, the rise of explosion pressure was slower compared to fine fraction. Fine particles with the ability to turn to volatiles due to more surface area resulted almost homogenous combustion of their volatile. For coarse size fraction, the time lag of conversion of big particles to gas resulted the slow build-up of pressure as shown in Figure 7.33. As a result, the mass burning of the coarse size fractions was low generating less explosion pressure.

The steep slope of the explosion pressure for fine fraction ends up at some specific peak explosion pressure after that it quenches and pressure decay starts. For coarse size fractions, the peak explosion pressure was observed to stay constant for small time interval before the quenching starts. This was due to the gasification of the coarse particles that continues; adding the pressure in the net explosion pressure.

As shown in Figure 7.34, the pressure time histories of three different biomass dusts for same nominal concentration but wide variation of their

average particle sizes were plotted. It was noticed that with increase in particle size from <63 to <1000µm, the build-up of explosion pressure for very coarse size fraction can be separated into two different sections. For coarse fraction of size <1000µm, the explosion pressure progressed very slowly with only 7.5% rise of pressure. In this time interval, the rise of pressure for peanut shell<500µm was almost 50% whereas for very fine fraction of bagasse<63µm, the explosion pressure reached to peak in half of this time interval. This stage mainly involved heating of coarse particles to generate volatile and a very small rise of pressure for <1000µm might be due to the gasification of coarse particles. In the second stage for <1000µm sample, the flame propagated through the gaseous mixture with 92.5% rise of pressure. Due to slow burning of coarse particles, the overall actual burnt equivalence ratio was smaller with less build-up of pressure compared to fine size fractions as shown in Figure 7.34.

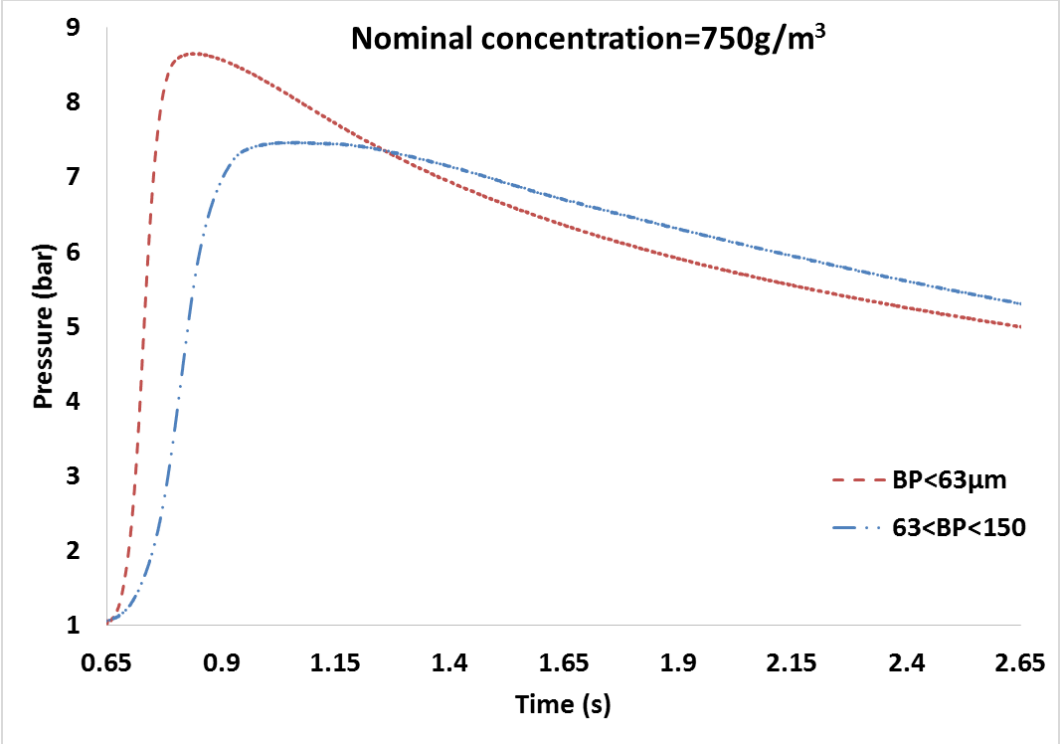

Figure 7.33: Comparison of explosion pressure of fine and coarse size fraction of steam exploded wood for same nominal concentration

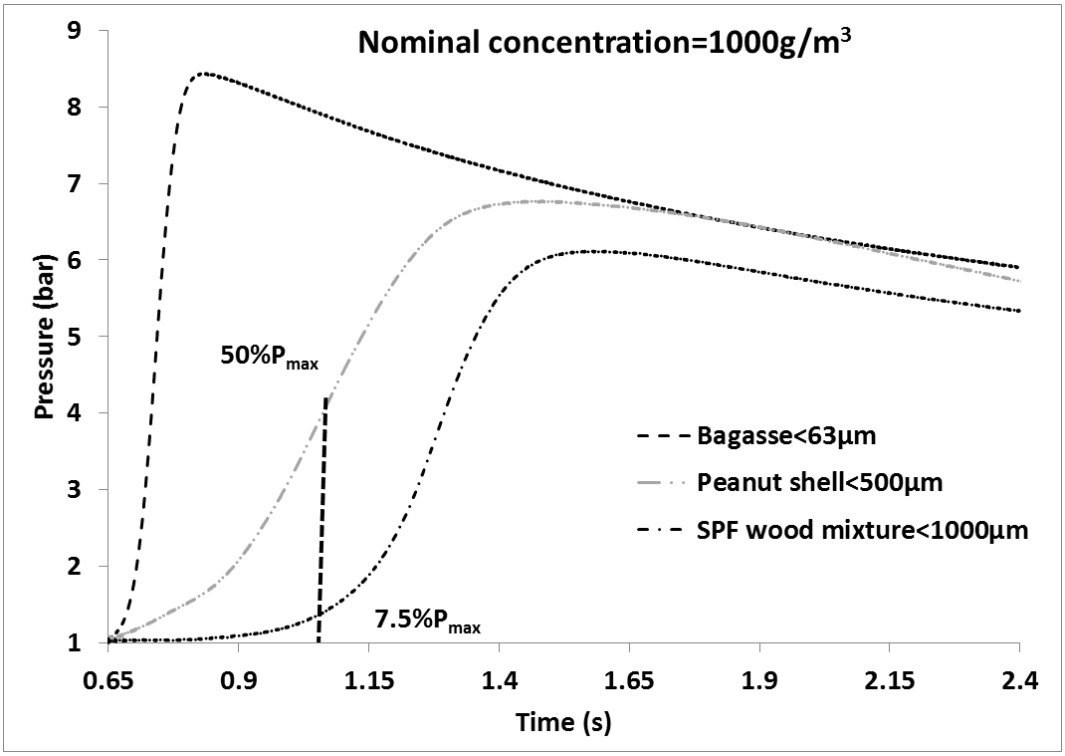

Figure 7.34: Pressure history plots for varying size fractions of biomass dusts

7.4.2 Dust layer thickness and rate of pressure decay

The explosion pressure increases with the burning until the flame quenches after touching with the vessel wall. Increase in the dust concentration raises the explosion pressure and higher flame temperature. It was noticed that after achieving most reactive concentration, further increase in concentration results in the slight reduction in the explosion pressure with almost constant explosion pressure for equivalence ratio depending on particle size distribution as shown in Figure 7.35. For higher concentration, the flame temperature almost remains constant with slight reduction of explosion pressure. As explained previously, the unburnt dust mass was pushed against wall during flame propagation. This mass forms a thin or thick layer with the wall and acts as insulating medium. This insulting layer acting as a barrier between the flame and the vessel wall affects the pressure loss. For the most reactive concentration, a further increase in concentration with constant adiabatic temperature resulted in a dropping of the pressure decay rate due to the direct effect of insulating layer thickness. The fine size fraction showed a sharp drop in the rate of pressure loss after the most reactive concentration, whereas the coarse sized particles continue to gasify with the drop of rate of pressure loss for very rich burnt equivalence ratio.

An attempt was made to calculate the dust layer thickness considering a uniform flame thickness for the unburnt mass. It was found that an increase in concentration resulted in the thicker insulating dust layer for different biomass dust as shown in Figure 7.36. Also, it can be observed that MEC is a strong function of particle size distribution with higher MEC for coarse size fractions. For very coarse size fractions (<500 or/and <1000µm), the MEC were higher than their stoichiometric concentration. It meant that for very coarse particles, more mass was required (higher than stoichiometric) to generate flammable mixture. This was due to the very slow evolution of volatiles from coarse particles as had already been explained above.

As presented in Figure 7.35 and 7.36, the increasing particle size shifts the most reactive concentration toward rich flammability limit. Also the flammability hazards associated with coarse particles were weak compared to fine particles but existed in contrast to coal samples. Mixing of the fine particles with the coarse particles act as a catalyst in speeding up the overall flame propagation. A higher proportion of fines in the sample increased the fire or/and explosion hazards with peak explosibility characteristics.

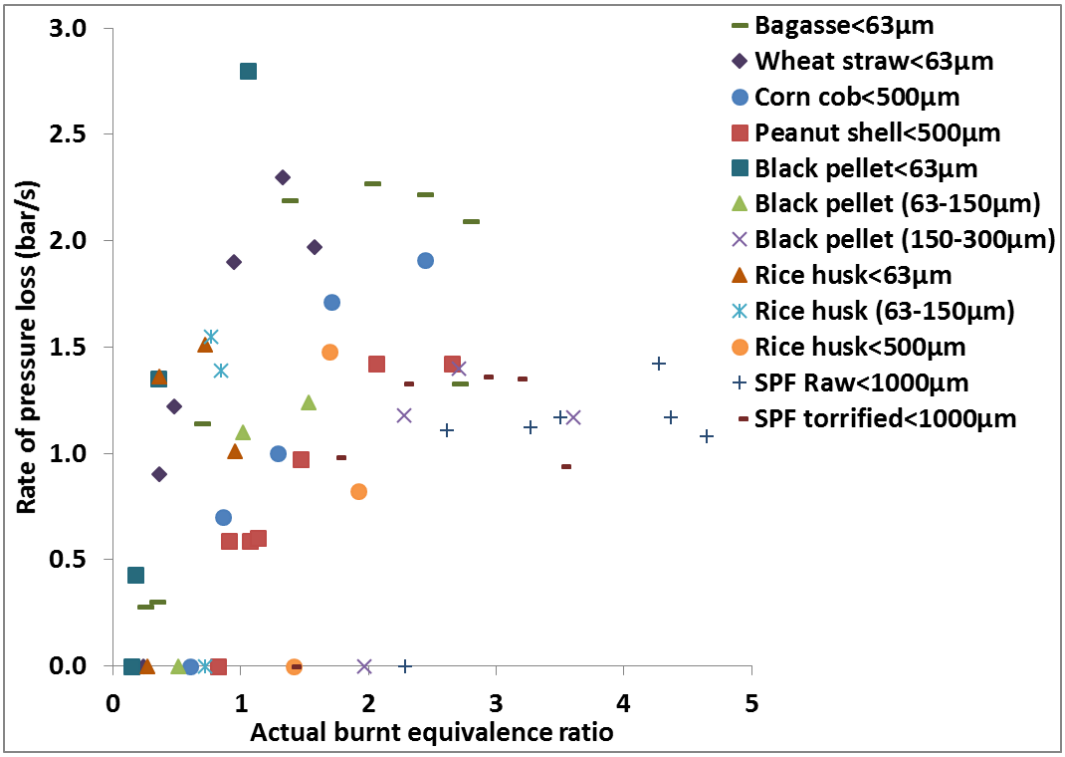

Figure 7.35: Rate of Pressure loss for different sized fractions biomass vs. burnt equivalence ratio

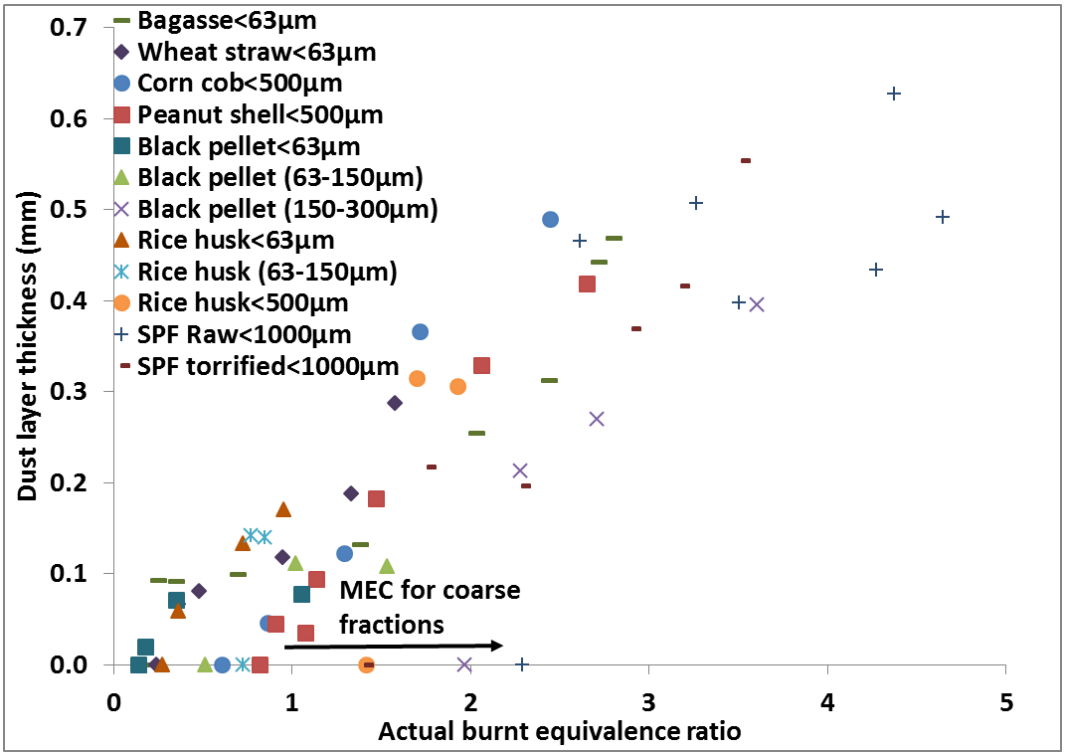

Figure 7.36: Actual burnt equivalence ratio vs. dust layer thickness for different biomass dusts

In Figure 7.37 and 7.38, peak turbulent flame speed and peak laminar burning velocity of selected biomass samples in combination with other biomasses were plotted against d_{50} obtained from Laser diffraction technique. There is a significant variation in the peak turbulent flame speed and laminar burning velocity for the different biomass compositions and the cause of this is thought to be related to the differences in particle size.

Most of the samples were sieved to <63µm size, but based on actual d_{50}, they were dispersed for a wide range of particle size. Biomass nut shell with regular and very fine particles were found to give the highest peak turbulent flame speed of up to 12m/s for corn flour and Lycopodium [18, 110]. Coal samples, despite of having comparable size with the nut shell biomass showed less severity in flame propagation. This is because of the higher inerts and less volatiles in their structures. Torrefied wood samples as tested by Clara et al.[168, 200, 201] were found to have less peak turbulent flame speed due to higher particle size in terms of d_{50} as shown in Figure 7.37. Biomass crop residues with more irregular shaped coarse fibrous particles have very small peak turbulent flame speed. The minimum value of peak turbulent flame speed of 1m/s was measured for SPF raw wood mixture with 50% proportions of particle size around 450µm. The range of S_L as shown

in Figure 7.38 is from 0.32 m/s for cornflour to 0.025 m/s for the SPF wood mixture in raw and torrefied form. This high S_L for cornflour is well below the value of 0.65 m/s measured by Dahoe et al. [121] but is similar to the S_L of 0.25 m/s from the results of Phylaktou et al. [123]. The most reactive standard biomass was walnut shells with an S_L of 0.27 m/s. Most of the biomass had S_L in the range 0.1 – 0.15 m/s and these are much lower values than for hydrocarbon gases where the maximum S_L is about 0.4 m/s [102].

In the end, the comparison of explosibility characteristics of different biomass including agricultural waste, nut shells, raw and torrefied wood were presented as shown in table 7.9. It was found that nut shell biomass having regular shape fine particles were more sensitive to explosion with higher bursting pressure. On the other hand, agricultural waste for the same particle size despite higher levels of inert ash were proven to be equally reactive as that of nut shell with higher explosibility hazards. However with increasing particle size, the explosibility threats of biomass materials were reduced but still existed for particle size as high as <1000µm.

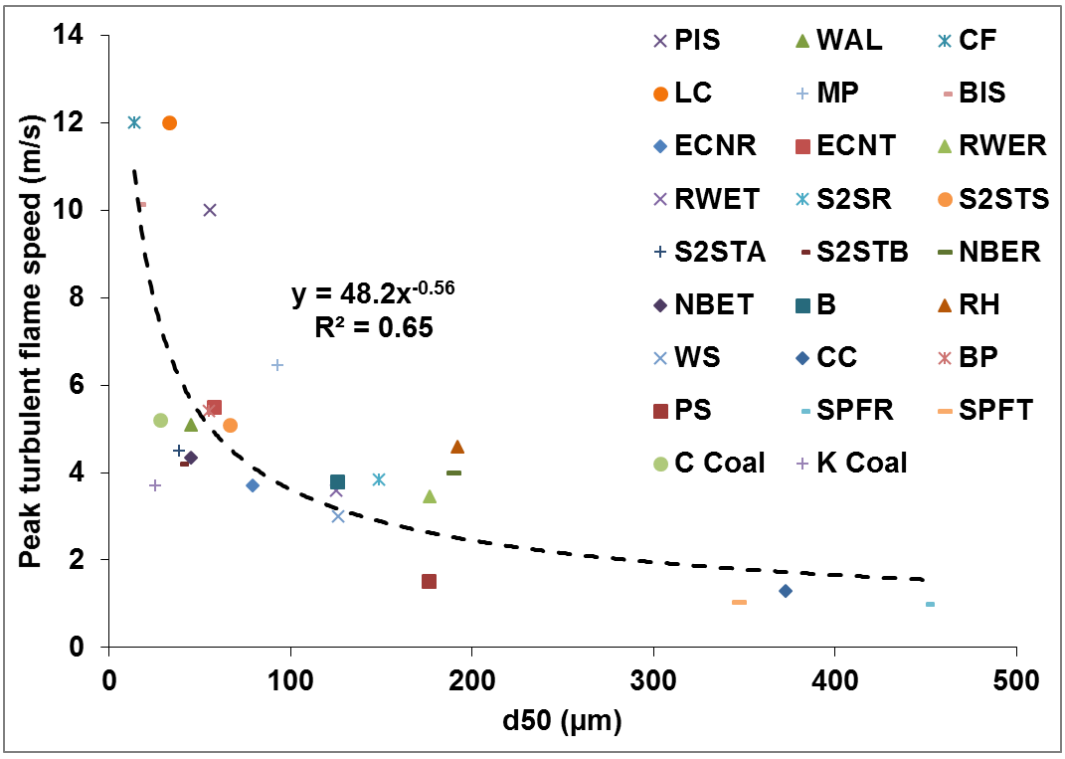

Figure 7.37: Peak turbulent flame speed as a function of d_{50} for different raw and treated biomass in combination with coals

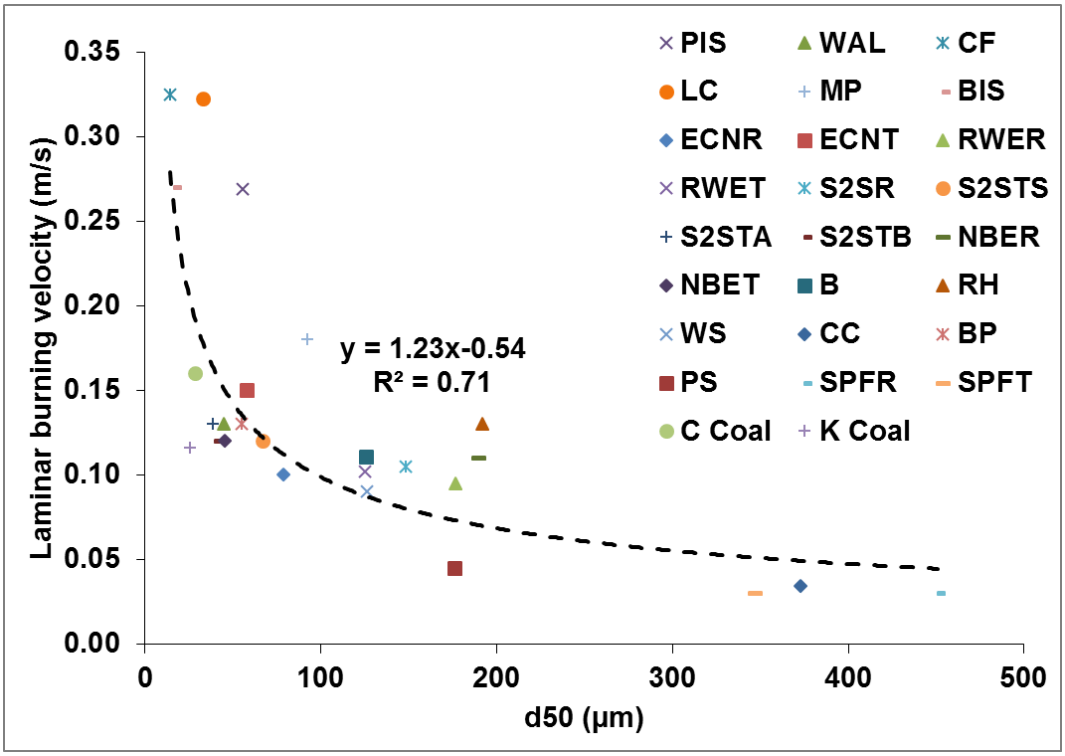

Figure 7.38: Peak laminar burning velocity as a function of d_{50} for different raw and treated biomass in combination with coals

It was also noticed that the thermal treatment of these biomass refine their properties with augmentation of their explosibility hazards. All the biomass samples tested were classified as Class 1 dust with Kst<200 bar m/s. Peak bursting pressure were recorded to be maximum 9.4 bar for Walnut shell. The least bursting pressure was measured to be 7.1 for coarse fraction of corn cob<500µm that is comparable with the coarser SPF wood and torrefied samples<1000µm. Turbulent flame speeds were measured to be 12m/s as maximum for corn flour and 1 m/s as minimum for coarse SPF wood mixture. Laminar burning velocities were measured to be small as compared to HC's gaseous mixture. Explosibility characteristics of most of the fine biomass samples were comparable with fine coal samples whereas the rest of the biomass can be thermally processed to refine their burning properties before their applications. So, these biomass were proved to be a good substitute of coals without significant changes in the existing coal power plants. Especially the agricultural waste without any major end use can be focussed in this regards. These agricultural waste should be dealt first in reducing the inert ash prior to feeding to the burner.

Table 7.9: Comparison of the explosibility characteristics of selected samples (with complete concentration profile) with others

Samples	***$Ø_{peak}$ K_{st}***	***Peak P_m/P_o***	***Peak K_{st} bar m/s***	***Peak S_T, m/s***	***Peak U_L, m/s***	***Refs.***
Bagasse, B<63µm	2.7	8.8	103	3.79	0.11	[21]
Wheat Straw, WS<63µm	1.6	8.5	82	3.0	0.13	[21]
Corn cob, CC<500µm	1.7	8.0	60	1.3	0.03	This work
Peanut shell, PS<500µm	1.13	7.1	25	1.3	0.04	This work
SPF Raw SPFR<1000µm	4.4	7.3	28.0	1.0	0.03	[203]
SPF torrefied SPFT<1000µm	2.9	7.4	35.7	1.05	0.03	[203]
Pistachio nut shells<63µm	2.4	9.3	82	3.7	0.27 Extrapolated	[18]
Walnut shells<63µm	2.8	9.4	98	5.1	0.13	[18]
Corn flour <63µm	2.6	9.2	156.4	12	0.32	[110]
Pine 1<63µm	4.2	9.0	109	3.7	0.1	[87]
Spruce<63µm	1.9	8.8	81	3.4	0.09	[201]
Torrefied Norway spruce<63µm	3.9	9.1	110	4.6	0.12	[200]
US Pine 2<63µm	2.5	9.0	105	4.5	0.11	[200]
Torrefied southern pine<63µm	2.0	8.8	115	4.4	0.12	[200]
Colombian coal<63µm	2.6	8.2	129	5.2	0.16	[168]
Kellingley coal<63µm	2.3	7.9	78.2	3.1	0.12	[168]

Chapter 8 MAIN FINDINGS AND FUTURE WORK

Pakistan has a large agricultural sector and produces a substantial amount of waste material that has little current economic use. At the same time Pakistan has a major electricity supply problem. This work showed that agricultural wastes are a significant energy resource that could be used to generate electricity using relatively small biomass generator-sets that could take all the waste biomass from the surrounding agricultural area if proper planning and strategies are made. Pakistan currently imports most of the oil used for electricity generation. The cost of this result in a high cost of electricity. It is shown that bio-electricity could be generated competitively in Pakistan. It was estimated, based on 30% thermal efficiency of an electric power generation, that the annual production of crop residues have the potential to generate 76% of the annual electricity requirements of Pakistan. To minimise transport costs it is proposed that a series of about 10MWe plants should be established (which are commercially available) with all farms in about a 10km radius delivering their agricultural solid waste to the plant at the farmers cost with direct payment by the power generator.

A similar approach could be adopted in other countries around the world. An additional advantage of the use of biomass as fuel is the reduction in carbon footprint in power generation and indeed legislation in many countries, including the UK, is incentivising the use of biomass in partial or full replacement of coal in power generation.

The change of fuel from coal to pulverised biomass, and the use of biomass only in new plants, requires consideration of the combustion characteristics of biomass for efficient design of the burners but also for operational safety of the storage, conveying and combustion facilities for biomass. The existing methods for the testing of explosibility characteristics are not suitable for fibrous biomass and coarse size fractions. Modified Hartmann with ignition delay under or overestimates the explosibility characteristics that are not related with the representative concentration. At no ignition delay, the relative reactivity of different size fractions can be studied only as demonstrated in this work. However further work suggested to use an ignition delay suitably within 50-120 ms. Standard 1 m^3 vessel was also modified to operate it for the testing of fibrous biomass dust and coarse size fraction. A hemispherical disperser with drilled pipe was designed previously and calibrated in this work using reference samples; corn flour and Colombian coal to get the optimum settings of ignition delay, dispersion pressure and valve off timings for comparative results of explosibility

characteristics as that of the standard system. Such data is scarce in the literature and it was one of the major objectives of this project to provide data for crop residues (bagasse, rice husk, wheat-straw, corn-cob and peanut-shell) and different raw and thermally treated woods.

8.1 Volatile release models

Two models were used to gain an understanding of the volatile release kinetics from biomass utilising TGA data at slow heating rates. Kinetic parameters were measured in terms of activation energy and pre-exponential factor considering 1^{st} order reaction. Two distinct phases of volatile release were identified that were because of the hemicellulose and cellulose decomposition at low temperature with mainly hard lignin decomposition at higher temperature.

In the first, “series reaction”, model, the primary release of volatiles from initial decomposition of hemicellulose and cellulose content form a major proportion of volatiles. Kinetic parameters were varied of this initial phase of volatile loss for different biomass samples with almost same kinetics for the second phase. It was found that biomass samples have lower activation energies (63-98 KJ/mol) than the coal samples (106-111 KJ/mol) for the release of major proportion of volatiles.

In competitive reaction model, it was proposed that the formation of char influences the release of volatiles and there were competitive reactions occurring side by side. Activation energies of volatile release under competitive reactions were again found to be lower for biomass samples (61-101 KJ/mol) compared to coal samples (182-333 KJ/mol). The difference in activation energies suggests that biomass is of the order of twice more reactive than coal.

Both approaches clearly showed the small energy requirement for fast release of volatiles from biomass at low temperatures. This was attributed to the soft and porous structure of biomass particles compared to coal. A good linear correlation was found between activation energy of the volatile release rate and minimum explosible concentration.

8.2 Explosion characteristics of varying sized biomass fractions (crop residues and woods)

Explosibility characteristics of different biomass fuels (crop residues and wood powders) were measured for different size range fractions and the

results were compared with Colombian and Kellingley coal samples, in the modified Hartmann tube and the 1m^3 explosion vessel.

Based on Hartmann results, the bagasse, rice husk and corn cob samples were found to explode for particle size distribution as coarse as 300-500µm. Coal samples would not explode at this particle size. It was also demonstrated that the proportion of fine particles within the mixture play an important role in the flame propagation. It was found that fraction with a larger proportion of fines size particles were sensitive to explosion showing a lower MEC. There was a longer time delay in the evolution of sufficient volatiles in larger size fractions, resulting in larger dust concentrations needed to achieve enough volatiles within the airborne (residence) time of the particles. Also the most reactive concentration giving higher rate of pressure rise was higher for coarser fraction compared to fine size fraction.

Crop residues were shown to sustain flame propagation even in the presence of 50% ash due to sufficient release of volatiles that was again never experienced with coal.

Based on 1m^3 vessel results, bagasse and wheat straw for size <63 µm, were found to be more reactive than the two selected coal samples having the same sieve size (< 63 µm). Minimum explosible concentration for these crop residues were leaner (0.22-0.29 equivalence ratio) than coal (0.39-0.49 equivalence ratio) whereas the maximum explosion pressures were comparable or higher (8.5-8.8 bar). The deflagration index and maximum flame speed for bagasse and wheat straw were 103 bar m/s, 3.8 m/s and 82 bar m/s, 3.0 m/s respectively despite of their higher ash contents.

Peanut shell and corn cob of higher sieve size <500µm were found to have comparable rise of pressure (7-8 bar) as that of coal samples, however the minimum explosible concentration exceeded from the coal samples due to their coarse sizes.

Post explosion residue samples showed almost the same chemical characterisation as the original samples. The increase of ash in the post explosion residue due to addition of ash from the burnt mass resulted in the corresponding proportional drop of volatile content.

Rice husk samples were additionally tested at higher size fractions and the MEC increased with increasing size fraction. However, the maximum explosion pressure remained fairly steady at 7.3-7.5 barg, but the

concentration at which this was achieved was richer for coarser size fractions.

Post explosion residues analysis revealed that for finer fractions there was greater mass burnt with correspondingly more ash content in the residue. For coarse particles there was an increase in char left in the residue.

It was concluded that particle size plays an important role in the rate of release of volatiles that are responsible for the flame propagation. It was found that the smaller the size of the particles, the more severe the explosion.

In agreement with the earlier volatile release kinetics work, the modified Hartmann tube and 1 m^3 vessel confirmed the findings of higher volatile yield from biomass compared to coal. SEM image analyses supported the concept of more porous structure for biomass and the elongated cylindrical particle shape (compared to a more spherical for coal). It was concluded that biomass samples do not need to grind as fine as coal to acquire the same explosion severity.

The higher reactivity of biomass may result in flashback in the burner for improper air flow rate and the higher feeding rate of biomass powder lift off the flame resulting the unsteady flame.

8.3 Flame propagation of steam exploded sample compared to raw pine

Steam exploded treatment on pine wood sample enhanced the brittleness with minor loss of volatiles. Raw pine wood sample after steam exploded treatment was more reactive with leaner minimum explosible concentration of 0.2 equivalence ratio compared to 0.39 for raw pine for same sieve size of less than 63µm. Rate of pressure rise for steam exploded pine was higher compared to raw pine wood. Most reactive concentration remained almost same at equivalence ratio of ~1.3. Also the flame speed were measured to be higher for steam treated pine compared to its raw pine with almost similar peak turbulent flame speed of ~2.5 m/s for raw and steam exploded pine. Chemical analysis of the pine wood and its steam exploded sample showed nearly same volatile yield with almost same total inert. However, the presence of higher proportions of fine in the steam exploded sample increased the rate of volatile release resulting quick build-up of pressure.

Later this steam exploded sample was tested on 1 m^3 explosion vessel for different size range fraction and similar trends were observed as expected

with leaner minimum explosible concentration (MEC) for finer fraction. Complete concentration profiles could not be obtained for finer sized fractions due to limited amount however, the very coarse fraction of size 150-300 µm propagated the flame with maximum explosion pressure of around 7 bar. The maximum deflagration index and peak turbulent flame speed were measured to be 42 bar m/s and 1.4 m/s respectively.

Steam explosion treatment refined the fuel with more brittle structure leading their easy milling. However, the more fines generation after milling make it more reactive than raw biomass sample. Implementation of this steam exploded black pellet, a refined advanced fuel, for power generation without the knowledge of its flame propagation rate and explosibility characteristics is threats for their safe exploitation. Higher reactivity of these steam exploded wood with their strong particle dependence demands more safety and careful consideration for their applications as substitute of coal for power generation.

8.4 Flame propagation of coarse size wood mixture in comparison to its torrefied sample

Coarse size SPF wood mixture of size less than 1 mm was tested using modified 1 m^3 vessel for its explosibility characteristics in comparison to its torrefied sample. This was the largest size range fraction tested ever on lab scale. It was found that this very coarse fraction of wood mixture propagated the flame with significant rise of pressure. The maximum rise of pressure of about 7.5 bar with this size fraction was not expected. It was found that the presence of fines with coarse particles facilitated the flame propagation. Also the lighter coarse particles of this SPF wood mixture suspended for longer time to evolve sufficient volatiles.

Torrefied sample of this SPF wood mixture was more sensitive to explosion with leaner minimum explosible concentration (1.4 equivalence ratio for SPF torrefied compared to 2.3 for SPF raw). Also the torrefied sample showed greater deflagration index (~36 bar m/s) compared to its raw wood mixture (28 bar m/s).

Post explosion residue analysis also showed more mass burnt of torrefied sample with greater ash in the residue sample. SEM imaging of the post explosion residues showed appearance of holes on the larger sized particles that revealed the release of volatiles from the surface of coarse sized particles. So, overall it was concluded that fine particles contribute fully whereas volatiles play an important role for the burning of coarse sized

particles. In a mixture of fine with coarse sized particles, flame propagates preferentially with fines and later sustained with release of volatile from coarse sized particles.

Number of factors influencing the flame propagation rate can be related as;

$$Reactivity \propto \frac{(Volatile) \times (Proportion\ of\ fines)}{(Inert) \times (Particle\ size)} \times \frac{(Soft\ porous\ structure)}{(Hard\ structure)}$$

Changes in the experimental methods can be used for the standardisation of testing of irregular shape coarse size dust mixtures. Based on these findings, it was concluded that biomass samples (crop residues and woods) are more reactive than coal samples despite of higher ash (especially for crop residues) and coarse size distribution. Fine particles along-with coarse particles play an important role for sustaining the propagation of flame. Coarse size fraction with higher proportion of fine was proved to be hazardous with higher flame propagation rate. Thermal treatments like torrefaction and steam explosion refine the biomass resulting their easy milling, generating more fines, exhibiting higher fire/explosibility hazards. So, the raw and especially thermally treated biomass not need to be milled as fine as that of coal to acquire the same flame propagation rate. This research work presented and established the flame propagation rate and explosibility characteristics results for crop residues and woody biomass materials with their particle size dependence.

8.5 Future work

Based on the experimental findings, there are several areas to be explored further as future work.

With the increased use of biofuels specifically as substitute of coal, various types of biomass materials particularly the low cost agricultural waste, can be employed. However, due to variability in the composition, each adopted fuels should be tested for its explosibility characteristics. Their distributions and effect of ignition delay on the modified dust explosion vessels needs to be studied. In the conventional processes, a high temperature and flash heating can significantly affect the kinetics for the volatile release. Kinetics of volatile release for the thermally thick and thermally thin biomass materials in combination with the effect of heating rate has to be investigated that has direct influence on the reactivity. The intermediate gaseous phase, due to pyrolysis and gasification with their characterisation, can help to understand the flame propagation mechanism.

The raw biomass after pre-treatments like torrefaction and steam explosion have significant reduction of particle size distribution posing greater fire/explosibility hazards. So, the flame propagation rate and explosibility characteristics should be studied as a function of the particle size. Similarly hybrid mixtures, using different proportions of different fuels, to achieve the best combination for efficient burning fuel are set as future plans. These future plans are split and listed below;

- Effect of ignition delay in the modified Hartmann for the testing of more biomass dusts.
- Kinetic study of biomass fuels in comparison to coal for high heating rate to see the effect of volatile release rate.
- Kinetic study for different sized fractions of biomass for high heating rate.
- Study the instantaneous volatile release at high temperature comparable to furnace conditions.
- Chemical characterisation of volatile for same conditions as that of furnace (higher heating rates and higher temperature).
- Study the role of hemicellulose, cellulose and lignin contents on the chemical characterisation of volatiles.
- Determination of most reactive concentration for coarse size fraction with complete concentration profile.
- Testing of coarse size range fraction of size similar to feedstocks in the conventional power generation plants.
- Study the effect of pre-treatments on biomass by testing different torrefied and steam exploded samples for varying treated conditions.
- Determination of explosibility characteristics of other agricultural waste and woody biomass.
- Study the influence of metallic components in ash content that act to catalyse the flame propagation.
- Study the testing of hybrid mixture by considering different HC’s fuel with biomass.

References

1. Schobert, H.H., *Chemistry of Fossil Fuels and Biofuels*, ed. P.U. Arvind Varma. 2013, United States of America: Cambridge University Press, New York.
2. Kyoto Protocol. *United Nations Framework Convention on Climate Change (UNFCCC)*. 2014 [cited 2014 20 March]; Available from: http://unfccc.int/kyoto_protocol/items/2830.php.
3. Climate Change Act. *Committe on Climate Change (CCC)*. 2008 [cited 2015 15 April]; Available from: https://www.theccc.org.uk/tackling-climate-change/reducing-carbon-emissions/carbon-budgets-and-targets/.
4. IEA. *Renewables, International Energy Agency*. 2013 [cited 2013 02 April]; Available from: http://www.iea.org/.
5. U.S. Energy Information Administration. *Independent Statistics and Analysis*. 2014 [cited 2016 06 March]; Available from: http://www.eia.gov/energyexplained/index.cfm?page=electricity_in_the_united_states.
6. Department-of-Energy-and-Climate-Change., *Digest of United Kingdom Energy Statistics (DUKES), UK*, 2015.
7. European-Commission, *Report from the Commission to the Council and the European Partiament on sustainability requirements for the use of solid and gaseous biomass sources in electricity, heating and cooling*, 2010.
8. Biomass and Biofuel. *the renewable energy centre*. 2015 [cited 2016 6 March]; Available from: http://www.therenewableenergycentre.co.uk/biomass-and-biofuel/.
9. Jenkins, B.M., et al., *Combustion properties of biomass.* Fuel Processing Technology, 1998. **54**(1–3): p. 17-46.
10. Vassilev, S.V., et al., *An overview of the organic and inorganic phase composition of biomass.* Fuel, 2012. **94**: p. 1-33.
11. Callé, F.R., *The biomass assessment handbook: bioenergy for a sustainable environment*. 2007: Earthscan.
12. McKendry, P., *Energy production from biomass (part 1): overview of biomass.* Bioresource technology, 2002. **83**(1): p. 37-46.

13. Gravalos, I., et al. *A study on calorific energy values of biomass residue pellets for heating purposes*. in *Proceedings on Forest Engineering: Meeting the Needs of the Society and the Environment, Padova, Italy*. 2010.

14. Kaliyan, N., *Densification of biomass*. 2008: ProQuest.

15. Badger, P.C. and P. Fransham, *Use of mobile fast pyrolysis plants to densify biomass and reduce biomass handling costs—A preliminary assessment.* Biomass and bioenergy, 2006. **30**(4): p. 321-325.

16. Davidsson, K.O., et al., *The effects of fuel washing techniques on alkali release from biomass.* Fuel, 2002. **81**(2): p. 137-142.

17. Saeed, M.A., et al., *Agricultural waste pulverised biomass: MEC and flame speeds.* Journal of Loss Prevention in the Process Industries, 2014. **36**: p. 308-317.

18. Sattar, H., et al. *Explosions and Flame Propagation in Nut-shell Biomass Powders*. in *Proc. of the IX International Seminar on Hazardous Process Materials and Industrial Explosions (IX ISHPMIE)*. 2012. Cracow.

19. Huéscar Medina, C., et al., *The development of an experimental method for the determination of the minimum explosible concentration of biomass powders.* Biomass and Bioenergy, 2013. **53**(0): p. 95-104.

20. Bergman, P.C. and J.H. Kiel. *Torrefaction for biomass upgrading*. in *Proc. 14th European Biomass Conference, Paris, France*. 2005.

21. Saeed, M.A., et al. *Flame Propagation of Pulverised Biomass Crop Residues and their Explosion Characteristics* in *25th International Colloquium on the Dynamics of Explosions and Reactive Systems (ICDERS)*. 2015. Leeds, UK.

22. Sattar, H., et al. *Pulverised Biomass Explosions: Investigation of the Ultra Rich Mixtures that give Peak Reactivity*. in *Proc. of the IX International Seminar on Hazardous Process Materials and Industrial Explosions (IX ISHPMIE)*. 2012. Cracow.

23. Huéscar Medina, C., et al. *Determination of the minimum explosible and most reactive concentrations for pulverised biomass using a modified Hartmann apparatus.* in *Proc. of the IX International*

Seminar on Hazardous Process Materials and Industrial Explosions (IX ISHPMIE). 2012. Cracow.

24. Andrews, G.E. and H.N. Phylaktou, *Explosion Safety*, in *Handbook of Combustion*. 2010, John Wiley and Sons, Inc. p. 377-413.
25. Forestry-Commission. *Biomass-Energy-Centre*. 2013 [cited 2013 11 May]; Available from: http://www.biomassenergycentre.org.uk/portal/page?_pageid=75,17301&_dad=portal&_schema=PORTAL.
26. World-Energy-Outlook. *Internationational Energy Agency*. 2013; Available from: http://www.oecd-ilibrary.org/energy/world-energy-outlook-2013_weo-2013-en;jsessionid=18bpy6u8bcoxe.x-oecd-live-02.
27. Blood, P. *A country study. US library of congresss*. 1994 [cited 2013 1st April]; Available from: http://countrystudies.us/pakistan/.
28. Indexmundi. *Factbook*. 2015 [cited 2015 1st April]; Available from: http://www.indexmundi.com/pakistan/.
29. Ministry-of-Water-&-Power. *Government of Pakistan*. 2013 [cited 2013 1 April]; Available from: http://www.mowp.gov.pk/gop/index.php?q=aHR0cDovLzE5Mi4xNjguNzAuMTM2L21vd3Av.
30. Fatima, N., *Shortage of gas needs to be tackled as early as possible to save CNG sector, Fuel fuss, Pakistan Renewable Energy Society*, 2013.
31. Pakistan-Energy-Yearbook 2011.
32. Khan, A., *Textile sector needs govt focus to stabilize economy*, 2013: Pakistan Observer.
33. National-Electric-Power-Regulatory-Authority. 2012 [cited 2014 12 September]; Available from: http://www.nepra.org.pk/.
34. Bazmi, A.A., G. Zahedi, and H. Hashim, *Progress and challenges in utilization of palm oil biomass as fuel for decentralized electricity generation.* Renewable and Sustainable Energy Reviews, 2011. **15**(1): p. 574-583.
35. Montzka, S., E. Dlugokencky, and J. Butler, *Non-CO2 greenhouse gases and climate change.* Nature, 2011. **476**(7358): p. 43-50.

36. Ministry-of-Finance, 2013.

37. Muneer, T. and M. Asif, *Prospects for secure and sustainable electricity supply for Pakistan.* Renewable and Sustainable Energy Reviews, 2007. **11**(4): p. 654-671.

38. Farooq, M.K. and S. Kumar, *An assessment of renewable energy potential for electricity generation in Pakistan.* Renewable and Sustainable Energy Reviews, 2013. **20**(0): p. 240-254.

39. Ali, T., J. Huang, and J. Yang, *Impact assessment of global and national biofuels developments on agriculture in Pakistan.* Applied Energy, 2013. **104**(0): p. 466-474.

40. Ashraf Chaudhry, M., R. Raza, and S.A. Hayat, *Renewable energy technologies in Pakistan: Prospects and challenges.* Renewable and Sustainable Energy Reviews, 2009. **13**(6–7): p. 1657-1662.

41. Andrews, S.S., *Crop residue removal for biomass energy production: Effects on soils and recommendations.* White paper, USDA Natural Resources Conservation Service, 2006.

42. Saxena, R., D. Adhikari, and H. Goyal, *Biomass-based energy fuel through biochemical routes: A review.* Renewable and Sustainable Energy Reviews, 2009. **13**(1): p. 167-178.

43. Ghaffar, M.A., *The energy supply situation in the rural sector of Pakistan and the potential of renewable energy technologies.* Renewable Energy, 1995. **6**(8): p. 941-976.

44. Pakistan-Renewable-Energy-Society. *Promoting Green Energy For Better Tomorrow*. 2013 [cited 2013 23rd May]; Available from: http://www.pres.org.pk/category/reaepakistan/country-profile/.

45. Siraj, M. *A model for developing ICT bases services for Agriculture Extension, Research for development project, Department for International Development*. 2011 [cited 2015 12 October]; Available from: http://r4d.dfid.gov.uk/Project/60818/.

46. Amur, G.Q. and S. Bhattacharya, *A study of biomass as a source of energy in Pakistan.* RERIC International Energy Journal, 1999. **21**(1): p. 25-36.

47. Mirza, U.K., N. Ahmad, and T. Majeed, *An overview of biomass energy utilization in Pakistan.* Renewable and Sustainable Energy Reviews, 2008. **12**(7): p. 1988-1996.

48. Bhutto, A.W., A.A. Bazmi, and G. Zahedi, *Greener energy: Issues and challenges for Pakistan—Biomass energy prospective.* Renewable and Sustainable Energy Reviews, 2011. **15**(6): p. 3207-3219.

49. FAO, *Fertilizer use by crop in Pakistan*, 2004.

50. Agriculture-Census, *Pakistan Report, Government of Pakistan , Statistics Division*, 2010.

51. Singh, J. and S. Gu, *Biomass conversion to energy in India—A critique.* Renewable and Sustainable Energy Reviews, 2010. **14**(5): p. 1367-1378.

52. Sacha Alberici, G.T., *Input to DRAFT PIR, UK biofuels industry overview, ECOFYS, Department for Transport*, 2013.

53. Bae, J.-S., et al., *Production of the glycerol-impregnated hybrid coal and its characterization.* Fuel, 2014. **118**: p. 33-40.

54. Scholtz, G., H. Van der Merwe, and T. Tylutki, *Sample preparation of Medicago sativa L. hay for chemical analysis.* South African Journal of Animal Science, 2009. **39**(5): p. 73-76.

55. OECD/IEA. *Energy Unit Converter*. 2013 [cited 2013 7th March]; Available from: http://www.iea.org/statistics/resources/unitconverter/.

56. Monfreda, C., N. Ramankutty, and J.A. Foley, *Farming the planet: 2. Geographic distribution of crop areas, yields, physiological types, and net primary production in the year 2000.* Global Biogeochemical Cycles, 2008. **22**(1).

57. Pakistan-Bureau-of-Statics. *Agriculture Statistics*. 2013 [cited 2013 15 March]; Available from: http://www.pbs.gov.pk/.

58. Aziz, N. *Biomass Energy Potential in Pakistan*. 2013.

59. Bagasse-Power, *Sugar makers have a sweet power advantage*, in *Biomass Magazine*2011.

60. Pakistan-Sugar-Mills-Association. *Sugar industry, list of mills*. 2011 [cited 2013 26 May]; Available from: http://www.psmacentre.com/sgindustry.php?sgid=3&type=listofmills&status=1.

61. Renewable-Energy-Policy, *Alternative-Energy-Development-Board.* 2006.

62. Awan, K.Y. and A. Rashid, *Overview of Pakistan's Electricity Crisis, Generation-Mix and Renewable energy scenarios.* International Journal of Engineering & Technology, 2012. **1**(4): p. 321-334.

63. IRENA, *Renewable Power Generation Costs in 2012, An Overview*, 2012.

64. Memon, M., et al. *Potential of crop residues as energy source in Pakistan*. in *Proceeding of World Renewable Energy Congress-IX*. 2006.

65. Alternative-Energy-Development-Board. *Ministry of Water & Power,Government of Pakistan*. 2013 [cited 2013 5 March]; Available from: http://www.aedb.org/Main.htm.

66. Private-Power-&-Infrastructure-Board. *Ministry of Water & Power, Government of Pakistan*. 2013 [cited 2013 1 June]; Available from: http://www.ppib.gov.pk/N_upcoming_cogen.htm.

67. NFPA-68, *Standard on Explosion Protection by Deflagration Venting*, 2007.

68. NFPA-68:2013 edt., *Standard on Explosion Protection by Deflagration Venting*, 2013.

69. Palmer, K.N., *Dust explosions and fires*. 1973: Chapman and Hall London;.

70. Amyotte, P.R. and R.K. Eckhoff, *Dust explosion causation, prevention and mitigation: An overview.* Journal of Chemical Health and Safety, 2010. **17**(1): p. 15-28.

71. Bardon, M. and D. Fletcher, *Dust explosions.* Sci. Prog. Oxf, 1983. **68**: p. 459-473.

72. Amyotte, P., S. Chippett, and M. Pegg, *Effects of turbulence on dust explosions.* Progress in Energy and Combustion Science, 1988. **14**(4): p. 293-310.

73. Eckhoff, R.K., *Dust Explosions in the Process Industries: Identification, Assessment and Control of Dust Hazards*. 3rd ed. 2003, Amsterdam: Gulf Professional Publishing.

74. Eckhoff, R.K., *Differences and similarities of gas and dust explosions: a critical evaluation of the European 'ATEX'directives in*

relation to dusts. Journal of Loss Prevention in the Process Industries, 2006. **19**(6): p. 553-560.

75. Combustible-dust. *United States, Department of Labor*. 2013 [cited 2013 10 May]; Available from: https://www.osha.gov/dsg/combustibledust/.

76. Randeberg, E., W. Olsen, and R.K. Eckhoff, *A new method for generation of synchronised capacitive sparks of low energy.* Journal of electrostatics, 2006. **64**(3): p. 263-272.

77. Abrahamsen, A.R., *The UK approach to dust explosibility assessment and its relevance to explosion prevention and protection*, in *Industrial Dust Explosions*. 1987, ASTM International.

78. Abbasi, T. and S. Abbasi, *Dust explosions–Cases, causes, consequences, and control.* Journal of Hazardous Materials, 2007. **140**(1): p. 7-44.

79. Wypych, P., D. Cook, and P. Cooper, *Controlling dust emissions and explosion hazards in powder handling plants.* Chemical Engineering and Processing: Process Intensification, 2005. **44**(2): p. 323-326.

80. Dahoe, A., et al., *Dust explosions in spherical vessels: the role of flame thickness in the validity of the 'cube-root law'.* Journal of Loss Prevention in the Process Industries, 1996. **9**(1): p. 33-44.

81. Going, J.E., K. Chatrathi, and K.L. Cashdollar, *Flammability limit measurements for dusts in 20-L and 1-m3 vessels.* Journal of Loss Prevention in the Process Industries, 2000. **13**(3–5): p. 209-219.

82. Sattar, H., et al. *Calibration of a 10L volume dust holding pot for the 1m3 standard vessel, for use in low-bulk-density biomass explosibility testing*. in *Proc. of the IX International Seminar on Hazardous Process Materials and Industrial Explosions (IX ISHPMIE)*. 2012. Cracow.

83. Jacobson, M., *Explosibility of agricultural dusts*. Vol. 5753. 1961: US Dept. of the Interior, Bureau of Mines.

84. Mittal, M., *Limiting oxygen concentration for coal dusts for explosion hazard analysis and safety.* Journal of Loss Prevention in the Process Industries, 2013.

85. Hertzberg, M. and K.L. Cashdollar, *Introduction to dust explosions.* American Society for Testing and Materials (ASTM), Special Technical Publication (STP), 1987. **958**: p. 5-32.

86. Cassel, H.M., *Some fundamental aspects of dust flames*. Vol. 6551. 1964: US Dept. of the Interior, Bureau of Mines.

87. Huéscar Medina, C., et al. *Torrefaction effects on the reactivity and explosibility of woody biomass*. in *Proc. of the 7th International Seminar on Fire and Explosion Hazards*. 2013. Providence, RI, USA.

88. Buschart, R.J., *Dust explosions in process plants.* Industry Applications Magazine, IEEE, 1999. **5**(1): p. 22-27.

89. Nifuku, M. and H. Katoh, *Incendiary characteristics of electrostatic discharge for dust and gas explosion.* Journal of Loss Prevention in the Process Industries, 2001. **14**(6): p. 547-551.

90. Gao, W., et al., *Effects of particle size distributions on flame propagation mechanism during octadecanol dust explosions.* Powder Technology, 2013(0).

91. Slatter., D.J.F., et al. *The Influence of Particle Size and Volatile Content on the Reactivity of CH and CHO Chemical and Biomass Dusts*. in *Proc. of the 7th International Seminar on Fire and Explosion Hazards*. 2013. Providence, RI, USA.

92. Eckhoff, R.K., *Influence of dispersibility and coagulation on the dust explosion risk presented by powders consisting of nm-particles.* Powder technology, 2013. **239**: p. 223-230.

93. Deguingand, B. and S. Galant. *Upper flammability limits of coal dust-air mixtures*. in *Symposium (International) on Combustion*. 1981. Elsevier.

94. Eckhoff, R., K. Fuhre, and G. Pedersen, *Dust explosion experiments in a vented 236 m< sup> 3</sup> silo cell.* Journal of Occupational Accidents, 1987. **9**(3): p. 161-175.

95. Wolanski, P., *Dust explosion research in Poland.* Powder technology, 1992. **71**(2): p. 197-206.

96. Mintz, K.J., *Upper explosive limit of dusts: Experimental evidence for its existence under certain circumstances.* Combustion and Flame, 1993. **94**(1–2): p. 125-130.

97. BS EN 1839:2003, *Determination of explosion limits of gases and vapours*, 2003, British Standard: London, UK.

98. Cashdollar, K.L., *Overview of dust explosibility characteristics.* Journal of Loss Prevention in the Process Industries, 2000. **13**(3): p. 183-199.

99. Yuan, J., et al., *Experimental investigation of dust MEC measurement.* Powder Technology, 2012. **217**(0): p. 245-251.

100. Nagy, J., J.W. Conn, and H.C. Verakis, *Explosion development in a spherical vessel*. 1969: US Department of the Interior, Bureau of Mines.

101. Horton, M., F. Goodson, and L. Smoot, *Characteristics of flat, laminar coal-dust flames.* Combustion and Flame, 1977. **28**: p. 187-195.

102. Andrews, G. and D. Bradley, *The burning velocity of methane-air mixtures.* Combustion and Flame, 1972. **19**(2): p. 275-288.

103. BS EN 15967:2011, *Determination of the maximum explosion pressure and the maximum rate of pressure rise of gases and vapours.*, 2011, British Standard Institute: London, UK.

104. BS EN 14034-2, *Determination of Explosion Characteristics of Dust Clouds.* , in *Part 2: Determination of the Maximum Rate of Explosion Pressure Rise (dP/dt)max of Dust Clouds.*2006, British Standard Institute: London, UK.

105. BS EN 14034-1:2004, *Determination of Explosion Characteristics of Dust Clouds.* , in *Part 1: Determination of the Maximum Explosion Pressure Pmax of Dust Clouds.*2004, British Standard Institute: London, UK.

106. BS EN 14994:2007, *Gas Explosion Venting Protective Systems*, 2007, British Standards Institute: London, UK.

107. BS EN 14491:2012, *Dust Explosion Venting Protective Systems.*, 2012, British Standard Institute: London, UK.

108. ISO 6184-1, *Explosion Protection Systems, Part 1: Method for determination of Explosion Indices of Combustible Dusts in Air.*, 1985.

109. Gardner, C.L., H.N. Phylaktou, and G.E. Andrews. *Turbulence and Turbulent Burning Velocities in the ISO 1 m3*. in *Proc. 17th ICDERS*. 2001. Seattle.

110. Sattar, H., et al., *Turbulent Flames Speeds and Laminar Burning Velocities of Dusts using the ISO 1 m3 Dust Explosion Method.* Chemical Engineering 2014. **36**.

111. W. Bartknecht, *Dust Explosions: Course, prevention, protection.* 1989, London: Springer.

112. National Fire Protection Association (NFPA-68):2002 edt., *Guide for venting of deflagration*, 2002.

113. Bartknecht, W., *Explosion protection, basics and application.* German, Springer-Verlag, 1993.

114. Chippett, S., *Modeling of vented deflagrations.* Combustion and Flame, 1984. **55**(2): p. 127-140.

115. Bradley, D. and A. Mitcheson, *Mathematical solutions for explosions in spherical vessels.* Combustion and Flame, 1976. **26**: p. 201-217.

116. Kumar, R., E. Bowles, and K. Mintz, *Large-scale dust explosion experiments to determine the effects of scaling on explosion parameters.* Combustion and flame, 1992. **89**(3-4): p. 320-332.

117. Proust, C. and B. Veyssiere, *Fundamental properties of flames propagating in starch dust-air mixtures.* Combustion Science and Technology, 1988. **62**(4-6): p. 149-172.

118. Proust, C. *Experimental determination of the maximum flame temperatures and of the laminar burning velocities for some combustible dust-air mixtures*. in *5. International Colloquium on Dust Explosions*. 1993.

119. P, W., *Dust Explosion.* EC CREDIT Project Contract No. EV5V-CT92-0082. Final Report, 1995.

120. Nagy, J., *Development and control of dust explosions*. Vol. 8. 1983: CRC Press.

121. Dahoe, A., K. Hanjalic, and B. Scarlett, *Determination of the laminar burning velocity and the Markstein length of powder–air flames.* Powder technology, 2002. **122**(2): p. 222-238.

122. Smoot, L.D., M.D. Horton, and G.A. Williams, *Propagation of laminar pulverized coal-air flames.* Symposium (International) on Combustion, 1977. **16**(1): p. 375-387.

123. Phylaktou, H., C. Gardner, and G. Andrews. *Flame speed measurements in dust explosions*. in *Proceedings of the Sixth International Seminar on Fire and Explosion Hazards*. 2010.

124. Kang Pu, Y., et al. *The investigation of the feature of dispersion induced turbulence and its effects on dust explosions in closed vessels*. in *Symposium (International) on Combustion*. 1989. Elsevier.

125. Kauffman, C., et al. *Turbulent and accelerating dust flames*. in *Symposium (International) on Combustion*. 1985. Elsevier.

126. Dahoe, A., et al., *On the transient flow in the 20-liter explosion sphere.* Journal of Loss Prevention in the Process Industries, 2001. **14**(6): p. 475-487.

127. Amyotte, P.R. and M.J. Pegg, *Lycopodium dust explosions in a Hartmann bomb: effects of turbulence.* Journal of Loss Prevention in the Process Industries, 1989. **2**(2): p. 87-94.

128. Bidabadi, M., A.H.A. Natanzi, and S.A. Mostafavi, *Thermophoresis effect on volatile particle concentration in micro-organic dust flame.* Powder Technology, 2012. **217**: p. 69-76.

129. Serafin, J., et al., *The influence of air flow on maximum explosion characteristics of dust–air mixtures.* Journal of Loss Prevention in the Process Industries, 2013. **26**(1): p. 209-214.

130. Jarosinski, J., J. Podfilipski, and Y. Pu, *Visualization of dust explosion under microgravity conditions.* Combustion science and technology, 2000. **158**(1): p. 183-194.

131. Han, O.-S., et al., *A study of flame propagation mechanisms in lycopodium dust clouds based on dust particles' behavior.* Journal of Loss Prevention in the Process Industries, 2001. **14**(3): p. 153-160.

132. Munir, S., et al., *Thermal analysis and devolatilization kinetics of cotton stalk, sugar cane bagasse and shea meal under nitrogen and air atmospheres.* Bioresource Technology, 2009. **100**(3): p. 1413-1418.

133. Norman, F., J. Berghmans, and F. Verplaetsen, *The dust explosion characteristics of coal dust in an oxygen enriched atmosphere.* Procedia Engineering, 2012. **45**: p. 399-402.

134. Cashdollar, K.L. and M. Hertzberg, *20-l explosibility test chamber for dusts and gases.* Review of Scientific Instruments, 1985. **56**(4): p. 596-602.

135. García-Torrent, J., et al., *Biomass dust explosibility at elevated initial pressures.* Fuel, 1998. **77**(9): p. 1093-1097.

136. Conde Lázaro, E. and J. García Torrent, *Experimental research on explosibility at high initial pressures of combustible dusts.* Journal of Loss Prevention in the Process Industries, 2000. **13**(3): p. 221-228.

137. Eckhoff, R. and K. Mathisen, *A critical examination of the effect of dust moisture on the rate of pressure rise in Hartmann bomb tests.* Fire Safety Journal, 1978. **1**(4): p. 273-280.

138. Yuan, J., et al., *Experimental investigations on the roles of moisture in coal dust explosion.* Journal of the Taiwan Institute of Chemical Engineers, 2014. **45**(5): p. 2325-2333.

139. Cashdollar, K.L. and K. CHATRATHI, *Minimum explosible dust concentrations measured in 20-L and 1-m3 chambers.* Combustion Science and Technology, 1993. **87**(1-6): p. 157-171.

140. Janes, A., et al., *MIKE 3 versus HARTMANN apparatus: Comparison of measured minimum ignition energy (MIE).* Journal of hazardous materials, 2008. **152**(1): p. 32-39.

141. Gao, W., et al., *Effect of ignition on the explosion behavior of 1-Octadecanol/air mixtures.* Powder Technology, 2013. **241**: p. 105-114.

142. Kuai, N., et al., *Experiment-based investigations on the effect of ignition energy on dust explosion behaviors.* Journal of Loss Prevention in the Process Industries, 2013. **26**(4): p. 869-877.

143. Kashiwagi, T., *A radiative ignition model of a solid fuel.* Combustion Science and Technology, 1973. **8**(5-6): p. 225-236.

144. Proust, C., *A few fundamental aspects about ignition and flame propagation in dust clouds.* Journal of Loss Prevention in the Process Industries, 2006. **19**(2): p. 104-120.

145. Di Benedetto, A., et al. *Flame Propagation of Dust and Gas-Air Mixtures in a Tube*. in *Proceedings of the 7th Mediterranean Combustion Symposium*. 2011. Chia Laguna Cagliari, Sardinia, Italy.

146. Khalili, I., et al., *Ignition sensitivity of gas–vapor/dust hybrid mixtures.* Powder Technology, 2012. **217**: p. 199-206.

147. Kosinski, P., et al., *Explosions of carbon black and propane hybrid mixtures.* Journal of Loss Prevention in the Process Industries, 2013.

148. Khalil, Y., *Experimental Investigation of the Complex Deflagration Phenomena of Hybrid Mixtures of Activated Carbon Dust/Hydrogen/Air.* Journal of Loss Prevention in the Process Industries, 2013.

149. Dahoe, A.E., *Dust explosions: a study of flame propagation.* 2000.

150. Lipatnikov, A. and J. Chomiak, *Turbulent burning velocity and speed of developing, curved, and strained flames.* Proceedings of the Combustion Institute, 2002. **29**(2): p. 2113-2121.

151. Zanzi, R., K. Sjöström, and E. Björnbom, *Rapid pyrolysis of agricultural residues at high temperature.* Biomass and Bioenergy, 2002. **23**(5): p. 357-366.

152. Pilão, R., E. Ramalho, and C. Pinho, *Overall characterization of cork dust explosion.* Journal of hazardous materials, 2006. **133**(1): p. 183-195.

153. Cuervoa, N., et al., *Experimental Study and Modelling of the Pyrolysis of Organic Dusts: Application to Dust Explosions.* CHEMICAL ENGINEERING, 2013. **31**.

154. Burhenne, L., M. Damiani, and T. Aicher, *Effect of feedstock water content and pyrolysis temperature on the structure and reactivity of spruce wood char produced in fixed bed pyrolysis.* Fuel, 2013.

155. Kletz, T.A., *The constraints on inherently safer design and other innovations.* Process Safety Progress, 1999. **18**(1): p. 64-69.

156. Bartknecht, W., *Dust explosions: Course, Prevention, Protection*. 1989, Berlin: Springer.

157. Van der Wel, P., et al., *An interpretation of dust explosion phenomena on the basis of time scales.* Powder technology, 1992. **71**(2): p. 207-215.

158. BS EN 14034-3:2006+A1:2011, *Part 3. Determination of the lower explosion limit LEL of dust clouds.*, 2011.

159. Zabetakis, M.G., *Flammability characteristics of combustible gases and vapors*, 1965, DTIC Document.

160. Lewis, B., *G. Von Elbe, Combustion, Flames and Explosions of Gases.* Academic Press, 1961. **2**: p. 226-308.

161. EN 13237:2012, *Potentially explosive atmospheres - Terms and definitions for equipment and protective systems intended for use in potentially explosive atmospheres.* .

162. BS EN 13821:2002, *Potentially explosive atmospheres - Explosion prevention and protection - Determination of minimum ignition energy of dust/air mixtures.*, 2002.

163. Maisey, H., *Gaseous and dust explosion venting.* Chem. Process Eng, 1965. **527**.

164. Field, P., *Explosibility assessment of industrial powders and dusts.* HMSO Books, P. O. Box 276, London SW 8 5 DT, England, 1983., 1983.

165. Razus, D., M. Molnarne, and O. Fuß, *Limiting oxygen concentration evaluation in flammable gaseous mixtures by means of calculated adiabatic flame temperatures.* Chemical Engineering and Processing: Process Intensification, 2004. **43**(6): p. 775-784.

166. Schröder, V. and M. Molnarne, *Flammability of gas mixtures: Part 1: Fire potential.* Journal of hazardous materials, 2005. **121**(1): p. 37-44.

167. Wilén, C., et al., *Safe handling of renewable fuels and fuel mixtures*. 1999: Technical Research Centre of Finland.

168. Huéscar Medina, C., et al., *Comparison of the explosion characteristics and flame speeds of pulverised coals and biomass in the ISO standard 1m 3 dust explosion equipment.* Fuel, 2015. **151**: p. 91-101.

169. Saeed, M.A., et al. *Effect of steam exploded treatment on the reactivity of wood sample*. in *Proceedings of the 8th Int. Conference on Sustainable Energy and Environmental Protection (SEEP2015)*. 2015. Paisley, Scotland, UK.

170. Industrial-Fire-World, *Incident logs*, 2015.

171. Cashdollar, K.L., *Coal dust explosibility.* Journal of loss prevention in the process industries, 1996. **9**(1): p. 65-76.

172. Hertzberg, M., et al. *Domains of flammability and thermal ignitability for pulverized coals and other dusts: particle size dependences and microscopic residue analyses*. in *Symposium (International) on Combustion*. 1982. Elsevier.

173. Staggs, J.E.J., *Modelling thermal degradation of polymers using single-step first-order kinetics.* Fire Safety Journal, 1999. **32**(1): p. 17-34.

174. Staggs, J.E.J. and R.H. Whiteley, *Modelling the combustion of solid-phase fuels in cone calorimeter experiments.* Fire and Materials, 1999. **23**(2): p. 63-69.

175. Staggs, J., *A theoretical investigation into modelling thermal degradation of solids incorporating finite-rate kinetics.* Combustion science and technology, 1997. **123**(1-6): p. 261-285.

176. Sheng, C. and J. Azevedo, *Modeling biomass devolatilization using the chemical percolation devolatilization model for the main components.* Proceedings of the Combustion Institute, 2002. **29**(1): p. 407-414.

177. Authier, O., et al., *Product Yields and Kinetics of Biomass Fast Devolatilization: Experiments and Modelling.* Chemical Engineering Transactions, 2014. **37**.

178. Yang, H., et al., *In-depth investigation of biomass pyrolysis based on three major components: hemicellulose, cellulose and lignin.* Energy & Fuels, 2006. **20**(1): p. 388-393.

179. Pasangulapati, V., *Devolatilization characteristics of cellulose, hemicellulose, lignin and the selected biomass during thermochemical gasification: experiment and modeling studies*, 2012, Oklahoma State University.

180. Friedl, A., Padouvas, E., Rotter, H. Vermuza, K, *Prediction of heating values of biomass fuel from elemental composition.* Anal Chim Acta, 2005. **544**(544): p. 191-8.

181. Raveendran, K., A. Ganesh, and K.C. Khilar, *Influence of mineral matter on biomass pyrolysis characteristics.* Fuel, 1995. **74**(12): p. 1812-1822.

182. Fagbemi, L., L. Khezami, and R. Capart, *Pyrolysis products from different biomasses: application to the thermal cracking of tar.* Applied energy, 2001. **69**(4): p. 293-306.

183. Hattwig, M. and H. Steen, *Handbook of explosion prevention and protection*. 2008: John Wiley & Sons.

184. Nicolas Cuervo, C.M., Olivier Dufaud, Nathalie Bardin, S.S.-L. Monnier, Jean-François Rémy, Pierre Auzolle,, and L. Perrin, *Combining CFD simulations and PIV Measurements to*

Optimize the Conditions for Dust Explosion Tests. AIDIC, 2014.

185. Murillo, C., et al., *Dust explosions: CFD modeling as a tool to characterize the relevant parameters of the dust dispersion.* Chemical Engineering Science, 2013. **104**: p. 103-116.

186. Carlos Murillo, O.D., Omar López, Laurent Perrin, Alexis Vignes, and F. Muñoz, *CFD Modelling of Nanoparticles Dispersion in a Dust*

Explosion Apparatus. AIDIC 2013.

187. Amjid, S.S., et al., *Biogas, renewable energy resource for Pakistan.* Renewable and Sustainable Energy Reviews, 2011. **15**(6): p. 2833-2837.

188. Dorosh, P. and J. Thurlow, *Agriculture Productivity Growth and Rural Welfare: Insights from Economy-wide Analysis.* 2015.

189. Saeed, M.A., et al. *Agricultural Waste Biomass Energy Potential in Pakistan*. in *Proc. International Bioenergy Exhibition and Asian Bioenergy Conference*. 2015. Shanghai.

190. Andrews, G. and D. Bradley. *Limits of flammability and natural convectionfor methane-air mixtures*. in *14th Symposium (International) on Combustion*. 1973. Elsevier.

191. Andrews, G.E. and D. Bradley, *Determination of burning velocities: A critical review.* Combustion and Flame, 1972. **18**(1): p. 133-153.

192. Basu, P., *Combustion and gasification in fluidized beds*. 2006: Taylor and Francis CRC press.

193. Saeed, M.A., et al. *Improvements to the Hartmann Dust Explosion Equipment for MEC Measurements that are*

Compatible with Gas Lean Limit Measurements. in *10th Asia-Oceania Symposium on Fire Science and Technology (10th AOSFST)*. 2015. Tsukuba, Japan.

194. Slatter., D.J.F., et al. *Biomass explosion residue analysis*. in *Proc. Tenth International Symposium on Hazards, Prevention, and Mitigation of Industrial Explosions (XISHPMIE)*. 2014. Bergen, Norway.

195. Asia-Rice-News. *Riceoutlook*. 2015 [cited 2015 23 November]; Available from: http://www.riceoutlook.com/category/rice-updates/asia-rice-news/pakistan-rice-news/.

196. Andrews, S.S., *Crop residue removal for biomass energy production: Effects on soils and recommendations.* US Department of Agriculture–Natural Resource Conservation Service, http://soils. usda. gov/sqi/files/AgForum_Residue_White_Paper. pdf (15 November 2012), 2006.

197. Stelte, W., *Steam explosion for biomass pre-treatment.* Danish Technological Institute, 2013.

198. Wechsler, M., et al., *Furnace including multiple trays and phase-change heat transfer*, 2013, Google Patents.

199. Mościcki, K.J., et al., *Commoditization of biomass: dry torrefaction and pelletization-a review.* Journal of Power Technologies, 2014. **94**(4): p. 233-249.

200. Huéscar Medina, C., et al. *Comparison of Explosion Characteristics of Torrefied and Raw Biomass*. in *Proc. 22nd European Biomass Conference and Exhibition*. 2014. Hamburg, Germany.

201. Huéscar Medina, C., et al., *Explosion reactivity characterisation of pulverised torrefied spruce wood.* Journal of Loss Prevention in the Process Industries, 2014.

202. Huéscar Medina, C., et al. *Explosibility of biomass and torrefied biomass powders: Determination of Minimum Explosible*

Concentrations. in *Proc. 20th European Biomass Conference and Exhibition*. 2012. Milan.

203. Saeed, M.A., et al. *Flame Propagation of Coarse Wood Mixture: Raw and Torrified*. in *Proc. 8th International Seminar on Fire and Explosion Hazards (ISFEH8)*. 2016. Heifei, China.: USTC Press.

Appendix A

List of dust fire/explosion incidents

Dust fire incidents				
	Date	**Facility**	**Details of incident**	**Internet ref**
1	05/04/2013	Marne, MI	Fire on the dust collection	http://www.woodtv.com/dpp/news/local/ottawa_county/fire-sparks-at-manufacturing-plant
2	14/03/2013	Troy, PA	Fire in a storage shed	http://thedailyreview.com/news/blaze-occurs-at-barefoot-pellet-in-troy-twp-one-worker-reportedly-suffers-smoke-inhalation-1.1458850
3	05/02/2013	Franconia, PA, Dalton, Ga., chemical plant	Fire in the sawdust collection	http://www.timesfreepress.com/news/2013/feb/05/fire-reported-dalton-ga-chemical-plant/
4	24/06/2012	Jaffrey Wood pellet plant, New England, USA	Fire (fourth since 2008)	http://industrialfireprevention.blogspot.co.uk/2012/05/pellet-plant-facing-osha-fine-on-fire.html
5	27/04/2012	New England wood pellet plant, Jaffrey, New England, Canada	Fire by the ignition of sawdust	http://www.unionleader.com/article/20120427/NEWS07/120429861
6	4/3/2012	Upper Leacock silo fire, Ironstonnes Mills, East Lampeter, PA, USA	Fire in the sawdust storage silo	http://www.witmerfire.com/fullstory.php?157763
7	23/02/2012	Geneva wood pellet Mill, Strong, Franklin County	Fire in the storage	http://www.sunjournal.com/news/franklin/1159177
8	01/01/2012	Wood-pellet manufacturing plant , Wiggins MS	Fire	http://www.fireworld.com/IncidentLogs/tabid/101/articleType/ArchiveView/Year/2012/Month/1/currentpage/8/Default.aspx
9	09/11/2010	Havco wood products , Scott County, MO	Fire on sawdust in a silo	http://www.kfvs12.com/story/13475742/another-fire-at-havco-wood-products-overnight
10	08/09/2010	Enligna Canada's wood pellet mill Upper Musquodoboit Halifax Nova Scotia	Fire on sawmill chipping waste	http://www.canadianbiomassmagazine.ca/content/view/1935/57/
11	28/06/2010	South Molton Chipboard factory, UK: wood processing factory.	Fire in the silos	http://www.edp24.co.uk/news/fire_at_south_molton_chipboard_factory_1_430441
12	21/04/2010	Wayerhaeuser, Grande Prayerie- pulp plant sawdust explosion & fire	Fire in sawdust due to friction	http://www.dailyheraldtribune.com/2010/04/21/friction-sawdust-start-fire-at-weyerhaeuser
13	03/01/2010	Elkhart County, IN: Fire broke out in a wood chip pile.	Fire	http://www.osha.gov/dsg/combustibledust/expert_forum_summary_report.pdf
14	20/11/2009	Adelanto, CA: A silo caught fire at a wood products plant.	Fire in the silo	http://www.vvdailypress.com/articles/adelanto-15809-factory-fire.html
15	23/10/2009	Pellet Factory Wismar, Germany	Fire	http://fireworld.com/IncidentLogs/tabid/101/articleType/ArchiveView/month/10/year/2009/Default.aspx
16	24/08/2009	Klamath Falls	Wood dust fire	http://www.fireworld.com/IncidentLogs/tabid/101/articleType/ArchiveView/Year/2009/Month/8/currentpage/2/Default.aspx

17	24/06/2009	Inverness, UK: Fire broke out at a wood chip factory,1 injuring	Fire	http://www.fireworld.com/IncidentLogs/tabid/101/articleType/ArchiveView/month/6/year/2009/Default.aspx
18	31/06/2009	Ferry hill, UK: Fire was reported at a wood chip factory.	Fire	http://www.fireworld.com/IncidentLogs/tabid/101/articleType/ArchiveView/month/6/year/2009/Default.aspx
19	02/05/2009	Westwood Fibre products, kelowna, BC, Canada	Fire in dust particles	http://www.castanet.net/news/West-Kelowna/46698/Another-fire-at-Westwood
20	18/09/2008	Granulles de lac Mauricie, Atikokan, ON	Fire	http://www.pellet.org/linked/2011-07-24%20g%20murray%20pfi.pdf
21	17/09/2008	Kremmling Pellet Plant, Collorado	Fire	http://www.skyhidailynews.com/article/20081027/NEWS/810289971
22	21/06/2008	Vancouver, B.C.	Fire	http://www.fireworld.com/IncidentLogs/tabid/101/articleType/ArchiveView/Year/2009/Month/8/currentpage/2/Default.aspx
23	20/06/2008	Pellet Mill, Corinth, Maine	Fire in the dust	http://woodpelletguru.blogspot.co.uk/2008/05/pellet-mill-fire.html

Dust explosion incidents

	Date	Facility	Details of incident	Internet ref
1	28/01/2013	Tandil, Argentina	Explosion in a grain silo	http://www.lu22radiotandil.com.ar/index.php/informacion-general/49-locales/7286-tras-el-accidente-en-la-planta-de-silos-desde-uatre-aseguran-que-qes-el-momento-de-acompanar-a-las-familias-y-respetar-su-dolorq
2	11/06/2012	Amagerværket, Vattanfall, Denmark	Explosion in the silo	http://ing.dk/artikel/129164-eksplosion-skete-under-rensning-af-silo
3	23/04/2012	Lakeland Mill Vancouver	Explosion & fire fatalities by the ignition of sawdust	http://news.nationalpost.com/2012/04/28/fatal-sawdust-blast-in-b-c-comes-after-five-explsions-at-similar-plants-since-2009/
4	08/03/2012	Laurinburg wood pellet mill, Laurinburg, NC Canada	Dust Explosion & Fire in the silo	http://www.carolinalive.com/news/story.aspx?id=728305
5	20/07/2011	Waycross, Jacksonville, Georgia, USA (incident after 1 month operation)	Flash type explosion in the dust	http://jacksonville.com/news/crime/2011-06-21/story/explosion-damages-waycross-plant-no-injuries-reported
6	06/01/2011	Tolko Soda Creek Mill, Williams Lake	Wood dust Explosion & Fire	http://www.vancouversun.com/news/sawmill+blast+went+unreported/6550344/story.html
7	25/10/2010	Pinskdrev plant	Dust Explosion & Fire in silo	http://charter97.org/en/news/2010/10/26/33260/
8	23/04/2010	Creative Biomass, Kimble Place, Fitchburg , Biomass silo	Dust Explosion & Fire in silo	http://lifeasajournalist.blogspot.co.uk/2010/06/nobody-hurt-in-dust-explosion.html
9	13/04/2010	Wood-Mode Inc KREAMER, PA.	Dust explosion & Fire in silo	http://dailyitem.com/0100_news/x27405087/Dust-fire-fourth-since-2003-at-plant
10	03/04/2010	Kreamer PA	Saw dust explosion	http://www.lewistownsentinel.com/page/content.detail/id/518520.html
11	06/03/2010	Forest Bio Products wood processing plant Perthshire, Scotland	Dust Exlosion & Fire	http://www.pressandjournal.co.uk/Article.aspx/1634354?UserKey=
12	24/08/2009	Williams Lake BC wood pellet facility	Dust Explosions and Fire	http://www.fireworld.com/IncidentLogs/tabid/101/articleType/ArchiveView/Year/2009/Month/8/currentpage/2/Default.aspx
13	08/08/2009	Pellet mill strong, Maine	Dust Explosion & Fire due to the use of unapproved spark	http://www.reliableplant.com/Read/23313/OSHA-cites-Maine-pellet-mill
14	01/08/2009	Pacific Bioenergy Pellet facility, Prince	Dust Explosion & Fire	http://woodworkingnetwork.com/ComDust-explosion-rips-BC-wood-pellet-mill/2010-12-

		George, BC, Canada		27/Article.aspx?oid=1294395&fid=WWN-ARTICLES
15	29/01/2009	Eibenstock, Germany: An explosion destroyed a plant that makes wood pellets.	Dust Explosion & Fire	http://www.fireworld.com/IncidentLogs/tabid/101/articleType/ArchiveView/month/1/year/2009/Default.aspx
16	01/03/2009	Northeast Pellets in Ashland	Dust Explosion & Fire	http://www.pressherald.com/archive/fires-put-maine-pellet-mills-on-hot-seat_2009-08-23.html
17	04/01/2009	Pellet Facility Ettenheim, Germany	Dust Explosion	http://dustexplosions.blogspot.com/2009/01/staubexplosion-german-pellet-mill.html
18	19/12/2008	Pacific Bioenergy Pellet facility, Prince George, BC, Canada	Dust Explosion & Fire	http://forestindustries.eu/content/explosion-pacific-bioenergy%E2%80%99s-pellet-plant-prince-george-bc
19	08/10/2008	New England Wood Pellets	Dust Explosion & Fire	http://dustexplosions.blogspot.com/2008/08/wood-pellet-dust-fire-non-issue.html
20	22/08/2008	AJ Stove and Pellets in Marion, PA	Dust Explosion	http://dustexplosions.blogspot.com/2008/08/wood-pellet-plant-dust-explosion-again.html
21	15/08/2008	Corinth Wood Pellets	Dust Explosion & Fire	http://dustexplosions.blogspot.com/2008/08/wood-pellet-dust-fire-non-issue.html
22	11/08/2008	New England Pellet Plant Jaffrey pellet plant New Hampshire	Dust Explosion & Fire	http://www.thebostonchannel.com/news/17155015/detail.html
23	15/07/2008	AJ Stove and Pellets in Marion, PA	Dust Explosion	http://dustexplosions.blogspot.com/2008/08/wood-pellet-plant-dust-explosion-again.html
24	01/07/2008	Westwood Fibre products, kelowna, BC, Canada	Dust Explosion & Fire	http://www.castanet.net/news/West-Kelowna/46698/Another-fire-at-Westwood
25	01/03/2008	Pacific Bioenergy Pellet facility, Prince George, BC, Canada	Dust explosion	http://www.princegeorgecitizen.com/article/20101218/PRINCEGEORGE0101/312189993/-1/PRINCEGEORGE/explosion-closes-down-pellet-plant

Pellet's fire Incidents

	Date	Facility	Details of incident	Internet ref
1	09/04/2013	Charleston, AR	Fire in the pellets	http://www.arkansasonline.com/news/2013/apr/11/fire-damages-charleston-plant-20130411/
2	27/02/2012	Tilbury biomass power station, UK	Fire in biomass pellets after starting in a hopper	http://www.guardian.co.uk/uk/2012/feb/27/firefighters-essex-power-station-blaze
3	16/12/2010	Wood-pellet factory in Barnstead, NH, USA	Fire on wood pellet	http://www.firehouse.com/news/10464625/nh-firefighters-again-called-to-wood-pellet-plant
4	12/04/2010	New England wood pellets/ Norbord	Fire in the dust deposit in bagging department	http://www.wbng.com/younews/59726207.html
5	29/07/2009	Pellet Mill, Rumford, RI	Fire in the pellets	http://www.fireworld.com/IncidentLogs/tabid/101/articleType/ArchiveView/month/7/year/2009/Default.aspx
6	01/01/2009	Lantmännen's silos in Kristinehamn, Norway	Fire in the pellet silo	http://www.aga.com/international/web/lg/aga/like35agacom.nsf/docbyalias/cust_high_lantm
7	20/05/2008	Corinth Wood Pellets	Fire in the pellets	http://dustexplosions.blogspot.com/2008/08/wood-pellet-dust-fire-non-issue.html

Fire/ Explosions in Conveyers

	Date	Facility	Details of incident	Internet ref
1	12/08/2012	810MW Avedore power plant in Copenhagen	Fire on conveyors	http://www.canadianbiomassmagazine.ca/content/view/3583/57/
2	02/05/2012	Wood pellet wharehouse Port of Panama	Fire on conveyors	http://www.newsherald.com/articles/port-102429-fire-city.html

Fire/Explosions (Spontaneous combustion)				
	Date	**Facility**	**Details of incident**	**Internet ref**
1	14/03/2013	Troy, PA;Barefoot wood pellet plant	Fire broke out in a storage shed	http://thedailyreview.com/news/blaze-occurs-at-barefoot-pellet-in-troy-twp-one-worker-reportedly-suffers-smoke-inhalation-1.1458850
2	03/08/2012	Green Circle Bio-Energy's wood pellet facility Panama	spontaneous combustion	http://www.canadianbiomassmagazine.ca/content/view/3550/57/
3	31/10/2011	Storage area Port of Tyne, UK	Fire	http://www.journallive.co.uk/north-east-news/todays-news/2011/10/31/firefighters-battle-huge-biomass-fire-at-port-of-tyne-61634-29689277/
Fire/Explosions in Venting and duct work				
	Date	**Facility**	**Details of incident**	**Internet ref**
1	18/03/2013	Gonic, NY, Rochester industrial plant	Dust ignition in the venting	http://www.unionleader.com/article/20130318/NEWS07/130319007&source=RSS
2	11/02/2013	Kreamer, PA, Oaklay paper plant	Fire in the empty sawdust silo	http://www.local12.com/news/local/story/Two-Alarm-Fire-At-Oakley-Paper-Plant/uNjjSvbgnUKtks5oY-iOiw.cspx?rss=30
3	01/02/2013	Vivescia, France	Overheated grain silo fire	http://champagne-ardenne.france3.fr/2013/02/02/menace-autour-d-un-silo-de-grains-acy-romance-192701.html
4	07/09/2010	Mingo County, WV: Fire broke out in a wood processing plant.	wood Dust fire in ventilation	http://wvgazette.com/News/201009071154
Fire/Explosions in Grinders				
	Date	**Facility**	**Details of incident**	**Internet ref**
1	01/04/2013	Glendale Heights sheet metal plant, IL	Aluminium dust ignition explosion in grinding	http://abclocal.go.com/wls/story?section=news/local&id=9048672
2	04/01/2013	Tilbrook, UK:	Straw caught fire in grinder	http://www.huntspost.co.uk/news/latestnews/fire_breaks_out_at_huntingdonshire_straw_factory_1_1784402
3	28/02/2011	Portsmouth, NH: A fire in a wood chip crushing machine spread through a power	Fire	http://www.fosters.com/apps/pbcs.dll/article?AID=/20110301/GJNEWS_01/703019953/-1/FOSNEWS
Miscellaneous				
	Date	**Facility**	**Details of incident**	**Internet ref**
1	21/01/2012	Babine Forest Products mill injuring 19, Burns Lake BC	By natural gas leakage	http://foresttalk.com/index.php/2012/01/21/explosion-destroys-babine-forest-products-injuring-19/
2	21/12/2011	Pinnacle Plant Houston BC, Canada. (several fires since 2006)	Under Investigation	http://www.cftktv.com/news/Story.aspx?ID=1630036
3	30/11/2011	Kremmling Pellet Plant, Collorado	No reason is mentioned	http://www.skyhidailynews.com/article/20111130/NEWS/111139999
4	20/10/2011	New England wood pellet plant, Jaffrey, New Hampshire, USA	Fire in cooling tower	http://www.unionleader.com/article/20111020/NEWS07/710219950/0/FRONTPAGE
5	27/04/2011	Pinnacle Plant Houston BC, Canada. (several fires since 2006)	No reason Is mentioned	http://foresttalk.com/index.php/2011/04/04/explosion-at-pinnacle-pellet-in-armstrong-b-c/
6	04/04/2011	Armstrong pellet plant, Pleasant Valley Road, Swan Lake , Canada	Under Investigation	http://www.firedirect.net/index.php/2011/04/blast-fire-at-plant/

7	10/3/2011	Pacific Bioenergy Pellet facility, Prince George, BC, Canada	Fire in pipe connecting two cyclones	http://www.canadianbiomassmagazine.ca/content/view/2352/57/
8	17/12/2010	Pacific Bioenergy Pellet facility, Prince George, BC, Canada	Explosion resulting fire due to Plant's fibre drying system ignition by spark	http://foresttalk.com/index.php/2011/01/06/cause-of-explosion-at-pacific-bioenergy-pellet-plant-determined/
9	07/12/2010	Michigan Fuel pellet plant, Holland, Michigan USA	Fire on pelletizing machine	http://www.hollandsentinel.com/news/x1171015614/Fire-starts-in-machinery-at-wood-pellet-plant
10	02/12/2010	The Ainsworth Lumber Co. Ltd.'s OSB plant, Mile House BC Canada	Explosion in the dryer area	http://foresttalk.com/index.php/2010/12/02/ainsworths-100-mile-osb-plant-operating-again-after-explosion/
11	18/11/2010	Ainsworth OSB Plant 100 Miles House British Columbia	Under Investigation	http://foresttalk.com/index.php/2010/11/18/ainsworth-osb-plant-in-100-mile-house-still-down-after-last-weeks-explosion/
12	16/09/2010	Pine Bluff Fibre resources wood pellet facility, Maryland USA	Under Investigation	http://www.chem.info/News/2010/09/Safety-Sawdust-Explosion-Fire-Guts-Plant/
13	18/07/2010	Lakeshore Wisconsin wood pallets and wood pellets	Suspicious fire	http://www.jsonline.com/news/wisconsin/99535874.html
14	30/03/2010	TinmberTech, Prairae Avenue	Undermines Explosion	http://wnewsj.com/main.asp?SectionID=49&SubSectionID=156&ArticleID=183186
15	04/02/2010	Waste to Energy Plant Jamesville, New York	Dust explosion in filters	http://www.cnycentral.com/news/news_story.aspx?id=438837
16	08/08/2009	Geneva Wood Fuels LLC wood pellet processing, Maine USA	Blast in the dryer in the start-up mode	http://www.dailybulldog.com/db/features/pellet-mill-damaged-in-massive-explosion/

Appendix B

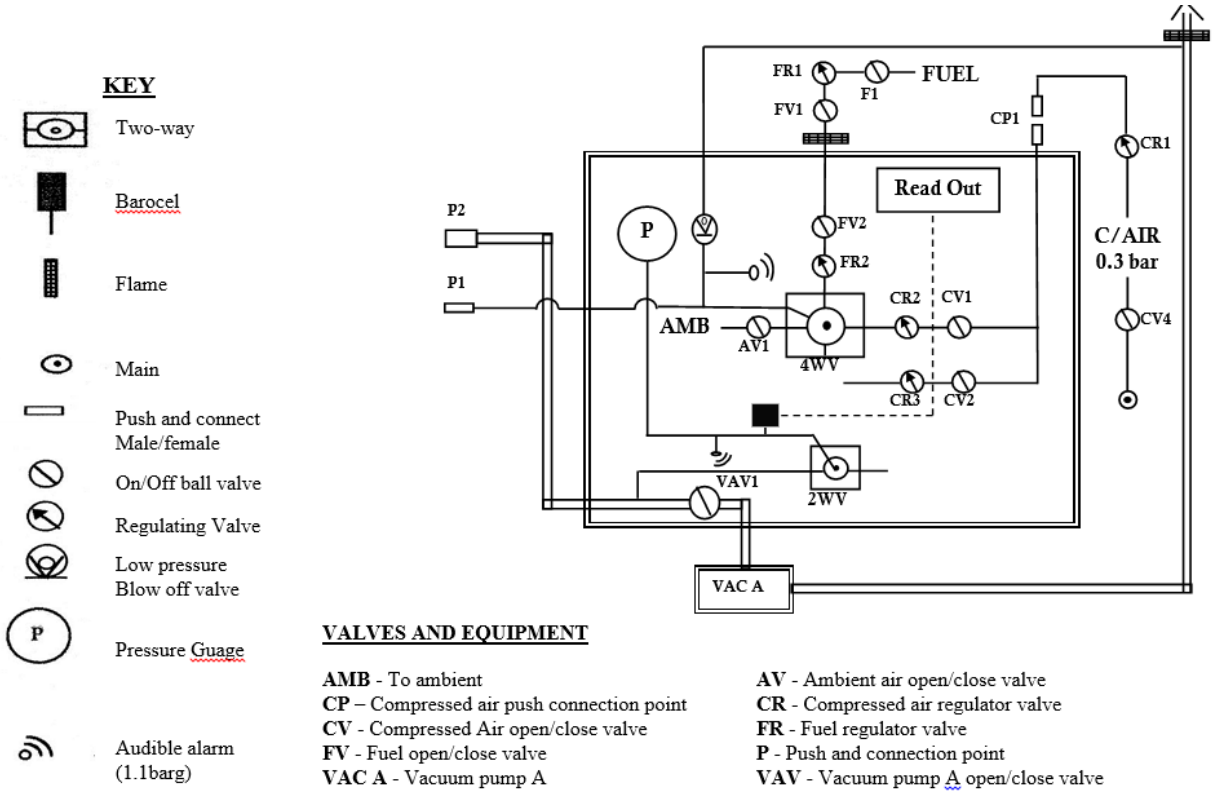

VALVES AND EQUIPMENT

AMB - To ambient
CP – Compressed air push connection point
CV - Compressed Air open/close valve
FV - Fuel open/close valve
VAC A - Vacuum pump A
AV - Ambient air open/close valve
CR - Compressed air regulator valve
FR - Fuel regulator valve
P - Push and connection point
VAV - Vacuum pump A open/close valve

Main Control Panel

Appendix C

KEY

- Two-way
- Barocel
- Flame
- Main
- Push and connect Male/female
- On/Off ball valve
- Regulating Valve
- Low pressure Blow off valve
- Pressure Guage
- Audible alarm (1.1barg)

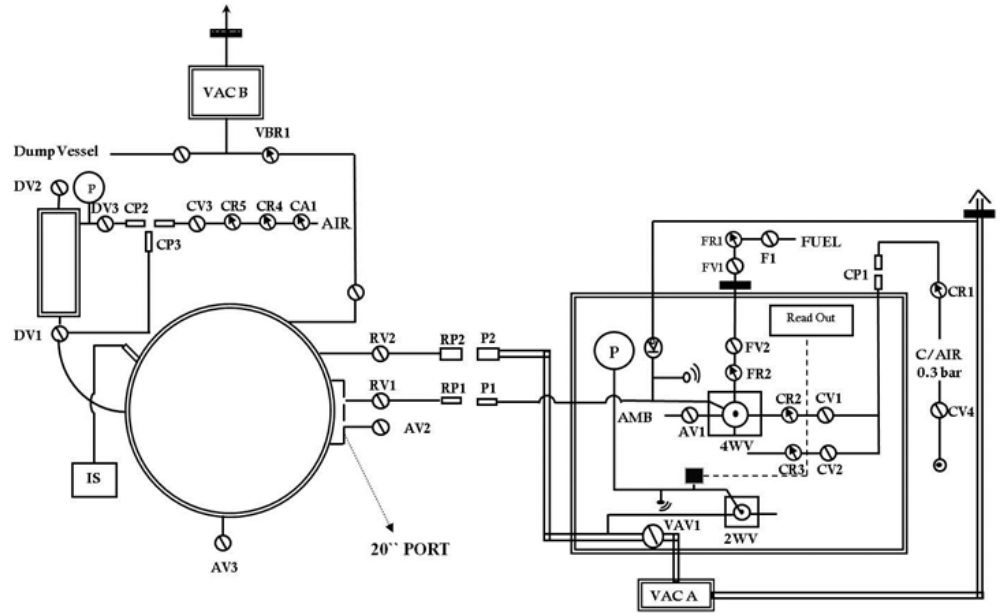

VALVES AND EQUIPMENT

AMB - To ambient
AV - Ambient air open/closed valve
CA – Compressed air bottle valve
CP – Compressed air push and connection point
CR - Compressed air regulator Valve
CV - Compressed air open/close valve
DV – Dust pot open/close valve
F – Fuel bottle open/close valve
FR - Fuel regulator valve
FV- Fuel Open/ closed valve
IS – Ignition Set
P-Push and connection point
RP – Rig push-on connection point
RV – Rig open/close isolation valve
VAC A - Vacuum pump A
VAC B – Vacuum pump B
VAV-Vacuum pump A open/close valve
VBR – Vacuum pump B regulatory valve

Dust Explosion Rig

Appendix D

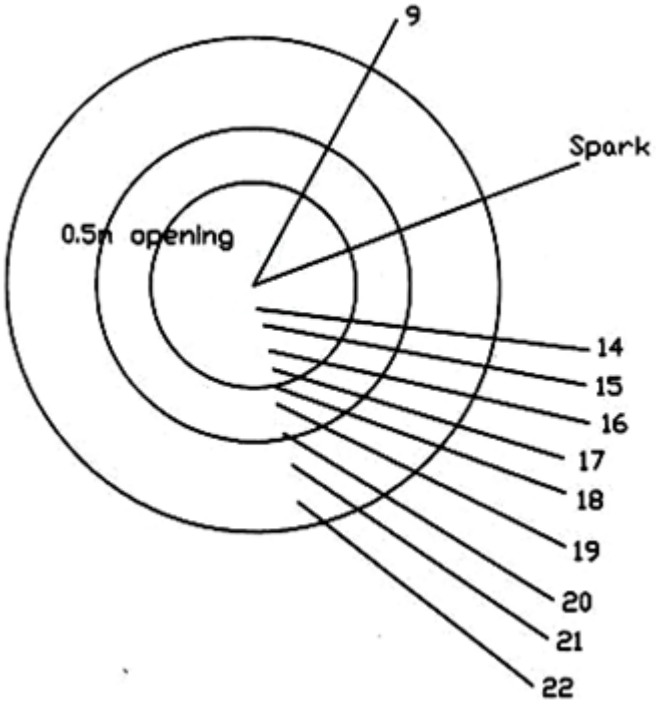

C.1: Schematic of the thermocouple arrangement in vessel (Vertical arrangement)

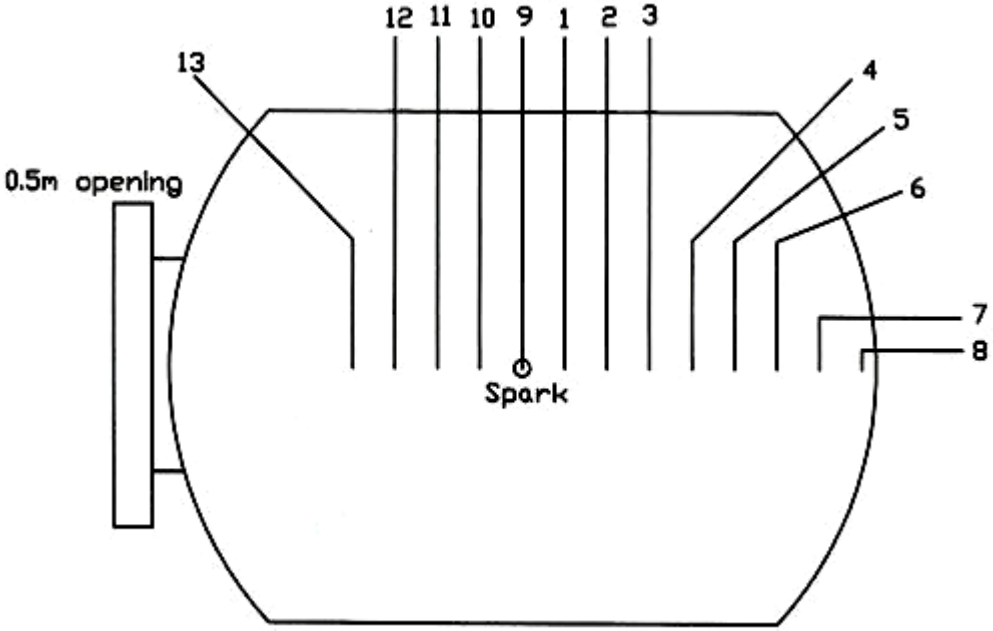

C.2: Schematic of the thermocouple arrangement in vessel (Horizontal arrangement)

Appendix E

Thermocouple Distances

Direction: Forward			**Direction: Backwards**			**Direction: Downwards**		
Thermocouples	Distance from Spark [mm]	Distance between adjacent thermocouples [mm]	Thermocouples	Distance from Spark [mm]	Distance between adjacent thermocouples [mm]	Thermocouples	Distance from Spark [mm]	Distance between adjacent thermocouples [mm]
Spark	0	0	**Spark**	0	0	**Spark**	0	0
1	68	68	**9**	7	7	**14**	78	78
2	132	64	**10**	69	62	**15**	125	47
3	198	66	**11**	131	62	**16**	200	75
S4	261	63	**12**	199	68	**17**	256	56
5	329	68	**13**	265	66	**18**	306	50
6	397	68				**19**	376	70
7	460	63				**20**	444	68
8	522	62				**21**	500	56
						22	556	56

Appendix F

Date	**Test No.**		**Description**
Previous Test No.			Authorised by
Operation	**Tick**	**Instruction/State**	**State/Action**
A. Initial state			
System purged			
Spark power OFF			
Ignition discharged			
20" port open			
B. Chemical ignitors			
See SPECIAL PROCEDURES for handling chemical ignitors		Ignitor energy = Number used = **Total energy =**	
Trim ignitor leads (if required)			
Fit to electrodes		Wire in parallel	Wear safety goggles
Close 20" port		Procedure given in [CONSTRUCTION]	
		dust name	
		Kst	
		dust concentration required (g/m^3) =	
		dust weight required [conc. x 1.138] (g) =	
Weigh out dust sample		Actual weighed mass (g) = m =	
		Actual conc. [actual mass/1.138] (g/m^3) =	
Open dust pot			
Check DV1 closed		Pour dust sample into pot	
Close dust pot		Procedure given in [CONSTRUCTION]	
C. Data Acquisition			
Power to Microlink			
Wavecap computer ON			
Load Wavecap			
Check Valves Closed			
RV1			
RV2			
AV2			
AV3			
VBV2			
DV1		Red indicator horizontal	
DV2			
DV3			
VBR1			
VBV1			
Check Disconnected			
CP2			
CP3			
Connect			
Push to connect P2 to RP2			
D. Control panel check			
Closed			
CV1			
CR2			
CV2			
CR3			

VAV1			
AV1			
FR2			
FV2			
4WV			
E. Pretest Conditions			
Power to barocel			
Open AV2			
Open RV2			
2WV to Test		**Ambient P =**	
		Ambient T =	
		Humidity =	
Power to audible P alarm			
F. Operating State			
F1. Evacuation			
Close AV2			
Open VBV2			
Open VBR1			
Start Vac		Vac to < 900 mbara	
Close VBV2			
Stop Vac			
Close VBR1		Allow P to settle Is leak rate < 2 mbar/min? YES NO If NO see [SPECIAL PROCEDURE]	
F2. Air filling			
Record required P		Final pre-ignition P mbara (A) =	
		Air injection P rise mbara (B) =	
		Pre-injection P mbara (A-B) =	
Open AV2 for initial air fill		Fill to 10 mbar less that pre-injection P	
Close AV2		Record actual metered Barocel P =	
Close RV2			
2WV to close			
F3. Disconnect			
P2 from RP2			
G. Dust-pot Air Filling			
Open CA1			
Check AIR bottle PG1 > 30 bar			
Set PG2 to 25 bar by CR4			
Connect CP2 to AIR bottle			
Open DV3			
Open CV3			
Open and control CV3		meter air to dust-pot to P of 22 bar on gauge	
Close DV3			
Close CV3			
Disconnect CP2			
Check power off to DV1			
Set PG2 to 10 bar by CR4			
Connect CP3 to AIR bottle			
H. System Check			

Power DV1				
Check all valves Closed				
Open CV3				
Check CP3 connected				
Check DV2 Closed				
Check DV3 Closed				
I. Ignition Sequence				
Connect ignition lead to spark box				
Power to spark box				
All to control room				
Connections to sequence gen				
Power to sequence gen				
Lock doors				
Time delay sequence	No.	Time	From	
Time units =	1			
	2			
	3			
	4			
Arm datalogger				
Reset Sequence generator				
Start Sequence generator				
Data logging ends				
Save data				
J. Data check				
Reset Sequence generator				
Load test results		Thermocouple and Pressure data indicate ignition? YES NO If no igntion see [SPECIAL PROCEDURE]		
P2Kel	P1 =			P1 - P2 =
	P2 =			
P53670	P1 =			P1 - P2 =
	P2 =			
Dust pot final P =				
K. System Purge				
Open dump vessel valve to ambient				
Slightly open VBV1				
Connect P2 to RP2				
Close the barocel by the valve behing the main control panel				
Open RV2				
Open VBV2				
Start Vacuum pump		After 2 min open the barocel valve		
Open AV2		Wait for at least 15min		
Close dump vessel valve to ambient				
Disconnect P2 to RP2				
Unbolt 20" port				
Close VBV2				
Turn off pump		Allow test pressure to reach ambient		
Give little crack to 20"door until the O-ring in place falls				
Open VBV2				
Turn on the vacuum pump		Wait for 10-15min		
NOTE: Keep the vacuum pump running at all time till the completion of howering				

L. Dust Pot and Vessel Cleaning			
Open dust pot			
		Weigh out an empty vacuum bag W1 =	
Attach vacuum bag to the vacuum cleaner			
Hover out all the residue from dust pot (if there is any)			
		Weigh out the vacuum bag after hovering W2 = Weight of residue in dust pot W2 - W1 = W3 = Mass explode m - W3 = W4 Actual conc of dust explode W4/1.138 =	
Open 20" port			
		Weigh out an empty vacuum bag W5 =	
Attach vacuum bag to the vacuum cleaner			
Hover out all the residue from the vessel			
		Weigh out the vacuum bag after hovering W6 = Weight of residue in the vessel W6 - W5 =	

Appendix G

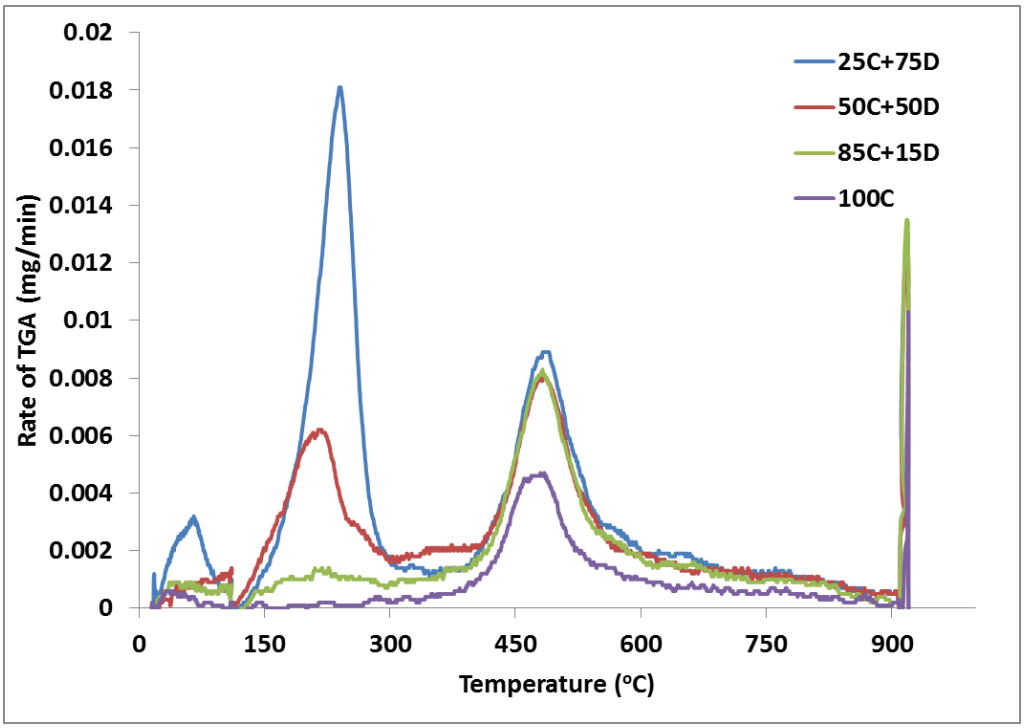

F.1: Rate of volatile rate vs. temperature for different coal-diesel mixtures

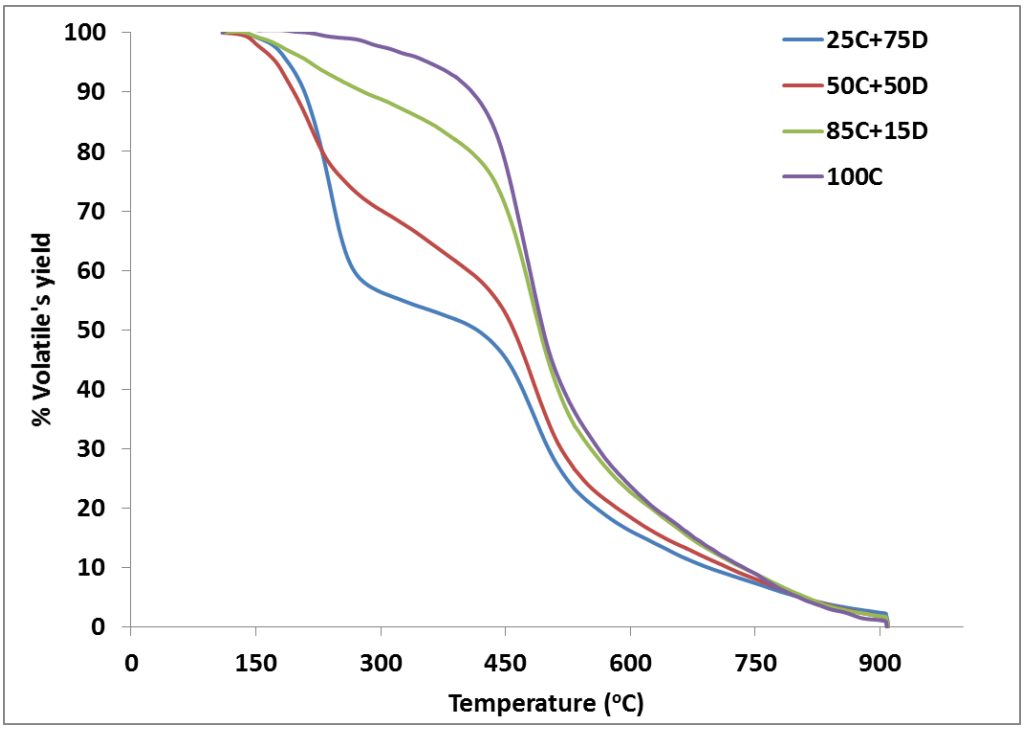

F.2: % volatiles loss vs. temperature for different coal-diesel mixtures

Appendix H

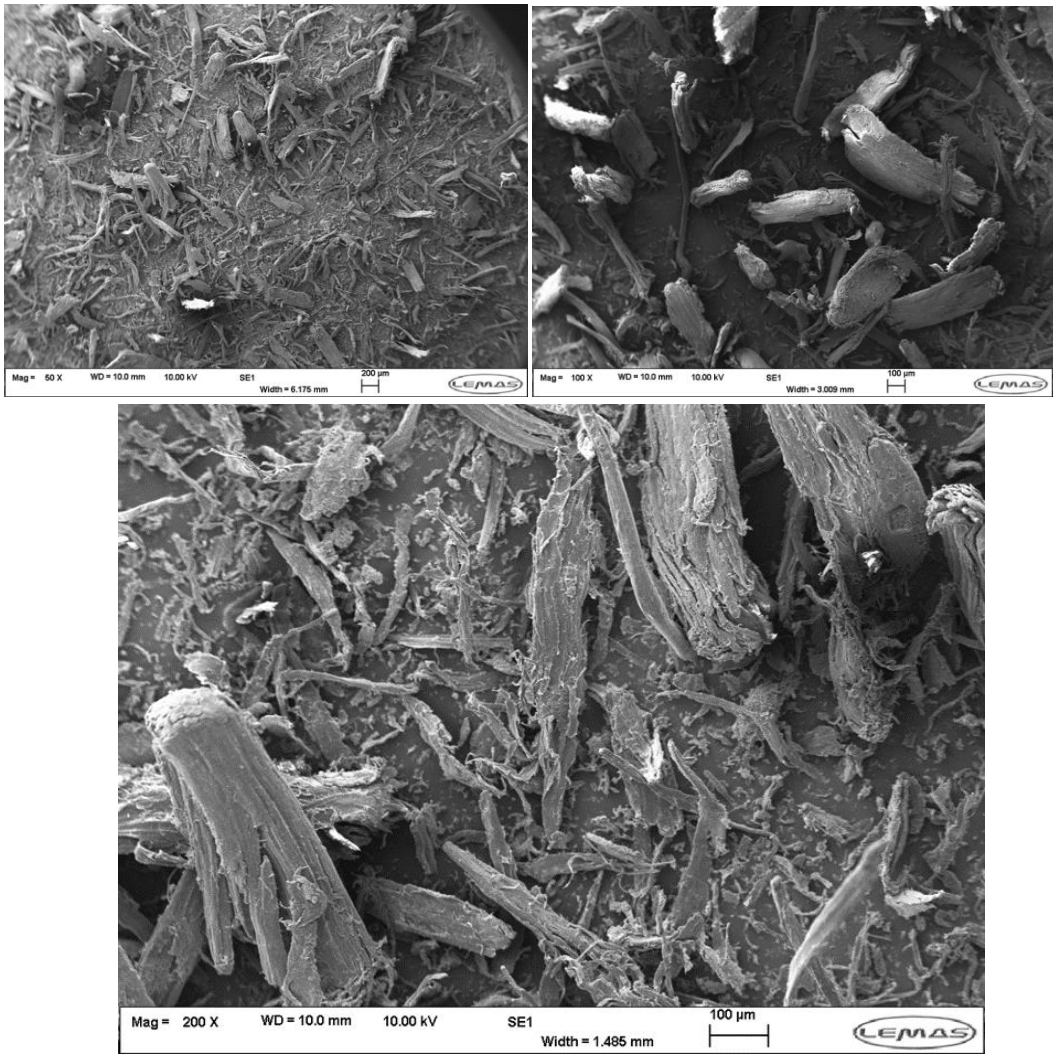

G.1: SEM images of Pinewood pellet (Blz) for different magnifications

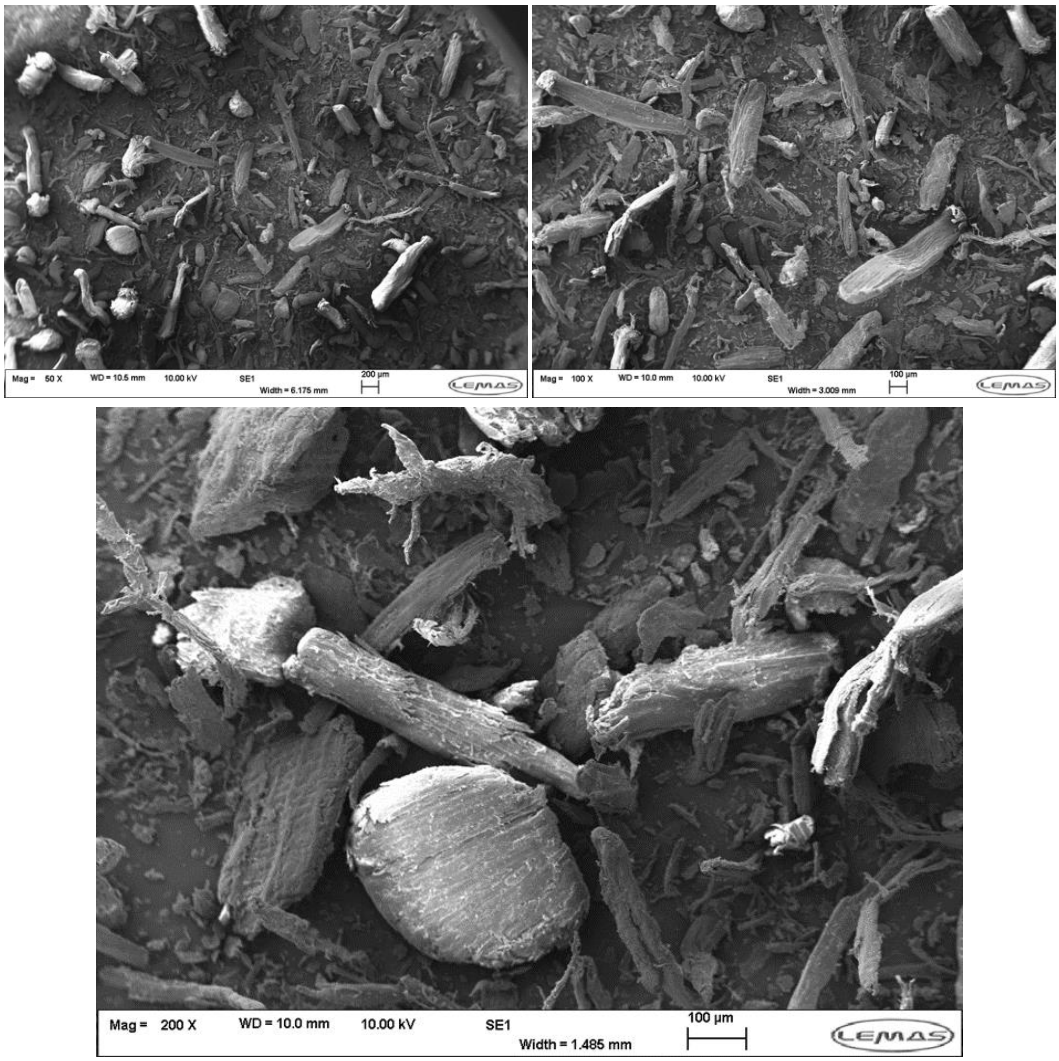

G.2: SEM images of HW sawdust (Dfl) for different magnifications

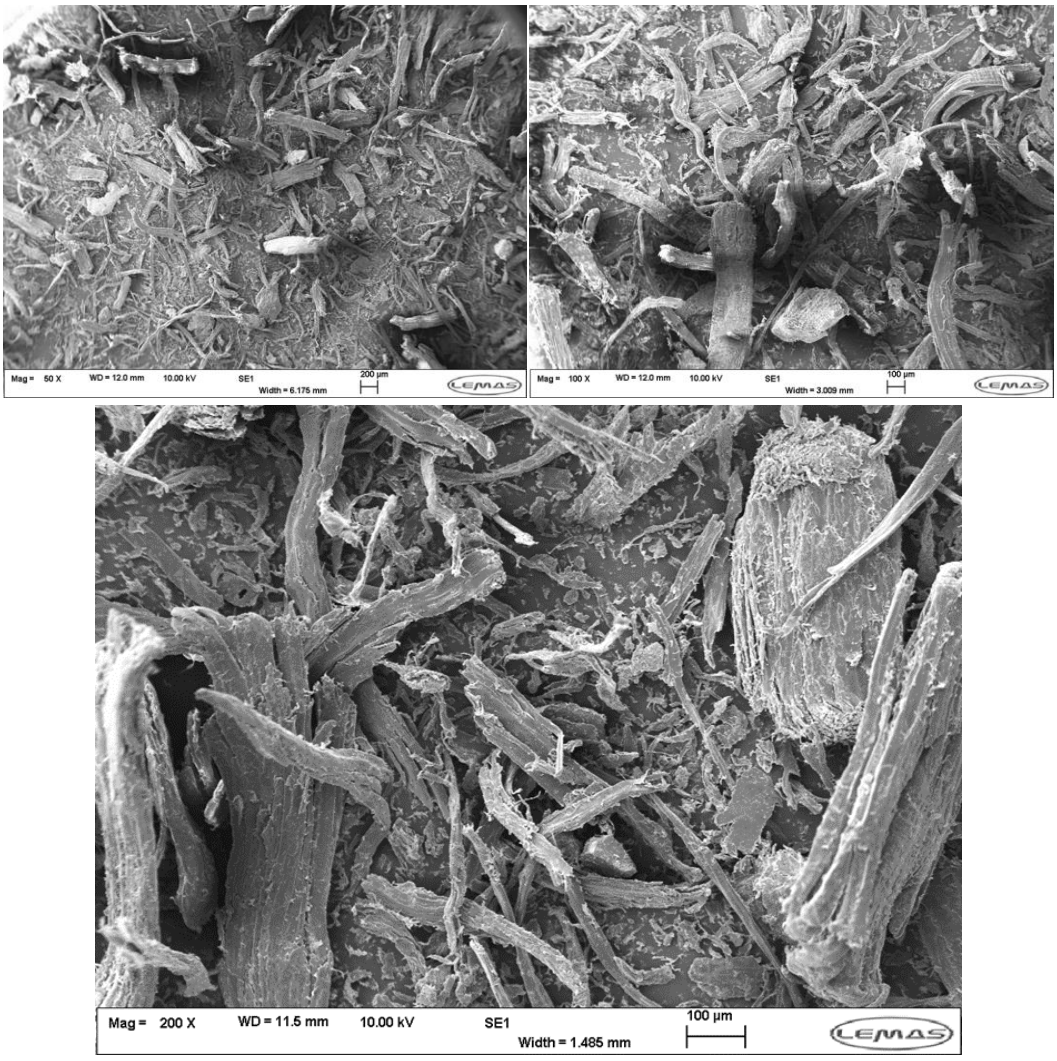

G.3: SEM images of Construction waste wood 1 (CWW1) for different magnifications

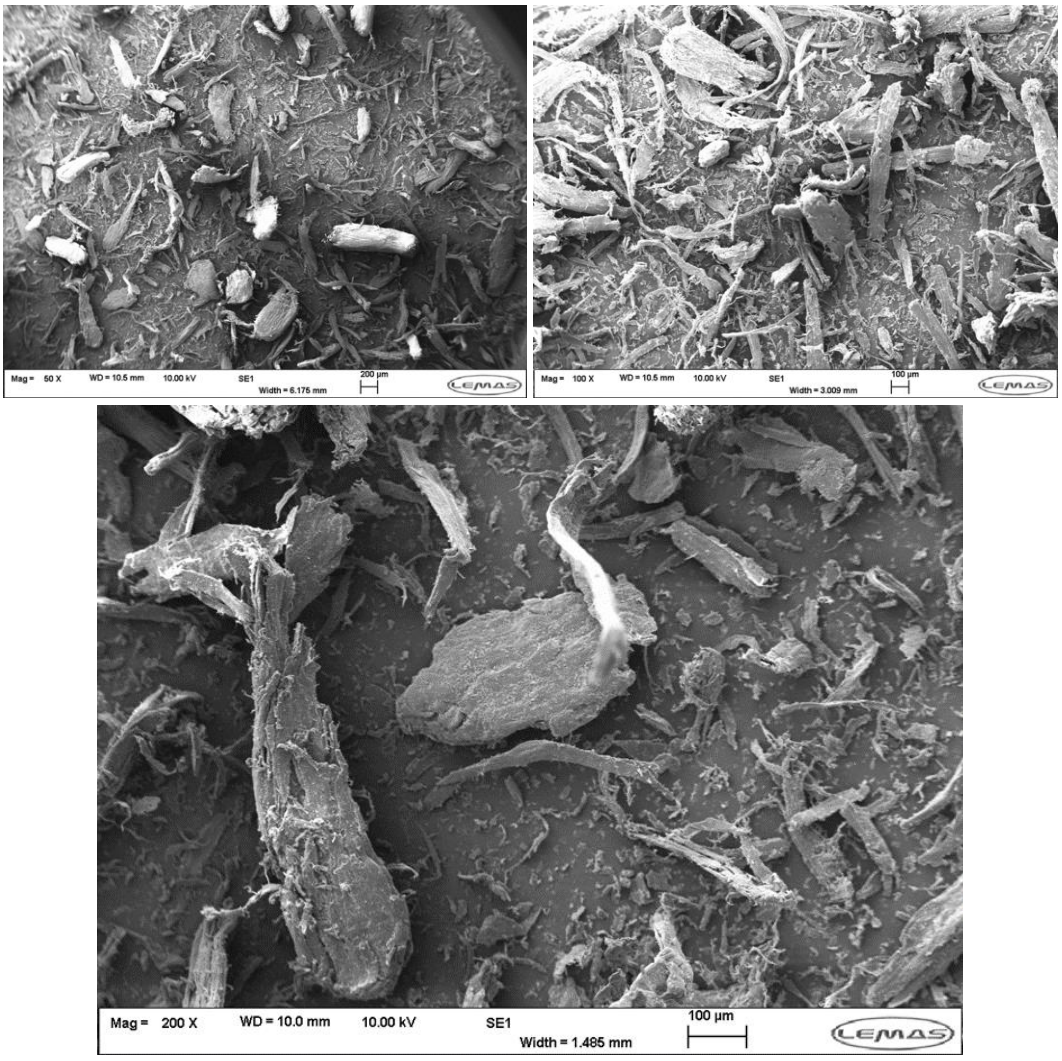

G.4: SEM images of Construction waste wood 2 (CWW2) for different magnifications

Appendix I

Particle size distribution of pine wood in comparison to its steam exploded wood and Kellingley coal samples

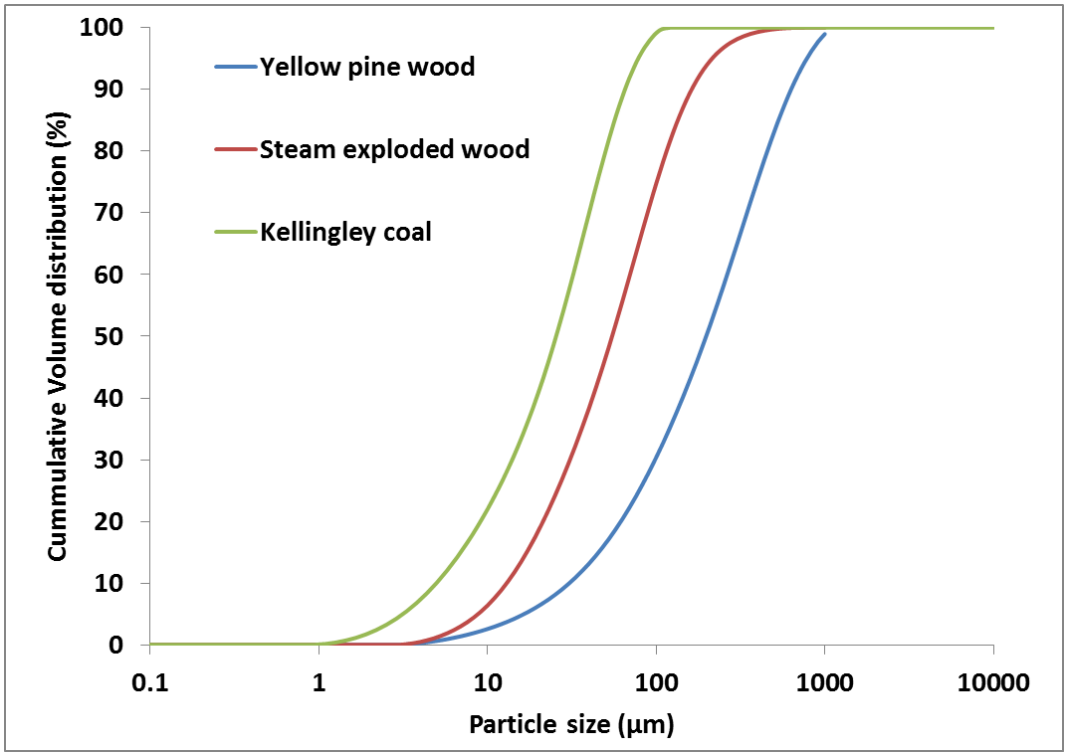

Appendix J

Pressure trace with thermocouples signals in Hartmann test

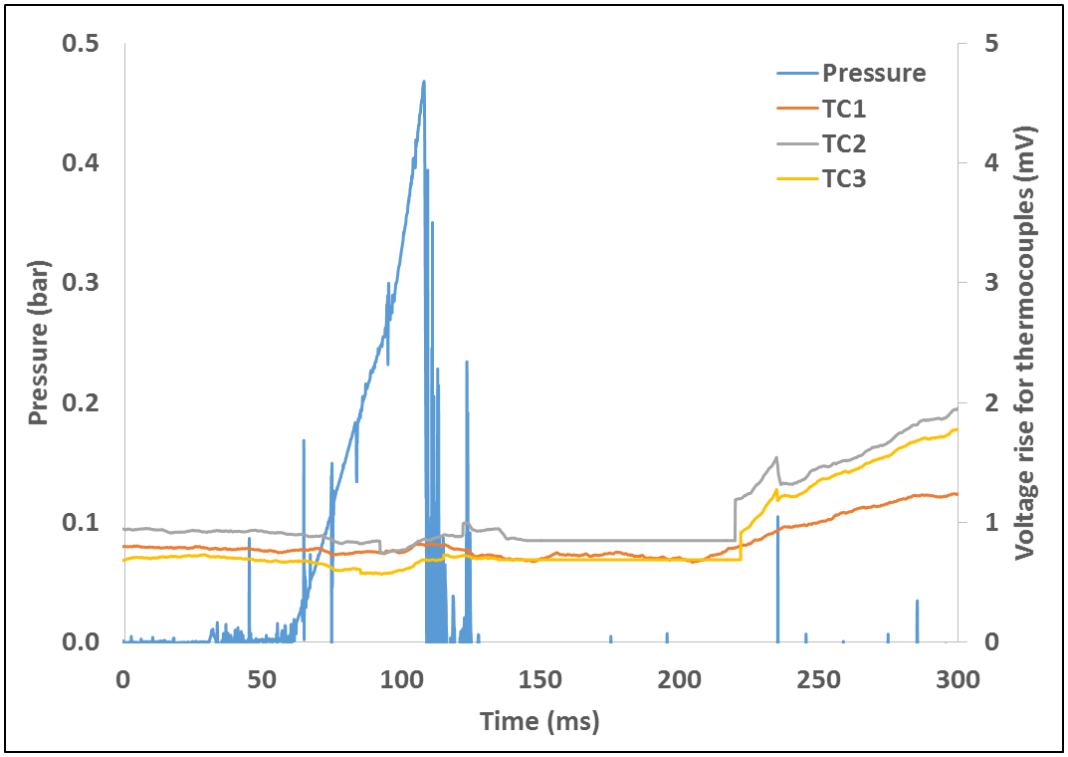

Appendix K

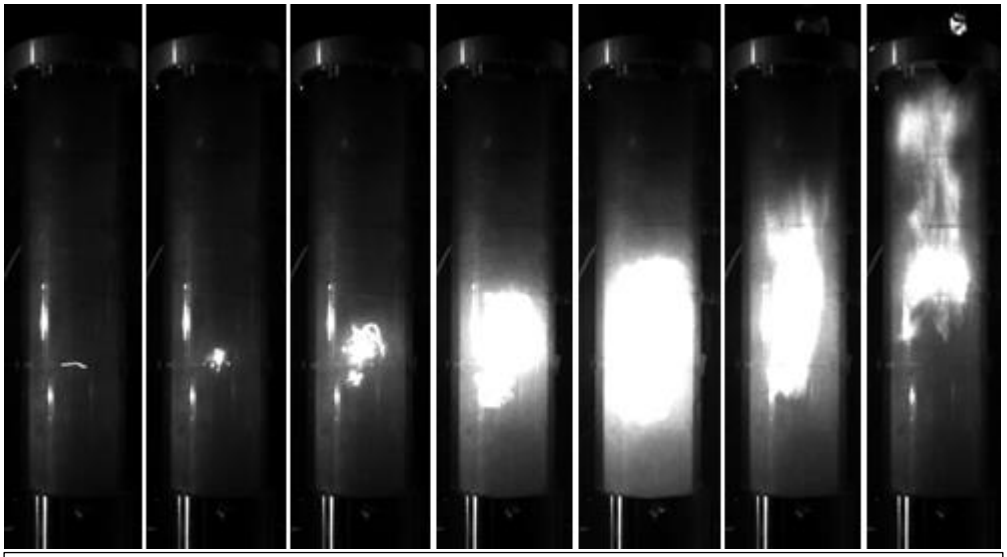

J.1: Flame propagation of polyethylene dust for 120 ms ignition delay

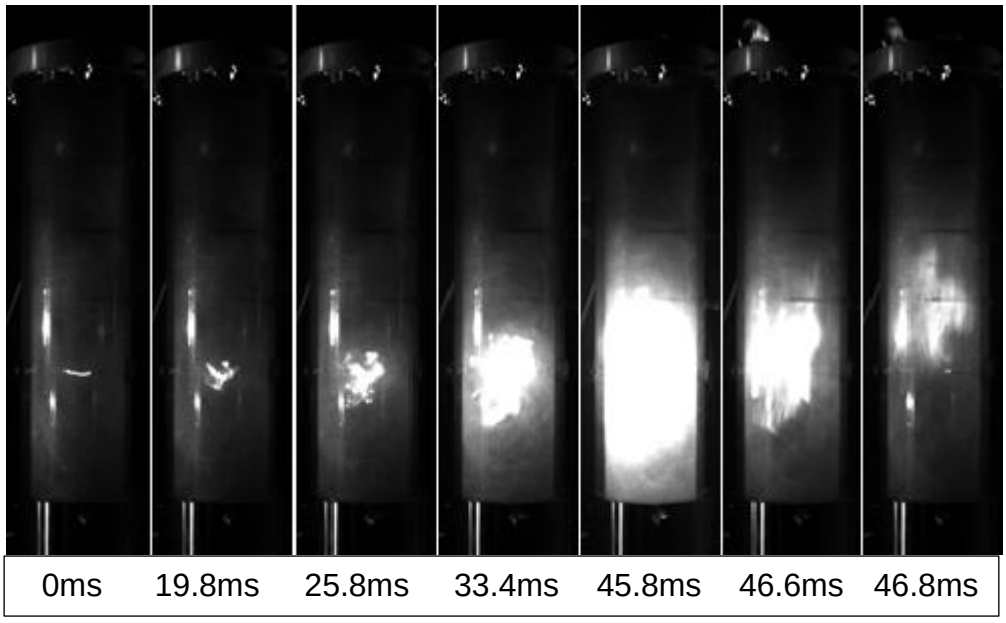

J.2: Flame propagation of polyethylene dust for 80 ms ignition delay

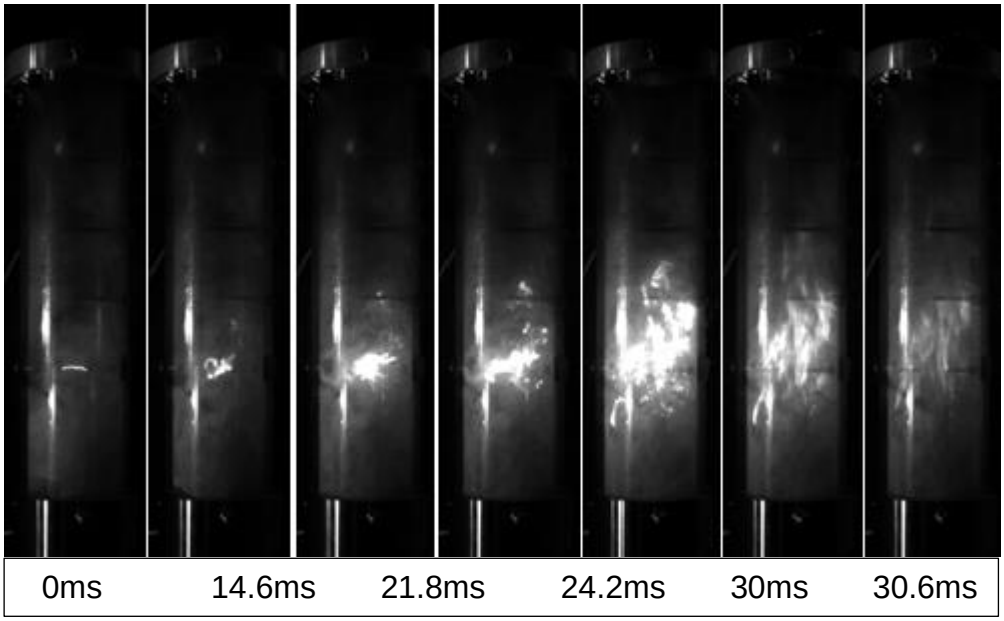

J.3: Flame propagation of polyethylene dust for 50 ms ignition delay

Appendix L

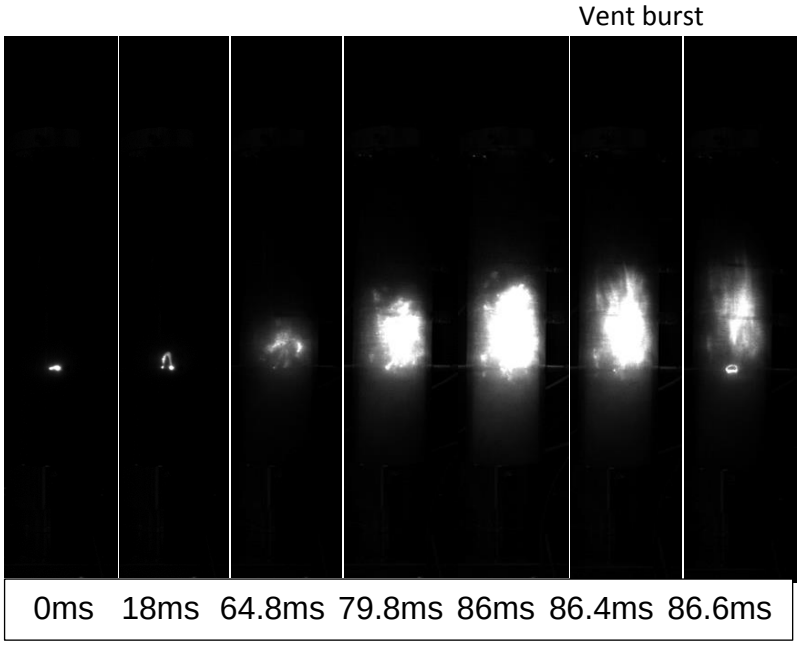

K.1: Flame propagation of yellow pine wood for 0 ms ignition delay

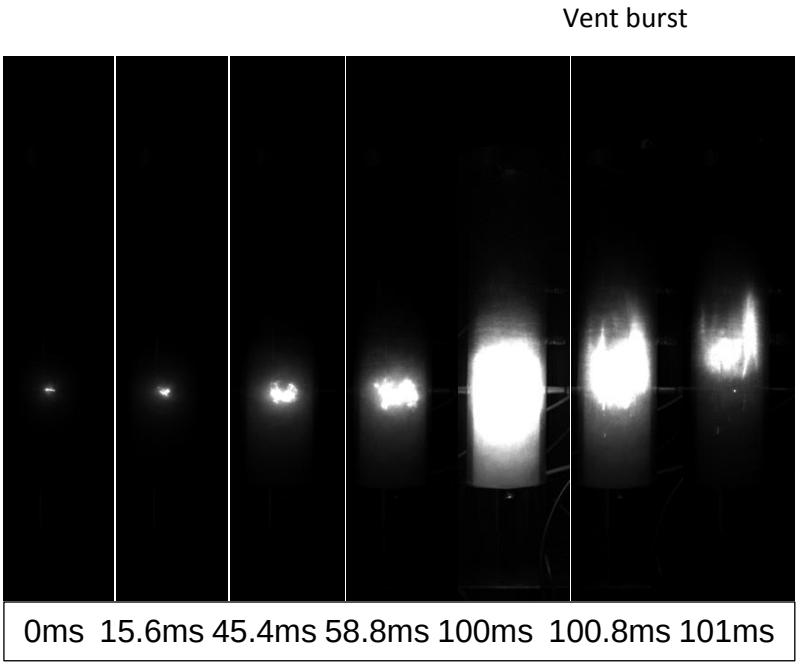

K.2: Flame propagation of yellow pine wood for 120 ms ignition delay

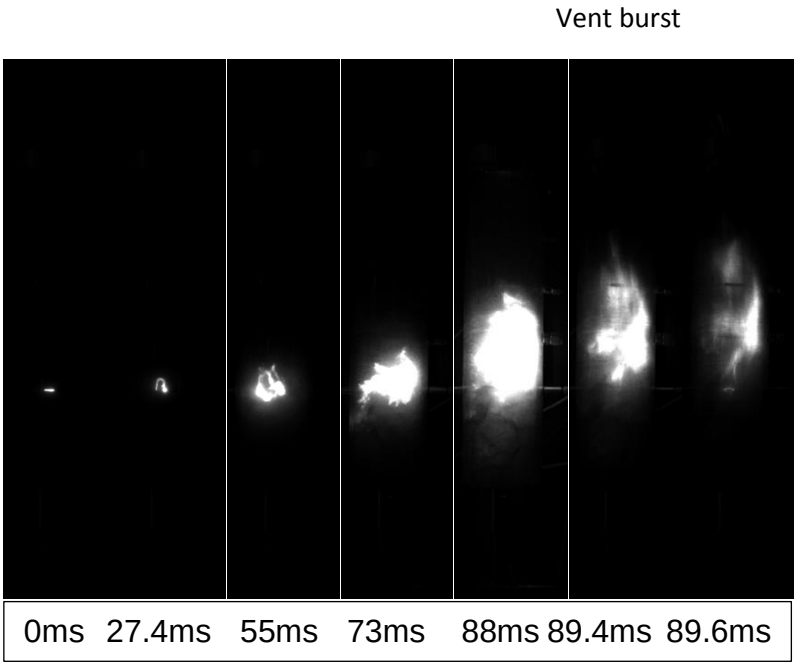

K.3: Flame propagation of steam treated yellow pine/black pellet (BP) for 0 ms ignition delay

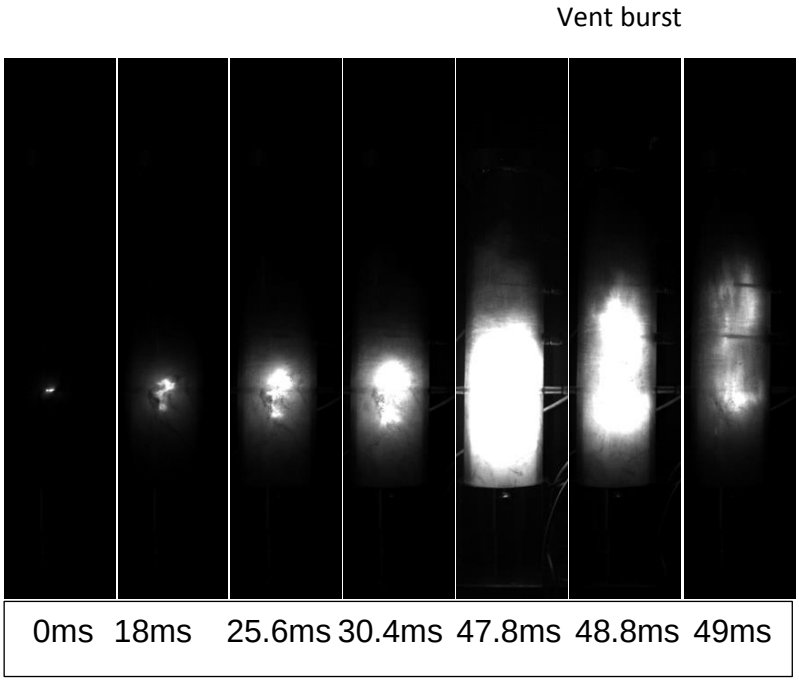

K.4: Flame propagation of steam treated yellow pine/black pellet (BP) for 120 ms ignition delay

Appendix M

Diesel test on modified Hartmann tube

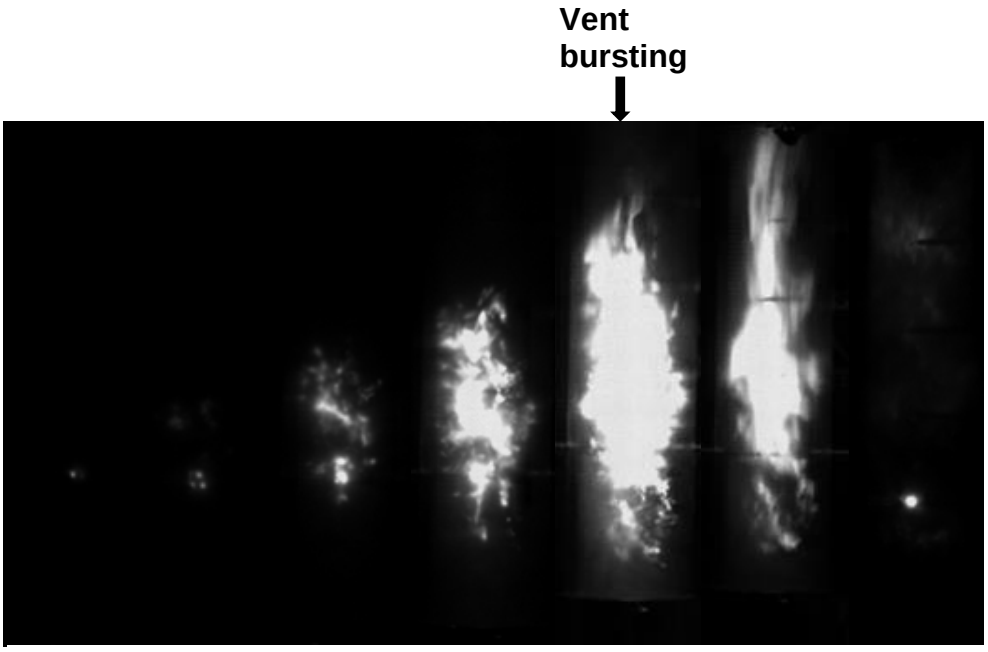

L.1: Flame propagation of diesel air mixture (Eq. ratio= 2.25) using modified Hartmann tube

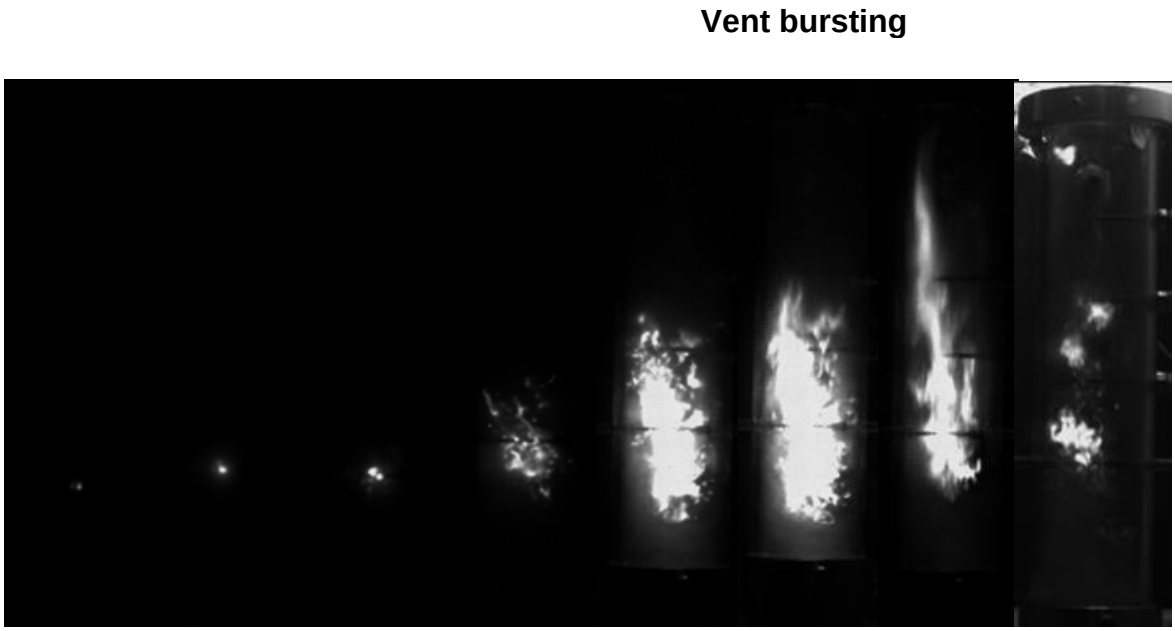

L.2: Flame propagation of diesel air mixture (Eq. ratio= 4.5) using modified Hartmann tube

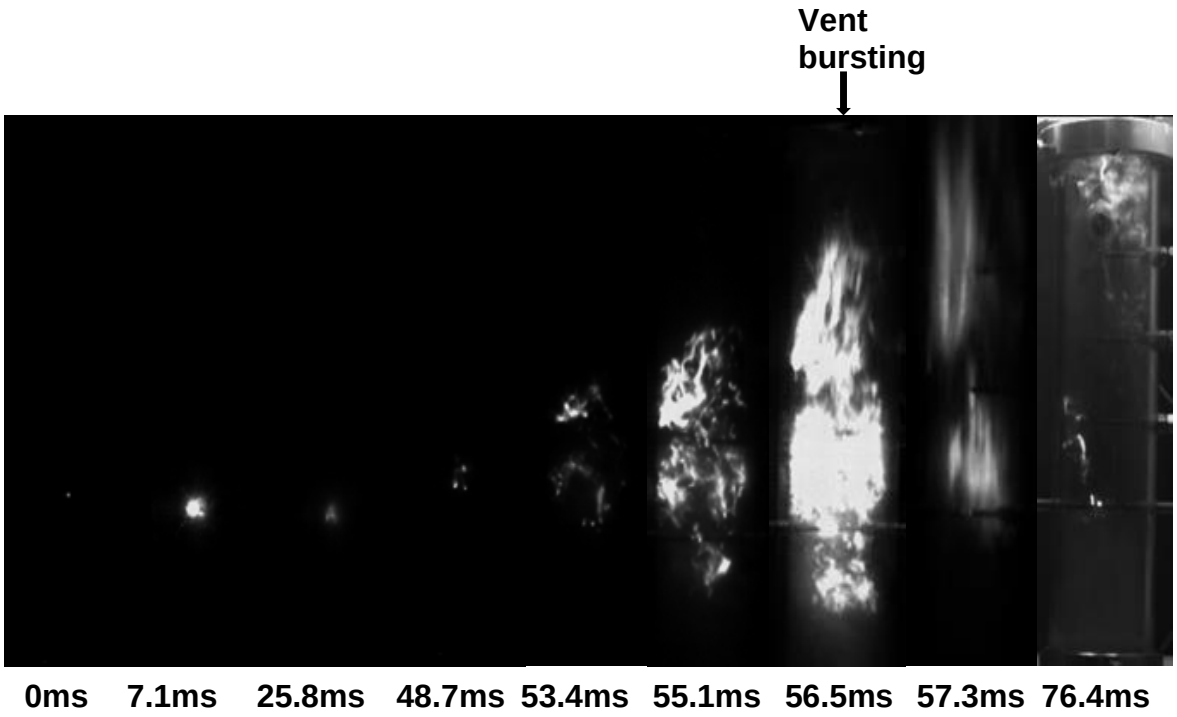

L.3: Flame propagation of diesel air mixture (Eq. ratio= 10.5) using modified Hartmann tube